2007

XENOBIOTIC TRANSPORTERS IN LACTATING MAMMARY EPITHELIAL CELLS: PREDICTIONS FOR DRUG ACCUMULATION IN BREAST MILK

Philip Earle Empey
University of Kentucky, pempey@pitt.edu

STUDENT AGREEMENT:

I represent that my thesis or dissertation and abstract are my original work. Proper attribution has been given to all outside sources. I understand that I am solely responsible for obtaining any needed copyright permissions. I have obtained needed written permission statement(s) from the owner(s) of each third-party copyrighted matter to be included in my work, allowing electronic distribution (if such use is not permitted by the fair use doctrine) which will be submitted to UKnowledge as Additional File.

I hereby grant to The University of Kentucky and its agents the irrevocable, non-exclusive, and royalty-free license to archive and make accessible my work in whole or in part in all forms of media, now or hereafter known. I agree that the document mentioned above may be made available immediately for worldwide access unless an embargo applies.

I retain all other ownership rights to the copyright of my work. I also retain the right to use in future works (such as articles or books) all or part of my work. I understand that I am free to register the copyright to my work.

REVIEW, APPROVAL AND ACCEPTANCE

The document mentioned above has been reviewed and accepted by the student's advisor, on behalf of the advisory committee, and by the Director of Graduate Studies (DGS), on behalf of the program; we verify that this is the final, approved version of the student's thesis including all changes required by the advisory committee. The undersigned agree to abide by the statements above.

Philip Earle Empey, Student

Dr. Patrick J. McNamara, Major Professor

Dr. Janice Buss, Director of Graduate Studies

ABSTRACT OF DISSERTATION

Philip Earle Empey

The Graduate School

University of Kentucky

2007

XENOBIOTIC TRANSPORTERS IN LACTATING MAMMARY EPITHELIAL CELLS: PREDICTIONS FOR DRUG ACCUMULATION IN BREAST MILK

ABSTRACT OF DISSERTATION

A dissertation submitted in partial fulfillment of the
requirements for the degree of Doctor of Philosophy in the
College of Pharmacy at the University of Kentucky

By

Philip Earle Empey

Lexington, Kentucky

Director: Patrick J. McNamara, Ph.D., Professor of Pharmaceutical Sciences

Lexington, Kentucky

2007

ABSTRACT OF DISSERTATION

XENOBIOTIC TRANSPORTERS IN LACTATING MAMMARY EPITHELIAL CELLS: PREDICTIONS FOR DRUG ACCUMULATION IN BREAST MILK

Recent literature has established that breast cancer resistance protein (ABCG2) is upregulated during lactation and is responsible for the greater than predicted accumulation of many drugs in breast milk. The objectives of this project were (1) to investigate the role of this transporter in the reported apically-directed nitrofurantoin flux in the CIT3 cell culture model of lactation, (2) to develop a mathematical model for drug transfer into breast milk to relate initial flux rates, steady-state concentrations, efflux ratios, and in vivo milk to serum ratios (M/S) and (3) to identify xenobiotic transporters that are highly expressed, and therefore potentially important for drug accumulation during lactation in mice and humans.

Expression, localization, and functional assays confirmed that Abcg2 is the molecular mechanism for the apically-directed nitrofurantoin flux in CIT3 cells despite an unchanged expression level following lactogenic hormone stimulation in this model.

A simple three compartment model for drug transfer into breast milk incorporating the permeability-surface area products for passive diffusion (PS_D), paracellular flux (PS_{PC}), endogenous transporters ($PS_{B,U}$, $PS_{A,E}$, $PS_{B,E}$, and $PS_{A,U}$), and ABCG2 ($PS_{A,E(ABCG2)}$) transfection was developed. A stably transfected ABCG2 overexpressing MDCKII cell line was successfully created and used to explore the theoretical relationships of this new model. Derivations and correlations presented herein show the relationships between the calculated efflux ratios, $PS_{A,E(ABCG2)}$, and M/S attributed to ABCG2.

Six xenobiotic transporters (Abcg2, Slc22a1, Slc15a2, Slc29a1, Slc16a1, and Abcc5) were identified as upregulated during lactation in murine developmental datasets analyzed by microarray expression profiling. As existing methods were inadequate to obtain pure populations of luminal epithelial cells in sufficient numbers from human breast milk or reduction mammoplasty samples for microarray analysis, a new fluorescence activated cell sorting method was developed and validated. ABCG2, SLC15A2, SLC22A12, SLC6A14, and SLCO4C1 were significantly upregulated 164-, 70-, 41-, 8-, and 2-fold during lactation, respectively. ABCC10, SLC10A1, SLC16A1, SLC22A4, SLC22A5, SLC22A9, SLC28A3, SLC29A1, SLC29A2, and SLCO4A1 had an expression level similar to, or greater than, levels in the kidney or liver. The significant upregulation of SLCO4C1 with ABCG2 is a novel finding that suggests a coordinated vectorial pathway for substrate movement into breast milk.

KEYWORDS: ABCG2, transporter, lactation, mathematical modeling, M/S prediction

XENOBIOTIC TRANSPORTERS IN LACTATING MAMMARY EPITHELIAL CELLS: PREDICTIONS FOR DRUG ACCUMULATION IN BREAST MILK

By

Philip Earle Empey

Patrick J. McNamara, Ph.D.
Director of Dissertation

Janice Buss, Ph.D.
Director of Graduate Studies

September 24, 2007
Date

RULES FOR THE USE OF DISSERTATIONS

Unpublished dissertations submitted for the Doctor's degree and deposited in the University of Kentucky Library are as a rule open for inspection, but are to be used only with due regard to the rights of the authors.

Bibliographical references may be noted, but quotations or summaries of parts may be published only with the permission of the author, and with the usual scholarly acknowledgments.

Extensive copying or publication of the dissertation in whole or in part also requires the consent of the Dean of the Graduate School of the University of Kentucky.

A library that borrows this dissertation for use by its patrons is expected to secure the signature of each user.

Name	Date

DISSERTATION

Philip Earle Empey

The Graduate School

University of Kentucky

2007

XENOBIOTIC TRANSPORTERS IN LACTATING MAMMARY EPITHELIAL CELLS: PREDICTIONS FOR DRUG ACCUMULATION IN BREAST MILK

DISSERTATION

A dissertation submitted in partial fulfillment of the
requirements for the degree of Doctor of Philosophy in the
College of Pharmacy at the University of Kentucky

By

Philip Earle Empey

Lexington, Kentucky

Director: Patrick J. McNamara, Ph.D., Professor of Pharmaceutical Sciences

Lexington, Kentucky

2007

DEDICATION

To my wife, Kerry, whose love and support made this journey through graduate school possible and to our twins, Piper and Caden, whose giggles keep life fun.

ACKNOWLEDGEMENTS

I would first like to thank my wife, Kerry McGarr Empey, for her continuous love and support through our time in Kentucky. I wish to thank my parents, Richard and Rosanne Empey for their love and always encouraging me to be curious and to pursue the knowledge afforded by ongoing education.

I thank my mentor, Patrick McNamara for providing this wonderful opportunity for me to develop as a scientist. I have truly enjoyed working with him and will always be grateful for the education, advice, and mentorship he has provided. I value the many lengthy discussions we have had; whether as specific as involving a particular experiment or more philosophically about academia and the pharmacy profession. I also acknowledge the contributions of each of my committee members Drs. Val Adams, Markos Leggas, Robert Yokel, Mary Vore, Jeffrey Moscow and that of my outside examiner, Dr. William Silvia. I would also like to thank the members of the McNamara Lab, past and present, Phillip Gerk, Jane Alcorn, Jeffrey Edwards, Michael Chen, Lipeng Wang, Yuxin Yang, and especially Maggie Abbassi for so many thoughtful discussions. I truly value the constant support, guidance, and close friendship of Dr. David Feola. All my friends and colleagues at the University of Kentucky will be sorely missed.

I appreciate the assistance of Mamta Goswami with transfection assays, Dr. Diane Davey with cytology, Dr. Beth Garvy with FACS, Dr. Justin Balko with microarray, Na Ren and Dr. Arnold Stromberg with the microarray statistics, Patti Cross with histology, Catina Rossell in the College of Pharmacy, Dr. Jennifer Strange and Dr. Greg Bauman at the Flow Cytometry Core Facility, the Microarray Core Facility, the Imaging Core Facility, and the General Clinical Research Center. Finally, I would like to acknowledge the financial support of the Research Challenge Trust, the American Foundation for Pharmaceutical Education, the Glavinos Student Endowment Travel Award, and to the Graduate School and the Department of Pharmaceutical Sciences for the travel support to various meetings to present my work.

TABLE OF CONTENTS

LIST OF TABLES

LIST OF FIGURES

CHAPTER 1: Background

A. Breastfeeding and the clinical problem of postpartum drug use

Breast milk is the most complete infant nutrition and breastfeeding is widely advocated as the best choice for most infants, their mothers, and society [1-3]. Breastfed infants have a decreased risk of infectious diseases such as diarrhea [4-7], lower respiratory tract disease [6,8-10], otitis media [7,11], bacterial meningitis [12,13], and urinary tract infections [10,14,15]. Studies suggest lower rates of sudden infant death syndrome in the first year of life [16-18] and a lower incidence of type 1 and 2 diabetes [19,20], some cancers [21,22], asthma [23,24], and obesity [25,26] in adults who were breastfed. Breastfeeding even offers potential advantages in terms of an infant's cognitive development, as a slightly enhanced performance on IQ tests has been documented [27-30]. Maternal benefits include a more rapid postpartum recovery [31], increased child spacing [32], a decreased risk of osteoporosis [33], a lower incidence of both breast cancer and ovarian cancer [34,35], an earlier return to pre-pregnancy weight [36], and emotional benefits such as empowerment and mother-infant bonding. Literature also suggests economic, family, and environmental benefits to society such as the potential for a decreased annual health care cost of $3.6 billion in the United States (estimated in 2001 dollars) and decreased parental employee absenteeism and associated loss of family income [37,38]. Few contraindications exist, but notably include infant galactosemia, maternal HIV or tuberculosis, and the use of illicit drugs. Mothers with exposure to radioactive materials and a short list of other medications such as antimetabolites and some cytotoxic drugs should also refrain from breastfeeding until these agents are no longer present in the milk [1].

Current policy statements by the American Academy of Pediatrics recommend that infants be exclusively breastfed for at least the first six months of life with the addition of complimentary foods to continued breastfeeding through at least 12 months of age [1]. Breastfeeding rates have steadily increased in the United States since the 1970s with 2003 data indicating that 66% of women initiating breastfeeding and 32.8% continuing to breastfeed their infants to 6 months (Figure 1-1) [39,40]. However, despite efforts of professional organizations and government agencies through aggressive public awareness campaigns, breastfeeding rates continue to fall short of the *Healthy People 2010 Initiative* goals of 75% of mothers choosing to breastfeed in the early postpartum period, 50% at six months, and 25% at one year. Additional goals specifically for

exclusive breastfeeding were recently added to the *Healthy People 2010 Initiative* in 2007. These new objectives are to increase the proportion of mothers who breastfeed exclusively through 3 months to 60%, and through 6 months to 25%. Many obstacles to achieving these metrics exist. Data indicate medication use in the postpartum period is highly prevalent with greater than 90% of women taking at least one medication postpartum [41]. Furthermore, Ito et al. document that 22% of lactating women who require antibiotics either stopped breastfeeding or did not start the prescribed medication despite the fact that the drugs were considered safe during breastfeeding. Schirm et al. reported that 82.1% of the patients surveyed in the Netherlands breastfed their baby at some time during the first 6 months postpartum and that 65.9% of these women had administered medications while breastfeeding [42]. These authors found that "drugs play an important role in women's decision to start or continue breastfeeding: women frequently hesitated to use drugs during breastfeeding, stopped either breastfeeding or drug use to avoid combining the two, took a measure to minimize exposure to the child, did not use any drug because of breastfeeding, or did not breastfeed because of drug use."

Figure 1-1: Breastfeeding trends in the United States.

Data compiled from the Mothers Survey conducted by the Ross Products Division of Abbott Laboratories [40].

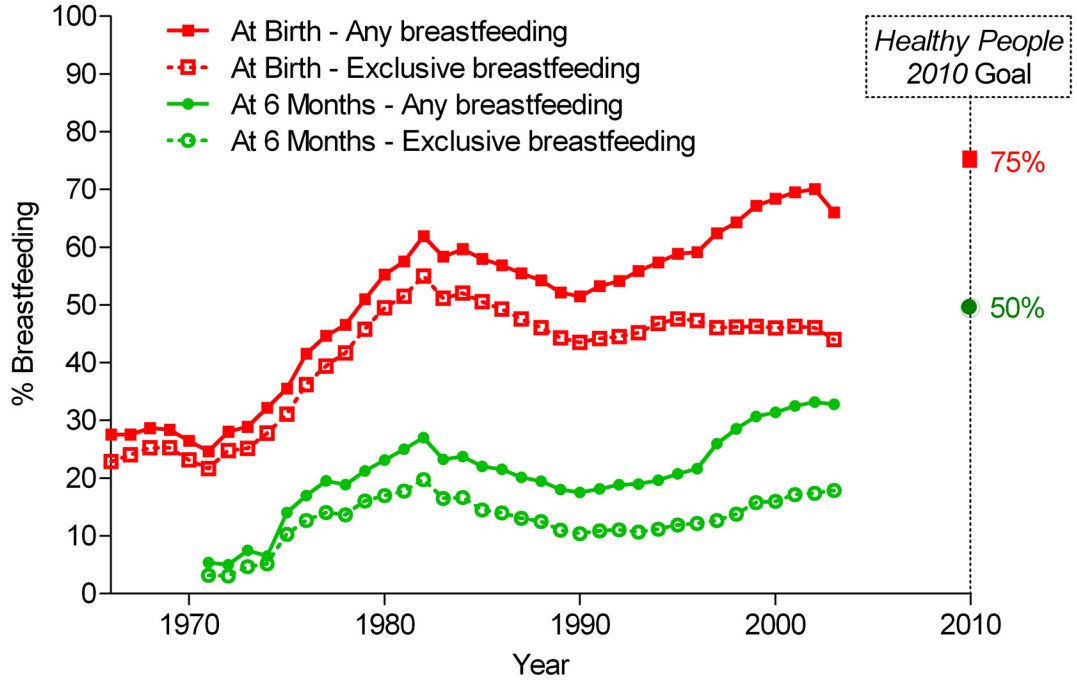

Complicating matters is the lack of data available to lactating mothers and health care professionals when making decisions involving medication initiation or continuation postpartum. A 2003 FDA analysis of the prescribing information of the 1625 drugs in the Physicians Desk Reference (PDR) underscores the problem (Figure 1-2) [43]. Only 34% of drugs had any information on their potential transfer into human milk and when the search was expanded to include animal data, over half still had no information to offer. The problem is also not confined to older drugs, as less than 10% of the new molecular entities approved between 1995 and 2002 gave any information on human milk transfer in their regulatory filings [43]. The FDA has since released a draft guidance for the industry to try to fill this gap in knowledge; requiring clinical studies in lactating women to be performed whenever (1) a new drug is expected to be used in women of reproductive age, (2) after approval, use in lactating women is evident, (3) a new indication is being sought for an approved drug and there is evidence of use or anticipated use of the drug by lactating women, or (4) marketed medications that are commonly used by women of reproductive age [44]. The comment period has passed, but it is unclear at this time when the final guidance will be released and what official recommendations will be made to the pharmaceutical industry.

Figure 1-2: 2003 FDA Analysis of prescription drug labeling for information regarding drug transfer into milk.

Prescribing information either provided no statement, a statement indicating drug transfer into breast milk is unknown, a specific recommendation to not use the drug during lactation, contained human data or provided information from animal studies, but not human data. Panel A includes labeling information from all drugs in the PDR at the time of the study. Panel B excerpts data from new molecular entities approved from 1995-2002. Created from data in reference [43].

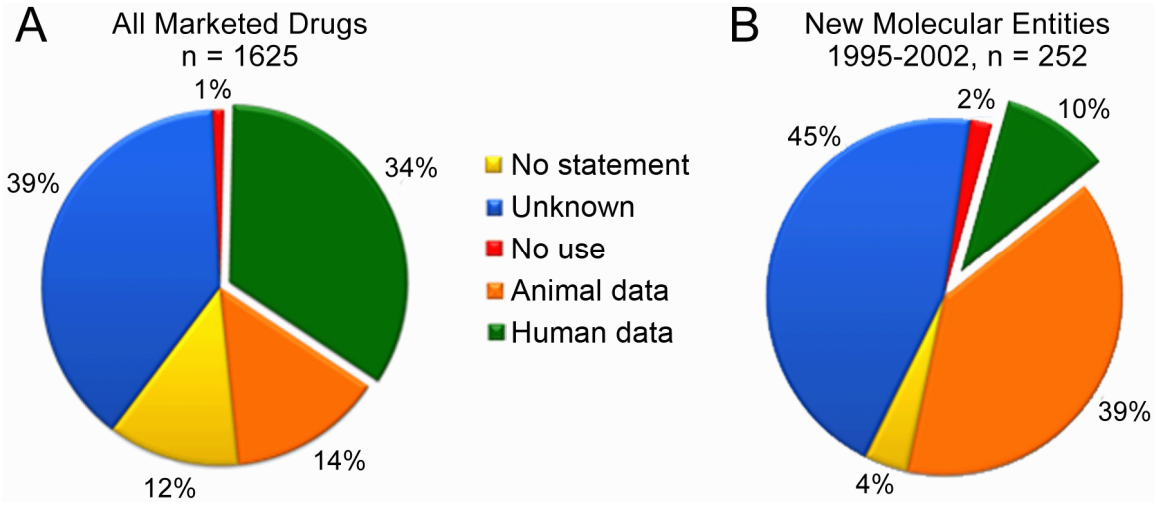

The overwhelming documented benefits of breastfeeding and paucity of data in the literature regarding milk transfer puts patients and health care professions in the precarious position of weighing maternal benefit and potential risks to the suckling infant. However, as stated in the draft guidance "the applicability and predictability of nonclinical models (e.g., predictions of drug transfer or milk/plasma (M/P) ratios using physicochemical properties of the drug) are still under consideration, but these models [currently] do not help in deciding whether to conduct a study in lactating women." A better understanding of the mechanisms of drug transfer into breast milk and further investigations of in vitro and mathematical models is clearly needed to provide the desperately needed data to support evidenced-based therapeutic decisions.

B. Mechanisms of drug transfer into breast milk

Comprehensive reviews of mammary gland anatomy and physiology are presented by Lawrence and Lawrence [45], Hennighausen and Robinson [46], Hale [47], and Neville et al. [48]. The mammary gland is comprised of epithelium and stroma (mammary fat pad). The epithelium forms the milk production functional unit, grape-like clusters called alveoli, and the ducts that connect them to the nipple (Figure 1-3). Two types of epithelial cells are present. The majority are luminal secretory cells which produce breast milk and secrete it into a central lumen. These cells form the barrier between the breast milk and the maternal circulation. Basal myoepithelial cells create the contractile framework surrounding the luminal secretory cells and are responsible for milk ejection following physiological stimuli. The stroma is connective tissue containing adipocytes, capillaries, lymphatics, sensory neurons, and fibroblasts, which the ductal alveolar systems grow into during mammogenesis. During pregnancy, the size and number of alveoli grows significantly and develops under hormonal stimulation (estrogen, progesterone, placental lactogen, prolactin, and oxytocin), but lactogenesis does not begin until after delivery when estrogen and progesterone levels rapidly decline. Initially, colostrum, a fluid rich in maternal lymphocytes, macrophages, lactoferrin, immunoglobulins, and other proteins is secreted. At this point, in the first few days postpartum, intercellular gaps exist between luminal epithelial cells allowing the relatively easy passage of large substances via the paracellular route. Milk secretion begins around day two as alveolar cells progressively enlargen and intercellular gaps close. By day five postpartum, mature milk secretion begins and transcellular diffusion

becomes the major path of drug transfer from maternal circulation into breast milk as tight junctions between cells exist.

Figure 1-3: Mammary gland anatomy

Panel A. Cross section of breast. Image obtained from NIH website (mammary.nih.gov). Panel B. Diagram of alveolar anatomy modified with permission from reference [45].

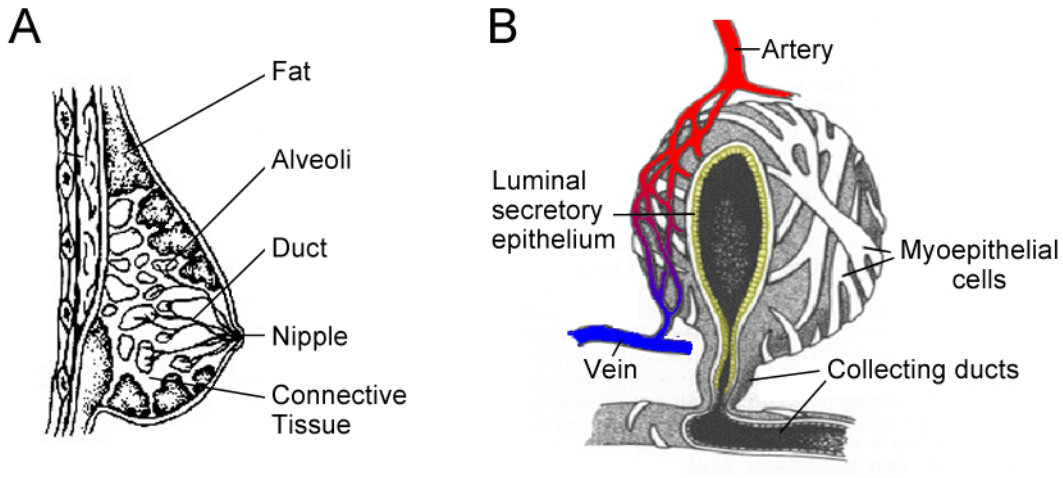

The majority of xenobiotics enter breast milk by passive or facilitated diffusion following a concentration gradient, although active transport processes have also been observed [49-53]. The overall rate and extent of accumulation in the milk compartment and subsequent exposure is controlled by maternal factors, infant factors, and drug physiochemical properties. Maternal factors include the stage of lactation and maternal dosing and pharmacokinetics. The stage of lactation is important for the existence of tight junctions (discussed above) and has implications for milk composition. Protein content declines and fat content increases with the transition of colostrum to mature milk [54,55]. Changes in breast milk pH are more minor with the colostrum, milk three months post-partum, and milk ten months post-partum averaging 7.45, 7.0-7.1, and 7.4 respectively [56]. Maternal drug pharmacokinetics is perhaps the most important variable affecting rate and extent of accumulation as the maternal plasma concentration creates the driving force in equilibrium processes. Higher clearance, shorter half-life, less bioavailable, higher protein bound drugs would produce lower maternal free concentrations. Lower dosing rates or nonparenteral administration routes would be expected to yield lower exposure risks [47]. Infant factors affecting exposure include suckling pattern (volume of milk consumed, frequency, and timing relative to maternal plasma concentrations) and drug oral bioavailability in the neonate. For short half-life drugs, although it is difficult to achieve in practice, altering the drug administration or

suckling pattern to dosing after feeding would be expected to decrease exposure [57]. The final factor influencing overall rate and extent of xenobiotic accumulation in breast milk are its physiochemical properties; molecular weight, degree of ionization (pKa), water and lipid solubility, and protein binding. Small molecular weight molecules such as urea and ethanol pass transcellularly by passive diffusion, whereas larger molecules in excess of 1000 daltons cannot pass capillary membranes and pass into the milk only in trace amounts [47,58,59]. Degree of ionization is also important as ionized or electrically charged xenobiotics cannot diffuse through biological membranes. The pKa determines ionization at a given pH and as milk pH averages 7.2, less than that of plasma, a phenomenon called "ion trapping" can occur as non-ionized weakly basic drugs become ionized in the more acidic conditions of the breast milk [60,61]. Lipophilicity also plays a role as water soluble compounds have difficulty crossing the biological membranes and nonpolar compounds can traverse the lipid bilayer easily. The relatively high lipid content of breast milk (3-5%) relative to plasma further favors the concentration of lipophilic drugs in milk fat [59]. Protein binding in either the maternal serum or breast milk would shift the balance of equilibrium processes as only free drug is available to pass through the mammary epithelial cell. Breast milk protein composition is lower than serum at approximately 0.9 g/dL and consists mostly of caseins and whey rather than albumin, as found in the serum [62]. Further, α-lactalbumin (the major whey protein found in milk) has a lower drug binding capacity relative to albumin, suggesting that drugs with greater protein binding are more likely to remain in the serum [63,64]. A detailed discussion of role of active processes is presented in Sections D and E.

C. Risk Assessment: The milk to serum ratio (M/S)

There are many factors contributing to the rate and extent of xenobiotic accumulation in breast milk making it difficult to estimate infant exposure risk. Pharmacokinetically, concentrations achieved in the infant serum ($C_{infant,serum}$) are determined by infant systemic clearance (Cl_{infant}), infant bioavailability (F_{infant}) and by the dose received through breastfeeding as described in Eq. 1-1:

$$C_{infant,\ serum} = \frac{F_{infant} \cdot Dose}{Cl_{infant}} \qquad \text{Eq. 1-1}$$

Neonatal bioavailability and systemic clearance are not well-categorized for most drugs as conducting pharmacokinetic studies in this population is often difficult due to ethical concerns. Exposure risk is therefore often expressed in terms of the infant dosing rate.

Dose is the product of the milk consumption rate (volume per time, V_{milk}/τ), maternal serum concentrations ($C_{maternal}$), and the proportion of the maternal serum concentration in the breast milk (milk to serum ratio, M/S) as shown in Eq. 1-2:

$$\text{Dose} = C_{\text{maternal, serum}} \left(\frac{M}{S}\right)\left(\frac{V_{milk}}{\tau}\right) \qquad \text{Eq. 1-2}$$

As maternal serum concentrations can be measured and milk consumption rate estimated, M/S ratio is the variable that is focused upon and used to determine the extent to which a xenobiotic is transferred into milk. Quantified appropriately, the M/S is either determined from the relative steady state concentrations or by the time-integrated drug concentrations (area under the concentration-time curve, AUC) as shown in Eq. 1-3 [58,60,61].

$$\frac{M}{S} = \left(\frac{C_{ss,\ milk}}{C_{ss,\ maternal,\ serum}}\right) = \left(\frac{AUC_{milk}}{AUC_{maternal,\ serum}}\right) \qquad \text{Eq. 1-3}$$

Unfortunately, in the literature it is often calculated from single paired milk and serum measurements. This milk to serum point ratio (M/S_{point}) can be inaccurate as it assumes milk and serum concentrations parallel one another, which is not always the case as concentrations in milk may peak later than observed in plasma [65]. This time lag would cause an underestimation of the time-averaged M/S ratio if determined during the maternal peak concentration or overestimate it if calculated when the peak in the breast milk occurs [58]. To emphasize this possibility and appropriate methologies for studying drugs in human milk, Begg et al, reviewed drug situations (sumatriptan, sertraline, paroxetine and bupriopion) when a 2-3 fold variability in the calculated M/S_{point} of each drug (dependent upon time of measurement) was observed [60]. Beyond suboptimal study designs, other factors that limit the amount and quality of published data is the difficulty in recruiting breastfeeding subjects and the overall lack of interest in conducting these experiments [66].

Several methods to predict the M/S ratio in vitro have been published in efforts to circumvent the difficulties associated with conducting clinical studies [50,67,68]. Fleishaker et al. developed a passive diffusion model that incorporates ionization, protein-binding in the serum and milk, and lipid partitioning into a M/S prediction as shown in Eq. 1-4:

$$\frac{M}{S}_{predicted} = \frac{\left(f_s^{un}\right)(f_s)(W)}{\left(f_m^{un}\right)(f_m)(Sk)} \qquad \text{Eq. 1-4}$$

where f_s^{un} and f_m^{un} are the calculated fraction of the drug unionized in the serum and milk, respectively; f_s and f_m are the experimentally-determined fractions protein bound in the serum and milk, respectively; and W and Sk are the experimentally-determined fat partitioning into whole and skim milk, respectively [68]. This passive diffusion model relies upon the assumption that only unbound, unionized drugs can cross the mammary epithelial barrier and performs well for several drugs tested in rabbits, rats, and humans. Figure 1-4 illustrates that for ten drugs (propranolol, phenobarbital, phenytoin, diazepam, acetaminophen, antipyrine, salicylic acid, caffeine, paraxanthine and cimetidine) studied in rabbits, the M/S observed in vivo was similar to that predicted by the model [69-72]. The majority of drugs studied in rats and human also fell upon the line of unity. The model, however, is inadequate to explain the accumulation of some drugs such as nitrofurantoin and cimetidine in the rat and human where active processes seem to be involved [51,73-77].

Figure 1-4: M/S predicted and observed in rabbit, rat, and human.

The majority of drugs fall on the line of identity between M/S predicted and observed in vivo with some exceptions (NF, nitrofurantoin; CM, cimetidine; RN, ranitidine; ACV, acyclovir; CP, ciprofloxacin).

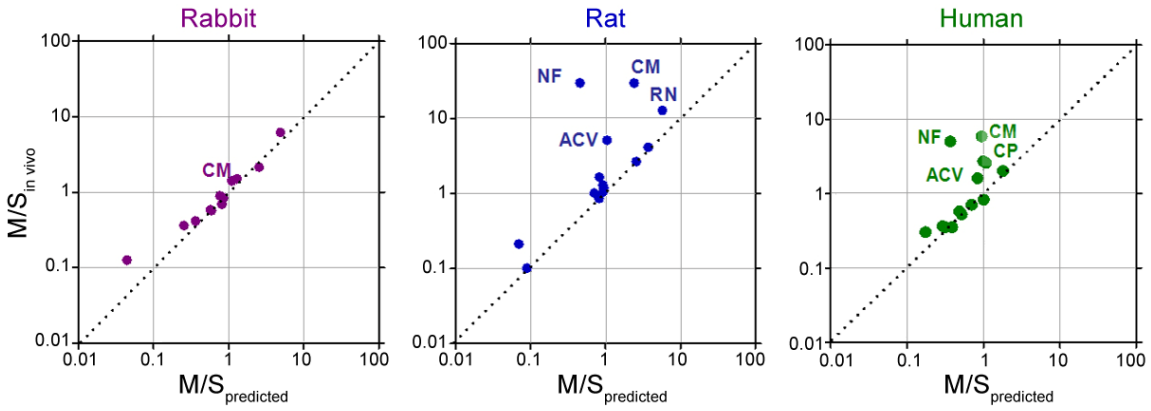

D. Evidence of drug accumulation by active transport

Although the transfer of most drugs into milk can be explained by passive diffusion, there are several drugs where the measured M/S ratio exceeds that of the value predicted by passive diffusion, suggesting the contribution of active processes. The involvement of active transport phenomena in xenobiotic milk accumulation has been observed in multiple species including humans, rats, mice, goats and cows and

has been proven through clinical and animal studies, knock-out and inhibition experiments, and in cell culture based transfection systems.

The most striking human data comes from a clinical study conducted by Gerk et al. in which four healthy lactating women received a single oral 100 mg dose of nitrofurantoin [51]. The $M/S_{in\ vivo}$ determined by a ratio of the nitrofurantoin AUC in the milk and serum was 6.21 ± 2.71, over 22 times that predicted by passive diffusion (0.28 ± 0.05). Oo et al. published similar observations in twelve healthy lactating women who were administered 100 mg, 600 mg, or 1200 mg cimetidine in a randomized crossover study design [77]. The $M/S_{in\ vivo}$ was similar at all dosing levels and was greater than 5.5 times that predicted (5.77 ± 1.24 vs. 1.05 ± 0.08, respectively). Studies suggest that active processes may exist for other drugs as well; ranitidine, acyclovir, and zidovudine all achieve high concentrations in human milk [78-80]. In vitro experiments with MCF12A cells, a human cell line derived from non-cancerous mammary gland epithelia, also showed the presence of a carrier-mediated uptake process. Kwok et al. demonstrated that carnitine and tetraethylammonium uptake in this cell line could be inhibited by other cationic compounds such as cimetidine, verapamil, or carbamazepime [81]. These in vivo and in vitro human data definitively demonstrate the presence of active transport systems for drug transfer into human milk.

Rat studies with nitrofurantoin and cimetidine yield similar results [73,74,82-85]. Oo et al. showed that an infusion of 0.5 mg/h nitrofurantoin resulted in a $M/S_{in\ vivo}$ that was nearly 100 times greater than the diffusion prediction (31.1 ± 4.0 vs. 0.3 ± 0.1, respectively) [85]. Kari et al. replicated this finding with a single orally administered 50 mg/kg dose of nitrofurantoin ($M/P_{in\ vivo}$ of 23.1; nearly 75-fold the $M/S_{predicted}$ of 0.31), but interestingly only observed a 2.5 fold difference ($M/P_{in\ vivo}$ 3.49 vs. $M/S_{predicted}$ 1.4) with the nitrofurantoin congener furazolidone [84]. Further, in the same study, another nitrofurantoin congener furaltadone exhibited a $M/P_{in\ vivo}$ equivalent to that predicted by passive diffusion. Cimetidine further provided specific evidence of an active transport process as the $M/S_{in\ vivo}$ was saturable, falling from 31.9 ± 9.0 to 26.5 ± 9.5 to 24.6 ± 6.4 with increasing infusion rate. Steady-state $M/S_{in\ vivo}$ values were also 6-fold higher than the $M/S_{predicted}$ of 4.19 [73]. In the same rat study, although the $M/S_{in\ vivo}$ achieved by a 0.4 mg/h cimetidine infusion was relatively unchanged by coadministration of ranitidine (30 mg/h), the converse did provide evidence for the inhibition of an active transport process. A 30 mg/h cimetidine infusion significantly decreased $M/S_{in\ vivo}$ resulting from a 0.4 mg/h ranitidine infusion from 16.1 ± 2.0 to 10.5 ± 2.0 [74].

Knock-out mice and murine-derived cells have primarily been used in efforts to identify the specific transport pathway or pathways responsible for the aforementioned observations. The murine CIT3 cell culture model developed by Dr. Margaret Neville has been used as an in vitro model of lactation that is suitable for flux experiments [86-88]. CIT3 cells are a subline of the Comma 1D normal mouse mammary epithelial cell that is a coculture of mammary epithelial cells and fibroblasts derived from pregnant BALB/c mouse mammary glands [89,90]. When grown on polycarbonate membranes and stimulated with lactogenic hormones (prolactin, hydrocortisone, and insulin), they form tight junctions with a high transepithelial electrical resistance (TEER) and synthesize the milk protein beta-casein. Toddywalla et al. first demonstrated the applicability of this in vitro cell culture system in transwell experiments with the same drug shown to accumulate in vivo, nitrofurantoin [86]. The radiolabelled nitrofurantoin flux rate was 50% higher in the basolateral to apical than in the apical to basolateral direction and was equalized (inhibited) in the presence of 500 μM unlabelled nitrofurantoin [86]. Gerk et al. further showed that the CIT3 nitrofurantoin active transport system was sodium-dependent, inhibited by dipyridamole, adenosine, and guanine, and was likely expressed on the basolateral surface, but these investigators were not able to identify the specific transporter [87,88]. It was not until Alfred Schinkel's lab investigated the role of breast cancer resistance protein, Abcg2, in the transport of xenobiotics into breast milk that an important molecular mechanism was elucidated. Using an Abcg2 knock-out mouse model his lab elegantly showed that the oral administration of 10 mg/kg nitrofurantoin produced a milk vs. plasma AUC ratio 76-fold higher in wild-type animals than was seen in the Abcg2 knock-outs (45.7 ± 16.2 vs. 0.6 ± 0.1) [53]. These investigators further extended their work to show that Abcg2 was responsible for the active secretion of cimetidine, topotecan, riboflavin, acyclovir, ciprofloxacin, 2-amino-1-methyl-6-phenylimidazo[4,5-b]pyridine (PhIP), 2-amino-3-methylimidazo[4,5-f]quinoline (IQ), and 3-amino-1,4-dimethyl-5H-pyrido[4,3-b]indole (Trp-P-1) into mouse milk [53,91-93]. Their observations are summarized in Table 1-1 and clearly demonstrate the important role that Abcg2 plays in drug transfer into breast milk.

Table 1-1: Milk to plasma ratios for certain drugs in wild-type and Abcg2 (Bcrp1-/-) knock-out mice.

	Wild-type	Bcrp1-/-	Ratio	Reference
Nitrofurantoin	45.7	0.6	76.2	[53]
Riboflavin	25.0	0.4	67.6	[91]
PhIP	12.8	0.5	28.1	[92]
Topotecan	6.7	0.7	10.1	[92]
Cimetidine	13.7	2.3	6.0	[92]
Aflatoxin B1	0.7	0.2	3.8	[92]
IQ	0.9	0.3	3.4	[92]
Acylcovir	1.3	0.4	3.3	[92]
Trp-P-1	1.1	0.4	2.6	[92]
Ciprofloxacin	3.1	1.6	1.9	[93]

Earlier investigations with other drugs in goats and cows have also suggested the presence of active transport systems. Rasmussen et al. documented ultrafiltrate M/S values of n-acetylated p-aminohippurate and sulfanilamide that were 10-fold higher than the value predicted by passive diffusion alone [94,95]. Schadewinkel-Scherkl et al. showed that benzylpenicillin accumulated in goat breast milk via an active process and this process was significantly decreased when probenecid was given concominantly [96]. Estrogen sulfate is also concentrated in goat milk with a milk to plasma ratio of 7.4 [97]. Finally, the coadministration of a known Abcg2 substrate albendazole, produced a decreased enrofloxacin M/S ratio in lactating goats providing evidence that enrofloxacin enters breast milk by an active process [98].

Taken together, these data provide strong functional evidence for the involvement of active transport processes in the transfer of xenobiotics into breast milk in humans and several other species. Pathways seem to exist for both organic cations (eg. cimetidine, ranitidine) and anionic compounds (eg. nitrofurantoin, benzylpenicillin). The significant role of one transporter, Abcg2, has been documented thus far; Section E will explore the molecular evidence for this transporter and the many others that may be involved in drug transfer into breast milk during lactation.

E. Drug transporters in lactating mammary epithelia

Identification of the xenobiotic transporters in lactating luminal mammary epithelial cells (LMECs) is necessary to improve M/S predictive models and to determine the drugs for which an active transport mechanism governs transfer into breast milk.

During lactation, the mammary gland becomes a specialized secretory tissue responsible for delivering essential nutrients to the infant. Some of these substances have physiochemical properties that limit their ability to efficiently cross the LMEC to enter the breast milk or accumulate at concentrations that could not be achieved by passive diffusion alone. As in other secretory tissues, such as the liver and the kidney, transporter systems have presumably evolved to meet these demands. There currently exist 420 genes in 53 transporter gene families that have been identified in the human genome [99]. These membrane proteins may be expressed in the basolateral (serum facing) or apical (milk facing) cell membranes and are driven by ATP, electrochemical potentials, or the cotransport of another compound. Transporters may have an unknown function or be involved in the transport of nutrients such as glucose, ions, vitamins, fatty acids, or amino acids and have no documented role in xenobiotic transport. A number of transporters such as SLC5A1 (SGLT1; a sodium/glucose transporter) [100], SLC12A2 (NKCC1, a sodium/potassium/chloride transporter) [101], and SLC5A5 (sodium iodide symporter) [102], have been identified in mammary tissue of various species, but few studies have focused on transporters known to be important for drug transfer. It is difficult to perform these experiments in humans to obtain an accurate representation of expression in LMECs specifically; however, screening studies as well as investigations focused on single transporters or transporter families have been published. The difficulties in conducting these experiments and the associated implications for interpretation are reviewed along with examples from the literature in the following sections. Molecular evidence for the presence of members of the solute carrier and ATP-binding cassette transporter superfamilies is also presented.

1. Experimental considerations

Several experimental techniques have been used to identify transporters in the mammary gland that may be relevant to drug transport into milk. Most commonly, whole tissue homogenates are prepared for RNA or protein expression level quantification by microarray analysis, northern blotting, PCR, or western blotting. This approach can complicate interpretation as the quantified level is a composite of the relevant expression in the luminal mammary epithelial cells that secrete milk and form the functional barrier and the less important supporting cells such as myoepithelial cells, fibroblasts, lymphatics, and stroma. Some investigators have solved this problem in animal studies by localizing the tissue expression by immunohistochemistry or confocal microscopy. In

humans, ethical issues make it difficult to obtain lactating mammary tissue from healthy human subjects. Gross tissue samples from patients undergoing reduction mammoplasty procedures can be analyzed, but these would be of undifferentiated cells not stimulated by lactogenic hormones; they would not necessarily be representative of the expression levels during lactation. Biopsies of apparently normal tissue adjacent to cancerous tissue is potentially available from lactating breast cancer patients, but would also be of questionable value as expression of transporters in these cells may be affected by growth-factor enriched microenvironments [103].

A recent study by Bleasby et al. illustrates the difficulties in evaluating what little human published data exists [104]. In a comprehensive microarray study designed to be a resource for investigations into drug disposition, the expression profile of 50 xenobiotic transporter genes was evaluated in 40 tissues from humans and compared to the corresponding expression levels in monkeys, dogs, rats, and mice. The RNA sources cited were the following: human, purchased from an external vendor, pooled from multiple subjects of both sexes; monkey, two male and two female matched for age; dogs, five male and five non-oestrus females; rats, sixteen male and sixteen female, 75 days old; mice, males and females, females were nulliparous and non-pregnant. No further information is provided and thus, all tissues are presumed to be whole tissue homogenates and nonlactating. Although species comparisons were made across 22 tissues, the mammary gland was not included in this part of the analysis. In contrast, in a screening study focused on LMECs, Alcorn et al. circumvented both the obstacle of finding a source of normal human lactating epithelial cells and that of measuring the transporter expression level in LMECs rather than in a whole tissue homogenate [49]. These investigators used immunomagnetic separation to isolate enough LMECs from the heterogeneous cell populations in breast milk to determine the RNA expression level of 30 transporter genes by quantitative PCR (qPCR). Nonlactating luminal mammary epithelial cells (MECs) were isolated from reduction mammoplasty tissue specimens to serve as a nonlactating control. The isolation procedure produced pure populations of luminal mammary epithelial cells, but unfortunately required the pooling of the six breast milk samples and four reduction mammoplasty specimens to assure adequate RNA for the single (n=1 in each group) comparison by qPCR and was not able to examine the expression level of all transporter genes of interest (eg. did not study ABCG2).

2. Solute carrier transporters

There are currently 46 known transporter gene families within the solute carrier (SLC) superfamily [99]. Not all have been fully characterized. However, several have individual members with a known role in xenobiotic transport and have been identified in mammary tissue.

The solute carrier transporter family 22 (SLC22) includes organic anion transporters (OCTs), zwitterion/cation transporters (OCTNs), and organic anion transporters (OATs) and its members have been associated with xenobiotic transport in other tissues. SLC22A1-3 (OCTs) are uniporters that mediate facilitated diffusion and are electrogenic, sodium-independent, and reversible in regards to direction [105]. SLC22A4 (OCTN1) is a proton/organic cation antiporter (SLC22A4) [106,107], whereas SLC22A5 (OCTN2) may function as a sodium-independent organic cation transporter or a sodium/carnitine cotransporter [108,109]. SLC22A6-8 (OAT1-3) are believed to be organic anion exchangers [105]. Several members of the SLC22 family have been detected in the mammary gland. Gerk et al. identified RNA transcripts for Slc22a1 (Oct1) and Slc22a3 (Oct3), but not Slc22a2 (Oct2) in lactating rat mammary tissue [110]. Kwok et al. replicated this finding in the human mammary gland derived MCF12A cell line and nonlactating human tissue and further detected SLC22A4 and SLC22A5 protein expression by western blotting [81]. SLC22A5 expression was specifically localized to the ductal-lobular-alveolar structures by immunohistochemistry. Alcorn et al. showed a similar finding in LMECs, documenting the presence SLC22A1, SLC22A3, SLC22A4, and SLC22A5 RNA, but not transcripts for SLC22A2 [49]. Interestingly, the RNA expression level of SLC22A1 was markedly increased in LMECs relative to the MEC comparators. No molecular evidence of any of the organic anion transporters in this family (SLC22A6-8) was found in rat mammary glands or LMECs [49,110].

The solute carrier organic anion transporter family (SLCO) is another major gene family that can transport organic anions and xenobiotics. The members of SLCO family, recently reclassified from the SLC21 designation, encode for the organic anion transporting polypeptides (OATPs) that seem to exchange a wide range of amphipathic compounds by a bidirectional, sodium-independent, pH-dependent, electroneutral mechanism [111]. There are currently six human subfamilies (SCLO1-6), containing 11 genes (SLCO1A2, SLCO1B1, SLCO1B3, SLCO1C1, SLCO2A1, SCLO2B1, SLCO3A1, SLCO4A1, SLCO4C1, SLCO5A1, SLCO6A1) with gene specific patterns of tissue

distribution and substrate specificities [99,103]. Pizzagalli et al. reported that SLCO2B1 (OATP-B) appeared to be the most abundantly expressed organic anion polypeptide expressed in the mammary gland, but also detected SLCO3A1 (OATP-D) and SLCO4A1 (OATP-E) in nonlactating human mammary gland total RNA by PCR and northern blotting [112]. When immunohistochemistry of the mammary tissue was performed, however, OATP-B was localized to the supporting myoepithelial cells rather than the luminal MECs that would eventually form the barrier between serum and milk. Transcripts for SLCO1A2 (OATP-A), SLCO1B1 (OATP-C), SLCO1B3 (OATP-8), and SLCO2A1 (PGT) had very low expression or were not detected in the whole tissue total RNA. In the study by Alcorn et al, SLCO1A2, SLCO2B1, SLCO3A1, and SLCO4A1 were detected in LMECs and MECs [49]. Relative to MEC pooled sample, the expression of SLCO1A2 and SLCO2B1 was higher in the LMEC pooled sample, whereas SLCO3A1 and SLCO4A1 were lower. The expression of SLCO3A1 was higher in both luminal mammary epithelial cell samples relative to the liver, kidney, and placenta comparators.

Amino acid or peptide transporters that are expressed in mammary tissue and that have been shown capable of transporting xenobiotics include members of the solute carrier transporter families 6 and 15. SLC6A14 (ATB(0+)) is sodium-dependent cotransporter with a broad affinity for neutral and cationic amino acids [113]. SLC15A1 (PEPT1) and SLC15A2 (PEPT2) are electrogenic proton/oligopeptide cotransporters [114]. SLC15A1 appears to be low-affinity/high-capacity and SLC15A2 the high-affinity/low-capacity variant, although both proteins essentially transport the same substrates into the cell. Sloan and Mager discovered SLC6A14 and documented that it was expressed in the mammary gland as well as other human tissues [115]. Kwok et al. further confirmed SLC6A14 RNA expression in nonlactating human mammary tissue and MCF12A cells by PCR [81]. This transporter was not one of the genes studied in the LMEC transporter gene expression study by Alcorn et al, however, both SLC15A1 and SLC15A2 were studied and were detected [49]. SLC15A1 expression was low in LMEC relative to comparator tissues, but SLC15A2 was higher. Groneberg, et al. focused their work on SLC15A2 in the mammary gland and documented RNA expression in both the rat mammary gland and in LMECs within expressed human milk [116]. Pept2 protein was further localized specifically to the ductal epithelium in the rat.

Finally, the nucleoside and nucleobase transporters are members of the solute carrier superfamily and have been identified in mammary tissue of various species.

Nucleoside transporters are classified into solute carrier transporter families 28 and 29 and include the three concentrative nucleoside transporters, SLC28A1-3 (CNT1-3) and the four equilibrative nucleoside transporters, SLC29A1-4 (ENT1-4). Nucleobase transporters include the two ascorbic acid transporting solute carrier transporter family 23 members, SLC23A1-2 (SVCT1-2). SLC28A1-3 are sodium-dependent, nucleoside cotransporters that have differing substrate specificities: SLC28A1 is pyrimidine-nucleoside preferring, SLC28A2 is purine-nucleoside preferring, and SLC28A3 transports both pyrimidine and purine nucleosides [117]. SLC29A1-4 are believed to be bidirectional transport systems that mediate facilitated diffusion [118]. SLC23A1-2 are sodium-dependent, high-affinity L-ascorbic acid cotransporters [119]. In the original paper describing SLC28A3, Ritzel et al. demonstrated RNA expression of this nucleoside transporter in human mammary gland total RNA [111]. Alcorn et al, reported that this transporter was also expressed in LMEC cells, as was SLC28A1, SLC29A1, SLC29A3, and SLC23A1 [49]. All but SLC29A1 were expressed at a markedly higher level in the single pooled LMEC sample relative to the MEC pooled sample. SLC28A3 expression level was also much higher than the liver, kidney, and placenta total RNA comparators. SLC28A2, SLC29A2, and SLC23A2 were not detected in LMECs whereas the SLC29A4 expression was not studied.

3. ATP-binding cassette transporters

The ATP-binding cassette (ABC) transporter superfamily consists of seven subfamilies; three (ABCB, ABCC, ABCG) contain members with roles in xenobiotic transport. ABC transporters use the energy derived from ATP hydrolysis to efflux a wide variety of substrates including sugars, amino acids, metal ions, peptides, proteins, and a large number of hydrophobic compounds out of the cell [120]. ABCB1 (MDR) encodes for P-glycoprotein and is perhaps most studied. It is found in the epithelia of many tissues including the intestine, liver, kidney, blood-brain barrier, testis, placenta, and lung, transporting mostly positively charged, hydrophobic compounds [121]. The ABCC family currently contains 13 known genes [99]. ABCC 1-6 (MRP1-6), ABCC10 (MRP7), ABCC11 (MRP8), and ABCC12 (MRP9) are transporters whereas the remainder are ion channels (CFTR/ABCC7) or sulfonylurea receptors ABCC8 (SUR1) and ABCC9 (SUR2) [121]. The MRPs transport mainly amphipathic anionic compounds and conjugates [103]. There exist 5 known members of the ABCG family, with breast cancer resistance protein, ABCG2 (BCRP), being the most relevant for xenobiotic transport. ABCG2

transports electroneutral amphipathic drugs and is expressed in several secretory tissues [121].

Several of the ABC transporters have been identified in mammary tissue. P-glycoprotein was identified in the normal human mammary gland by immunohistochemistry over 15 years ago [122,123]. ABCB1 RNA and its protein product, P-glycoprotein, were also detectable in human MCF12A cells but functional activity was not observed [103]. Interestingly, Jonker et al. showed a decrease in P-glycoprotein expression level in murine mammary gland whole tissue homogenates at 2-weeks lactating relative to virgin animals [124]. Alcorn et al. also documented that lactation appeared to substantially down-regulate ABCB1 in LMEC cells specifically, showing a 50-fold lower level in the LMEC vs. MEC sample [49]. This group also detected ABCC1, ABCC2, and ABCC5 in the LMEC and MEC samples. ABCC1 was lower and ABCC5 was higher in the LMEC sample relative to the MEC sample. ABCC3 and ABCC4 were not detected. The remainder of the transporter encoding genes of the ABCC subfamily was not evaluated in this study. Transcripts for ABCC8 and ABCC9 were however, detected by Bera et al. in normal mammary gland tissue by PCR [125,126]. Several recent studies by the research group of Alfred Schinkel have demonstrated that ABCG2 plays a significant role in xenobiotic accumulation in breast milk [91,124,127-129]. ABCG2 is expressed in cow, murine, and human lactating mammary tissues and appears to be developmentally regulated in mice, achieving the highest protein expression level during lactation [124]. ABCG2 was immunohistochemically localized to a few cells in the virgin mammary gland of cows and mice and to the alveolar epithelial cells in the lactating tissue [92,124,130]. As murine Abcg2 is associated with the stem cell phenotype, it is possible that the cells observed in the virgin tissues are the mammary epithelial stem cells that undergo proliferation during lactogenic hormone stimulation [130]. ABCG2 was not studied in the LMEC vs. MEC study by Alcorn et al., so it is currently not known if the increased expression level in whole mammary epithelial glands during lactation is a result of increased expression within MECs/LMECs or simply due to an increased proportion of these cells within the entire mammary gland following differentiation to the lactation stage. The role of ABCG2 in xenobiotic transport is discussed in greater detail in the next section.

F. ABCG2

The considerable recent interest in the structure and function of Breast Cancer Resistance Protein has resulted in the publication of several good review papers [92,131-134]. ABCG2 was first cloned by Doyle et al. from a multidrug resistant breast cancer cell line (MCF-7/AdrVp) and given the name Breast Cancer Resistance Protein based on this derivation, despite the fact it is not highly expressed in breast cancer [135]. The gene is comprised of 16 exons and encodes for a 655 amino acid protein that contains a single N-terminal ATP binding cassette followed by six pututative transmembrane spanning regions [92]. The protein is much smaller than P-glycoprotein, only 70 kDA, but is termed a "half-transporter" as it is believed to function as a homodimer, although higher form oligomers have been reported [136]. Nonsynonymous single nucleotide polymorphisms have been reported; notably, the C421A (Q41K) is prevalent in the Japanese population (~35%), resulting in reduced protein expression levels and potential clinical significance [137-139]. The promoter is predicted to be TATAless and studies have begun to functionally evaluate some of the regulatory elements. Recent evidence suggests that hypoxia [140], aryl hydrocarbon receptor (AhR) agonists [141], and peroxisome proliferator activator receptor alpha (PPARα) agonists [142] increase the expression of ABCG2. Progesterone upregulated ABCG2 expression, but controversy exists regarding the regulatory effects of estradiol [133,143,144].

RNA and protein expression of ABCG2 are greatest in the placenta, although high expression is also found in the liver, intestine, and breast [145]. It is also expressed in stem cells, endothelial cells of the blood-brain barrier, lung, ovary and testis [131]. Species differences are evident as Abcg2 is highly expressed in the murine kidney (RNA not detected in human kidney samples) and only moderately expressed in the murine placenta [132]. Tissue-specific sex differences also exist with Bcrp1 expression and function in the male murine liver exceeding that of the female [146]. Localization is apical and the protein functions to efflux its substrates from the cell.

ABCG2 is capable of transporting a diverse array of substrates; however, the spectrum is not as structurally diverse as for P-glycoprotein or MRP1 [147]. A recent listing compiled by Krishnamurthy and Scheutz includes drug classes such as anticancer drugs (eg. anthracyclines, camptothecans, methotrexate, tyrosine kinase inhibitors, but not vinca alkaloids), HIV nucleoside reverse transcriptase inhibitors, natural compounds

(eg. flavonoids, dietary carcinogens such as PhIP, porphyrins), and fluorescent dyes (eg. Hoechst 33342, Rhodamine 123) [132]. More recent studies have added nitrofurantoin [53], cimetidine [127], dipyridamole [148], several HMG-CoA reductase inhibitors [149,150], fluoroquinolones [93,151], and benzimidazoles such as the antithemintics and pantoprazole [152,153] to the rapidly growing list. ABCG2 appears to have a preference for sulfate conjugates of steroids and xenobiotics rather than glucuronide conjugates and is not dependent on intracellular glutathione to transport drugs [147]. Potent inhibitors such as fumitremorgan C (FTC) and its derivative Ko143, GF120918, novobiocin, and imatinib have been discovered and are used experimentally. GF120918 is a mixed inhibitor, with a potent activity versus P-glycoprotein as well as ABCG2. Ko143, in contrast, is highly specific for ABCG2 with almost 300-fold more inhibitory potency vs. ABCG2 compared to P-glycoprotein [133]. In vitro screening systems have identified many other drugs with the capability to inhibit ABCG2-mediated transport [154,155].

Conclusive evidence for the physiological role of breast cancer resistance protein and its endogenous substrate(s) has been elusive. Investigators initially looked to the expression in hematopoetic stem cells for the answer. The ability of these cells to export Hoechst 33342 had previously been used to identify the subpopulation of stem cells in murine bone marrow [156]. Abcg2 has recently been shown to be responsible for this phenotype [130]. Further, high expression in pluripotent stem cells and little to no expression in more differentiated lineages suggests Abcg2 may have a specific importance for pluripotent stem cell biology [92]. Interestingly, a high concentration of the toxic heme precursor protoporphyrin IX accumulates in Abcg2-/- progenitor cells under hypoxic conditions [140,157]. These knock-out animals also exhibited high erythrocyte levels of the phototoxic chlorophyll-breakdown product pheophorbide a, leading to lethal diet-induced lesions suggesting the physiological role of Abcg2 may involve protection against natural dietary toxins [158].

The high expression in the placental syncytiotrophoblast at the chorionic villus suggests a protective role for the fetus by effluxing substances that enter the placenta back into maternal circulation [131,159]. Jonker et al. demonstrated that the fetal topotecan plasma levels in Abcb1-deficient mice administered GF120918 were twice that of controls [160]. Staud et al. further showed that cimetidine is transported towards the maternal circulation, against its concentration gradient, in a placental perfusion model [161]. Interestingly, a recent study by Grube et al. suggested ABCG2, together with OATP2B1, may form a vectorial transport system for the efficient transfer of

common substrates across the placental barrier [162]. Their data indicated a correlation between ABCG2 and OATP2B1 RNA expression levels, that ABCG2 is expressed in the apical and OATP2B1 in the basolateral membrane, and that they both transport the steroid sulfates estrone 3 sulfate and dehydroepiandrosterone.

ABCG2 also seems to take a protective role in the small intestine and liver. In the same study presented above by Jonker et al. using Abcb1-deficient mice, GF120918 increased the topotecan AUC by decreasing hepatobiliary excretion and increasing intestinal reuptake [160]. The increase in topotecan bioavailability with GF120918 coadministration was replicated in humans in a clinical study by Kruijtzer et al. [163]. The development of the Abcg2 knock-out mouse has been a truly powerful tool in uncovering the importance of Acbg2 in limiting systemic xenobiotic exposure. A series of studies show that the AUC of nitrofurantoin, the dietary carcinogen PhIP, and ciprofloxacin is nearly 4-fold, 3-fold, and over 2-fold higher in Abcg2 deficient mice compared to wild type, respectively [53,93,128].

The high apical expression of ABCG2 in the mammary gland however seems illogical if its physiological role is that of xenotoxin elimination. It is likely that it functions in the breast to secrete nutrients into milk, a hypothesis supported by van Herwaarden and colleagues' recent observation that riboflavin is an ABCG2 substrate and that the milk secretion of riboflavin is reduced over 60-fold in Abcg2 knock-out relative to wild-type animals [91,92]. Specific evidence for its role in the transfer of xenobiotics into breast milk is provided in a preceding section (Section E). It is interesting to note that the majority of the drugs for which the passive diffusion prediction fails (detailed in Section D), nitrofurantoin, cimetidine, acyclovir, ciprofloxacin, have since been shown to be ABCG2 substrates. This suggests that a transport pathway involving Abcg2 may be an important route of drug transfer into breast milk and that knowledge of a drug's ability to interact with ABCG2 may improve our ability to predict accumulation into breast milk.

G. Summary

Despite the documented benefits of breastfeeding and major governmental advocacy efforts, a paucity of data exists regarding the transfer of most drugs into breast milk. For most of the drugs that have been studied, passive diffusion governs the extent of accumulation and the exposure risk can be predicted using mathematical models. However, examples of xenobiotic accumulation into breast milk well above that predicted

by passive diffusion have been documented and attributed to active transport processes. ABCG2 clearly transports many drugs known to accumulate in breast milk. Despite some inconsistencies with the properties of nitrofurantoin flux in the CIT3 cell culture model, ABCG2 was found to be responsible for nitrofurantoin accumulation in breast milk in vivo. The large body of ABCG2 data suggests that knowledge of a xenobiotic's potential interaction with this transporter may help improve in vitro M/S predictions. The expression of several other members of the SLC and ABC transporter superfamilies has also been reported in a variety of species but interpretation is complicated by the fact that expression data is often from nonlactating tissues and/or whole tissue homogenates rather than LMECs. No study has comprehensively studied the expression of all known xenobiotic transporters in nonpooled human LMEC samples.

This dissertation work will address many of these unanswered questions to drive future predictive models and enhance our understanding of the mechanisms of drug transfer into breast milk. It aims: (1) to clarify the existing CIT3 nitrofurantoin flux observations through an evaluation of the potential role of Abcg2 in this model system; (2) to extend the in vitro paradigm for M/S prediction by determining if an ABCG2-transfection model system can estimate the extent of in vivo xenobiotic breast milk accumulation; and (3) to provide a comprehensive analysis of the expression level of all known xenobiotic transporters in lactating LMECs obtained from individual patients.

CHAPTER 2: Plan of Work

A. Hypothesis 1: Breast cancer resistance protein (Abcg2) is responsible for the basolateral to apical transport of nitrofurantoin in CIT3 cells.

- *Specific Aim 1: To determine if Abcg2 is detectable in CIT3 cells with and without lactogenic hormone stimulation.*
- *Specific Aim 2: To determine if nitrofurantoin is transported in unstimulated CIT3 cells.*
- *Specific Aim 3: To evaluate if established Abcg2 inhibitors decrease the transport of nitrofurantoin and if known Abcg2 substrates are transported in CIT3 cells.*

Significant past efforts of our lab have focused on nitrofurantoin transfer into human milk and the identification of the transport system in stimulated CIT3 cells. Recent data demonstrate the role of Abcg2 in transporting nitrofurantoin in the mouse and substantial upregulation of this transporter during lactation [53,124]. Data from Gerk et al. suggest the system is sodium-dependent, inhibited by dipyridamole, and is likely expressed on the basolateral surface of CIT3 cells when stimulated with lactogenic hormones [87,88]. Specific Aim 1 will determine Abcg2 RNA (qPCR) and protein (western blotting and confocal microscopy) expression levels in unstimulated and stimulated CIT3 cells. Specific Aim 2 will employ transwell flux assays to determine if the preferential basolateral to apical nitrofurantoin flux is also observed in unstimulated CIT3 (not stimulated with lactogenic hormones). Specific Aim 3 will determine if Abcg2 plays a role in nitrofurantoin transport in the CIT3 cell culture system through the use of specific inhibitors. Well-characterized Abcg2 substrates will also be tested to confirm any role Abcg2 plays in this model system.

B. Hypothesis 2: Flux experiments in an ABCG2-transfection model system can estimate the extent of in vivo xenobiotic accumulation (M/S ratio) in breast milk.

- *Specific Aim 4: To create a stable ABCG2-transfected cell line that has appropriate characteristics for flux experiments.*
- *Specific Aim 5: To validate the model system with known ABCG2 substrates (PhIP, nitrofurantoin, cimetidine, methotrexate) and ABCG2 inhibitors (GF120918 and fumitremorgin C).*
- *Specific Aim 6: To establish a mathematical model for xenobiotic transport in an ABCG2-overexpressed cell culture system and to compare measurements of efflux activity.*
- *Specific Aim 7: To define the relationship between in vitro efflux ratios and the in vivo M/S ratio.*

A large number of xenobiotics known to significantly accumulate in breast milk have recently been shown to be substrates of the apical efflux transporter ABCG2 [53,93,127]. The objective of this series of experiments is to determine if a flux-based ABCG2-transfected cell system could be utilized to predict the extent of drug accumulation in vivo. Specific Aim 4 will use molecular biology techniques to establish a stably transfected ABCG2 overexpressing cell line derived from a single clone that can be used for monolayer flux studies. The model system will be validated in Specific Aim 5 with a series of expression and functional assays with known ABCG2 substrates and inhibitors. Specific Aim 6 will then create a mathematical model to define the relationships between permeability-surface area product specifically attributed to apical efflux ($PS_{a,efflux}$) and the commonly used experimental measurements efflux activity (ER_A, ER_α). This model will be used to explain experimental data (Aim 5) and literature-derived efflux ratios from other ABCG2 overexpressed cell lines to gain insight into the best measure of efflux activity for future work. Finally, Specific Aim 7 will model the relationship between in vitro efflux ratios and in vivo M/S to understand the utility and limitations of the developed cell culture model.

C. Hypothesis 3a: The determination of xenobiotic transporter genes with increased expression in lactating mammary epithelial cells relative to the nonlactating cells and other secretory tissues will identify transporters responsible for drug accumulation in breast milk.

D. Hypothesis 3b: The increased Abcg2 expression in mammary tissue observed during lactation is a due to increased expression of Abcg2 within luminal mammary epithelial cells rather than an expansion of this cell type relative to others within the mammary gland.

- *Specific Aim 8: To identify xenobiotic transporters highly expressed in mice during lactation (in vivo).*
- *Specific Aim 9: To develop a robust methodology to isolate a pure population of epithelial cells from human breast milk and reduction mammoplasty clinical samples.*
- *Specific Aim 10: To identify xenobiotic transporters highly expressed in human lactating mammary epithelial cells relative to nonlactating mammary epithelial cells and other secretory tissues.*

Several investigators have undertaken screening approaches to quantify the expression level of various transporters in tissue homogenates and often include the mammary gland in these studies. These efforts only provide limited information as: (1) the expression level represents an average from all cell types in the tissue, not just the cells forming the barrier for flux; (2) the tissue condition chosen for analysis is often the nonlactating mammary gland; (3) this approach also does not provide information as to the potential regulation of transporter genes during lactation; (3) nor are they complete enough to evaluate the potential for the involvement of multiple transport systems. Previous efforts in our lab utilized qPCR to determine the β-actin normalized expression level of 30 transporters in a single pooled sample of human luminal mammary epithelial cells from breast milk and from the same cell type in nonlactating reduction mammoplasty tissue. This dissertation work will use microarray to build upon, and address the limitations of, existing knowledge. Specific Aim 8 will explore xenobiotic transporter expression during lactation relative to other stages of development by mining

existing murine development datasets. Specific Aim 9 will develop and validate a new methodology necessary to obtain a pure population of human luminal mammary epithelial cells in sufficient numbers from clinical samples for microarray. Specific Aim 10 will identify transporters with high expression in lactating mammary epithelial cells relative to similar nonlactating cells and other secretory tissues (liver and kidney).

CHAPTER 3: Materials and Methods

A. Materials

CIT3 cells (passage 9) were generously provided by Dr. Margaret Neville at the University of Colorado. Other cell lines were purchased from the established vendors: LLC-PK1 cells (an epithelial cell line comprised of porcine kidney proximal tubule cells originally deposited by Eli Lilly and Company) from American Type Culture Collection (ATCC, Manassas, VA), and MDCKI and MDCKII cells (sub-types I and II cell lines originally isolated from a canine kidney by H. Madin and N. B. Darby) from European Collection of Cell Cultures (ECACC, Salisbury, Wiltshire, UK). All cell culture plates, #3412 and #3414 transwells, and #3407 snapwells were obtained from Corning Costar (Cambridge, MA). All cell culture media, enzymes, and reagents including human epidermal growth factor were purchased from Invitrogen (Carlsbad, California). Human insulin, hydrocortisone, 10x Tris-borate EDTA (TBE) buffer, Trizma® base, Trizma® HCL, magnesium chloride, EDTA, mannitol, sucrose, bovine serum albumin (BSA), sodium azide, methanol, nitrofurantoin, cimetidine, hyaluronidase, collagenase, dimethyl sulfoxide (DMSO), and the monoclonal mouse anti-β-actin antibody were obtained from Sigma-Aldrich (St. Louis, MO). Ciprofloxacin was obtained from ICN Biomedical (Aurora, OH). GF120918 was a generous gift from GlaxoSmithKline (Research Triangle, NC). Fumitremorgin C (FTC) was purchased from Alexis Biochemicals (San Diego, CA). DB-67 was a generous gift from Dr. Markos Leggas. Ovine prolactin was purchased from the National Hormone and Pituitary Program (Torrance, CA).

RNeasy® Micro Kit and Qiashredder columns were obtained from Qiagen (Valencia, CA). Phosphate-buffered saline (PBS), Hanks balanced salt solution (HBSS), the SuperScript™ First-Strand Synthesis System for RT-PCR kit, NuPAGE® 4-12% Bis-tris gels, NuPAGE® MOPS SDS buffers, NuPAGE® reducing agent and antioxidant, PVDF sandwich membrane and filter paper, Magic Mark™ XP protein ladder, genecitin, Alexa Fluor® 488 goat anti-mouse IgG (H+L) secondary antibody, Alexa Fluor® 568 goat anti-rabbit IgG (H+L) secondary antibody, Prolong® Gold antifade reagent containing DAPI, and Hoechst 33342 were purchased from Invitrogen (Carlsbad, California). The SYBR® Green PCR Core Reagents kit was obtained from Applied Biosystems (Foster City, CA). Fluorescein calibration dye was purchased from Bio-Rad (Hercules, CA). All primers were purchased from Integrated DNA Technologies (Coralville, IA). Sea-Kem LE agarose was obtained from Cambrex (Rockland, ME).

Ethidium bromide, Tween-20, sodium hydroxide, and Triton®-X-100 were purchased from Fisher Scientific (Hampton, NH). The BCA Protein Assay kit, goat anti-mouse HRP conjugate secondary antibody, and Supersignal® West Pico chemiluminescent kit were obtained from Pierce (Rockford, IL). PNGase F was purchased from New England Biolabs (Ipswich, MA). Complete Mini EDTA-free protease inhibitor tablets, FuGENE 6® transfection reagent, and DNAse I was obtained from Roche Diagnostics (Indianapolis, IN).

Goat serum was purchased from Vector Laboratories (Burlingame, CA). The BXP-21 mouse anti-human ABCG2 monoclonal antibody and the BXP-53 rat anti-mouse Abcg2 monoclonal antibody was obtained from Kamiya Biomedical (Thousand Oaks, CA). The anti-ZO-1 (n-terminus) rabbit polyclonal primary antibody was obtained from Zymed (San Francisco, CA). The phycoerythrin (PE) labeled mouse anti-human ABCG2 (clone 5d3) and mouse IgG2b isotype control were purchased from eBioscience (San Diego, CA). The fluorescein isothiocyanate (FITC) conjugated mouse anti-human ABCG2 (clone 5d3) was obtained from Chemicon International (Temecula, CA). The monoclonal rat anti-human epithelial basement membrane antigen (MUC1) IgG2a subtype antibody (MFGM/5/11[ICR.2]) was obtained from Immunologicals Direct/AbD Serotec (Raleigh, NC). Rat IgG2a isotype control (clone R35-95), FITC-conjugated mouse IgG1 isotype control antibody and the FITC-conjugated mouse anti-rat IgG2a (clone RG7/1.30) secondary antibody were purchased from BD Biosciences/Pharmingen (San Jose, CA). The EasySep® human MUC1 selection kit, "The Big Easy" EasySep® magnet, anti-human MUC1 mouse IgG1 subtype (clone 214D4) antibody, and mouse monoclonal FITC-conjugated anti-dextran antibody (clone DX1) were obtained from StemCell Technologies (Vancouver, Canada). The Vectastain ABC kit and the monoclonal mouse anti-human (IgG1) cytokeratin cocktail CK22 (40-68 kDa) antibody was obtained by the UK Cytology department from Vector Laboratories (Burlingame, CA) and Biomeda Corp (Foster City, CA), respectively. Human kidney and liver total RNA was purchased from Clonetech (Mountain View, CA).

The following radiochemicals were purchased: ^{14}C-nitrofurantoin (58 mCi/mmol) from Chemsyn Labs (Lexena, KS), ^{3}H-cimetidine (25 Ci/mmol) from Amersham (Piscataway, NJ), ^{14}C-PhIP (10mCi/mmol) from Toronto Research Chemicals (Toronto, CA), ^{14}C-sucrose (495 mCi/mmol) and ^{14}C-ciprofloxacin (20 mCi/mmol) from Moravek (Brea, CA), ^{3}H-mannitol (27 Ci/mmol) from MP Biomedicals (Solon, OH). Bio-safe® II

scintillation cocktail was obtained from Research Products International (Mount Prospect, IL).

B. Expression and functional role of Abcg2 in CIT3 cells

1. Cell culture

CIT3 cells were cultured following established protocols [87]. Briefly, 1 x 10^6 cells (passages 15-19) were seeded on 0.4 µm 4.66 cm^2 polycarbonate #3412 transwells and grown in "growth media" (DMEM/12 medium with 2% inactivated fetal bovine serum, 2.38 g/L HEPES, 1.2 g/L sodium bicarbonate, 5 ng/mL epidermal growth factor, 10 µg/mL insulin, 100 U/mL penicillin, and 100 µg/mL streptomycin). TEER was measured every other day with a Millicell ohmmeter and a Millicell-ERS probe (Millipore, Bedford, MA) for 10-18 days until > 800 Ω•cm^2 was achieved. Cells were then differentiated for 4 days in "secretion media" which was identical to the growth media except that the epidermal growth factor was replaced with 3 µg/mL ovine prolactin and 3 µg/mL hydrocortisone.

2. RNA isolation and quantitative PCR

Cells were grown on #3412 transwells in growth media to a TEER > 800 Ω•cm^2, then in either growth media or secretion media for an additional 4 days. Following a wash with ice-cold PBS, cells were scraped off the transwells, and pelleted by centrifugation at 300 *g* for 5 min. Isolation of total RNA from pelleted cells was performed using the RNeasy® Micro Kit per manufacturer protocol with sample disruption using Qiashredder® and on-column DNAse treatment. Mammary gland tissue from a lactating CD1 mouse 7 days post-partum served as a positive control. Total RNA isolation from this fibrous tissue was performed in parallel to the CIT3 cells following an additional tissue pulverization step using liquid nitrogen with a mortar and pestle. The resulting total RNA concentration was determined by the measurement of optical density at 260 nm with a small volume UV-Vis Spectrophotometer (ND-1000, NanoDrop, Wilmingon, DE). Total RNA integrity was verified by an OD260/OD280 absorption ratio greater than 1.9. Reverse-transcription of 1.5 µg RNA to cDNA was performed with the SuperScript™ First-Strand Synthesis System for RT-PCR kit following manufacturer's protocol using oligo(dT) to prime the reaction preferentially for mRNA. All samples to be compared were run together using master mixes to limit potential sources of variation.

Quantification of the expression level of Abcg2, milk proteins β-casein (Csn2) and α-lactalbumin (lalba), and the house-keeping gene β-actin (Actb) was performed using the quantitative polymerase chain reaction (qPCR) on the iCycler Multicolor Real-Time PCR Detection System (Bio-Rad, Hercules, CA). Gene-specific primer sequences were either designed (Csn2 and Lalba) or obtained from published literature (Actb and Abcg2). Primers were designed using reference sequences deposited in NCBI's Entrez Gene with the software assistance of Primer3 (Whitehead Institute for Biomedical Research, Cambridge, MA*)* and Oligo Tool Kit (Operon, Huntsville, AL) [164]. All primers utilized were confirmed to generate unique products using NCBI's BLAST. Reference accession numbers, primer sequences, and product sizes are provided in Table 3-1. qPCR reaction master mixes (50 µL) were made using the SYBR® Green PCR Core Reagents kit and contained 200 nM of each primer, 1.25 mM dNTPs, 1x SYBR Green buffer, 0.025 U/µL Taq polymerase, optimized concentrations of magnesium chloride for each primer pair, 20 nM fluorescein, and 0.15 µg of sample cDNA. The amplification protocol included a "hot-start" (95ºC for 5 min) followed by 50 cycles of a denaturation step (95ºC for 45 sec), an annealing step (optimized annealing temperature for each primer pair for 1 min) and an extension step (72ºC for 1 min). SYBR Green fluorescence was quantified during each cycle at the end of the extension step. Following amplification, a melting curve program was run to aid in determining the specificity of the reaction. Each reaction mixture was heated to 95ºC and then cooled 1ºC/min while monitoring the rate of change in fluorescence. When plotted against temperature, this allows for the discrimination of specific amplification products from one another [165]. Finally, to confirm the generation of a single product of appropriate size, all amplification products were separated by 3% agarose gel electrophoresis in 1 x TBE running buffer for 50 min at 150 mV, visualized by staining with ethidium bromide, and imaged on an Image Station 2000 MM (Eastman Kodak, New Haven, CT). Optimization of the best conditions for each primer pair (annealing temperature and magnesium) was performed using high and low dilutions of the positive control and water only reactions. Conditions producing fluorescence above a threshold level in the fewest number of cycles while generating a single product of the appropriate size via melt curve analysis and gel electrophoresis were accepted.

Table 3-1: Murine primers and conditions for qPCR.

Gene	Reference Sequence	Forward Primer (5'→3') / Reverse Primer (5'→3')	Prod. Size (bp)	Mg Conc (mM)	Anneal Temp (ºC)	Ref.
Actb	NM_007393	TGTTACCAACTGGGACGACA	165	3.5	62	[166]
		GGGGTGTTGAAGGTCTCAAA				
Csn2	NM_009972	TGTGCTCCAGGCTAAAGTTC	103	3.5	62	-
		GATGTTTTGTGGGACGGGAT				
Lalba	NM_010679	GACAACGGCAGCACAGAGTA	133	3.5	62	-
		CATCATCCAACTCGTCATCC				
Abcg2	NM_011920	GAACTCCAGAGCCGTTAGGAC	166	3.5	62	[167]
		CAGAATAGCATTAAGGCCAGGTT				

Data analysis was performed using the iCycler IQ Optical System software version 3.1 (Bio-Rad, Hercules, CA) according to the relative quantification with an external standard method [168]. Briefly, a standard curve consisting of a serial dilution for each gene was made from the lactating mammary gland positive control sample in triplicate and run simultaneously with the samples in the same plate. SYBR Green fluorescence captured during each cycle of the run was plotted vs. the cycle number in real-time. An arbitrary fluorescence level was then set in the exponential phase of the amplification such that it was above any background fluorescence level. The cycle at which each standard's amplification curve crosses this threshold level (threshold cycle) was plotted vs. relative copy number and a best fit line was generated by linear regression. Relative copy number of each gene in the samples was then determined in triplicate and normalized to relative copy number of the housekeeping gene β-actin within each sample. Negative controls from the reverse transcription and the PCR reactions were incorporated into all runs.

3. Western blot

CIT3 cells were grown to confluence in growth media and then an additional 4 days in either growth media or secretion media to determine if Abcg2 protein was detectable in the cell line with and without lactogenic hormone stimulation. Following a wash with ice-cold PBS, cells were scraped and pelleted by centrifugation at 300 *g* for 5

min. Mammary gland tissue from a lactating CD1 mouse 7 days post-partum previously pulverized for RNA isolation served as a positive control. To isolate crude membrane fractions from these samples, 1 mL "Dounce Buffer" (Tris buffer pH 7.6 at 4ºC, 0.5 mM magnesium chloride) with protease inhibitors (Complete Mini EDTA-free tablets) was first added to allow the cells to swell. Membrane disruption was achieved with brief pulses of sonication using a probe ultrasonic processor (Fisher Scientific, Hampton, NH) and the tonicity restored to 150 mM with sodium chloride. Following another centrifugation at 300 *g* for 5 min, the supernatant was removed and EDTA was added to a final concentration of 5 mM. The sample was then centrifuged further at 100,000 *g* for 1 hour at 4ºC to pellet the crude membrane fractions. Pellets were resuspended in "resuspension buffer" (0.2 M mannitol, 0.07 M sucrose, 50 µM Tris HCl, 1 µM EDTA) and protein concentrations were measured using the BCA Protein Assay kit.

Western blot analysis was then performed on these samples with or without a deglycosylation step using PNGase F according to the manufacturer's protocol. Gel electrophoresis was completed using NuPAGE® 4-12% Bis-tris gels and NuPAGE® MOPS SDS buffers in the X-Cell SureLock™ Mini-Cell system (Invitrogen, Carlsbad, CA). NuPAGE® reducing agent was added to all samples prior to heating to 70ºC for 10 min. Samples and the Magic Mark XP protein ladder were run for 200 V for 1 h and then transferred to a PVDF membrane using 30 V for 1.25 h at room temperature. The membrane was blocked for 1 h with 3% BSA in TBST (10 mM Tris buffer pH 7.4, 150 mM sodium chloride, 0.05% Tween-20) prior to overnight incubation with either 1:50 BXP-53 (for Abcg2) or 1:2000 anti-β-actin in TBST and then washed for 10 min X 3 with TBST. Labeling was accomplished with 1:10,000 goat anti-mouse HRP conjugate in 3% BSA in TBST for 1 h. Following 3 more 10 min TBST washes, Abcg2 protein on the membrane was visualized using the Supersignal® West Pico chemiluminescent kit and the Image Station 2000 MM (Eastman Kodak, New Haven, CT). Quantification was achieved with band densitometry within the Molecular Imaging Software version 4.04 (Eastman Kodak, New Haven, CT).

4. Confocal microscopy

Expression level and cellular localization of Abcg2 in CIT3 with and without lactogenic hormone stimulation were determined by confocal microscopy. As with previous experiments, cells were grown in growth media on polycarbonate filter membranes to a TEER > 800 $\Omega \bullet cm^2$ to allow for polarization, then in either growth media

or secretion media for an additional 4 days. As the membranes were to be eventually repositioned to glass slides, 0.4 μm 1 cm^2 #3407 snapwells were used. Membranes were initially washed with ice-cold PBS, cut, and transferred to a 24-well plate for easier processing and staining. Cells were fixed with -20ºC methanol for 10 min, rehydrated with room temperature PBS for 5 min, and permeabilized with room temperature 0.2% Triton®-X-100 in PBS for 15 min. Membranes were then blocked through the addition of 10% goat serum to the permeabilization solution for 30 min at room temperature. Abcg2 and the tight-junction protein ZO-1 were then labeled with 1:20 BXP-53 and 1:100 anti-ZO-1 in the same blocking solution for 1 h at room temperature respectively. Three 5 min washes with permeabilization buffer then removed residual primary antibody prior to a 1 h incubation with 1:500 Alexa Fluor® 488 anti-mouse and 1:500 Alexa Fluor® 568 anti-rabbit secondary antibodies in blocking solution. Finally membranes were again washed with permeabilization solution three times, rinsed with PBS, mounted on glass slides with Prolong Gold® containing DAPI to visualize nuclei, sealed under a cover slip, and allowed to cure overnight. Fluorescence emission was captured using the 100x oil-immersion objective at 3 distinct wavelengths with an inverted laser-scanning confocal microscope (Leica, Germany) equipped with He-Ne and argon lasers at the UK Imaging Facility. Appropriate negative controls (without the Abcg2 primary antibody) were run to set background fluorescence.

5. Flux assay procedures

Two different flux systems were utilized. Early radiolabelled nitrofurantoin experiments (Specific Aim 2) were performed following published protocols using 0.4 μm 1 cm^2 #3407 snapwells and vertical diffusion chambers (Navicyte, Sparks, NY) and manifold (Harvard Apparatus, Holliston, MA) [87,88]. When the supply of radiolabelled nitrofurantoin was exhausted, all subsequent experiments (Specific Aim 3) were performed using the larger surface area 0.4 μm 4.66 cm^2 #3412 transwell filters in the horizontal orientation to allow for greater mass transfer to increase the sensitivity of the system. For the snapwell experiment, approximately 0.5 x 10^6 cells were seeded whereas 1 x 10^6 cells were seeded to transwells for all subsequent experiments. Regardless of approach used, cells were grown for similar lengths of time (10-18 days initially, then 4 days in either growth or secretion media) to achieve TEER > 800 Ω•cm^2. On the day of the experiment, cells were preincubated with 37ºC DMEM/F12 containing only 2.38 g/L HEPES and 1.2 g/L sodium bicarbonate (free of serum, proteins,

hormones, and antibiotics) and any inhibitors or vehicle only controls to be tested in specific wells on that day. Experiments were initiated by replacing the preincubation solutions with fresh solution and adding the "loading solution" containing the substrate to be tested and either 0.01 μM ^{3}H-mannitol or 0.2 μM ^{14}C-sucrose as a marker of paracellular flux to either the basolateral (B) or apical (A) chamber. Vertical chambers were maintained at 37ºC by perfusing the manifold with solution from a recirculating waterbath and constantly mixed by bubbling 95% oxygen/5% carbon dioxide into the chambers. Horizontal chambers were kept at 37ºC in a 5% carbon dioxide incubator and constantly mixed with a 10º 3-D Rotator (Barnstead International, Dubuque, Iowa). B and A chambers were sampled at specific times and samples were frozen for subsequent HPLC analysis (nitrofurantoin) or mixed with 3.5 mL Bio-safe II™ liquid scintillation cocktail for later counting on the Tri-Carb 2200CA (PerkinElmer, Waltham, MA). Permeability in the basolateral to apical (B→A) and apical to basolateral (A→B) directions were determined as described in the Flux assay data analysis section on page 34. Experiments involving nitrofurantoin were performed in a darkened room due to this drug's sensitivity to light.

6. Flux assay study designs

The initial experiment to determine if there was a directionality to nitrofurantoin flux in unstimulated CIT3 cells as was previously demonstrated for CIT3 cells following lactogenic hormone stimulation was performed by loading 0.2 μCi/well (approx 1.5 μM) ^{14}C-nitrofurantoin (greater than 97% pure) to either the B or A snapwell chamber (n=3 of each). One hundred microliter samples were obtained at 1, 20, 40, 60, 80, 100, and 120 min from both chambers and immediately mixed with liquid scintillation cocktail for counting. TEER and nitrofurantoin permeability of unstimulated cells vs. those stimulated with lactogenic hormones for 4 days were then compared.

The ability to inhibit the predominantly B→A directed flux of 10 μM nitrofurantoin in unstimulated and stimulated CIT3 cells with Abcg2 inhibitors was determined using the Abcg2 inhibitor FTC at 10 μM. The inhibitor was added to all preincubation buffers and both B and A chambers of the #3412 transwells. The experiment was initiated by adding nitrofurantoin and ^{3}H-mannitol to final concentration of 10 μM and 0.01 μM, respecitively, to the B or A chamber (n=3 of each). One hundred fifty microliters was sampled from both chambers at 0.5, 1, and 2 h for determination of pmol nitrofurantoin transferred at each timepoint by HPLC and 50 μL was collected at 1 and 2 h for similar

mannitol mass quantification by liquid scintillation counting. Permeability of nitrofurantoin in both directions was then compared with and without inhibitors in either unstimulated or stimulated conditions.

Finally to further demonstrate the potential role of Abcg2 in unstimulated CIT3 cells, two known Abcg2 substrates were tested using similar experimental procedures. 2 μM ^{14}C-PhIP and 0.01 μM ^{3}H-mannitol and the same inhibitor were used in the first experiment and 5 μM cimetidine (traced with 500 μCi/μmol ^{3}H-cimetidine) and 0.2 mM ^{14}C-sucrose was used in the second. In the PhIP experiment, 200 μL was sampled from both sides of each chamber at 0.5, 1, and 2 h, whereas 150 μL was sampled from both sides of each chamber at 0.5, 1, 2, and 4 h in the cimetidine experiment. All samples were immediately added to liquid scintillation cocktail. Permeability of each drug in both directions was then compared with and without inhibitors. Chemical structures of all agents used in the transport studies can be found in Appendix 2.

7. Nitrofurantoin HPLC analysis in cell culture media

The amount of nitrofurantoin transferred at each timepoint was calculated by HPLC analysis using a published assay with minor modifications [53]. Briefly, 50 μL of the sample from each timepoint in cell culture was injected onto the Shimadzu HPLC 6A series HPLC system (Kyoto, Japan) without extraction. Samples were only vortexed and briefly centrifuged to pellet any debris. The mobile phase was modified from 75:25 to 80:20 acetonitrile:3.5 mM potassium phosphate pH 3.0 at 1 mL/min to shorten the run time to 5 min. The retention time of nitrofurantoin was 3.5 min on the Lichrosorb 5 RP-18 125 x 4 mm column (Phenonemex, Torrance, CA) with good peak separation. UV absorbance was measured at 366 nm. Sample and standard injection order was randomized. Peak heights were used for interpolation on the standard curve.

8. Flux assay data analysis

The apparent permeability (Papp, (μL/h)/cm^2) of each drug or paracellular marker was determined by calculating its flux (J, pmol/h) across the cell layer and dividing by the surface area (A, cm^2) of the transwell or snapwell and the initial concentration (C_0, pmol/mL) in the donor chamber as shown in Eq. 3-1.

$$Papp = \frac{J}{A \cdot C_0} \qquad \text{Eq. 3-1}$$

Cumulative amount of drug moving to the recipient chamber was assumed to be negligible relative to donor concentration such that initial donor concentrations were maintained (sink conditions). Flux of each drug was determined by best fit line through the linear region of the graph of the cumulative pmol transferred vs. time. Linear regression was performed using GraphPad Prism 5.0 (San Diego, CA). Regression lines were forced through the origin for PhIP as less than 3 points were available in the linear range of the curve. Consistent with similar flux assays in the published literature, leakage of the paracellular marker used in each experiment was tolerated up to an apparent permeability of 1%/h (4.3 (μL/h)/cm^2) [127].

9. Statistical Analysis

Normalized relative RNA expression of β-casein, α-lactalbumin, and Abcg2 in CIT3 cells with and without lactogenic hormone stimulation were compared with an unpaired t-test. Sucrose permeabilities in unstimulated CIT3 cells were also compared with an unpaired t-test. All other directionality and inhibition studies were compared using one-way ANOVA with Bonferroni's multiple comparisons as above except that only select comparisons were considered in post-hoc testing. In the stimulated vs. unstimulated nitrofurantoin directionality experiment, the following comparisons were made: unstimulated B→A vs. A→B, stimulated B→A vs. A→B, unstimulated B→A vs. stimulated B→A, and unstimulated A→B vs. stimulated A→B. In all inhibition experiments, the comparisons selected were B→A vs. A→B, B→A vs. B→A inhibited, A→B vs. A→B inhibited, and B→A inhibited vs. A→B inhibited. All statistical analyses were performed using GraphPad Prism 5.0 (San Diego, CA) with a p-value < 0.05 considered significant.

C. Creation of an ABCG2 stably transfected model system

1. Selection of a cell line

Several cell lines (LLC-PK1, MDCKI and MDCKII) were evaluated prior to transfection to identify the candidate with the best properties for subsequent experiments: ease of maintenance in culture, an ability to form a monolayer on transwells exhibiting high TEER and low flux of a paracellular flux marker (mannitol), no background expression of Abcg2, limited expression of other xenobiotic transporters, and ease of selection post-transfection. Each was purchased from an established

source and was grown in the media specified by that vendor. To compare TEER and mannitol flux, cells were grown on #3414 transwells until a maximal TEER was achieved and mannitol flux experiments were performed as described with CIT3 cells in the Flux assay procedures section on page 32. Background expression of Abcg2 and other xenobiotic transporters was evaluated by reviewing of published literature. The concentration of genecitin necessary for selection of transfected cells was estimated by visually inspecting growth following exposure of the parent cell line to a range of concentrations (100-1000 µg/mL) of this agent.

2. Transfection

The pcDNA3 plasmid construct alone (empty vector) and the pcDNA3 plasmid containing wild-type ABCG2 were generously provided by Dr. Markos Leggas (Figure 3-1). MDCKII cell transfection was performed at 50% confluence with the lipid-based FuGENE 6® transfection reagent at a 3:1 ratio per manufacturer's protocol. Success of transfection was initially evaluated at 48 h by western blot analysis of cell lysates for ABCG2 following procedures described in the Western blot on page 37. Transfected cells were then selected through the addition of 800 µg/mL genecitin to the parent cell line media (MEM containing glutamax, 5% FBS, 100 U/mL penicillin, and 100 µg/mL streptomycin).

Figure 3-1: pcDNA3/ABCG2 plasmid construct.

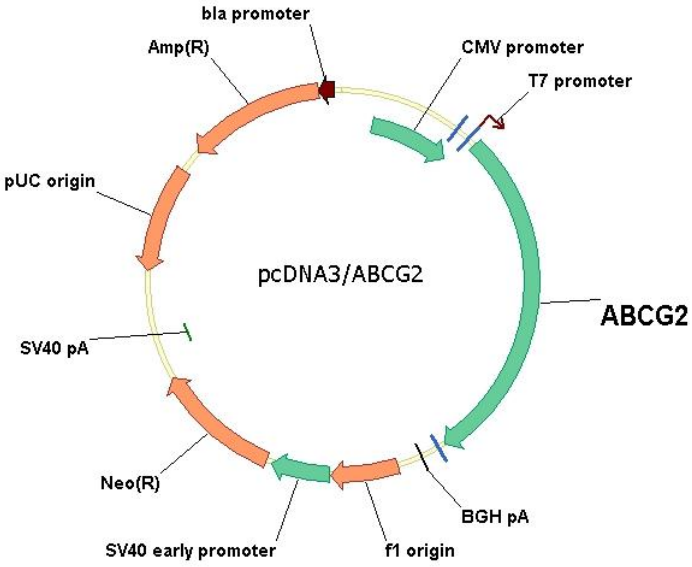

3. Western blot

Procedures for western blot analysis of ABCG2 expression in crude membrane fractions were the same as those described for CIT3 cells on page 30 with different antibodies. The ABCG2 primary antibody used was 1:500 BXP-21 and the secondary antibody was therefore 1:10,000 goat anti-mouse HRP conjugate. When protein from cell lysates rather than crude membrane fractions was desired, it was prepared by scraping the cells, washing with ice-cold PBS, pelleting by centrifugation at 300 *g* for 5 min, and adding "lysis solution" (50 mM HEPES, 1 mM EDTA, protease inhibitors (from Complete Mini EDTA-free tablets)) to the pellet. Protein isolated from ABCG2-transfected Saos-2 cells (Saos-2-ABCG2) served as a positive control [169,170].

4. Flow cytometry and fluorescence-activated cell sorting (FACS)

Relative quantification of ABCG2 surface expression was performed by flow cytometry using a PE-conjugated primary antibody raised against an external epitope of ABCG2. Cells were trypsinized, pelleted by centrifugation at 300 *g* for 5 min, resuspended in ice-cold HBSS (without calcium/magnesium) containing 1 mM EDTA and counted on a hemocytometer. Five hundred thousand cells were added to a 12 x 75 mm polystyrene tube, again pelleted by centrifugation, and labeled with 0.5 µg of the Anti-ABCG2(clone 5d3)-PE or IgG2b-PE isotype control antibody for 30 min at 4ºC in 50 µL of HBSS (without calcium/magnesium) containing 2% FBS, 1 mM EDTA, and 0.1% sodium azide. Following labeling, cells were washed with the same labeling solution to remove residual antibody, centrifuged at 300 *g* for 5 min, resuspended, and brought to the UK Flow Cytometry Core Facility on ice for immediate analysis. Cell clumps or debris were gated out using forward and side scatter and following excitation at 488 nm the PE fluorescence of 3 x 10^4 events per tube were captured at 575 nm on the FACSCalibur cytofluorimeter (BD Biosciences, San Jose, CA). Relative expression level was quantified by subtracting the geometric mean fluorescence intensity (MFI) of the PE histogram of the isotype control from that of the anti-ABCG2 antibody. Antibody titrations were performed for all new batches of the anti-ABCG2-PE antibody using Saos-2-ABCG2 cells and mouse IgG2b isotype-control antibody.

Sorting of individual live cells with high surface expression of ABCG2 for clonal selection was achieved using FACS and the same antibody, this time conjugated to FITC. Transfected cells selected in 800 µg/mL genecitin for 2 weeks were trypsinized,

pelleted by centrifugation at 300 *g* for 5 min and counted on a hemocytometer. Cells (5 x 10^5) were added to a 12 x 75 mm polypropylene tube and blocked with 10% goat serum in HBSS for 5 min at room temperature. Cells were then washed, centrifuged, and the pellets were labeled with 10 µL of the Anti-ABCG2(clone 5d3)-FITC antibody for 30 min at room temperature in HBSS + 2% FBS. Residual antibody was removed following centrifugation and cells were resuspended in HBSS with 2% FBS containing 2 µg/mL propidium iodide (PI). At the UK Flow Cytometry Core Facility, cell clumps or debris were removed from the analysis using forward and side scatter and following excitation at 488 nm cells with low PI fluorescence at 575 nm (presumed viable) and with high FITC fluorescence at 525 nm were sorted into individual wells of a 96-well plate using the MoFlo™ High-Performance Cell Sorter (DakoCytomation, Fort Collins, Colorado). Gates were set based on fluorescence of single color controls.

5. Hoechst 33342 efflux

ABCG2 functional activity was assessed by efflux of the fluorescent ABCG2 substrate Hoechst 33342 by flow cytometry. Following clonal expansion of single cells plated via FACS, 1 x 10^5 were seeded in 12-well plates and grown to confluence. On the day of the experiment, these MDCKII-ABCG2 cells were first washed with PBS and preincubated with OptiMEM with or without 1 µM GF120918 for 15 min. Hoechst 33342 (10 µM) was then added and allowed to accumulate for 45 min at 37ºC while mixing in an incubator containing 5% carbon dioxide. Cells were next washed with PBS, OptiMEM with or without the inhibitor replaced, and efflux was allowed for 10 min. Efflux was stopped by placing the wells on ice and washing with ice-cold PBS (without calcium or magnesium). Three hundred microliters of 10X trypsin/EDTA containing no phenol red was subsequently added to loosen the cells from the plate. The resulting cell suspension was centrifuged at 300 *g* for 5 min at 4ºC and resuspended in PBS (without calcium or magnesium) containing 2.5% FBS and 2 µg/mL PI and brought to the UK Flow Cytometry Core Facility for analysis on the MoFlo™ High-Performance Cell Sorter (DakoCytomation, Fort Collins, Colorado). Cell clumps, debris, and presumed nonviable cells were removed from analysis using forward/side scatter and PI fluorescence. Hoechst 33342 fluorescence of each cell was analyzed by excitation at 325 nm and a measurement of the emission at 440 nm. A gate set at the beginning of the Hoechst 33342 histogram of the GF120918-treated samples of each clone was used to assess ABCG2 functional activity of each sample. Specifically, the number of cells with

fluorescence intensity less than this level (dim population) was quantified and expressed as a percentage of total cells in the sample. All gates were set based on fluorescence of unstained and single color controls. Empty vector-transfected cells were used as a negative control. Hoechst 33342 accumulation and efflux times were optimized using Saos-2-ABCG2 cells prior to experiments with MDCKII-ABCG2 clones.

6. DB-67 accumulation

The accumulation of the camptothecin analog DB-67 was assessed in several of the clones by similar procedures. Four hundred thousand MDCKII-ABCG2 cells expanded from single clones were plated in 6-well plates (n=3 of each condition), grown to confluence, and preincubated with or without 1 μM GF120918 in OptiMEM for 15 min. One micromolar DB-67 was then added and allowed to accumulate for 20 min at 37ºC while mixing in an incubator containing 5% carbon dioxide. Substrate accumulation was stopped by placing the plate on ice and washing three times with ice-cold HBSS containing 10% FBS. Cells were lysed with 0.5 N sodium hydroxide and an aliquot was used to determine protein concentrations using the BCA Protein Assay kit. The remaining sample was analyzed by HPLC with fluorescence detection for total DB-67 (lactone and carboxylate forms) following previously published methods [171]. Data was expressed as total DB-67 accumulation normalized to protein content and compared with and without the inhibitor in each cell line by t-tests.

7. Confocal microscopy

Procedures for the determination of expression level and cellular localization of ABCG2 in MDCKII-ABCG2 cells were the same as those described for CIT3 cells on page 31 except that the anti-ABCG2 primary antibody used was 1:40 BXP-21. Empty vector-transfected cells were used as a negative control.

8. Flux assays

Evaluation of the MDCKII-ABCG2 model system with known ABCG2 substrates and inhibitors was performed using procedures detailed in the Flux assay procedures and Flux assay data analysis sections on pages 32 and 35. All experiments were performed with 1 x 10^6 cells grown for 3-4 days on #3414 transwells in the horizontal orientation. Directionality experiments were performed in OptiMEM with 10 μM nitrofurantoin, 2 μM ^{14}C-PhIP, 5 μM cimetidine (traced with 2 mCi/μmol ^{3}H-cimetidine), 5

nM ^{3}H-methotrexate, or 10 µM ciprofloxacin (traced with 8 µCi/µmol ^{14}C-ciprofloxacin) added to the donor chamber. Inhibition experiments were also performed in OptiMEM with either 1 µM GF120918, 10 µM FTC, or vehicle-only control with all of these substrates except for methotrexate and ciprofloxacin. Sampling was performed as detailed: nitrofurantoin, 130 µL at 0.5 h, 1 h, 2 h, 3 h (directionality), 120 µL at 0.5 h, 1 h, 2 h, 3 h; PhIP, 50 µL at 0.5 h, 1 h, 2 h, 3 h, 4 h (directionality), 300 µL at 0.5 h, 1 h (inhibition); cimetidine, 200 µL at 0.5 h, 1 h, 2 h; methotrexate, 200 µL at 0.5 h, 1 h, 2 h; and ciprofloxacin, 50 µL at 0.5 h, 1 h, 2 h, 4 h. All substrates except nitrofurantoin were assayed by liquid scintillation counting. Nitrofurantoin was assayed by HPLC as described on page 34. A paracellular marker (^{14}C-sucrose or ^{3}H-mannitol) was used in all experiments and leakage was tolerated up to an apparent permeability of 1%/h (4.3 (µL/h)/cm^2). Permeabilities were calculated for each drug and statistical tests were performed as described on page 35 except that comparisons were made between the empty vector and the MDCKII-ABCG2 clone 40 for directionality experiments and between control and the various inhibitor treated samples within each cell type in the inhibition assays. The percentage inhibition of the component of the B→A permeability attributed to ABCG2 was also calculated as shown in Eq. 3-2. The difference in the ABCG2-transfected B→A permeability and the empty vector-transfected B→A permeability with the inhibitor ($Papp_{ABCG2, I} - Papp_{Empty, I}$) is subtracted from that of wells without the inhibitor ($Papp_{ABCG2} - Papp_{Empty}$) and dividing by the same difference in the uninhibited condition.

$$\% \text{ Inhibition} = \frac{(Papp_{ABCG2} - Papp_{Empty}) - (Papp_{ABCG2, I} - Papp_{Empty, I})}{(Papp_{ABCG2} - Papp_{Empty})} \times 100 \quad \text{Eq. 3-2}$$

D. Mathematical modeling and derivation of commonly used measurements of efflux activity.

1. Development of a model for drug transfer into milk

A simple mathematical model, built upon the recently published work of Kalvass and Pollack, was developed to describe drug transfer into breast milk (Figure 3-2) [172]. This three compartment system incorporates the permeability-surface area product attributed to: paracellular flux between the cells (PS_{PC}), passive diffusion across the LMEC basolateral and apical membranes (PS_D), basolateral uptake ($PS_{B,U}$), apical efflux ($PS_{A,E}$), basolateral efflux ($PS_{B,E}$) and apical uptake ($PS_{A,U}$).

Figure 3-2: Simple kinetic model for flux across a LMEC monolayer

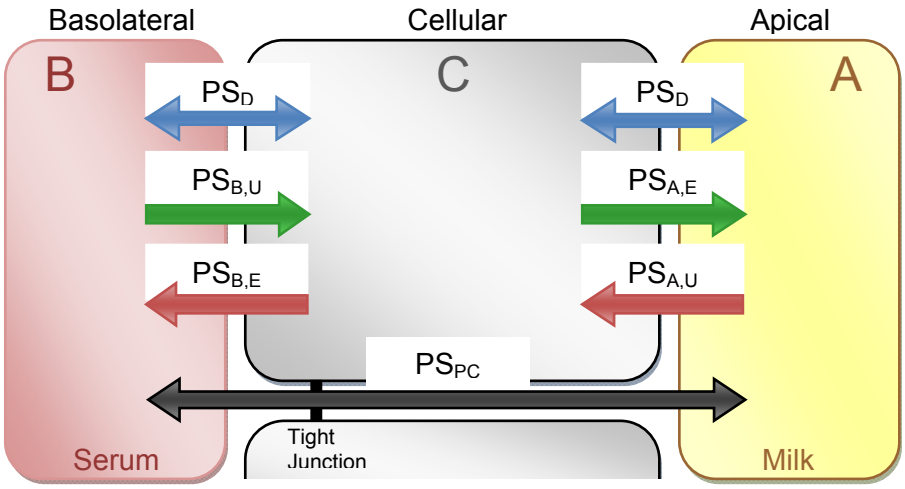

Assuming passive diffusion is equal for the basolateral and apical membranes and ignoring any potential protein binding, ionization, or fat partitioning phenomena, the kinetic model can be described by the following set of equations:

$$\frac{dX_B}{dt} = C_C(PS_D+PS_{B,E}) - C_B(PS_D+PS_{B,U}) + (C_A-C_B)PS_{PC} \qquad \text{Eq. 3-3}$$

$$\frac{dX_C}{dt} = C_A(PS_D+PS_{A,U}) + C_B(PS_D+PS_{B,U}) - C_C(2PS_D+PS_{A,E}+PS_{B,E}) \qquad \text{Eq. 3-4}$$

$$\frac{dX_A}{dt} = C_C(PS_D+PS_{A,E}) - C_A(PS_D+PS_{A,U}) + (C_B-C_A)PS_{PC} \qquad \text{Eq. 3-5}$$

where dX_A/dt, dX_B/dt, and dX_C/dt represent the substrate flux into and out of the apical (A, milk), basolateral (B, serum), and cellular compartments (C, LMEC), respectively; and C_A, C_B, and C_C, represent the substrate concentrations in each compartment. The complete derivations of all equations discussed in this and subsequent sections can be found in Appendix 3.

2. Initial rate: B→A

Assuming initial unidirectional flux into the apical compartment ($C_A = 0$), and rapid equilibration between the B and C compartments such that $dX_C/dt = 0$, B→A flux can be described by:

$$\frac{dX_{A,B\rightarrow A}}{dt} = C_B^0\left[\frac{(PS_D+PS_{B,U})(PS_D+PS_{A,E})}{(2PS_D+PS_{A,E}+PS_{B,E})}+PS_{PC}\right] \qquad \text{Eq. 3-6}$$

In the complete absence of substrate active uptake into or efflux out of the cell ($PS_{B,U}$, $PS_{A,E}$, $PS_{B,E}$, and $PS_{A,U}$ = 0), for example in a parent cell line with no endogenous transporter expression, the relationship collapses to:

$$\left(\frac{dX_{A,B\rightarrow A}}{dt}\right)_{parent} = C_B^0\left[\frac{PS_D}{2}+PS_{PC}\right] \qquad \text{Eq. 3-7}$$

Subsequently, transfection of a single apical efflux transporter into the parent cell line (eg. The MDCKII-ABCG2 cells created in section C), yields the following:

$$\left(\frac{dX_{A,B\rightarrow A}}{dt}\right)_{ABCG2} = C_B^0\left[\frac{(PS_D)(PS_D+PS_{A,E(ABCG2)})}{(2PS_D+PS_{A,E(ABCG2)})}+PS_{PC}\right] \qquad \text{Eq. 3-8}$$

$PS_{A,E(ABCG2)}$ represents the permeability-surface area product attributed to the transfected transporter ABCG2.

3. Initial rate: A→B

Assuming initial unidirectional flux into the apical compartment (C_B = 0), and rapid equilibration between the A and C compartment such that dX_C/dt = 0, A→B flux can be described by:

$$\frac{dX_{B,\,A\rightarrow B}}{dt} = C_A^0\left[\frac{(PS_D+PS_{A,U})(PS_D+PS_{B,E})}{(2PS_D+PS_{A,E}+PS_{B,E})}+PS_{PC}\right] \qquad \text{Eq. 3-9}$$

In the complete absence of substrate active uptake into or efflux out of the cell ($PS_{B,U}$, $PS_{A,E}$, $PS_{B,E}$, and $PS_{A,U}$ = 0), for example in a parent cell line with no background transporter expression, the relationship collapses to:

$$\left(\frac{dX_{B,\,A\rightarrow B}}{dt}\right)_{parent} = C_A^0\left[\frac{PS_D}{2}+PS_{PC}\right] \qquad \text{Eq. 3-10}$$

Subsequently, transfection of a single apical efflux transporter into the parent cell line (eg. The MDCKII-ABCG2 cells created in section C), yields the following:

$$\left(\frac{dX_{B,\,A\rightarrow B}}{dt}\right)_{ABCG2} = C_A^0\left[\frac{(PS_D)^2}{(2PS_D+PS_{A,E(ABCG2)})}+PS_{PC}\right] \qquad \text{Eq. 3-11}$$

4. Apical efflux ratio: ER_A

The apical efflux ratio, ER_A, is defined as the ratio of the initial rate of B→A flux when all active transport processes are not inhibited divided by the initial rate of B→A flux when all active transport processes are inhibited completely:

$$ER_A = \frac{\frac{dX_{A,B\rightarrow A}}{dt}}{\frac{dX_{A,B\rightarrow A}}{dt}_{inhibited}} = \frac{C_B^0\left[\frac{(PS_D+PS_{B,U})(PS_D+PS_{A,E})}{(2PS_D+PS_{A,E}+PS_{B,E})}+PS_{PC}\right]}{C_B^0\left[\frac{PS_D}{2}+PS_{PC}\right]} \quad \text{Eq. 3-12}$$

If we assume permeability-surface area product for passive diffusion is much greater than that for paracellular flux between cells ($PS_D >> PS_{PC}$) or that paracellular flux between cells is negligible ($PS_{PC}\rightarrow 0$), the equation for ER_A can be rearranged to:

$$ER_A = \frac{\frac{dX_{A,B\rightarrow A}}{dt}}{\frac{dX_{A,B\rightarrow A}}{dt}_{inhibited}} = \frac{2(PS_D+PS_{B,U})(PS_D+PS_{A,E})}{PS_D(2PS_D+PS_{A,E}+PS_{B,E})} \quad \text{Eq. 3-13}$$

If the same assumption is made when determining ER_A for transfection of the single apical efflux transporter ABCG2 into the parent cell line with no background endogenous transporter expression (Eq. 3-8 divided by Eq. 3-7), the following relationship results:

$$ER_A = \frac{2[PS_D+PS_{A,E(ABCG2)}]}{2PS_D+PS_{A,E(ABCG2)}} \quad \text{Eq. 3-14}$$

5. Asymmetry efflux ratio: ER_α

The asymmetry efflux ratio, ER_α, is defined as the ratio of the initial rate of B→A flux (Eq. 3-6) divided by the initial rate of A→B (Eq. 3-9):

$$ER_\alpha = \frac{\frac{dX_{A,B\rightarrow A}}{dt}_{ABCG2}}{\frac{dX_{B,A\rightarrow B}}{dt}_{ABCG2}} = \frac{C_B^0\left[\frac{(PS_D+PS_{B,U})(PS_D+PS_{A,E})}{(2PS_D+PS_{A,E}+PS_{B,E})}+PS_{PC}\right]}{C_A^0\left[\frac{(PS_D+PS_{A,U})(PS_D+PS_{B,E})}{(2PS_D+PS_{A,E}+PS_{B,E})}+PS_{PC}\right]} \quad \text{Eq. 3-15}$$

If we assume the initial donor concentrations in the basolateral and apical compartments are equal experimentally ($C_B^0 = C_A^0$), and that PS_{PC} is negligible ($PS_{PC}\rightarrow 0$), the equation can be simplified to:

$$ER_\alpha = \frac{(PS_D+PS_{A,E})(PS_D+PS_{B,U})}{(PS_D+PS_{A,U})(PS_D+PS_{B,E})} \quad \text{Eq. 3-16}$$

Finally, if the same assumption is made when determining ER_α for transfection of the single apical efflux transporter ABCG2 into the parent cell line with no background endogenous transporter expression (Eq. 3-8 divided by Eq. 3-11), the following relationship results:

$$ER_\alpha = \frac{PS_D+PS_{A,E(ABCG2)}}{PS_D} \quad \text{Eq. 3-17}$$

6. Steady-state concentrations in compartments A, B, and C

The steady-state substrate concentrations in compartments A, B, and C (dX_A/dt, dX_B/dt, and $dX_C/dt = 0$) can be determined by rearranging the differential equations Eq. 3-3, Eq. 3-4, and Eq. 3-5 to produce:

$$C_{B,SS} = \frac{C_{A,SS}PS_{PC} + C_{C,SS}(PS_D + PS_{B,E})}{(PS_D + PS_{B,U} + PS_{PC})} \quad \text{Eq. 3-18}$$

$$C_{C,SS} = \frac{C_{A,SS}(PS_D + PS_{A,U}) + C_{B,SS}(PS_D + PS_{B,U})}{(2PS_D + PS_{A,E} + PS_{B,E})} \quad \text{Eq. 3-19}$$

$$C_{A,SS} = \frac{C_{B,SS}PS_{PC} + C_{C,SS}(PS_D + PS_{A,E})}{(PS_D + PS_{A,U} + PS_{PC})} \quad \text{Eq. 3-20}$$

If we assume PS_{PC} is negligible relative to the other processes ($PS_{PC} \rightarrow 0$), equations Eq. 3-18 and Eq. 3-20 for the steady state concentrations in the basolateral and apical compartments can be reduced to Eq. 3-21 and Eq. 3-22, respectively:

$$C_{B,SS} = \frac{C_{C,SS}(PS_D + PS_{B,E})}{(PS_D + PS_{B,U})} \quad \text{Eq. 3-21}$$

$$C_{A,SS} = \frac{C_{C,SS}(PS_D + PS_{A,E})}{(PS_D + PS_{A,U})} \quad \text{Eq. 3-22}$$

Recalling that concentrations in this model are unbound drug, the steady-state ratio of a drug in the apical vs. the basolateral compartment can be determined by dividing $C_{A,SS}$ by $C_{B,SS}$ (Eq. 3-22 by Eq. 3-21). This results in the same asymmetry efflux ratio (ER_α) presented earlier:

$$\frac{C_{A,SS,unbound}}{C_{B,SS,unbound}} = \frac{(PS_D + PS_{A,E})(PS_D + PS_{B,U})}{(PS_D + PS_{A,U})(PS_D + PS_{B,E})} = ER_\alpha \quad \text{Eq. 3-23}$$

7. Relationships to M/S ratio

To extend the model to the in vivo situation, we assume the clearance terms that define the in vivo unbound ratio of the drug at steady state in the milk and serum are comparable to the in vitro permeability-surface area product terms that define the similar ratio in the model (Eq. 3-23), such that:

$$\frac{C_{milk,unbound}}{C_{serum,unbound}} = \frac{(Cl_D + Cl_{A,E})(Cl_D + Cl_{B,U})}{(Cl_D + Cl_{A,U})(Cl_D + Cl_{B,E})} \quad \text{Eq. 3-24}$$

The Passive Diffusion model for drug transfer into breast milk is based on total drug concentrations and provides the following prediction for the M/S ratio:

$$\frac{M}{S}_{\text{in vivo}} \approx \frac{M}{S}_{\text{diffusion}} = \frac{(f_s^{un})(f_s)(W)}{(f_m^{un})(f_m)(Sk)} \qquad \text{Eq. 3-25}$$

where f_s^{un} and f_m^{un} are the fraction of the drug unionized in the serum and milk, respectively; f_s and f_m are the fraction protein bound in the serum and milk, respectively; and W and Sk are the fat partitioning into whole and skim milk, respectively [68]. It assumes that the ratio of unbound concentrations in the milk and serum are equal ($C_{milk,unbound} = C_{serum,unbound}$) and suggests that M/S ratio observed in vivo is governed by protein binding and ionization in the milk, and serum and partitioning into milk fat. If active processes exist, $C_{milk,unbound}$ would not equal $C_{serum,unbound}$ and another component would need to be added to the prediction to account for differences in these unbound concentrations.

$$\frac{M}{S}_{\text{in vivo}} = \left[\frac{C_{milk,unbound}}{C_{serum,unbound}}\right]\left[\frac{(f_s^{un})(f_s)(W)}{(f_m^{un})(f_m)(Sk)}\right] \qquad \text{Eq. 3-26}$$

Replacing the unbound ratio in the milk and serum at steady state with the clearance terms that govern that ratio (Eq. 3-24) allows the incorporation of active processes to put forth a new in vivo conceptual model:

$$\frac{M}{S}_{\text{in vivo}} = \left[\frac{(Cl_D+Cl_{A,E})(Cl_D+Cl_{B,U})}{(Cl_D+Cl_{A,U})(Cl_D+Cl_{B,E})}\right]\left[\frac{(f_s^{un})(f_s)(W)}{(f_m^{un})(f_m)(Sk)}\right] \qquad \text{Eq. 3-27}$$

It also suggests that it may be possible to predict the in vivo M/S ratio using in vitro ER_α determinations and simple in vitro measurements of protein binding, ionization potential, and skim to whole milk partitioning:

$$\frac{(Cl_D+Cl_{A,E})(Cl_D+Cl_{B,U})}{(Cl_D+Cl_{A,U})(Cl_D+Cl_{B,E})} \approx \frac{(PS_D+PS_{A,E})(PS_D+PS_{B,U})}{(PS_D+PS_{A,U})(PS_D+PS_{B,E})} \qquad \text{Eq. 3-28}$$

$$\frac{M}{S}_{\text{in vivo}} = \left[\frac{(PS_D+PS_{A,E})(PS_D+PS_{B,U})}{(PS_D+PS_{A,U})(PS_D+PS_{B,E})}\right]\left[\frac{(f_s^{un})(f_s)(W)}{(f_m^{un})(f_m)(Sk)}\right] \qquad \text{Eq. 3-29}$$

$$\frac{M}{S}_{\text{in vivo}} = ER_\alpha\left[\frac{(f_s^{un})(f_s)(W)}{(f_m^{un})(f_m)(Sk)}\right] \qquad \text{Eq. 3-30}$$

8. Application of the model

The theoretical limits of the initial B→A and A→B rates and efflux ratios with increasing $PS_{A,E(ABCG2)}$ and PS_D were simulated to gain a greater understanding of the

model. Apparent permeability data from the published literature as well as generated through this dissertation work were analyzed to examine the applicability of this kinetic model to experimental data. Graphed flux data from all publications using two different cell lines (MDCKII transfected with either Abcg2 or ABCG2) created by the lab of Dr. Alfred Schinkel was gathered for calculation of the apical efflux ratio (ER_A) and the asymmetry efflux ratio (ER_α) in an external data set [53,91,93,127-129,152,153,173]. The flux of each drug per unit time, expressed as a percentage of initial donor mass, was extracted from each graph and linear regression was used to determine a flux rate using methods previously described. Efflux ratios were then generated from the external data sets and are presented as a single value as only mean permeabilities were available in the literature. The ER_A and the ER_α for nitrofurantoin, PhIP, cimetidine, ciprofloxacin, and methotrexate in the MDCKII-ABCG2 model system created in Section C (Specific Aim 5) were also determined. As each condition in each experiment was performed in triplicate and the resulting individual permeabilities used in the calculations of the efflux ratios were unmatched, the mean and standard deviation of these ratios were calculated by determining all efflux ratios possible from the experimental data (eg. n=3 ABCG2 B→A and n=3 Empty B→A ABCG2 observations yields nine possible ER_A values). The simulations and efflux ratios were then used to provide some guidance as to which efflux ratio (eg. ER_A, ER_α) is a better experimental measurement of apical efflux attributed to ABCG2 ($PS_{A,E(ABDG2)}$) in flux assays.

Experimental constraints for the model were then considered. The assumption that there exists no other active flux processes in the parent cell line and that the permeability-surface area product for diffusion is much greater than that of paracellular flux ($PS_D >> PS_{PC}$) were challenged.

Finally, correlations were conducted to gain a greater understanding of the relationships between in vitro efflux ratios and in vivo M/S ratios. Pearson's Correlations between various efflux ratios (measurements of the ABCG2/Abcg2-mediated efflux in the in vitro model system) and the ratio of the M/S in a wild-type mouse vs. that of the Abcg2 knockout animal (an in vivo estimation of the M/S attributed to Abcg2) were also performed and the correlation coefficients (r) reported (GraphPad Prism 5.0, San Diego, CA). To illustrate any possible relationship between the variables graphically, orthogonal (Deming) regression (GraphPad Prism 5.0, San Diego, CA) was also performed to generate the best-fit line as both variables are independent. Despite the use of all possible combinations of the unmatched permeabilities to generate an

estimate of the “true” mean and standard deviation of each efflux ratio, it would not be appropriate to use all these datapoints in the correlation as the experiment was truly only performed in triplicate. Therefore, correlations were performed using these estimates of the mean and standard deviation with a sample size of three for each experiment.

E. Microarray expression profiling of transporter gene expression in murine developmental datasets

1. Developmental datasets

Microarray analysis was used to identify murine xenobiotic transporters that were differentially expressed during lactation. The published literature and NCBI Gene Expression Omnibus (http://www.ncbi.nlm.nih.gov/projects/geo/) were searched and three existing datasets found. The work by Stein el al, Clarkson et al, and Medrano et al. captured gene expression in the mammary gland at various time points during development, but none specifically focused on xenobiotic transporters and lactation [174-176]. Stein et al. provided the most robust set of data with one Balb/C mouse used per chip and 3 chips (biological replicates) per time point. The murine developmental time points available from this study included virgin weeks 10 and 12; pregnancy day 1, 2, 3, 8.5, 12.5, 14.5, and 17.5; lactation day 1, 3, and 7; and involution day 1, 2, 3, 4, and 10. Clarkson et al. included 3 C57/Bl/6 mice per chip and 2 chips (biological replicates) per time point. The 12 stages of adult mammary gland development included virgin week 8; gestation day 5, 10, and 15; lactation day 0, 5, and 10; and 12, 24, 48, 72, and 96 hours after forced weaning. Medrano included one C57 mouse per chip and variable number of chips at each time point: 3 virgin at 6 weeks, 2 at pregnancy day 14, 2 at lactation day 10, and 2 at involution day 4. Stein et al. and Clarkson et al. specifically noted removing the lymph nodes from the whole mammary gland during excision.

2. Data and statistical analysis

Data from all 17 time points of the Stein et al. dataset were obtained in the form of a tab-delineated file containing detection calls, normalized MAS5 signal data, gene symbols, and annotations from all 12488 probesets of the GeneChip® Mu74v2A Array (Affymetrix, Santa Clara, CA). The Clarkson et al. and Medrano et al. data was obtained as raw .cel files and were analyzed by the Expression Console 1.1 (Affymetrix, Santa Clara, CA) software using the MAS5 algorithm normalizing to a target intensity of 100.

This analysis scheme was chosen to replicate that used by Stein et al. for comparison purposes. Stein et al. data from virgin mice at weeks 10 and 12 (6 chips), Clarkson et al. data from virgin mice at 8 weeks (2 chips), and Medrano et al. data from virgin mice at 6 weeks (3 chips) were grouped into a "nonlactating" group. Similarly, Stein et al. data from lactation day 1, 3, and 7 (9 chips), Clarkson et al. data from lactation day 5 and 10 (4 chips) and Medrano data from lactation day 10 (2 chips) were grouped into a "lactating" group.

In order to decrease the number of comparisons made several filtering approaches were used. In the detection call, a one-sided Wilcoxon Signed Rank test performed within MicroArray Suite 5.0 (Affymetrix, Santa Clara, CA) during original analysis, the hybridization signal from each probe set was designated as being Present, Marginal or Absent. Signal intensity data for probesets identified as Absent in all 15 arrays in the lactating group were removed from the analysis. To further decrease the likelihood of false positives from multiple comparisons, two approaches to filter for probesets representing only xenobiotic transporters were explored. In the first, gene symbols of the transporter families Abc(A-G), Slc(1-43), and Slco were retrieved from Entrez Gene (search date: 1/9/07). The 395 hits were then submitted to Affymetrix NetAffyx™ Analysis Center (http://www.affymetrix.com/analysis/) to determine which could be detected by the Mu74v2 GeneChip® array set. Two hundred probeset IDs were returned by the query, with the majority detecting transcripts that had no known role in xenobiotic transport. The second filtering approach (the method eventually chosen) used the published literature to establish a list of genes with a proposed role in xenobiotic transport. This list of genes of interest was built by first combining the human gene symbols analyzed in three comprehensive surveys of transporter gene expression in various tissues by Alcorn et al, Calcagno et al, and Bleasby et al. [49,104,177]. Mouse homologs of these genes were then identified using NCBI Entrez Gene (http://www.ncbi.nlm.nih.gov/sites/entrez?db=gene) and NCBI Homologene (http://www.ncbi.nlm.nih.gov/sites/entrez/query.fcgi?db=homologene). These fifty-two genes from the ABCA, ABCB, ABCC, ABCG, SLC6, SLC10, SLC15, SLC16, SLC17, SLC22, SLC23, SLC 28, SLC29, SLC6, and SLCO families with potential relevance for xenobiotic transport were finally submitted to NetAffyx™, resulting in only 32 probeset hits (Table 3-2). Unfortunately, even though many of the genes of interest could be detected by the entire array set, few were on chip A, the only chip run by these three research groups [174-176].

Table 3-2: Human and mouse transporter genes of interest and number of probesets available for each on the U133 plus 2.0 and Mu74v2A GeneChips®.

Human			Mouse	
Common Name	Gene Symbol	Number of probesets on U133 plus 2.0	Gene Symbol	Number of probesets on Mu74v2A
ABC2	ABCA2	3	Abca2	1
ABC-C	ABCA3	1	Abca3	0
MDR1	ABCB1	2	Abcb1a	1
MDR3	ABCB4	3	Abcb4	1
BSEP	ABCB11	2	Abcb11	0
MRP1	ABCC1	2	Abcc1	1
MRP2	ABCC2	1	Abcc2	1
MRP3	ABCC3	6	Abcc3	1
MRP4	ABCC4	5	Abcc4	0
MRP5	ABCC5	3	Abcc5	1
MRP6	ABCC6	2	Abcc6	1
MRP7	ABCC10	2	Abcc10	0
MRP8	ABCC11	2	--	
MRP9	ABCC12	2	Abcc12	0
BCRP	ABCG2	1	Abcg2	1
OSTalpha	OSTalpha	1	Osta	1
NTCP	SLC10A1	1	Slc10a1	3
ASBT	SLC10A2	1	Slc10a2	1
PEPT1	SLC15A1	2	Slc15a1	0
PEPT2	SLC15A2	3	Slc15a2	1
MCT1	SLC16A1	5	Slc16a1	1
MCT2	SLC16A7	3	Slc16a7	1
NaPiI	SLC17A1	5	Slc17a1	2
OCT1	SLC22A1	1	Slc22a1	1
OCT2	SLC22A2	1	Slc22a2	1
OCT3	SLC22A3	3	Slc22a3	0
OCTN1	SLC22A4	2	Slc22a4	1
OCTN2	SLC22A5	1	Slc22a5	1
OAT1	SLC22A6	3	Slc22a6	1
OAT2	SLC22A7	5	Slc22a7	0
OAT3	SLC22A8	2	Slc22a8	0
UST3	SLC22A9	2	Slc22a19	0
OAT4	SLC22A11	1	--	
URAT1	SLC22A12	1	Slc22a12	1
SVCT1	SLC23A1	1	Slc23a1	1
SVCT2	SLC23A2	4	Slc23a2	1

Table 3-2 cont.

Human			Mouse	
Common Name	Gene Symbol	Number of probesets on U133 plus 2.0	Gene Symbol	Number of probesets on Mu74v2A
CNT1	SLC28A1	4	Slc28a1	0
CNT2	SLC28A2	2	Slc28a2	0
CNT3	SLC28A3	1	Slc28a3	0
ENT1	SLC29A1	2	Slc29a1	2
ENT2	SLC29A2	5	Slc29a2	1
ENT3	SLC29A3	1	Slc29a3	0
ENT4	SLC29A4	1	Slc29a4	0
ATB(0+)	SLC6A14	1	Slc6a14	0
OATP-A	SLCO1A2	3	Slco1a4	0
OATP-C	SLCO1B1	1	--	
OATP-8	SLCO1B3	1	Slco1b2	0
OATP-F	SLCO1C1	1	Slco1c1	0
PGT	SLCO2A1	1	Slco2a1	0
OATP-B	SLCO2B1	3	Slco2b1	0
OATP-D	SLCO3A1	3	Slco3a1	1
OATP-E	SLCO4A1	3	Slco4a1	0
OATP-H	SLCO4C1	1	Slco4c1	0
OATP-J	SLCO5A1	1	Slco5a1	1
OATP-I	SLCO6A1	1	Slco6b1	0

The first analysis performed was a test of the signal concordance within and between chips of each group to gauge overall variability of the samples as they originated from different mouse strains in experiments performed by three separate research groups. It was evaluated using Pearson's correlations to compare the signal values generated by the MAS5 algorithm.

Next, to determine which genes in the filtered list were differentially expressed, individual t-tests were performed on the 32 probesets to compare signal intensity in lactating versus nonlactating arrays; a p-value < 0.05 considered significant. The calculated fold change, the ratio of the mean signal intensity from a given probeset on the lactating arrays (n=15) to the signal intensity of the nonlactating arrays (n=11), was reported.

As multiple testing is performed in microarray analysis, false positives are of concern. Although there are several different methods available to adjust the p-value downwards to some arbitrary level in attempts to protect against this problem, it is

unclear how strict one needs to be. To maintain the greatest sensitivity and not "miss" potential transporters of interest, the alpha was maintained at 0.05; it was understood that this approach may lead to a higher rate of false positives.

F. Identification of xenobiotic transporters highly expressed in human LMEC and MEC clinical samples

1. Tissue sources and subject selection

Patient surgical reduction mammoplasty specimens served as the source of MECs. UK Surgical Pathology and the UK Tissue Procurement Service provided three anonymized mammary tissue samples under a local Institutional Review Board (IRB) approved protocol. Each specimen was comprised of resected mammary tissue from the left and right breasts that was declared histologically normal per Attending Pathologist reports. Samples were immediately stored in RPMI 1640 media containing 5% FBS, 100 U/mL penicillin, and 100 µg/mL streptomycin at 4ºC for later processing.

Human breast milk served as the source of LMECs and was obtained fresh from three healthy lactating volunteers utilizing the UK General Clinical Research Center facilities under an IRB-approved protocol. Exclusion criteria included: clinically significant cardiovascular, gastrointestinal, renal, hepatic, pulmonary, or hematological disease; a history of cerebral trauma; tobacco use within two years; consumption of caffeine or alcohol within 48 h; or any medication usage (other than prenatal vitamins, analgesics, or antihistamines) within 7 days of a study visit. Subjects were specifically asked if they were taking any oral contraceptives. Volunteers provided up to eight ounces of breast milk each visit (up to 16 visits) using the provided breast pump (Lactina® Select, Medela, McHenry, IL) and a sterile collection apparatus. Each sample was immediately put on ice and was processed through RNA isolation individually. RNA samples from the same patient were eventually pooled for microarray expression profiling.

2. Heterogeneous single cell suspensions from reduction mammoplasty tissue

All histologically normal reduction mammoplasty specimens were processed fresh (within 6 hours of procedure), processed to breast organoids, and frozen at -80°C until all samples had been collected according to published methods [49,178]. Briefly, skin and fat was excised from each specimen using two opposing scalpel blades and

resulting tissue was minced into < 0.5 cm cubed pieces (Figure 3-3). The minced tissue was transferred to 50 mL conical vials and “digestion media” (RPMI 1640 containing 5% FBS, 100 U/mL penicillin, 100 µg/mL streptomycin, 1 mg/mL hyaluronidase, 1 mg/mL collagenase) was added leaving 5 mL of air in the tube for mixing purposes. Following an overnight incubation at 37ºC on a rotating mixer (Dynal, New Hyde Park, NY), organoids were pelleted by centrifugation at 300 *g* for 5 min at 4ºC and the entire supernatant (containing the fat layer) was discarded. Organoids were then washed three times with RPMI 1640 containing 5% FBS, 100 U/mL penicillin, and 100 µg/mL streptomycin at 37ºC. To remove red blood cells, organoids were allowed to sediment from the 30 mL of the same media for 30 minutes. The supernatant was carefully removed and the procedure was repeated two more times. Finally, “cell preservation media” (RPMI 1640 containing 15% FBS and 10% DMSO) was added and organoids were aliquoted and frozen at -80ºC (by cooling at -1ºC/min in a Mr. Frosty®, Nalgene, Rochester, NY) until all subject recruitment had been completed.

Figure 3-3: Photo of reduction mammoplasty specimen with fat excised.

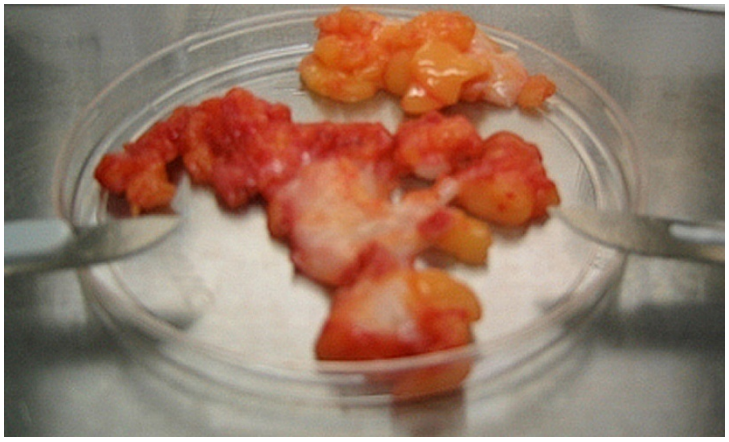

To achieve heterogeneous single-cell populations, thawed samples were washed once with cold RPMI containing 1% FBS, once with cold HBBS (containing no calcium or magnesium), and then digested by gentle pipetting in 10 mL 0.25% trypsin/EDTA containing 0.4 mg/mL DNAse 1 at 37°C for 5-15 minutes until no clumps were observed. The digestion was stopped by the addition of 5 mL cold RPMI containing 5% FBS and the mixture was further diluted with 10 mL cold HBSS (containing no calcium or magnesium), 2% FBS, and 1 mM EDTA. Overall cell yield was increased significantly with the addition of a second 10 min incubation with 5 mL HBSS containing 0.4 mg/mL DNAse to decrease cell clumping. This second digestion step was stopped by the

addition of cold HBSS (containing no calcium or magnesium) containing 2% FBS and 1 mM EDTA. Finally, a heterogeneous single cell suspension was achieved by filtering through a 40-μm cell strainer and was counted on a hemocytometer. A small volume of this cell suspension was saved for immunocytostaining.

3. Heterogeneous single cell suspensions from breast milk

Milk samples were centrifuged in 50 mL conical polypropylene vials at 600 *g* for 15 min. The fat layer was removed with a spatula and the remaining milk layer was aspirated with a pipette. The resulting cell pellets were washed twice with 30 mL cold HBSS (containing no calcium or magnesium), 2% FBS, and 1 mM EDTA, pooled, and filtered through a 40-μm cell strainer to yield a single cell suspension. The resulting heterogeneous population of cells was counted on a hemocytometer and a small volume was saved for immunocytostaining.

4. Luminal MEC isolation by immunomagnetic separation

Immunomagnetic separation was evaluated as a methodology to isolate a pure population of luminal MECs from the heterogeneous single cells suspension in sufficient numbers for subsequent microarray analysis. The method previously developed by Alcorn et al. used magnetic Dynabeads® coated with a primary antibody for epithelial basement membrane antigen (MUC1) (clone MFGM/5/11[ICR.2]), a surface marker specific to MECs, to isolate cells for qPCR [49]. This technique, although specific, was not robust enough to provide the quantity of cells needed for microarray analysis and another system had to be developed.

The EasySep® human MUC1 selection kit was tested with breast milk samples. The system consists of magnetic iron dextran nanoparticles conjugated to a different MUC1 antibody (clone 214D4) via a novel tetrameric antibody complex (Figure 3-4). Single cell suspensions derived from breast milk were blocked with cold 2% human serum in HBSS containing 2% FBS for 15 min. Cells were then pelleted by centrifugation, resuspended in HBSS containing 2% FBS at a concentration of 1 x 10^8 per milliliter and processed according to manufacturer protocol. Isolated populations were counted on a hemocytometer and purity was assessed by flow cytometry through quantification of the nanoparticle-MEC complexes with 5 μg/mL FITC-conjugated anti-dextran antibody vs. isotype control. A small volume was also saved for cytospin preparations and immunocytostaining.

Figure 3-4: Schematic drawing of EasySep® magnetic labeling of human cells [179].

The anti-cell antibody used was a murine anti-MUC1 (clone 214D4). Purity of the resulting populations was quantified by detection of the nanoparticle-cell complexes with an antibody directed against the nanoparticle (not shown in diagram).

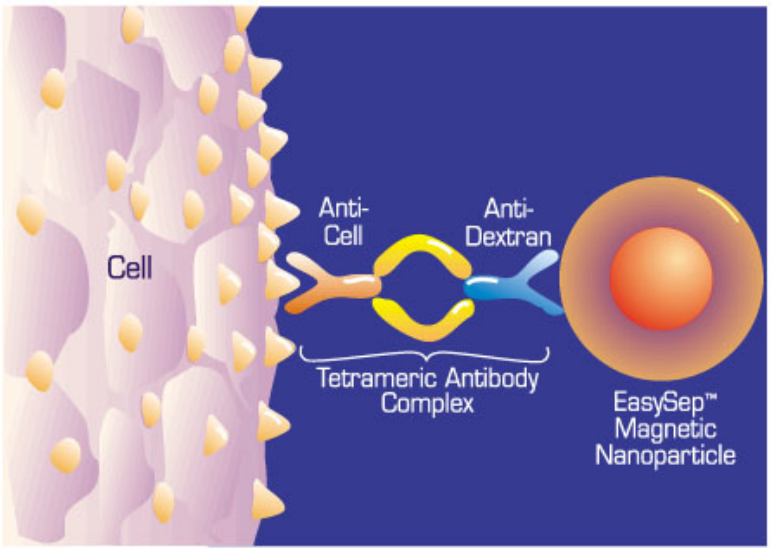

5. Luminal MEC isolation by FACS

FACS was also evaluated as a technique to isolate luminal MECs in sufficient numbers from the heterogeneous single cell suspension. Again, the MEC-specific surface expression of EMA/MUC1 was probed, but this time using the original EMA/MUC1 antibody (MFGM/5/11[ICR.2]) and protocols modified from the literature [49,178,180-182]. Single cell suspensions derived from breast milk and reduction mammoplasty specimens were blocked with cold 2% human serum in HBSS containing 2% FBS and 1 mM EDTA for 15 min. Cell pellets were then stained with a monoclonal rat anti-human epithelial basement membrane antigen IgG2a antibody or isotype control for 20 min on ice. Followed a wash with HBSS containing 2% FBS and 1 mM EDTA, luminal mammary epithelial cells were visualized using a secondary FITC-conjugated mouse anti-rat IgG2a. MUC1 positive and negative populations were identified utilizing the isotype control antibody and were sorted into HBSS containing 10% FBS. Due to the large numbers of dead cells in the previously frozen reduction mammoplasty samples, the addition of propidium iodide before FACS was found useful to exclude presumed nonviable cells from the analysis (as described on page 37). Isolated populations were counted with a hemocytometer and a small volume was saved for cytospin preparations and immunocytostaining.

6. Immunocytostaining

Cytospins of each cell population (approximately 1 x 10^5 cells) were made using the Shandon Cytospin 3 cytocentrifuge (IMEB, San Marcos, CA). Preparations were then air dried and fixed with alcohol. Slides were stained at the UK Cytology Department using the Vectastain ABC kit and a monoclonal mouse anti-human (IgG1) cytokeratin cocktail CK22 (40-68 kDa) specific for simple epithelial cells to verify purity of the sorted populations.

7. RNA isolation

RNA was immediately isolated from purified luminal mammary epithelial cells following FACS using the RNeasy Micro kit per manufacturer's protocol including sample homogenization and on-column DNA digestion and quantified as described on page 28. Resulting RNA quality was further tested using the Bioanalyzer 2100 (Agilent, Santa Clara, CA) at the UK Microarray Core Facility. RNA from breast milk samples obtained from the same patient was pooled to achieve the 2.5 µg necessary for microarray analysis (~1.5 µg) and qPCR validation (~1 µg). Although final elution from the RNeasy columns was performed with only 14 µL of water, pooled samples were still too dilute for microarray analysis and qPCR and were evaporated in a vacuum centrifuge to a concentration of least 100 ng/mL prior to subsequent procedures.

8. Microarray expression profiling and statistical analysis

Isolated total RNA (1 - 1.5 µg) from the three MEC samples and three LMEC samples were used for probe generation and hybridization to Human Genome U133 Plus 2.0 Arrays (Affymetrix, Santa Clara, CA) at the UK Microarray Core Facility. Each GeneChip® array contains probesets for about 47,000 transcripts and variants representing 38,500 well-characterized genes and expressed sequence tags (ESTs) in the human genome. For comparison of transporter gene expression in LMEC versus other secretory tissues, an external dataset needed to be identified. The microarray data repositories EMBL-EBI ArrayExpress (http://www.ebi.ac.uk/arrayexpress), NCBI Gene Expression Omnibus (http://www.ncbi.nlm.nih.gov/projects/geo/), and the published literature were searched for experiments containing healthy human liver and kidney data from the same U133 Plus 2.0 arrays. Suitable raw chip data was obtained from the ArrayExpress repository experiment E-AFMX-11 (http://www.ebi.ac.uk/

arrayexpress/experiments/E-AFMX-11) in which six mixed male and female healthy liver and kidney samples were analyzed [183].

Following hybridization of the LMEC and MEC samples, expression level was determined with MicroArray Suite 5.0 (Affymetrix, Santa Clara, CA). The microarray data from all 18 arrays were analyzed in unison and scaled to the same threshold to normalize for variances in chip intensity. As described in the mouse microarray expression profiling section on page 47, the first analysis performed was a test of the signal concordance within and between chips of each group to gauge overall variability of the samples. Next, signal intensity data for probesets identified as Absent across all LMEC arrays were removed from the analysis. As before, to decrease the likelihood of false positives, two approaches to filter for probesets representing xenobiotic transporters were explored. In the first, gene symbols of the transporter families ABC(A-G), SLC(1-43), and SLCO were retrieved from Entrez Gene (search date: 1/9/07). The 417 hits were then submitted to Affymetrix NetAffyx™ Analysis Center (http://www.affymetrix.com/analysis/) to determine which could be detected by the U133 Plus 2.0 GeneChip® array. Eight hundred and ninety probeset IDs (often more than 1 for a transcript) were identified with the majority again detecting transcripts that had no known role in xenobiotic transport. In the second filtering approach (the method eventually chosen), the fifty-five genes with potential relevance for xenobiotic transport identified from the literature (as described on page 47) were submitted and resulted in 122 probesets that spanned every gene of interest (Table 3-2).

In order to determine transporters of potential importance for xenobiotic transport in LMEC, a two step screening paradigm was designed (Figure 3-5). In the first, individual t-tests were performed on the 122 probesets to compare signal intensity in LMEC versus MEC arrays; a p-value < 0.05 was considered significant. Those transporter genes whose expression was significantly upregulated during lactation were of interest whereas those significantly downregulated were not. The transporter probeset comparisons that did not achieve significance were not discarded as similar gene expression in LMEC and MEC cells could still be of importance if that expression level was high. To determine that relative expression level, it was compared to the expression level in two other secretory tissues, the kidney and liver. T-tests were again performed and probesets with a signal intensity equivalent to, or significantly higher than each comparator were identified.

Figure 3-5: Microarray analysis screening paradigm for identifying human transporters potentially responsible for drug accumulation in breast milk.

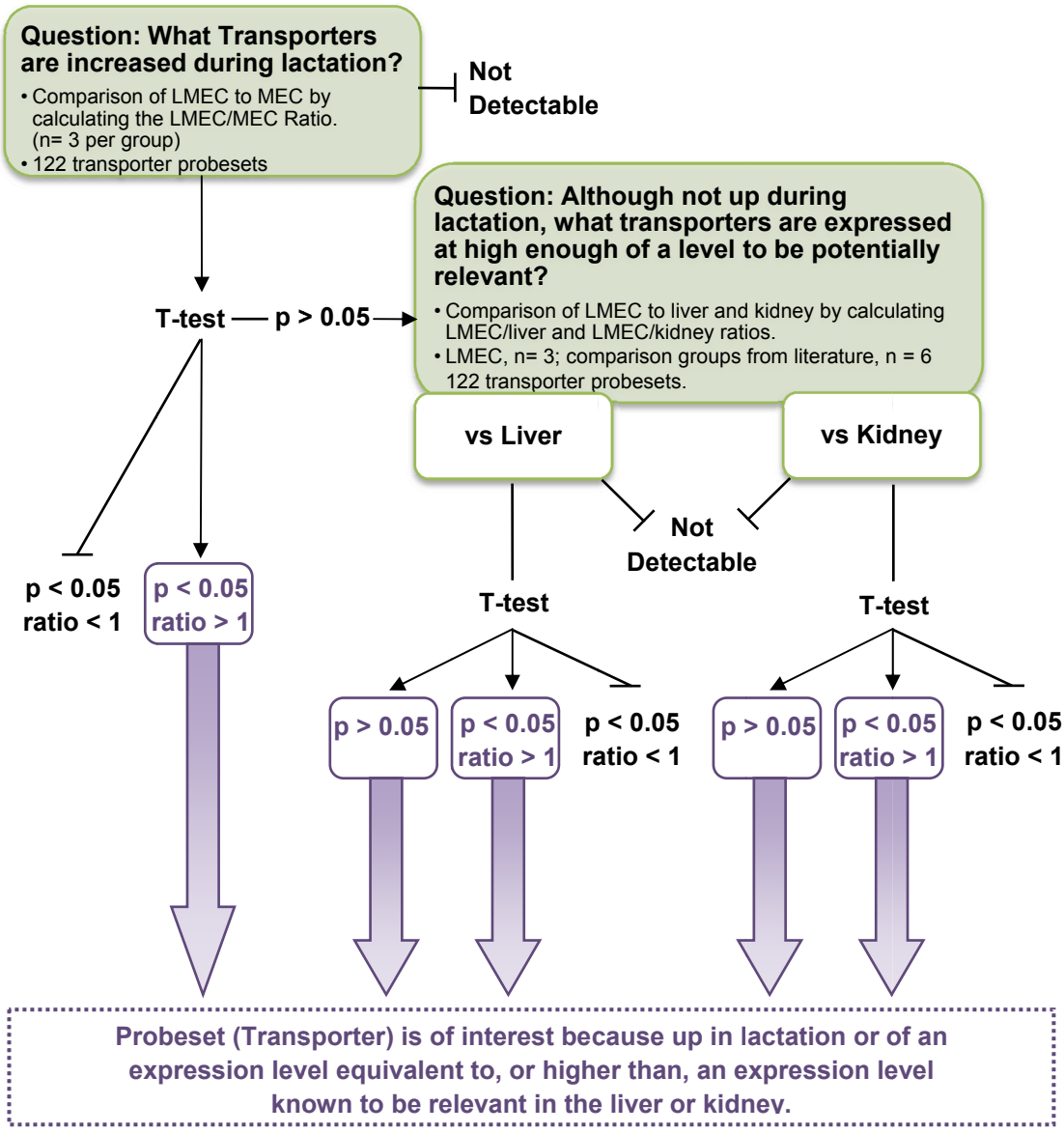

9. qPCR

Reverse-transcription and qPCR analysis of SLCO4C1 and the human milk protein β-casein (CSN2) were performed as described with CIT3 cells on page 28. To validate the expression level relative to the liver and kidney performed in the microarray analysis, total RNA pooled from 250 subjects that was previously purchased from Clonetech (Mountain View, CA) was used. These kidney and liver RNA comparators were exactly the same samples that were measured by Alcorn et al. [49]. One microgram of total RNA from each sample was added to the reaction and all samples to be compared were run together using master mixes to limit potential sources of variation.

Gene-specific primer sequences for SLCO4C1 and CSN2 were designed, optimized, and expression level detected in the samples as described previously. Reference accession numbers, primer sequences, and product sizes are provided in Table 3-3. RNA from cells isolated from breast milk samples pooled from several subjects was used to generate the standard curves.

Table 3-3: Human primers and conditions.

Gene	Reference Sequence	Forward Primer (5'→3') / Reverse Primer (5'→3')	Prod. Size (bp)	Mg Conc (mM)	Anneal Temp (ºC)	Ref.
CSN2	NM_001891	AAGGGAGACCATAGAAAGCCT	138	3.5	62	-
		GGCTGGAAAGAGGGGTAGATTT				
SLCO4C1	NM_180991	GAGAAGCTCCGGTCACTGTC	149	3.5	62	-
		ACTACAATACCTTGCGTGAC				

CHAPTER 4: Results

A. Expression and functional role of Abcg2 in CIT3 cells

1. Specific Aim 1: To determine if Abcg2 is detectable in CIT3 cells with and without lactogenic hormone stimulation

qPCR was performed to determine if transcripts for Abcg2 could be detected in CIT3 cells and if expression was increased following lactogenic hormone stimulation. The milk proteins β-casein and α-lactalbumin, were used as positive controls and mammary gland from a lactating CD1 mouse 7 days post-partum was used as the comparator for relative quantification (to generate the standard curves). Quality of the primer pairs used for the quantification of each gene was demonstrated by correlation coefficients > 0.99, PCR efficiencies of 95-100%, and single products on the melt curve analysis and agarose gel electrophoresis (Figure 4-1, Figure 4-2, Figure 4-3, Figure 4-4). Figure 4-5 depicts the β-actin normalized RNA expression level in CIT3 cells with and without hormone stimulation run in triplicate. β-casein and α-lactalbumin were significantly upregulated following 4 days of lactogenic hormone stimulation (3 μg/mL ovine prolactin and 3 μg/mL hydrocortisone added, epidermal growth factor removed). Abcg2 was detected, but the RNA expression was not significantly increased. The expression level in CIT3 cells (unstimulated or stimulated) was lower than that of in vivo mouse mammary gland comparator.

Figure 4-1: Mouse β-casein amplification curve, melt curve analysis, standard curve, and agarose gel electrophoresis generated from standards over a 6-$\log_{10}$ dilution series.

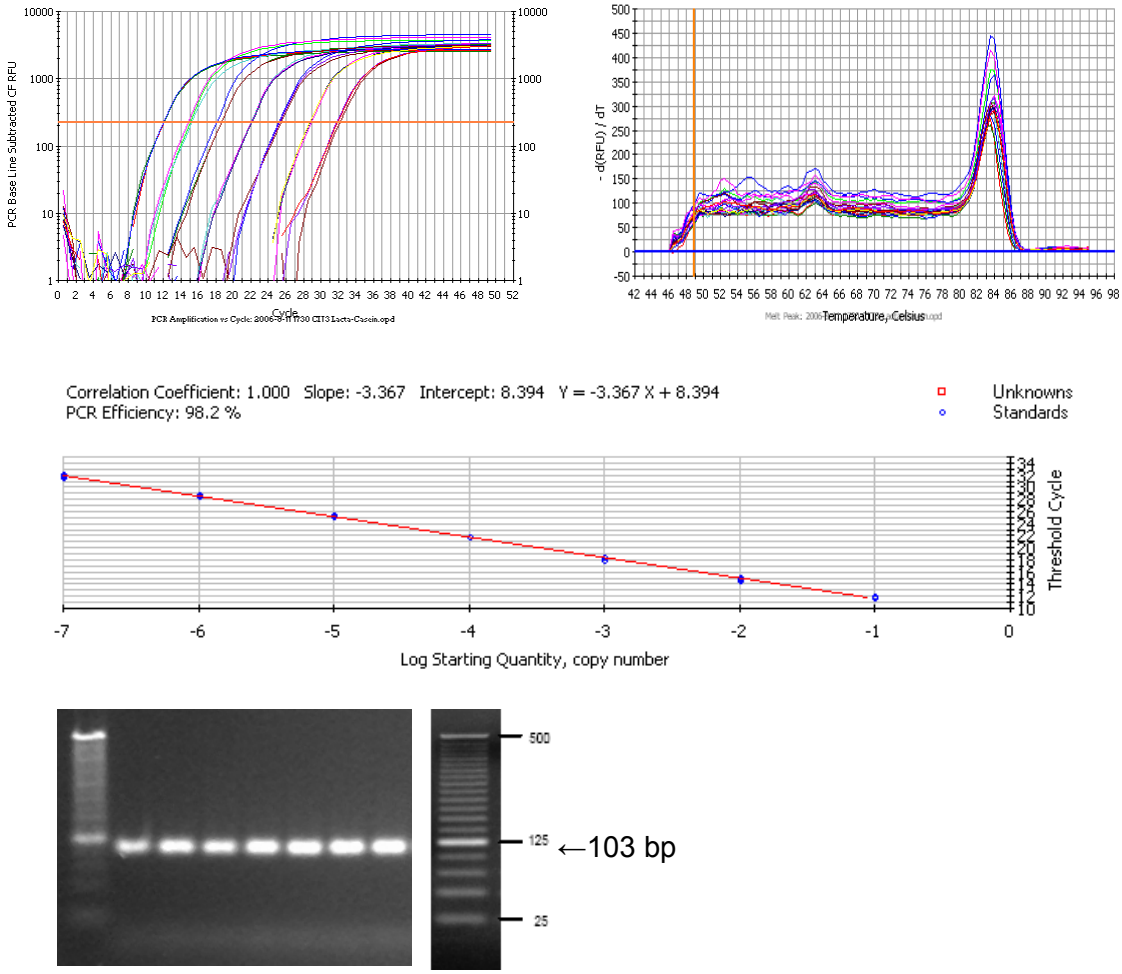

Figure 4-2: Mouse α-lactalbumin amplification curve, melt curve analysis, standard curve, and agarose gel electrophoresis generated from standards over a 5-$\log_{10}$ dilution series.

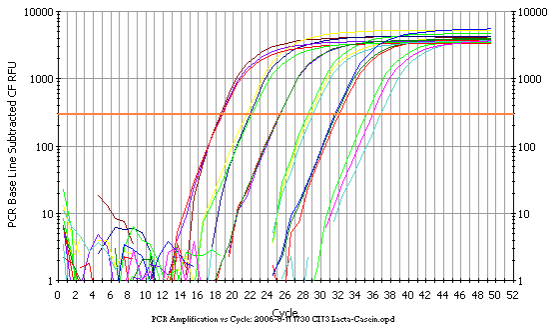

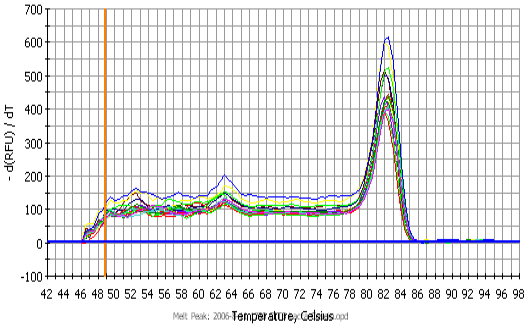

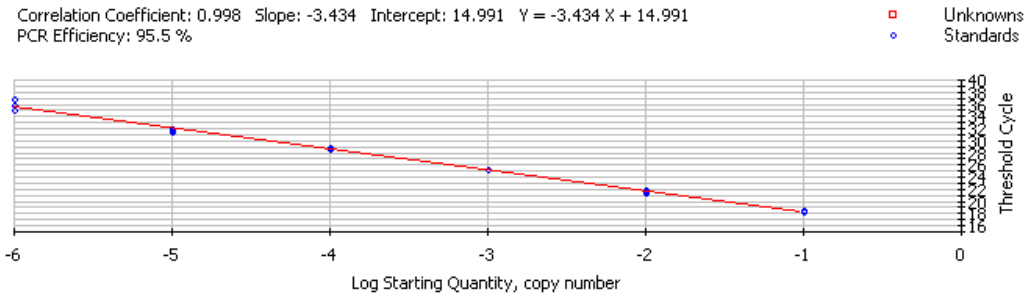

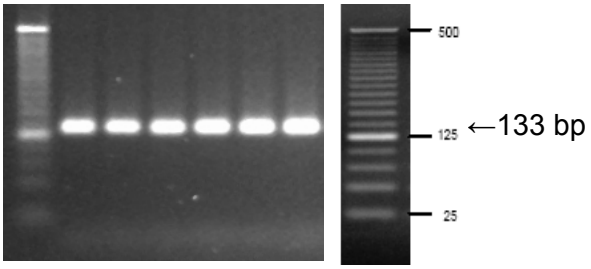

Figure 4-3: Mouse Abcg2 amplification curve, melt curve analysis, standard curve, and agarose gel electrophoresis generated from standards over a 3-$\log_{10}$ dilution series.

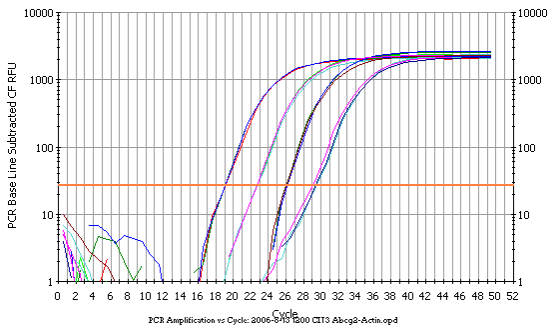

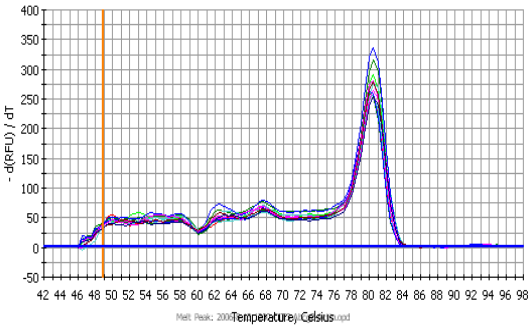

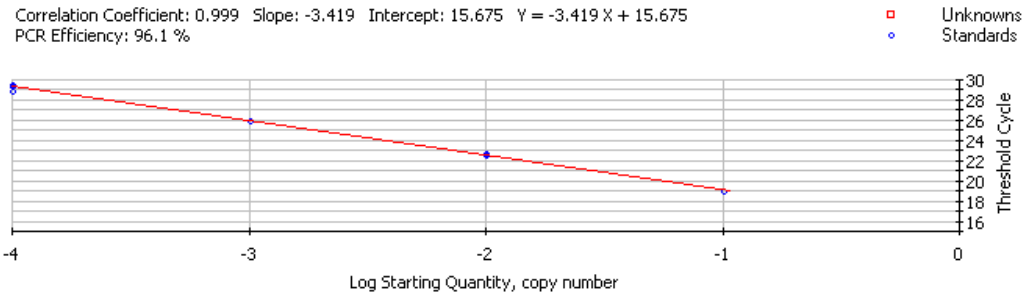

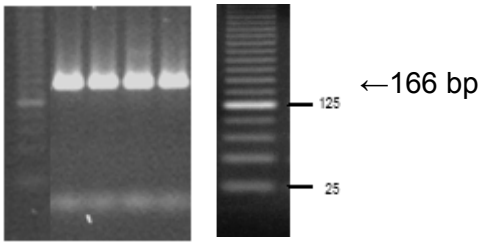

Figure 4-4: Mouse β-actin amplification curve, melt curve analysis, standard curve, and agarose gel electrophoresis generated from standards over a 2-$\log_{10}$ dilution series.

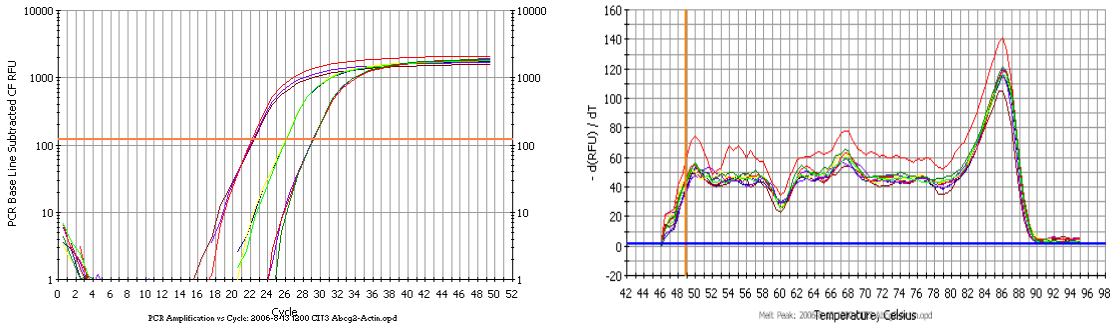

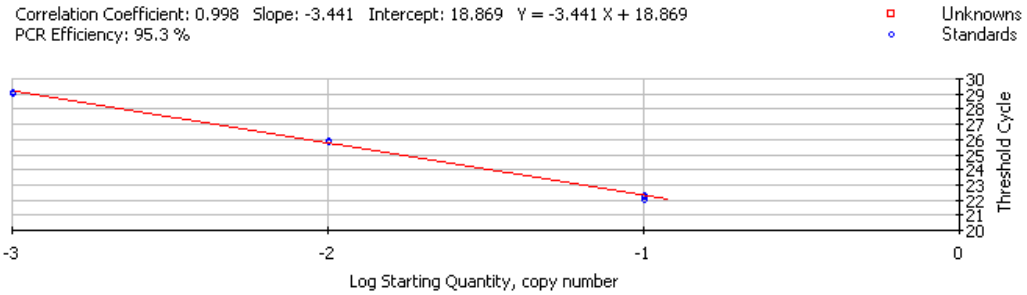

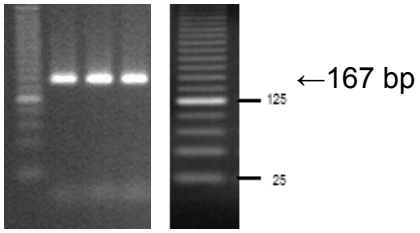

Figure 4-5: Relative RNA expression of β-casein, α-lactalbumin, and Abcg2 in unstimulated CIT3 cells and CIT3 cells following 4 days of lactogenic hormone stimulation.

Murine lactating mammary gland was used for generation of standard curves (Abcg2: $10^{-1} \rightarrow 10^{-4}$, β-casein: $10^{-1} \rightarrow 10^{-7}$, α-lactalbumin: $10^{-1} \rightarrow 10^{-6}$, and β-actin: $10^{-1} \rightarrow 10^{-3}$) and all samples were prepared at a 1:10 dilution. An asterisk denotes $p < 0.05$ for the comparison indicated.

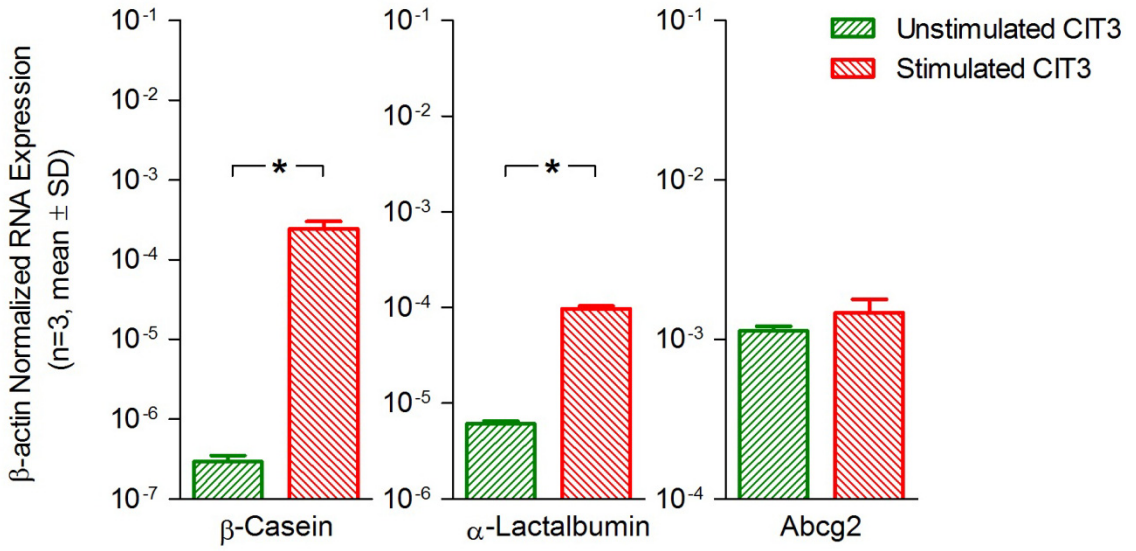

Western blot analysis was performed to determine if Abcg2 protein could be detected in CIT3 cells and if expression was increased following lactogenic hormone stimulation. Crude membrane fractions were prepared from unstimulated and stimulated CIT3 cells in parallel to the cells that underwent qPCR analysis. Again, mammary gland tissue from a lactating CD1 mouse 7 days post-partum was used as a positive control, but was loaded on the gel at a much lower amount to be able to visualize it along with the CIT3 cells under similar exposure conditions. Due to variations in protein size that were detected by the BXP-53 antibody in initial western blots, paired samples underwent a deglycosylation step and were loaded in parallel to the native protein in each sample to confirm band identity. Figure 4-6 shows the expected Abcg2 band at ~70 kDa in the positive control. This band was reduced to ~60 kDa following treatment with PNGase F. In CIT3 cells, the native Abcg2 protein was detectable at ~80 kDa and was also reduced to ~60 kDa following deglycosylation. Native Abcg2 protein expression was greater in the ovein prolactin and hydrocortisone stimulated CIT3 cells as the β-actin-normalized band density of native Abcg2 was 18% greater than in the unstimulated cells.

Figure 4-6: Western blot of native and deglycosylated Abcg2 in mouse lactating mammary gland (7 days post-partum), unstimulated CIT3 cells, and CIT3 cells following 4 days of lactogenic hormone stimulation.

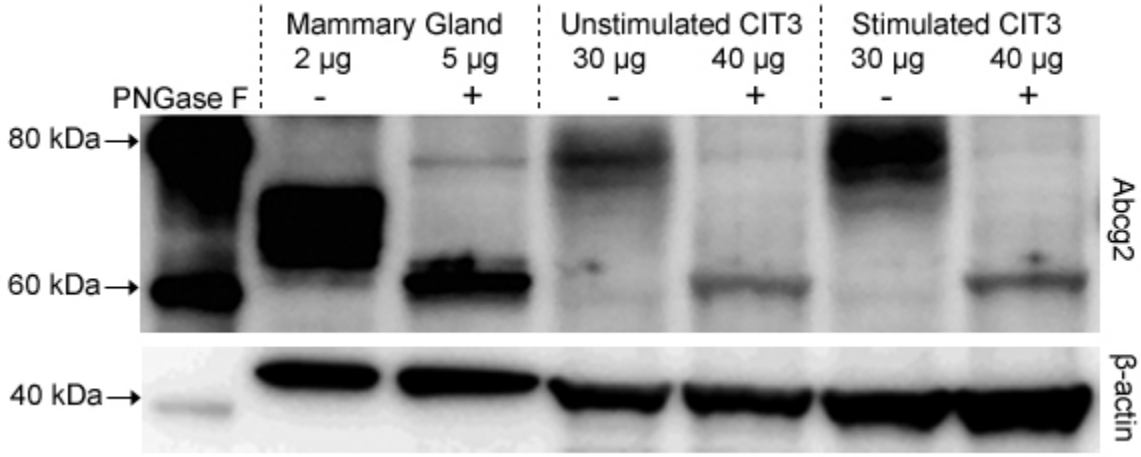

Expression level of Abcg2 was also visualized in unstimulated and stimulated CIT3 cells by confocal microscopy, with cellular localization in the X-Z plane demonstrated in stimulated cells. Cells exposed to lactogenic hormone stimulation had noticeably greater Abcg2-associated fluorescence relative to unstimulated cells when imaged with equivalent background FITC exposure (Figure 4-7). Figure 4-8 demonstrates that the localization of Abcg2 in stimulated CIT3 cells is in the apical membrane.

Figure 4-7: Fluorescent microscopy of Abcg2 in unstimulated and stimulated CIT3 cells.

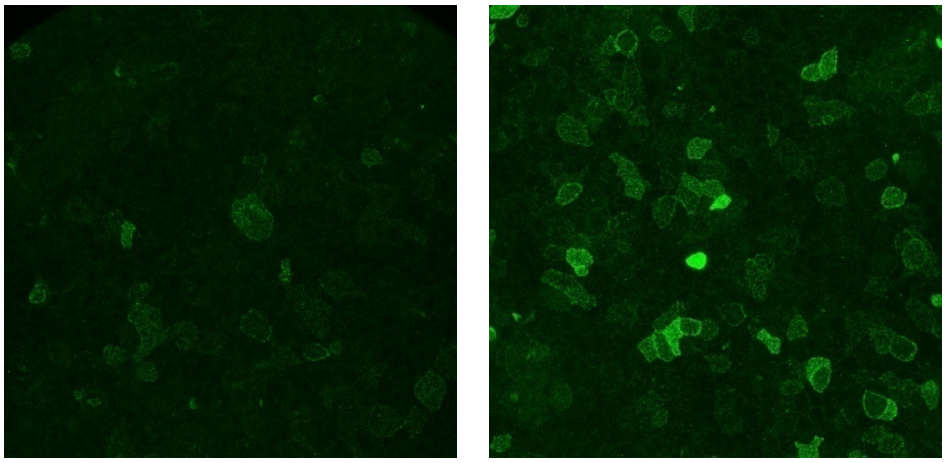

Unstimulated Stimulated

Figure 4-8: X-Z confocal microscopy of Abcg2 localization in stimulated CIT3 cells.

Abcg2 (FITC-green) is localized in the apical membrane of stimulated CIT3 cells grown on snapwells. The tight junction protein ZO-1 (PE-red) and cell nuclei (DAPI-blue) were stained for orientation. All antibodies except for BXP-53 were added to stimulated cells for a negative control. Abcg2-associated fluorescence in unstimulated cells was too dim to determine cellular localization.

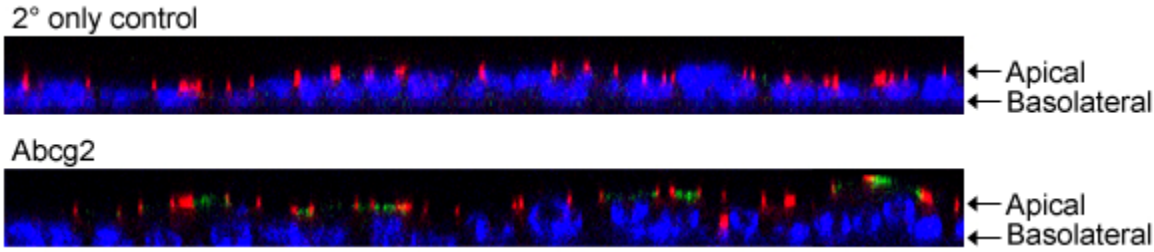

2. Specific Aim 2: To determine if nitrofurantoin is transported in unstimulated CIT3 cells.

The purpose of this initial flux experiment was to determine if there is directionality to nitrofurantoin flux in unstimulated CIT3 cells as was previously demonstrated in CIT3 cells exposed to lactogenic hormones. Unstimulated CIT3 cells did form the tight junctions necessary for flux assays as TEER exceeded 800 Ω•cm^2 and followed a similar profile as stimulated cells (Figure 4-9). The nitrofurantoin HPLC assay performed well with a limit of quantification of 3.9 ng/mL and the intra-day coefficients of variation of < 10% (Figure 4-10). Figure 4-11 illustrates that nitrofurantoin flux was linear over the 2 h experiment and that a greater apically directed permeability was observed in both unstimulated (50.7 ± 5.6 µL/h/cm^2 B→A vs. 19.2 ± 0.4 µL/h/cm^2 A→B) and stimulated (68.0 ± 0.2 µL/h/cm^2 B→A vs. 20.1 ± 4.3 µL/h/cm^2 A→B) conditions. The B→A permeability in stimulated cells (68.0 ± 0.2 µL/h/cm^2) was greater than that of the unstimulated cells (50.7 ± 5.6 µL/h/cm^2), but the A→B permeabilities (20.1 ± 4.3 µL/h/cm^2 vs. 19.2 ± 0.4 µL/h/cm^2) were similar.

Figure 4-9: TEER of unstimulated and stimulated CIT3 cells grown on snapwells.

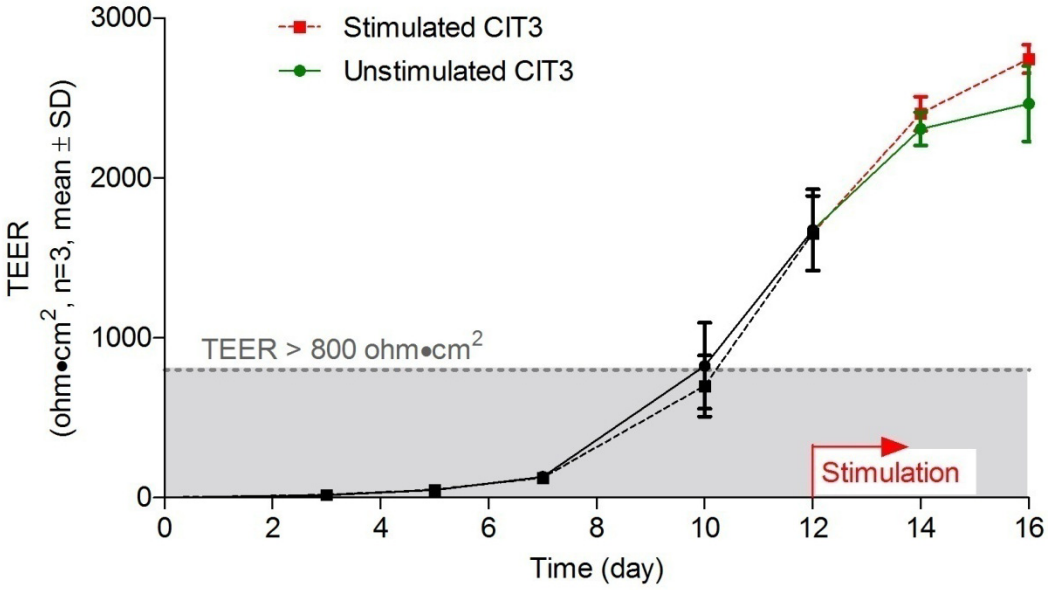

Figure 4-10: Nitrofurantoin HPLC chromatogram and standard curve in CIT3 cell culture media without serum, proteins, hormones or antibiotics.

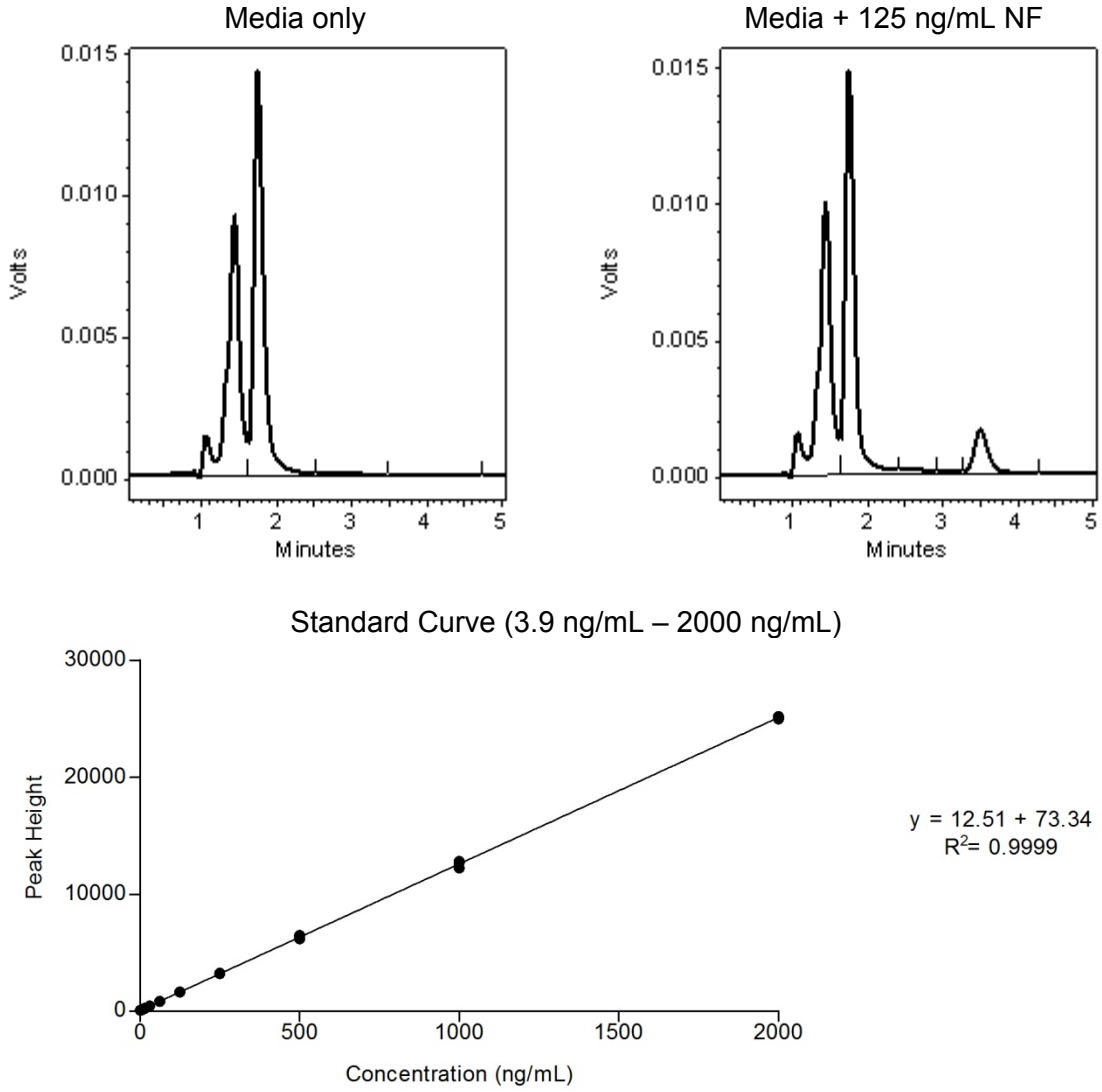

Figure 4-11: Directionality of radiolabelled nitrofurantoin transport in unstimulated and stimulated CIT3 cells grown on snapwells.

Flux in each well was normalized to a donor concentration of 1.5 µM. An asterisk denotes $p < 0.05$ for the comparison indicated.

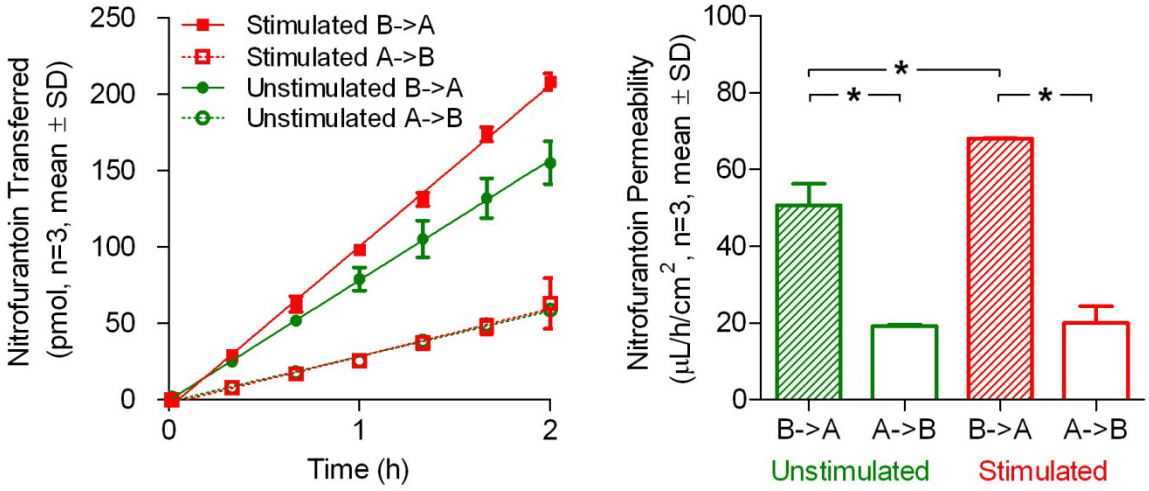

3. Specific Aim 3: To evaluate if established Abcg2 inhibitors decrease the transport of nitrofurantoin and if known Abcg2 substrates are transported in CIT3 cells.

The goal of this next series of flux experiments was to determine if Abcg2 is responsible for the transport of nitrofurantoin in both stimulated and unstimulated CIT3 cells through inhibition studies with the Abcg2 inhibitor, FTC. Figure 4-12 shows that the B→A permeability significantly decreased with the addition of 10 µM FTC in both unstimulated (14.2 ± 0.6 µL/h/cm^2 down to 8.96 ± 0.3 µL/h/cm^2) and stimulated (16.3 ± 0.7 µL/h/cm^2 down to 10.9 ± 0.1 µL/h/cm^2) conditions. The corresponding A→B permeabilities increased, but did not achieve significance. However, the addition of 10 µM FTC did cause the B→A and A→B permeabilities to collapse to a common value in both unstimulated (8.96 ± 0.3 µL/h/cm^2 B→A vs. 8.4 ± 1.9 µL/h/cm^2 A→B) and stimulated (10.9 ± 0.1 µL/h/cm^2 B→A vs. 10.9 ± 1.0 µL/h/cm^2 A→B) conditions.

Finally, to further demonstrate a potential role of Abcg2 in this model system, the flux of two Abcg2 substrates that are known to accumulate in breast milk was tested in unstimulated CIT3 cells. Panel A of Figure 4-13 depicts the directionality and inhibition of the transport of 2 µM PhIP. Only the first two time points (and the origin) were used to determine the flux rates as the amount of PhIP in the recipient chamber beyond that time appeared to violate the assumption of sink conditions. The B→A permeability (98.80 ± 7.4 µL/h/cm^2) was significantly greater than the reverse direction (60.0 ± 2.1 µL/h/cm^2)

and both significantly collapsed to a common value (B→A decreased from 98.80 ± 7.4 μL/h/cm^2 to 68.2 ± 3.0 μL/h/cm^2 and A→B increased from 60.0 ± 2.1 to 71.2 ± 1.8 μL/h/cm^2) with the addition of FTC. Cimetidine permeabilities did not show the expected results. Flux of 5 μM cimetidine was linear over the entire four hours of the experiment (Panel B of Figure 4-13). Although a greater mean B→A permeability (2.0 ± 0.3 μL/h/cm^2) was observed relative to A→B (1.7 ± 0.1 μL/h/cm^2), it did not achieve significance. Similarly, the addition of FTC did not significantly alter the permeabilities in either direction (B→A was 2.0 ± 0.3 μL/h/cm^2 alone vs. 1.7 ± 0.1 μL/h/cm^2 with FTC and A→B was 1.7 ± 0.1 μL/h/cm^2 alone vs. 1.7 ± 0.1 μL/h/cm^2 with FTC). The relative magnitude of the permeabilities was much smaller with cimetidine than with nitrofurantoin and PhIP.

Figure 4-12: Directionality of nitrofurantoin transport and inhibition by the Abcg2 inhibitor, fumitremorgin C (FTC), in unstimulated and stimulated CIT3 cells grown on transwells.

Flux in each well was normalized to a donor concentration of 10 μM. An asterisk denotes $p < 0.05$ for the comparison indicated.

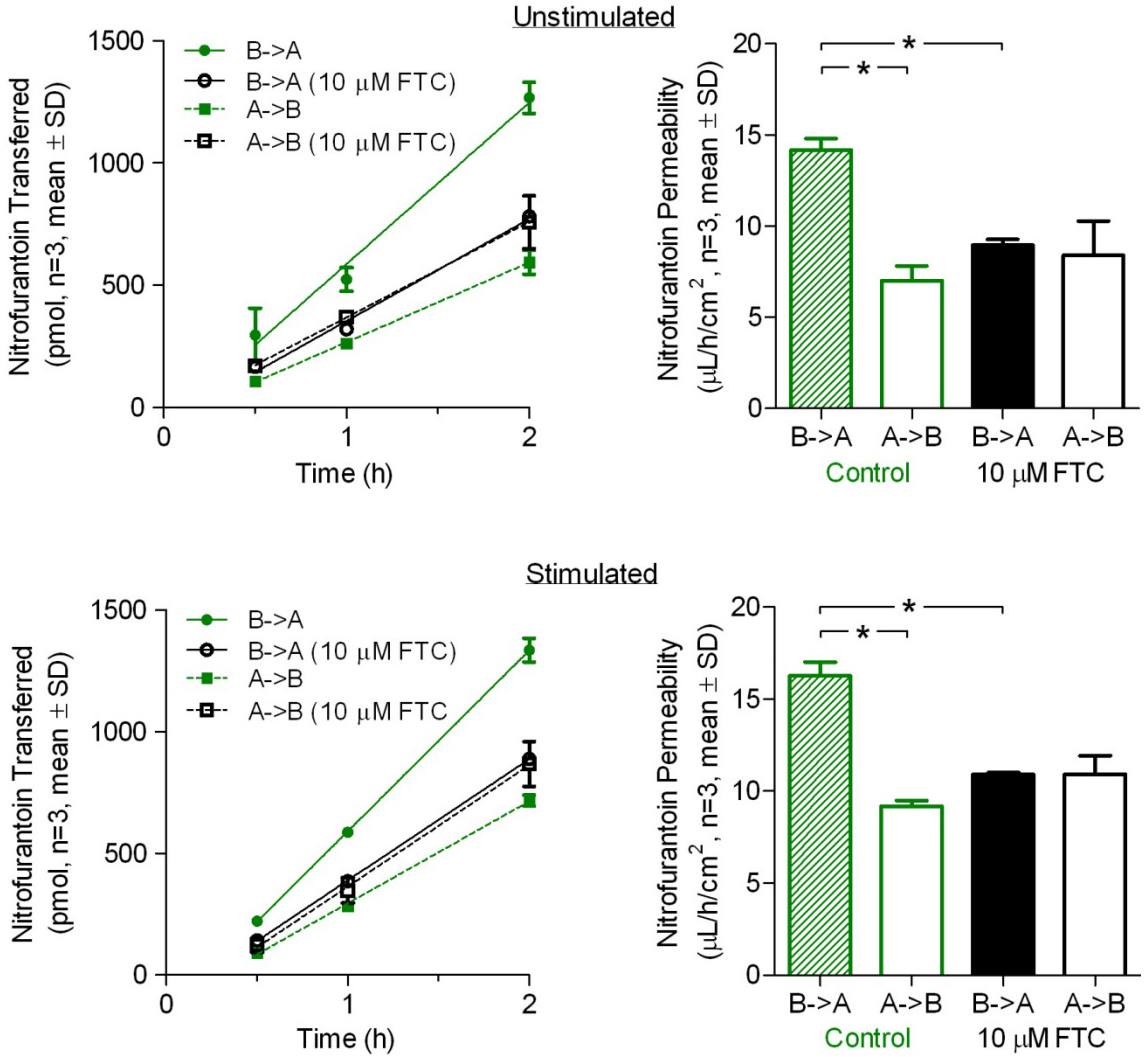

Figure 4-13: Directionality of PhIP and cimetidine transport and inhibition by the Abcg2 inhibitor, fumitremorgin C (FTC), in CIT3 cells grown on transwells.

A. Flux of 2 μM PhIP. Flux rate for permeability calculations based on linear portion of curve, 0.5 - 1 h, forced through the origin. B. Flux of 5 μM cimetidine. An asterisk denotes $p < 0.05$ for the comparison indicated.

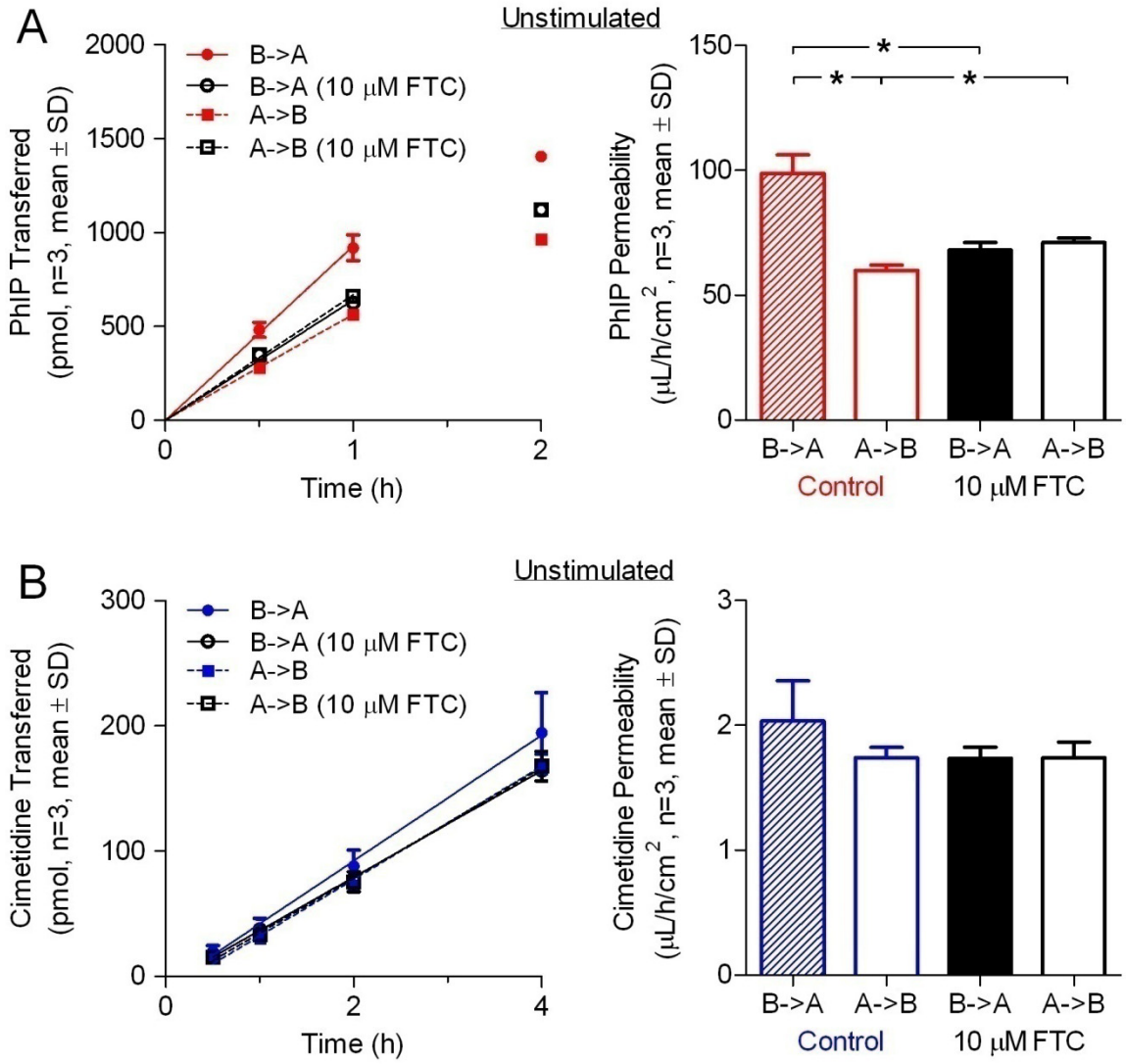

B. Creation of an ABCG2 stably transfected model system

1. Specific Aim 4: To create a stable ABCG2-transfected cell line that has appropriate characteristics for flux experiments.

To select an appropriate cell line for the ABCG2 transfection, LLC-PK1, MDCKI, and MDCKII cell lines were compared. The MDCKI and MDCKII cells are both sub-clones of a canine cocker spaniel kidney heterogeneous cell line derived in 1958. MDCKI cells are lower passage number and reportedly attain much higher TEER values. However, this epithelial phenotype is unstable and overgrowth or incomplete trypsinization during passaging may select for an altered phenotype (product labeling, ECACC). MDCKII cells are higher passage cells and have reportedly lower TEER values, but have been used extensively for transfection and flux assays. LLC-PK1 cells are also kidney-derived and have been extensively used for transfection and flux assays, but are porcine. In terms of background transporter gene expression, RNA transcripts for the orthologs of human ABCB1, ABCC1, and ABCC2 have been found in MDCKII and LLC-PK1 [184]. SLCO1A2 was detected in the original MDCK cell line, but not in either MDCKII or LLC-PK1 cells. SLCO1B1 was not found. Most importantly, neither MDCKII cells or LLC-PK1 cells had any background Abcg2 activity as measured by topotecan flux [160]. Data for MDCKI cells was not found in the literature. To determine ease of selection post-transfection with genecitin, each cell line was exposed to a concentration range of 100 – 1000 µg/mL. The MDCKII cells were most sensitive as all cells that were exposed to 800 µg/mL were dead by 4 days. The LLC-PK1 cells needed marginally more genecitin, 1000 µg/mL, for the same result. MDCKI cells took over a week at 1000 µg/mL for a similar effect. Finally, to confirm each cell lines' ability to form tight junctions, TEER and the flux of 0.01 µM mannitol was measured. Maximal TEER achieved in the LLC-PK1, MDCKI, and MDCKII cells was ~140 $\Omega \bullet cm^2$, >6000 $\Omega \bullet cm^2$, and ~130 $\Omega \bullet cm^2$, respectively. Figure 4-14 shows the mannitol permeabilities of each cell line with LLC-PK1 cells greatly exceeding the others. Based on these comparisons, MDCKII cells were selected for development of the model system.

Figure 4-14: Paracellular flux of radiolabelled mannitol in candidate parent cell lines grown on snapwells.

Flux in each well was normalized to a donor concentration of 0.01 μM. Equal numbers of snapwells were tested in the B→A and A→B directions and were pooled as there was no directionality to the flux. An asterisk denotes $p < 0.05$ for the comparison indicated.

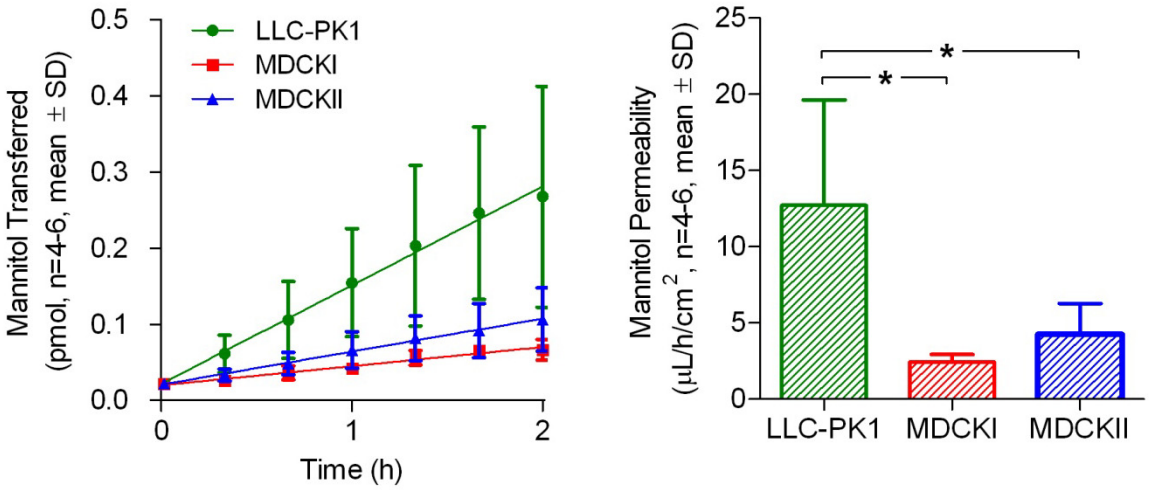

The pcDNA3-ABCG2 plasmid or empty vector control was successfully transfected into MDCKII cells, as demonstrated by western blot and Hoechst 33342 efflux of the heterogeneous population at 48 hrs ("dim" population, Figure 4-15). Following selection, initial attempts at clonal selection using a limiting dilution approach produced seven clones that were expanded and once again tested for ABCG2 function by Hoechst 33342 efflux. Only clone 2 had any appreciable GF120918-inhibitable ABCG2 function as indicated by the presence and absence of a small dim population with and without the inhibitor. Clone 2 was resorted using FACS, where presumed viable cells with high ABCG2 expression were identified and sorted individually into a 96-well plate (Figure 4-16). Ten clones were expanded and ABCG2 expression and function were determined by western blotting, flow cytometry, Hoechst 33342 efflux, and DB-67 accumulation. Results from select MDCKII-ABCG2 clones with varying levels of expression are presented in Figure 4-17, Figure 4-18, and Figure 4-19. Finally, apical localization of ABCG2 was confirmed in MDCKII-ABCG2 clone 40, the highest ABCG2 expressing clone, by confocal microscopy (Figure 4-20). This clone was selected for use in all subsequent experiments based on performance in aforementioned assays.

Figure 4-15: Successful transfection of ABCG2 into MDCKII cells as determined by western blot and Hoechst 33342 efflux assays at 48 h.

A. Western blot of ABCG2 in 12 µg of cell lysates. B. Efflux of Hoechst 33342. Abcg2-transfected cells efflux Hoechst 33342, producing a "dim" phenotype. Empty vector and 1 µM GF120918 inhibition of this "dim" phenotype were run as negative controls. Cell clumps and debris and presumed nonviable cells (PI-positive) were removed from the analysis.

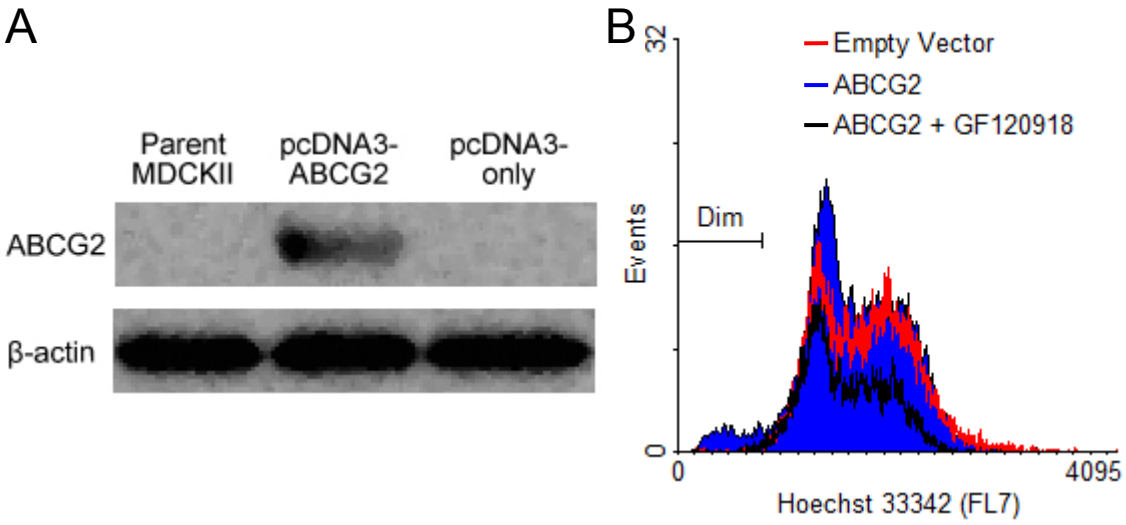

Figure 4-16: Fluorescence activated cell sorting (FACS) of individual cells with high surface expression of ABCG2

MDCKII-ABCG2 Clone 2 cells with high ABCG2 expression were identified (black box) and sorted individually into a 96-well plate. Cell clumps and debris and presumed nonviable cells (PI-positive) were removed.

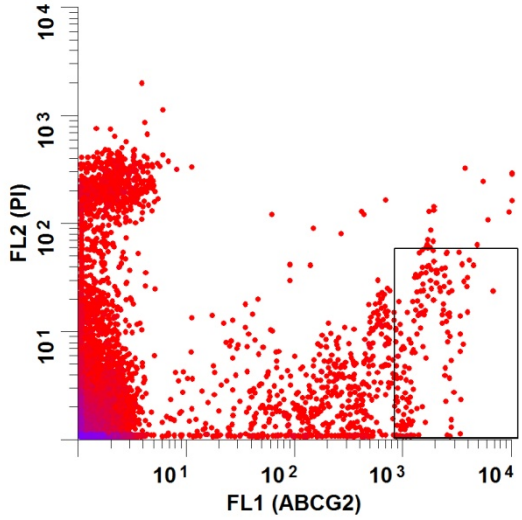

Figure 4-17: Western Blot for ABCG2 in crude membrane fractions of select MDCKII-ABCG2 clones.

Western blot of ABCG2 (~72 kDA) and β-actin (~42 kDa) in 10 µg of crude membrane fractions. Saos-ABCG2 and empty vector was loaded as a positive and negative control, respectively.

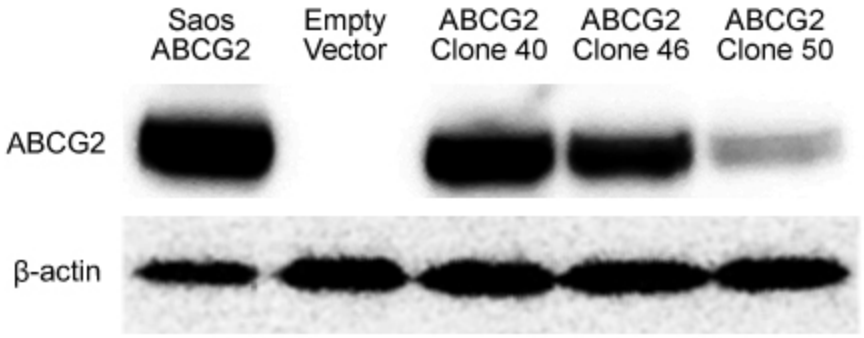

Figure 4-18: Flow cytometric analysis of surface ABCG2 expression and Hoechst 33342 efflux with or without the ABCG2 inhibitor, GF120918, in select MDCKII-ABCG2 clones.

A. Surface expression of ABCG2. The MFI difference between the ABCG2 labeled (red shaded) and isotype control (black line) in each clone was calculated as a surrogate for expression level (mean, n=3). B. Hoechst 33342 efflux. Percentage of cells in the dim gate (blue shaded) relative to each clone's GF120918-inihibited control (black line) was used as a surrogate for ABCG2 activity.

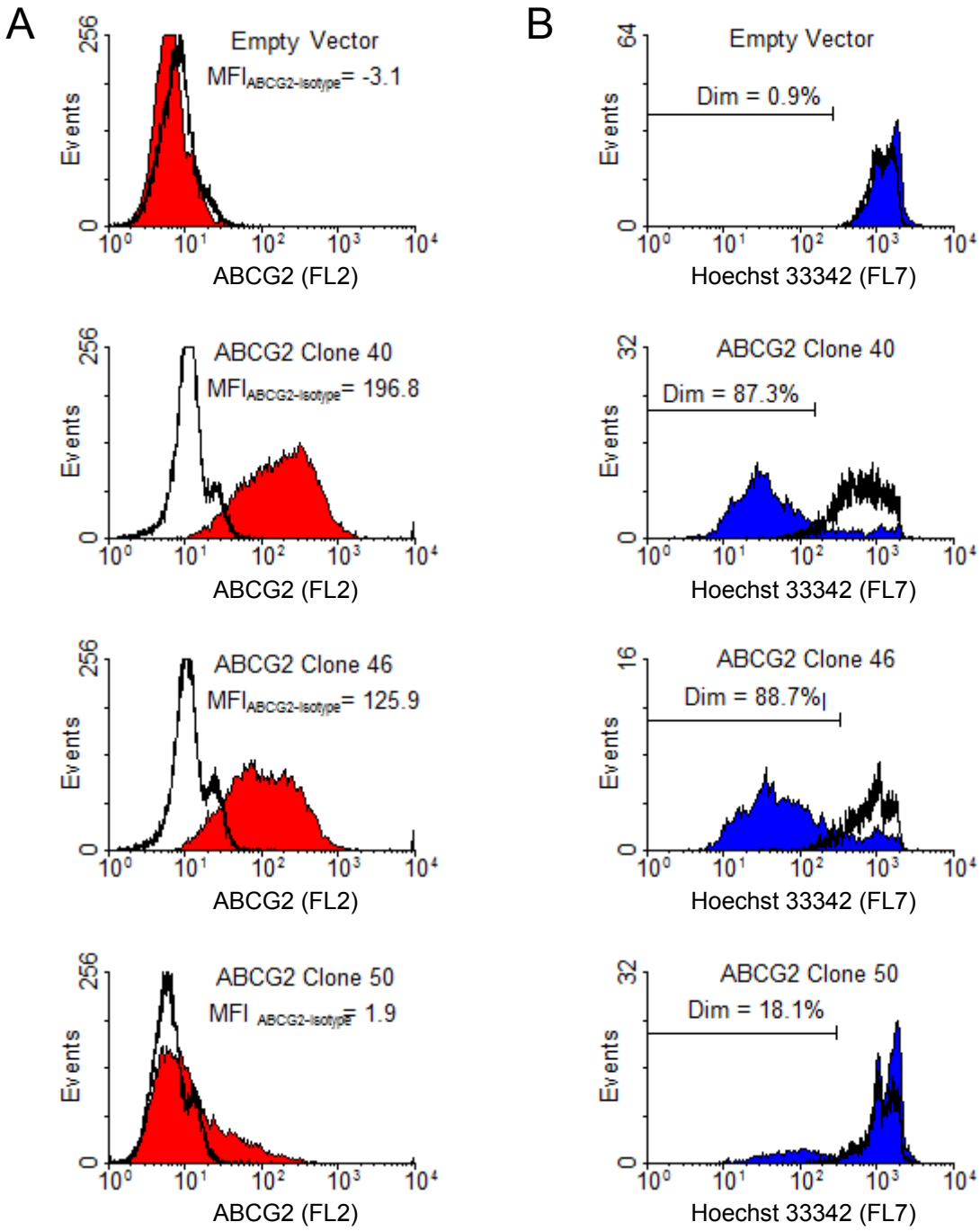

Figure 4-19: DB-67 accumulation in select MDCKII-ABCG2 clones with or without the ABCG2 inhibitor, GF120918.

Accumulation of 1 μM DB-67 with or without 1 μM GF120918 preincubation. An asterisk denotes $p < 0.05$ for the comparison indicated.

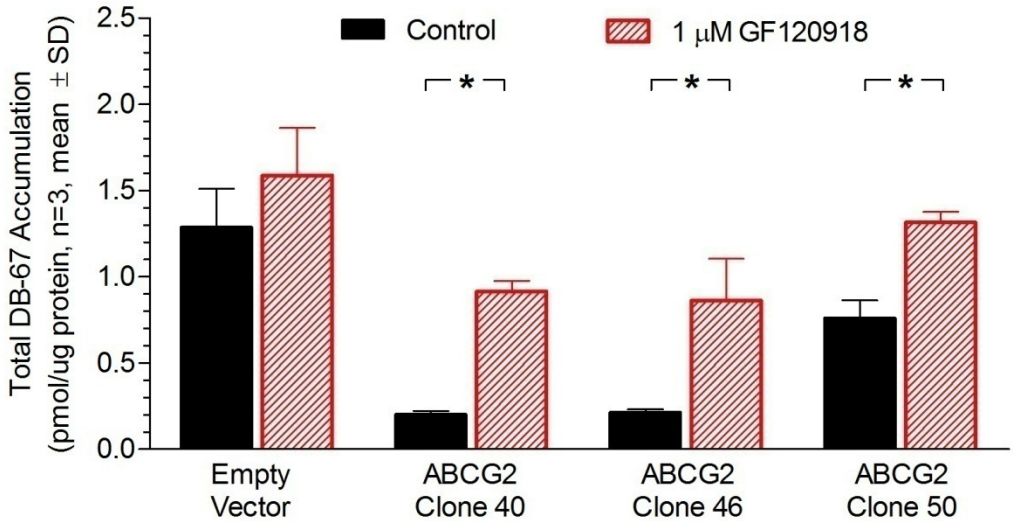

Figure 4-20: Confocal microscopy of ABCG2 expression and localization in MDCKII-ABCG2 Clone 40 cells.

Panel A. A high expression level of ABCG2 (FITC-green) is visualized in MDCKII-ABCG2 Clone 40 cells relative to empty vector cells. Panel B. X-Z section shows that ACGB2 is localized in the apical membrane. Cell nuclei (DAPI-blue) were stained for orientation.

A

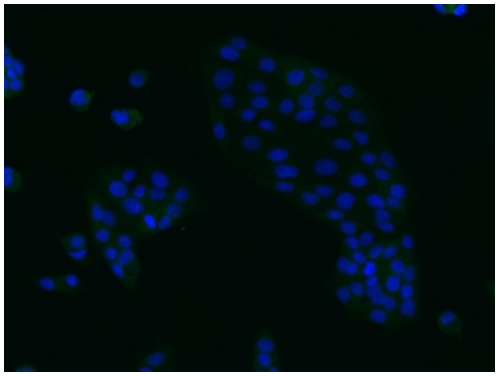

Empty Vector

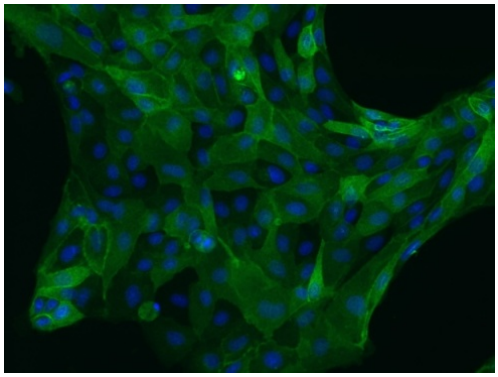

MDCKII-ABCG2 Clone 40

B

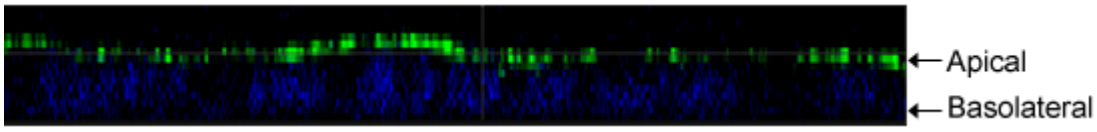

2. Specific Aim 5: To validate the model system with known ABCG2 substrates (nitrofurantoin, PhIP, cimetidine, methotrexate, ciprofloxacin) and ABCG2 inhibitors (GF120918 and FTC).

The stably transfected ABCG2 overexpressing model system was thoroughly validated for monolayer flux assays with a series of directionality and inhibition experiments with known ABCG2 substrates and inhibitors. In directionality experiments, the B→A and A→B flux in ABCG2-transfected and empty vector-transfected cells were compared. In inhibition experiments, the ability of 1 μM GF120918 and 10 μM FTC to inhibit the B→A flux attributed to ABCG2 was evaluated. Graphs of results for each substrate are presented in a consistent format with linearity of the time points chosen to determine flux rate on the left (represented by the plotted regression line) and the calculated permeabilities presented on the right.

The first substrate evaluated was nitrofurantoin. Figure 4-21 panel A illustrates the linearity of the flux of 10 μM nitrofurantoin over the 3 h experiment. Background permeability in the empty vector-transfected cells was predominantly directed towards the B chamber (5.3 ± 0.3 μL/h/cm^2 B→A vs. 9.5 ± 0.3 μL/h/cm^2 A→B) and the transfection of ABCG2 reversed this phenomenon (32.2 ± 0.3 μL/h/cm^2 B→A vs. 2.3 ± 0.3 μL/h/cm^2 A→B). Panel B shows that both 1 μM GF120918 and 10 μM FTC reversed the increase in B→A flux in the ABCG2-transfected cells relative to the empty vector-transfected cells, decreasing the permeability by 84.5% and 96.3% respectively.

Figure 4-21: Directionality of nitrofurantoin transport and inhibition of B→A flux by various inhibitors in empty vector and ABCG2-transfected cells grown in transwells.

Each transwell was normalized to a donor concentration of 10 µM. An asterisk denotes $p < 0.05$ for the comparison indicated.

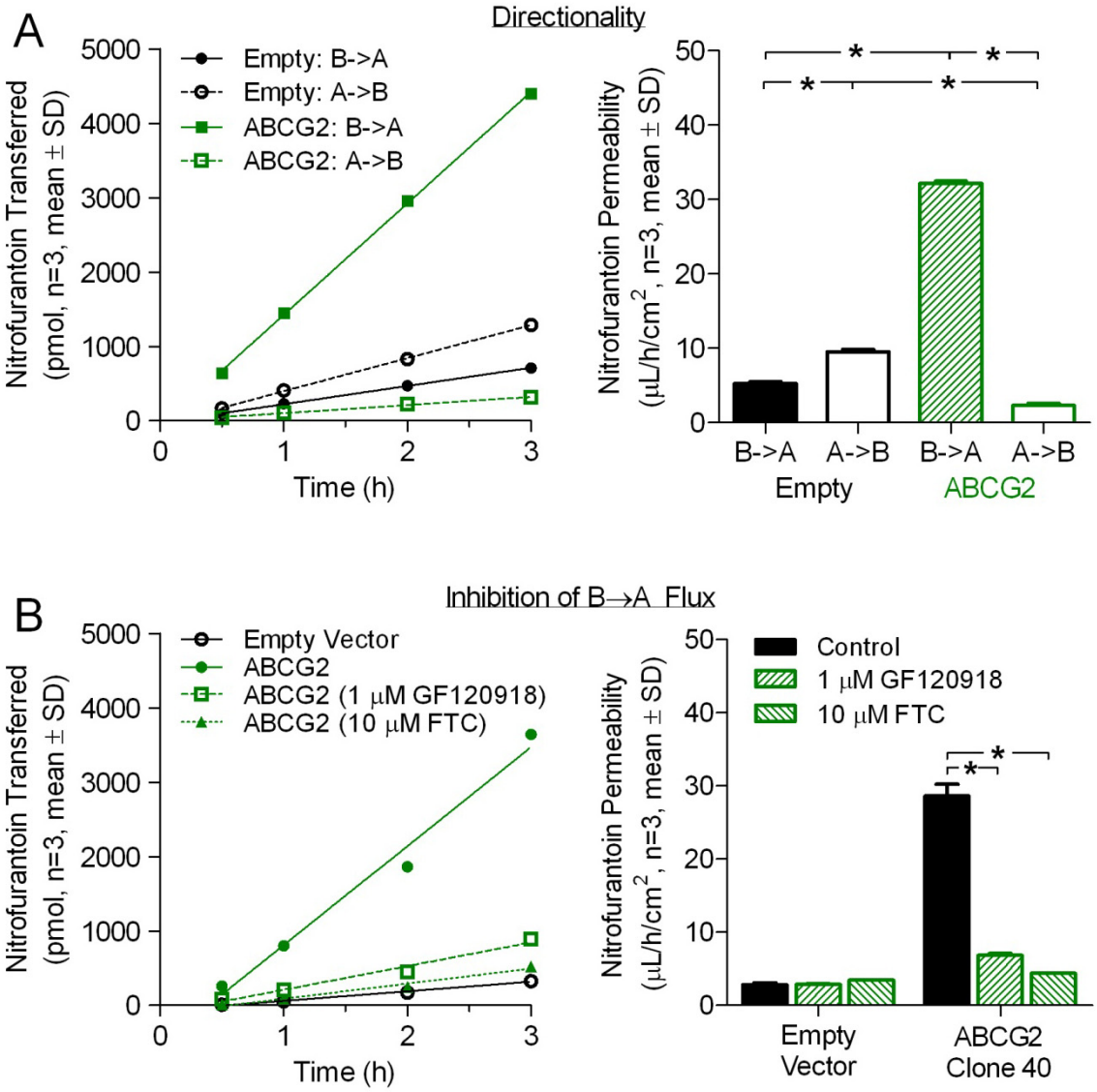

PhIP flux was only linear up to 1 h so the flux rate was determined by linear regression of only the first two time points and was forced through the origin. Figure 4-22 Panel A shows there was no difference in the B→A and A→B permeabilities in the empty vector-transfected cells (39.1 ± 4.8 μL/h/cm^2 B→A vs. 38.9 ± 2.0 μL/h/cm^2 A→B). However, the addition of ABCG2 to the cell line both significantly increased the flux in the B→A direction (39.1 ± 4.8 μL/h/cm^2 B→A in the empty vector to 97.3 ± 4.8 μL/h/cm^2 B→A in the ABCG2-transfected) and significantly decreased flux in the A→B direction (38.9 ± 2.0 μL/h/cm^2 A→B in the empty vector to 4.1 ± 0.3 μL/h/cm^2 A→B in the ABCG2-transfected). Panel B illustrates that addition of 10 μM FTC completely ablated the higher B→A permeability observed in the ABCG2-transfected cells relative to the empty vector cells. The 1 μM addition of GF120918, however, had no effect.

Figure 4-22: Directionality of PhIP transport and inhibition of B→A flux by various inhibitors in empty vector and ABCG2-transfected cells grown in transwells.

Each transwell was normalized to a donor concentration of 2 µM. Flux rate for permeability calculations based on linear portion of curve, 0.5 - 1 h, forced through the origin. An asterisk denotes $p < 0.05$ for the comparison indicated.

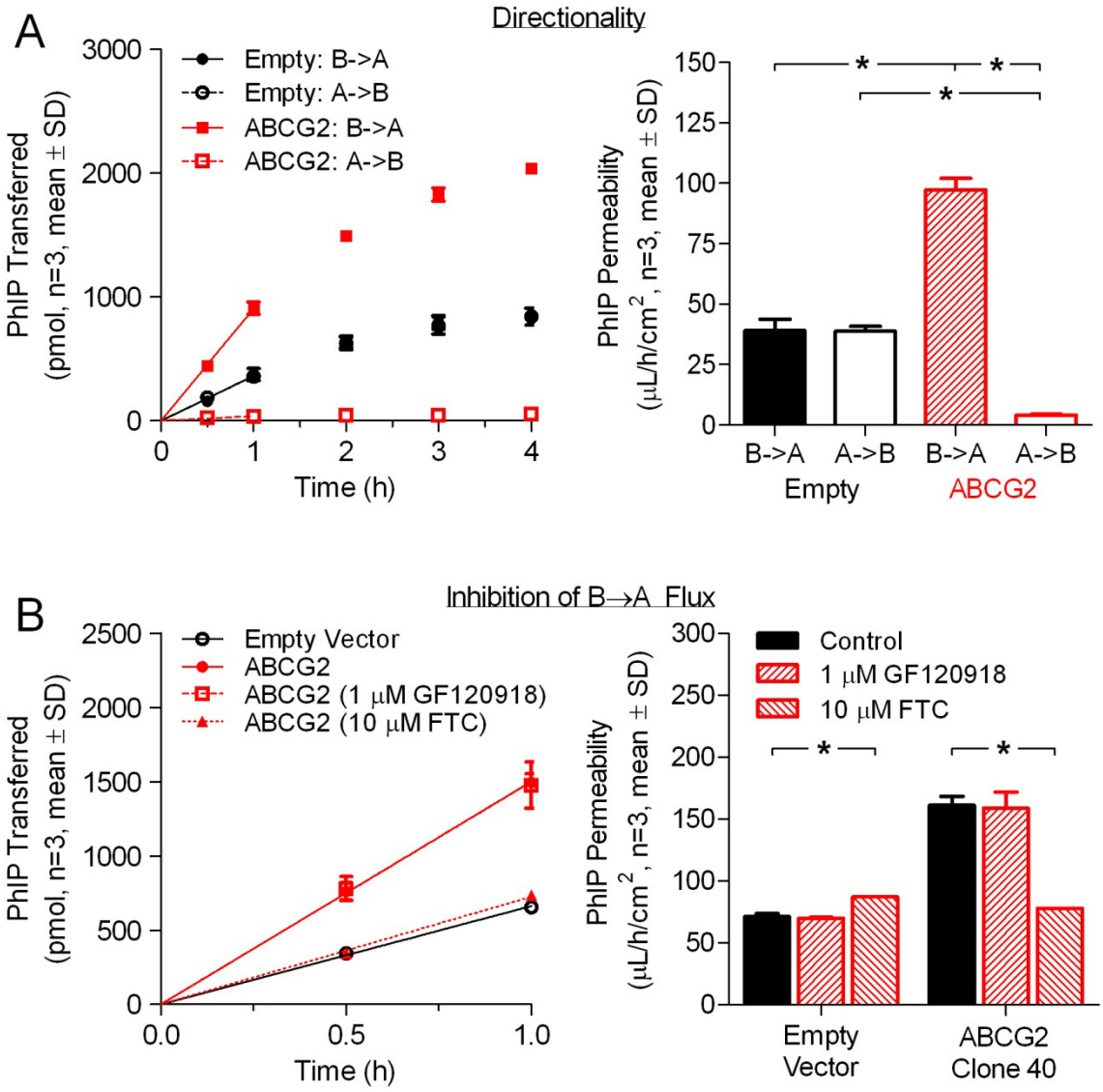

The magnitude of cimetidine flux was less than the previous two substrates, but was linear over the entire time course of the experiment. Figure 4-23 Panel A shows there was no difference in the B→A and A→B permeabilities in the empty vector-transfected cells (2.3 ± 0.4 μL/h/cm^2 B→A vs. 1.6 ± 0.3 μL/h/cm^2 A→B). The ABCG2 cells both significantly increased the flux in the B→A direction (2.3 ± 0.4 μL/h/cm^2 B→A in the empty vector to 8.4 ± 0.2 μL/h/cm^2 B→A in the ABCG2-transfected) and significantly decreased flux in the A→B direction (1.6 ± 0.3 μL/h/cm^2 A→B in the empty vector to 0.5 ± 0.06 μL/h/cm^2 A→B in the ABCG2-transfected). Panel B shows that both 1 μM GF120918 and 10 μM FTC completed ablated B→A flux attributed to ABCG2 in the ABCG2-transfected cells.

Figure 4-23: Directionality of cimetidine transport and inhibition of B→A flux by various inhibitors in empty vector and ABCG2-transfected cells grown in transwells.

Each transwell was normalized to a donor concentration of 5 μM. An asterisk denotes $p < 0.05$ for the comparison indicated.

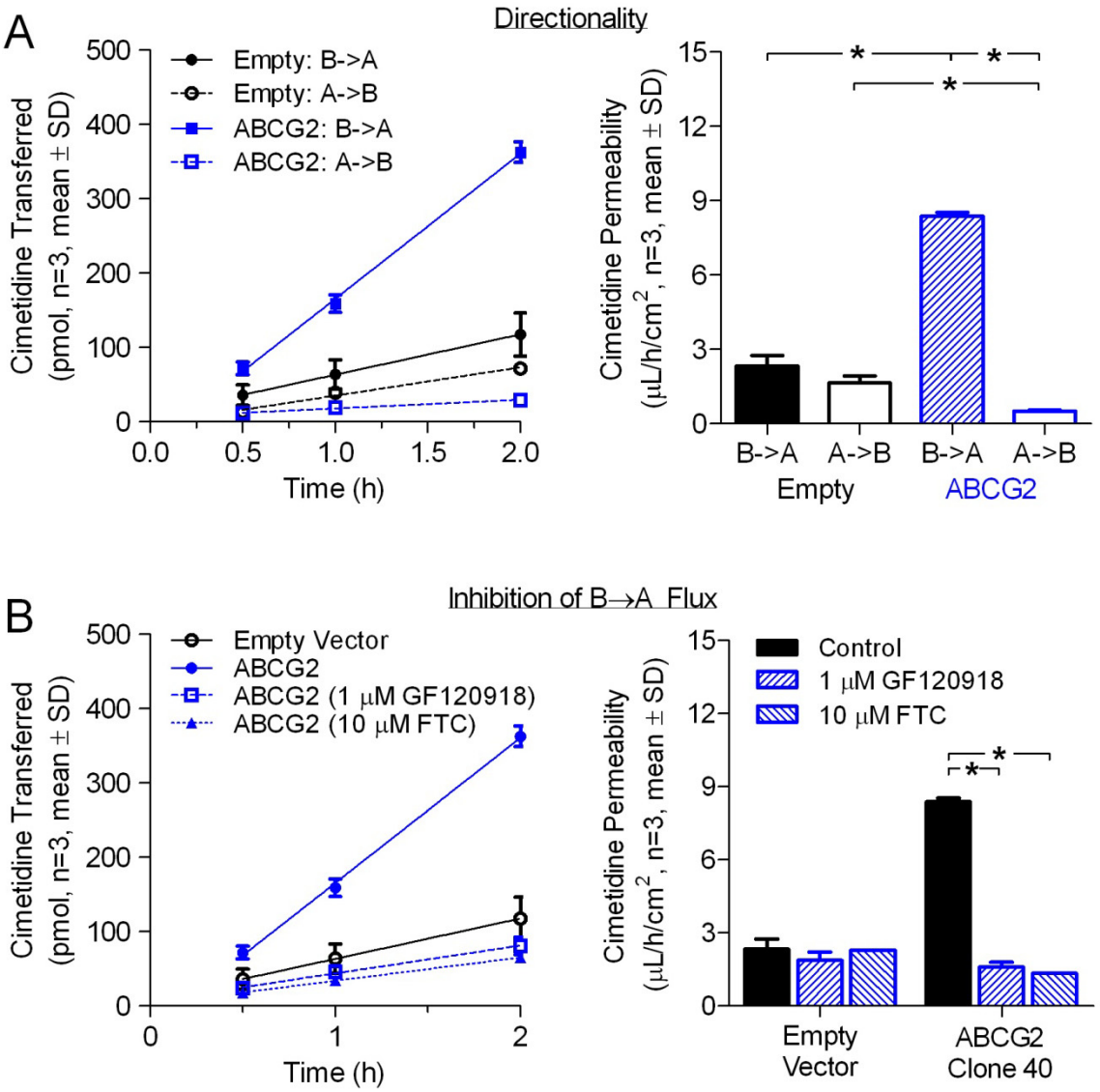

Although the flux of methotrexate appeared linear over the course of the experiment (Figure 4-24 Panel A), the overall magnitude was much lower than cimetidine and was nearly equal to that of the paracellular marker sucrose (Figure 4-24 Panel B). There was still a predominant B→A directionality in the ABCG2 transfectants (0.4 ± 0.08 μL/h/cm^2 B→A vs. 0.3 ± 0.04 μL/h/cm^2 A→B) that was not seen in the empty vector transfected cells (0.8 ± 0.06 μL/h/cm^2 B→A vs. 0.9 ± 0.03 μL/h/cm^2 A→B), but it is difficult to interpret as the B→A flux in the ABCG2-transfected cells were lower than that of their empty vector controls (0.4 ± 0.08 μL/h/cm^2 vs. 0.8 ± 0.06 μL/h/cm^2, respectively). Inhibition studies were not performed due to the extremely low permeability of methotrexate.

Figure 4-24: Directionality of methotrexate and sucrose transport in empty vector and ABCG2-transfected cells grown in transwells.

Panel A. Methotrexate flux and permeability. Each transwell was normalized to a donor concentration of 5 nM. Panel B. Sucrose flux and permeability. Each transwell was normalized to a donor concentration of 0.2 µM. An asterisk denotes $p < 0.05$ for the comparison indicated.

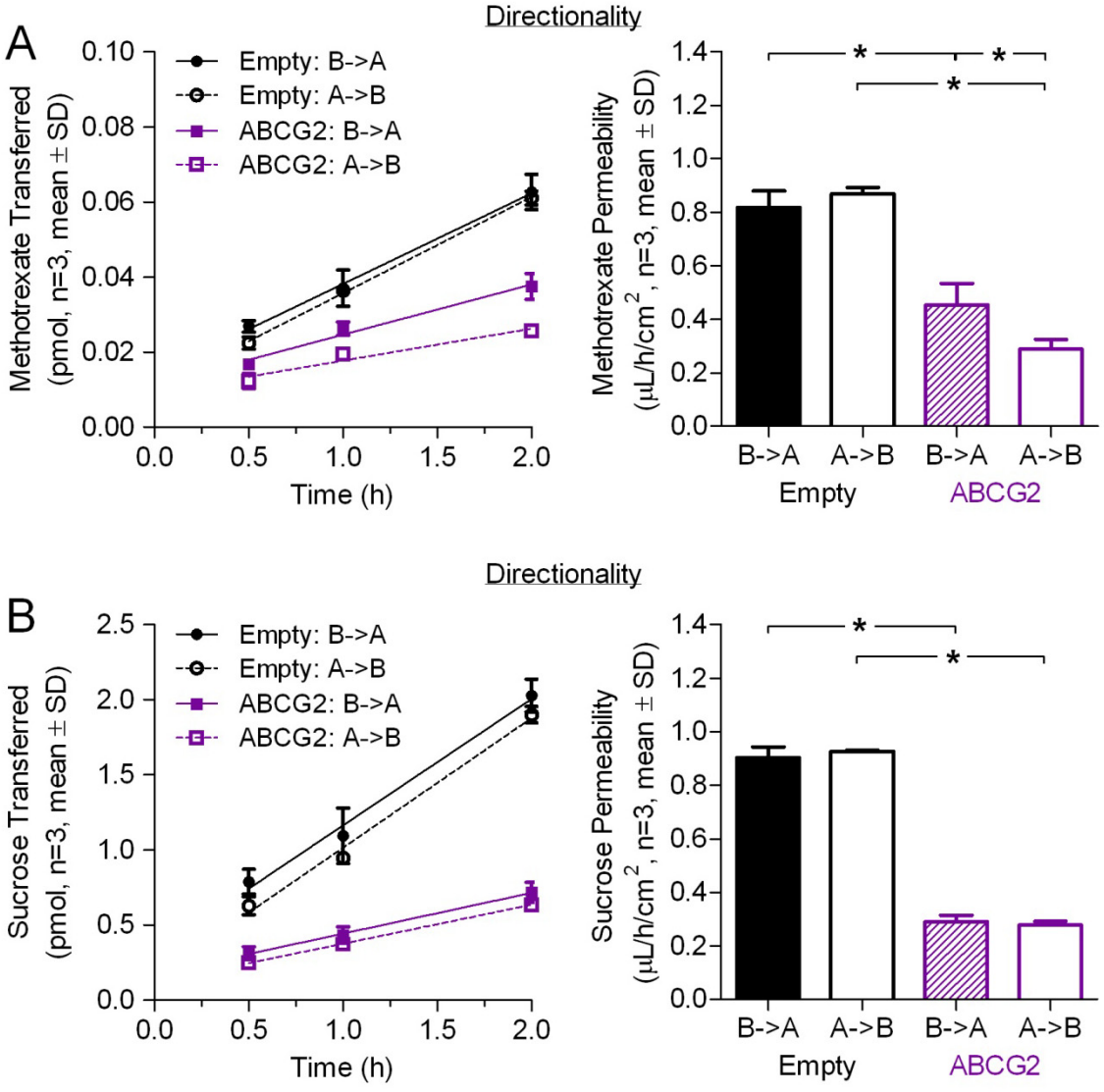

The flux of the final substrate studied, ciprofloxacin, was also linear over the 4 h experimental time course and was greater than that of methotrexate and cimetidine, but less than nitrofurantoin and PhIP. Figure 4-25 demonstrates that there was no difference in the B→A and A→B permeabilities in the empty vector-transfected cells (3.2 ± 0.1 μL/h/cm^2 B→A vs. 4.2 ± 0.4 μL/h/cm^2 A→B). The transfection of ABCG2 into the cells both significantly increased the flux in the B→A direction (3.2 ± 0.1 μL/h/cm^2 B→A in the empty vector to 16.2 ± 1.0 μL/h/cm^2 B→A in the ABCG2-transfected) and significantly decreased the flux in the A→B direction (4.2 ± 0.4 μL/h/cm^2 A→B in the empty vector to 2.5 ± 0.5 μL/h/cm^2 A→B in the ABCG2-transfected). Inhibition studies were not performed.

Figure 4-25: Directionality of ciprofloxacin transport in empty vector and ABCG2-transfected cells grown in transwells.

Each transwell was normalized to a donor concentration of 10 μM. An asterisk denotes $p < 0.05$ for the comparison indicated.

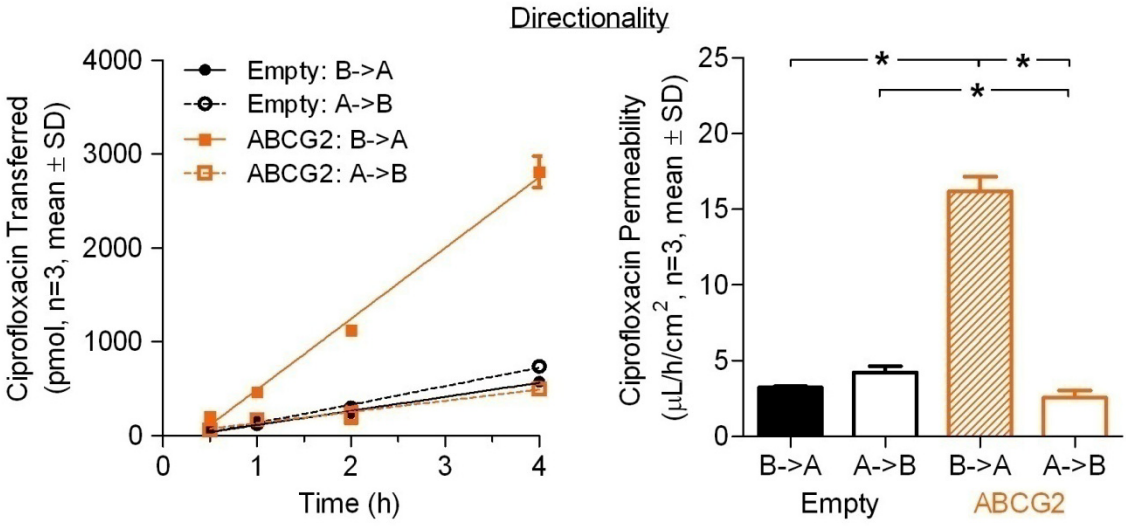

C. Mathematical modeling and derivation of commonly used measurements of efflux activity.

1. Specific Aim 6: To establish a mathematical model for xenobiotic transport in an ABCG2-overexpressed cell culture system and to compare measurements of efflux activity.

To explore the utility of the simple three compartment kinetic model presented in Figure 3-2, the theoretical limits of the initial rates with increasing $PS_{A,E(ABCG2)}$ were first determined. The initial B→A rate for a single transfected system with an apical efflux transporter is described by Eq. 3-8 and is dependent upon C_B^0, $PS_{A,E(ABCG2)}$, PS_D, and PS_{PC}. Inherent in this relationship is the observation that as $PS_{A,E(ABCG2)}$ becomes much greater than PS_D, dX_A/dt increases until it achieves a maximal flux for a given initial basolateral concentration (Eq. 4-1, depicted in Figure 4-26 below):

$$\lim_{PS_{A,E}\to\infty}\left(\frac{dX_{A,B\to A}}{dt}_{ABCG2}\right) = C_B^0\,[PS_D+PS_{PC}] \qquad \text{Eq. 4-1}$$

Figure 4-26: Effect of increasing permeability-surface area product attributed to apical efflux ($PS_{A,E(ABCG2)}$) on flux (dX_A/dt).

Flux (dX_A/dt) increases as $PS_{A,E(ABCG2)}$ increases to a maximum of $C_B^0\,[PS_D+PS_{PC}]$. PS_{PC}, PS_D, and C_B^0 were fixed at 0.1, 0.5, and 10 respectively. As the apparent permeability and permeability-surface area product are proportional to flux, substituting any of these parameters on the y-axis would yield the same relationship.

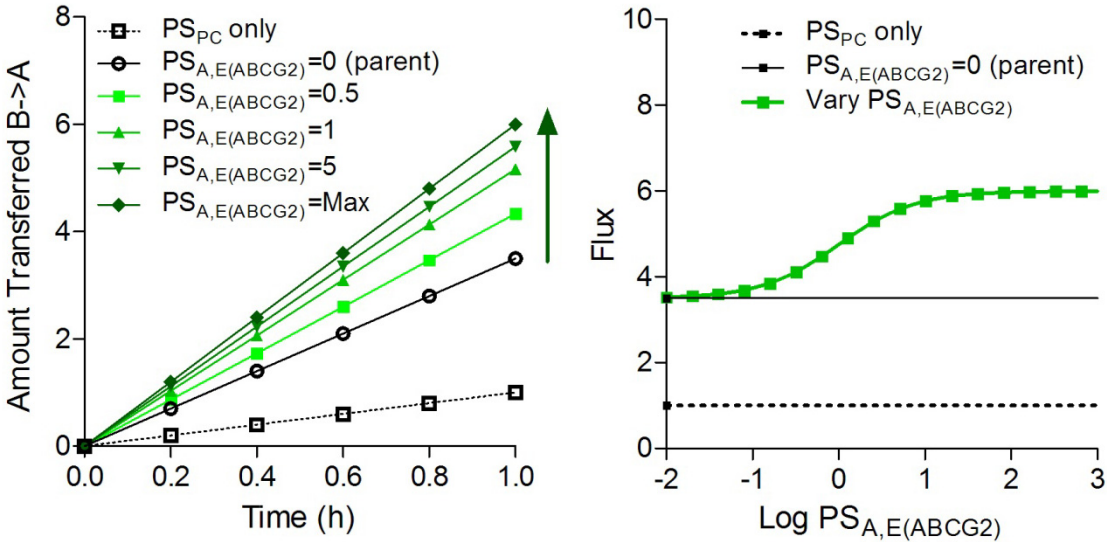

The initial A→B rate in a single transfected system with an apical efflux transporter is described by Eq. 3-11 and is dependent upon C_A^0, $PS_{A,E(ABCG2)}$, PS_D, and PS_{PC}. As $PS_{A,E(ABCG2)}$ becomes much greater than PS_D, dX_B/dt decreases until it achieves a minimum flux for a given initial basolateral concentration (Eq. 4-2, illustrated below in Figure 4-27):

$$\lim_{PS_{A,E}\to\infty}\left(\frac{dX_{B,\,A\to B}}{dt}_{ABCG2}\right) = C_A^0\,[PS_{PC}] \qquad \text{Eq. 4-2}$$

Figure 4-27: Effect of increasing permeability-surface area product attributed to apical efflux ($PS_{A,E(ABCG2)}$) on A→B flux (dX_B/dt).

Flux (dX_B/dt) decreases as $PS_{A,E}$ increases to a minimum of $C_A^0\,[PS_{PC}]$. PS_{PC}, PS_D, and C_A^0 were fixed at 0.1, 0.5, and 10 respectively. As the apparent permeability and permeability-surface area product are proportional to flux, substituting any of these parameters on the y-axis would yield the same relationship.

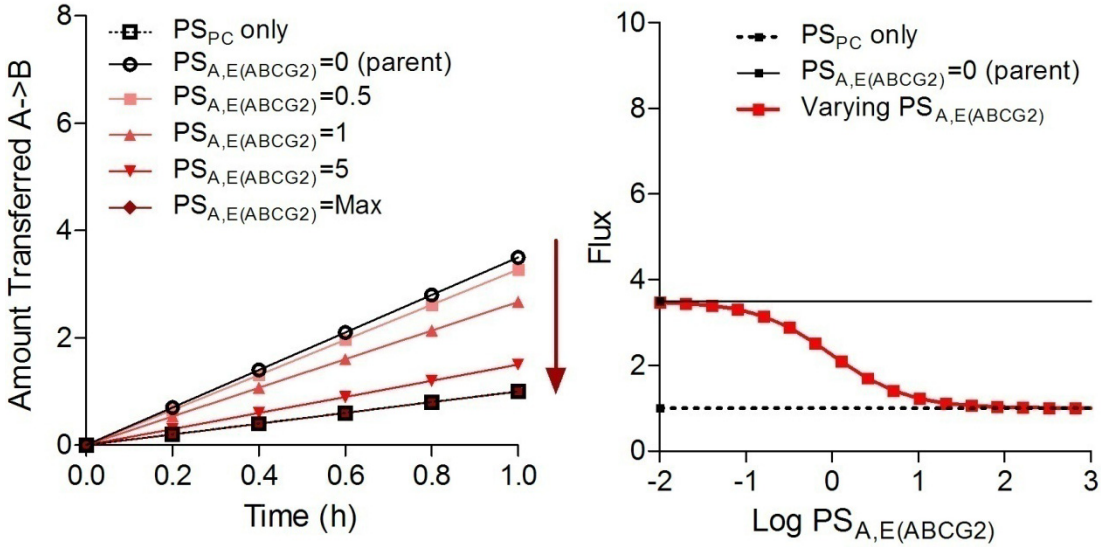

Next, the theoretical limits of ER_A in a single apical efflux transporter system were explored in a similar manner. This efflux ratio was derived in Eq. 3-14 for the single transfection of an apical efflux transporter when PS_{PC} is assumed to be insignificant. As presented in the work of Kalvass and Pollack, if the permeability-surface area product for apical efflux is much greater than that for passive diffusion ($PS_{A,E(ABCG2)} >> PS_D$) an ER_A upper limit of 2 is reached [172]. Conceptually, an infinitely large $PS_{A,E(ABCG2)}$ serves to essentially remove one of the two transcellular diffusion barriers (the apical membrane), therefore doubling the B→A permeability and ER_A.

$$\lim_{PS_{A,E}\to\infty}\left(ER_{A,\frac{ABCG2}{parent}}\right) = 2 \qquad \text{Eq. 4-3}$$

A maximal value was not observed for the ER_α when $PS_{A,E(ABCG2)}$ is increased under the same conditions (single transfection of an apical efflux transporter and $PS_{PC}\to 0$). The equation presented in Eq. 3-17 shows that this efflux ratio is expected to remain proportional to $PS_{A,E(ABCG2)}$. Rearrangement of the equation emphasizes this proportionality as shown in Eq. 4-4 below. In contrast, solving for $PS_{A,E(ABCG2)}$ in the apical efflux ratio equation given in Eq. 3-14 results in a much more complex relationship where no direct proportionality to ER_A exists (Eq. 4-5).

$$PS_{A,E(ABCG2)} = PS_D(ER_\alpha - 1) \qquad \text{Eq. 4-4}$$

$$PS_{A,E(ABCG2)} = \frac{(2PS_D)(ER_{A,\frac{ABCG2}{parent}} - 1)}{2 - ER_{A,\frac{ABCG2}{parent}}} \qquad \text{Eq. 4-5}$$

To apply these theoretical relationships to actual data and to test the assumptions of the model experimentally, two data sets were examined. The first was built from flux data in all publications using two different cell lines (MDCKII transfected with either ABCG2 or Abcg2) created by the lab of Dr. Alfred Schinkel. Table 4-1 compares the ER_A and ER_α of several Abcg2/ABCG2 substrates in a murine Abcg2-transfected (Panel A) or human ABCG2-transfected (Panel B) MDCKII cell lines. Substrates that appear to violate the assumption of the single apical efflux transporter system ($PS_{B,U}$, $PS_{A,E}$, $PS_{B,E}$, and $PS_{A,U} = 0$) as evidenced by an ER_α Empty ≠ 1 (ratio of the B→A and A→B flux rates in the empty vector-transfected cell line), are identified by shading. Data from the remaining drugs suggest that the calculated ER_A did appear insensitive to expected variations in $PS_{A,E}$ as different Abcg2 substrates yielded similar ER_A values that all approximated the maximum theoretical value of two. The ER_α

however, spanned a much wider range, presumably reflecting the proportionality of the efflux ratio with $PS_{A,E}$.

Table 4-1: Comparison of the ER_A and ER_α of several Abcg2/ABCG2 substrates in murine and human Abcg2/ABCG2-transfected MDCKII cell lines in the literature.

Apical efflux ratios (ER_A), asymmetry efflux ratios (ER_α), and the ratio of the asymmetry ratios in Abcg2/ABCG2-transfected vs. empty vector-transfected cells (ER_α Ratio) in Abcg2 (Panel A) or ABCG2 (Panel B) transfected MDCKII cells were calculated using flux data compiled from the literature. Drugs where the mean of ER_α Empty was not within 20% of unity were identified (shaded rows).

A	ER_α Empty	ER_A Abcg2	ER_α Abcg2	ER_α Ratio (g2/Empty)	Reference
Nitrofurantoin	0.64	2.63	8.70	13.62	[53]
Ciprofloxacin	0.88	2.52	4.37	4.96	[93]
Ofloxacin	0.90	2.22	6.17	6.88	[93]
Norfloxacin	0.91	2.92	3.26	3.58	[93]
Topotecan	2.23	3.13	14.85	6.66	[153]
PhIP	1.20	1.27	16.43	13.67	[128]
Cimetidine	1.26	3.01	7.14	5.67	[127]
Aflatoxin	1.12	1.58	9.32	8.29	[129]
IQ	1.09	1.84	16.70	15.30	[129]
Trp-P-1	1.09	2.89	4.25	3.91	[129]
Pantoprazole	1.00	1.34	5.05	5.05	[153]
Imatinib	1.03	2.39	35.27	34.11	[173]
Riboflavin	0.13	2.33	1.65	12.49	[91]
Albendazole	1.14	1.70	18.33	16.04	[152]
Oxfendazole	1.14	2.35	5.70	5.00	[152]

Table 4-1 cont.

B	ER_α Empty	ER_A ABCG2	ER_α ABCG2	ER_α Ratio (G2/Empty)	Reference
Nitrofurantoin	0.64	2.66	3.21	5.02	[53]
Ciprofloxacin	0.88	1.18	2.13	2.42	[93]
Ofloxacin	0.90	1.29	1.56	1.73	[93]
Norfloxacin	0.91	1.29	1.32	1.45	[93]
Topotecan	2.08	1.46	5.79	2.79	[127]
PhIP	0.60	1.89	12.74	21.29	[127]
Cimetidine	1.26	2.44	3.11	2.47	[127]
Estradiol	0.68	0.83	0.66	0.98	[127]
Aflatoxin	1.12	1.15	1.91	1.70	[129]
IQ	1.09	1.30	2.47	2.26	[129]
Trp-P-1	1.09	1.64	1.39	1.28	[129]
Albendazole	1.14	1.36	2.11	1.84	[152]
Oxfendazole	1.14	0.87	1.17	1.02	[152]

The second data set that included efflux ratios calculated using the newly developed ABCG2-transfected MDCKII cell line created in Aim 5 is presented in Table 4-2. Three of five ABCG2 substrates studied exhibited a predominant B→A or A→B flux in the empty vector-transfected controls as exhibited by an ER_α Empty ≠ 1 and were removed from the comparison. The ER_A for PhIP once again approximated the maximum model predicted value of two whereas its ER_α was much higher.

Table 4-2: Comparison of the ERA and ERα of several Abcg2/ABCG2 substrates in the newly created ABCG2-transfected MDCKII cell line.

Apical efflux ratios (ER_A), asymmetry efflux ratios (ER_α), and the ratio of the asymmetry ratios in ABCG2-transfected vs. empty vector-transfected MDCKII cells (ER_α Ratio) were calculated using flux data presented in Aim 5. Several experiments were performed with PhIP and grouped. Drugs where the ERα Empty was not within 20% of unity were identified (shaded rows). Data is presented as the mean and standard deviation of all possible efflux ratios from the unmatched individual experimental permeabilities.

	ER_α Empty		ER_A ABCG2		ER_α ABCG2		ER_α Ratio	
	Mean	SD	Mean	SD	Mean	SD	Mean	SD
Nitrofurantoin	0.55	0.03	6.13	0.28	13.93	1.43	25.31	2.78
Cimetidine	1.46	0.34	3.68	0.62	16.94	2.02	12.18	2.98
PhIP	0.98	0.08	2.35	0.17	42.55	4.89	43.83	5.86
	1.01	0.12	2.52	0.30	23.86	1.81	24.00	3.23
Methotrexate	0.94	0.07	0.56	0.09	1.59	0.30	1.69	0.33
Ciprofloxacin	0.77	0.07	5.04	0.29	6.55	1.27	8.61	1.74

These data sets provide some challenges to the assumptions of the model. First, the existence of other active transport processes in the parent MDCKII cell line has been documented in the literature and was observed in the ER_α Empty ratios. However, allowing endogenous $PS_{B,U}$, $PS_{A,E}$, $PS_{B,E}$, and $PS_{A,U}$ processes to persist in the model complicates efforts to establish relationships between the passive permeability-surface area product attributed the transfection of ABCG2 ($PS_{A,E(ABCG2)}$) and experimentally measured efflux ratios as described below.

The relationships that describe the initial flux rate in the B→A or A→B direction (Eq. 3-6 and Eq. 3-9) were updated to reflect the addition of ABCG2 into a parent cell line with endogenous active uptake and efflux processes in both the apical and basolateral membranes to produce Eq. 4-6 and Eq. 4-7:

$$\frac{dX_{A,B\rightarrow A}}{dt} = C_B^0 \left[\frac{(PS_D+PS_{B,U})(PS_D+PS_{A,E}+PS_{A,E(ABCG2)})}{(2PS_D+PS_{A,E}+PS_{B,E}+PS_{A,E(ABCG2)})} + PS_{PC} \right] \qquad \text{Eq. 4-6}$$

$$\frac{dX_{B,\,A\rightarrow B}}{dt} = C_A^0 \left[\frac{(PS_D+PS_{A,U})(PS_D+PS_{B,E})}{(2PS_D+PS_{A,E}+PS_{B,E}+PS_{A,E(ABCG2)})} + PS_{PC} \right] \qquad \text{Eq. 4-7}$$

If ER_A and ER_α are redefined using these new rate equations and we again assume $C_B^0 = C_A^0$ experimentally and $PS_{PC} \rightarrow 0$:

$$ER_A = \left[\frac{PS_D + PS_{A,E} + PS_{A,E(ABCG2)}}{2PS_D + PS_{A,E} + PS_{B,E} + PS_{A,E(ABCG2)}}\right]\left[\frac{(2PS_D + PS_{A,E})}{(PS_D + PS_{A,E})}\right] \quad \text{Eq. 4-8}$$

$$ER_\alpha = \left[\frac{(PS_D + PS_{A,E} + PS_{A,E(ABCG2)})}{(PS_D + PS_{A,U})}\right]\left[\frac{(PS_D + PS_{B,U})}{(PS_D + PS_{B,E})}\right] \quad \text{Eq. 4-9}$$

An examination of these efflux ratios demonstrates that ER_A is still restricted to values between 1 and 2 and that ER_α can fall in a much larger range. ER_A is dependent upon PS_D, $PS_{A,E}$, $PS_{B,E}$, and $PS_{A,E(ABCG2)}$, whereas ER_α could also be affected by any of the endogenous processes. In an attempt to isolate the apical efflux terms attributed to ABCG2 transfection ($PS_{A,E(ABCG2)}$), the ER_α was further divided by ER_α of the empty vector-transfected cells to produce the ER_α Ratio ($ER_{\alpha(ABCG2)}/ER_{\alpha(Empty)}$):

$$\frac{ER_{\alpha(ABCG2)}}{ER_{\alpha(Empty)}} = \left[\frac{(PS_D + PS_{A,E} + PS_{A,E(ABCG2)})}{(PS_D + PS_{A,E})}\right] \quad \text{Eq. 4-10}$$

$$PS_{A,E(ABCG2)} = (PS_D + PS_{A,E})\left[\left(\frac{ER_{\alpha(ABCG2)}}{ER_{\alpha(Empty)}}\right) - 1\right] \quad \text{Eq. 4-11}$$

As shown in the rearrangement of Eq. 4-10 to Eq. 4-11, it is not possible to remove effects of endogenous apical efflux processes ($PS_{A,E}$) from the relationship; however proportionality between $PS_{A,E(ABCG2)}$ and this ER_α Ratio still does exist. Experimentally, any variability in the cell line $PS_{A,E(ABCG2)}$ and $PS_{A,E}$ (transporter expression levels) or a substrate's ability to cross the membrane by passive diffusion (PS_D) or to interact with either transport process ($PS_{A,E(ABCG2)}$ and $PS_{A,E}$) would be expected to affect the ratio. The effects of changes in PS_D, $PS_{A,E}$, and $PS_{A,E(ABCG2)}$ on ER_A and the ER_α Ratio are illustrated graphically in Figure 4-28. Increases in $PS_{A,E}$ or a higher relative substrate PS_D lowers the maximal achievable ER_A and blunts the ER_α Ratio. The final columns of Table 4-1 and Table 4-2 show that the ER_α Ratio does appear to "correct" the ER_α ABCG2 by accounting for the endogenous processes observed in the empty vector transfected cells (eg. nitrofurantoin and ciprofloxacin with ER_α Empty < 1 in Table 4-2).

Figure 4-28: Effect of changes in PS_D and $PS_{A,E}$ on the relationship between the individual efflux ratios and $PS_{A,E(ABCG2)}$.

Panel A. Effect of changes in endogenous apical efflux activity ($PS_{A,E}$) ranging from 0 to 5 on the relationship between the permeability-surface area product attributed to ABCG2 ($PS_{A,E(ABCG2)}$) and the apical efflux ratio (ER_A) or ratio of the asymmetry ratio in the ABCG2-transfected to that of empty vector cells (ER_α Ratio). Arrows depict the changes in efflux ratios with increasing $PS_{A,E}$. $PS_{B,E}$ and PS_D were fixed at 0 and 0.1, respectively. Panel B. Effect of different permeability surface area products attributed to passive diffusion (PS_D) ranging from 0.2 – 10 on the relationship between the permeability-surface area product attributed to ABCG2 ($PS_{A,E(ABCG2)}$) and the apical efflux ratio (ER_A) or ratio of the asymmetry ratio in the ABCG2-transfected to that of empty vector cells (ER_α Ratio). Arrows depict changes in efflux ratios with increasing PS_D. $PS_{A,E}$ and $PS_{B,E}$ were fixed at 0.

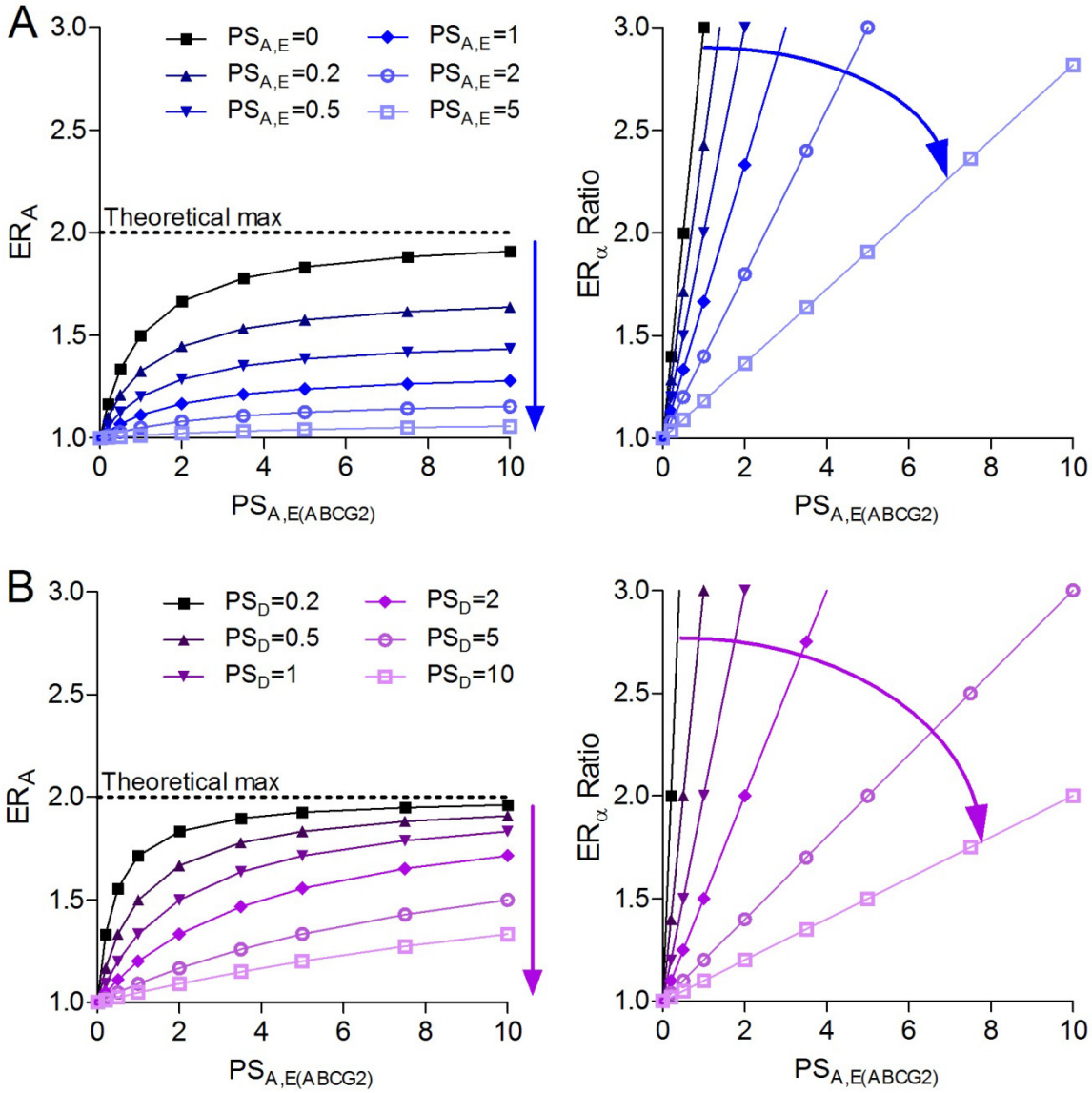

The second challenge to the constraints of the model involves the assumption that PS_D is much greater than that of PS_{PC} or that $PS_{PC} \rightarrow 0$. Table 4-3 again presents the five substrates studied in Aim 5, but this time provides the calculated permeability of the paracellular marker used each study beside that of each ABCG2 substrate. For methotrexate and ciprofloxacin in general and for virtually every calculated ABCG2 A→B permeability, the PS_{PC} was not negligible in comparison to that of the substrate studied. To understand the effect of a PS_{PC} that is not zero and that may be variable from experiment to experiment the relationship between $PS_{A,E(ABCG2)}$ and the ER_A or ER_α Ratio was graphed in the setting of an increasing PS_{PC} (Figure 4-29). As with increases in PS_D and $PS_{A,E}$, increases in PS_{PC} lowers the maximal achievable ER_A and blunts the ER_α Ratio. Perhaps even more importantly, the relationship between ER_α Ratio and $PS_{A,E(ABCG2)}$ was also no longer linear.

To control for the potential ramifications of variable PS_{PC} in the experimental data, the permeability of the paracellular marker was subtracted from that of the drug being studied. This approach has a theoretical basis in the model as demonstrated by the rearrangement of Eq. 4-6 and Eq. 4-7 to Eq. 4-12 and Eq. 4-13 below but is dependent on one major assumption; that the PS_{PC} of the paracellular marker being measured is equal to the PS_{PC} of the drug being studied.

$$\frac{\frac{dX_{A,B\rightarrow A}}{dt}}{C_B^0} - PS_{PC} = \frac{(PS_D+PS_{B,U})(PS_D+PS_{A,E}+PS_{A,E(ABCG2)})}{(2PS_D+PS_{A,E}+PS_{B,E}+PS_{A,E(ABCG2)})} \qquad \text{Eq. 4-12}$$

$$\frac{\frac{dX_{B,\,A\rightarrow B}}{dt}}{C_A^0} - PS_{PC} = \frac{(PS_D+PS_{A,U})(PS_D+PS_{B,E})}{(2PS_D+PS_{A,E}+PS_{B,E}+PS_{A,E(ABCG2)})} \qquad \text{Eq. 4-13}$$

Table 4-3 provides the ER_α and ER_α Ratio of the five ABCG2 substrates studied in the new model system recalculated using these equations. Relative to the values calculated earlier and presented in Table 4-2, the correction increased both efflux ratios for nitrofurantoin and substantially increased both values for ciprofloxacin. Efflux ratios for cimetidine and PhIP were less affected as the ABCG2 A→B permeability difference was relatively unchanged from the original ABCG2 A→B permeability (permeability of the paracellular marker was not large compared to that of the substrate being studied). Methotrexate could not be evaluated as the permeability of the drug was nearly identical and sometimes less than that of sucrose resulting in negative permeability differences. The PS_{PC} subtraction also led to a very small ABCG2 A→B permeability and substantially increased the variability in the ER_α and ER_α Ratio for ciprofloxacin.

Table 4-3: The relative permeabilities of the paracellular marker and the drug being studied in each flux experiment and corrected efflux ratios.

ER_α and ER_α Ratio were calculated accounting for PS_{PC}. Permeability of the paracellular marker mannitol (*) or sucrose (†) was assumed to be equivalent to paracellular permeability of the drug being studied in the same transwell and was subtracted from the total permeability to yield the transcellular permeability of each drug. Data is presented as the mean and standard deviation of all possible efflux ratios from the unmatched individual experimental permeabilities.

		Papp (drug)		Papp (paracellular)		Papp Difference		ER_α ABCG2		ER_α Ratio	
		Mean	SD	Mean	SD	Mean	SD	Mean	SD	Mean	SD
Nitrofurantoin*	Empty B→A	5.26	0.27	2.19	0.31	3.07	0.23	31.30	4.79	78.05	12.37
	Empty A→B	9.54	0.33	1.92	0.36	7.62	0.18				
	ABCG2 B→A	32.18	0.27	1.74	0.44	30.45	0.18				
	ABCG2 A→B	2.33	0.29	1.34	0.40	0.99	0.18				
Cimetidine†	Empty B→A	2.33	0.43	0.85	0.47	1.48	0.14	26.53	2.24	17.36	2.27
	Empty A→B	1.64	0.29	0.67	0.20	0.96	0.09				
	ABCG2 B→A	8.38	0.16	0.76	0.12	7.62	0.10				
	ABCG2 A→B	0.50	0.06	0.21	0.05	0.29	0.03				
PhIP*	Empty B→A	62.79	5.12	1.27	0.25	61.52	5.27	49.50	6.96	50.76	7.91
	Empty A→B	64.40	3.18	1.61	0.29	62.79	3.17				
	ABCG2 B→A	147.16	3.85	1.13	0.28	146.03	4.13				
	ABCG2 A→B	3.50	0.49	0.50	0.06	3.00	0.51				
	Empty B→A	39.05	4.81	2.23	0.39	36.82	5.19	27.53	1.95	28.07	4.11
	Empty A→B	38.86	1.96	1.83	0.24	37.02	2.08				
	ABCG2 B→A	97.27	4.77	0.71	0.11	96.56	4.67				
	ABCG2 A→B	4.09	0.30	0.57	0.08	3.52	0.23				
Methotrexate†	Empty B→A	0.82	0.06	0.90	0.04	-0.09	0.06				
	Empty A→B	0.87	0.02	0.93	0.00	-0.06	0.02				
	ABCG2 B→A	0.45	0.08	0.29	0.02	0.16	0.08				
	ABCG2 A→B	0.29	0.04	0.28	0.01	0.01	0.02				
Ciprofloxacin*	Empty B→A	3.22	0.10	1.76	0.27	1.46	0.23	281.1	348.8	467.2	560.4
	Empty A→B	4.22	0.41	1.84	0.24	2.38	0.25				
	ABCG2 B→A	16.20	0.97	2.14	0.78	14.06	0.29				
	ABCG2 A→B	2.54	0.50	2.34	0.66	0.21	0.17				

Figure 4-29: Effect of variable PS_{PC} on the relationship between the individual efflux ratios and $PS_{A,E(ABCG2)}$.

Effect of variable PS_{PC} ranging from 0 to 0.5 on the relationship between the permeability-surface area product attributed to ABCG2 ($PS_{A,E(ABCG2)}$) and the apical efflux ratio (ER_A) or ratio of the asymetry ratio in the ABCG2-transfected to that of empty vector cells (ER_α Ratio). Arrows depict the changes in efflux ratios with increasing PS_{PC}. $PS_{A,E}$, $PS_{B,E}$, and PS_D were fixed at 0, 0, and 0.5 respectively.

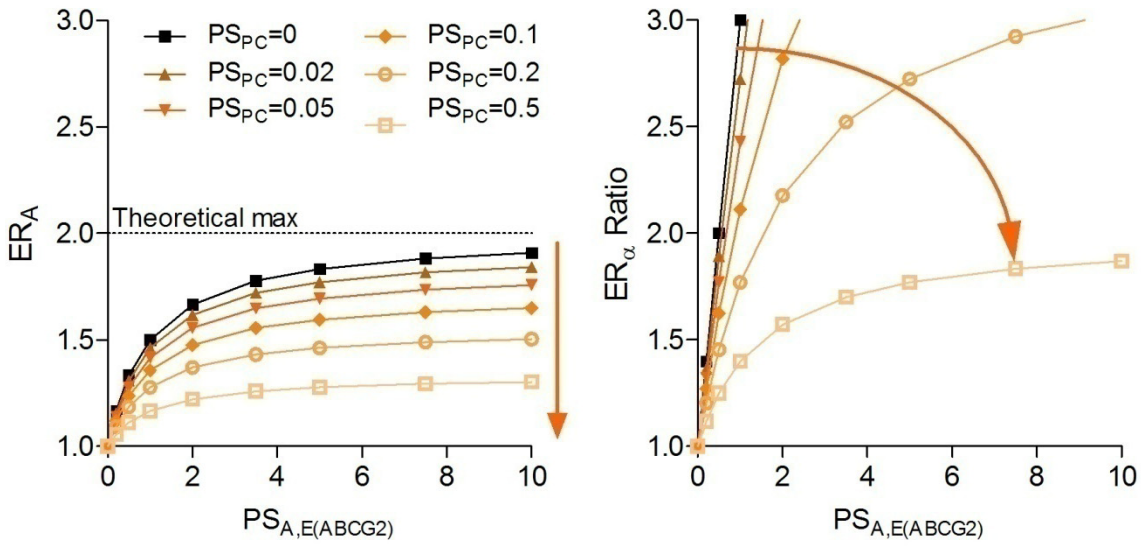

2. Specific Aim 7: To define the relationship between in vitro efflux ratios and the in vivo M/S ratio.

To explore the relationships between flux attributed to ABCG2/Abcg2 in both in vitro and in vivo systems, milk to plasma ratios of several Abcg2 substrates in wild-type and Abcg2 knock-out mice were gathered from the literature (Table 1-1). Correlations between the ratio of the milk to plasma ratios (M/P) in the wild-type and Bcrp1-/- mice and the murine and human ER_{α} and ER_{α} Ratio (presented previously in Table 4-1, Table 4-2, and Table 4-3) were then performed. Figure 4-30 Panel A shows the correlation for murine ER_{α}. Nitrofurantoin, riboflavin, topotecan, and cimetidine are plotted, but not included in the correlation as these drugs showed directional flux in the empty vector-transfected cells, thereby violating the constraint of the ER_{α}, that no other transport processes were present. Nitrofurantoin and riboflavin also demonstrated a large Abcg2-attributed effect in vivo that was not observed in vitro. A correlation coefficient of 0.60 was achieved with the remaining 5 datapoints. The disproportionate Abcg2 affect in vivo with nitrofurantoin and riboflavin may be as a result of other transporter systems that were present in the in vitro system that cannot be controlled for in the ER_{α} calculation. Theoretically, the ER_{α} Ratio can control for these endogenous active transport processes (all except $PS_{A,E}$) that may be present in the single transfection cell line (Eq. 4-10), so correlations were performed using this term versus the same M/P ratio. Figure 4-30 Panel B presents the correlations with and without the drugs excluded in Panel A. The correlation coefficient was 0.52 without these substrates and when they were added, it improved to 0.58; a value similar to what was achieved with the murine ER_{α} correlation that did not contain these drugs. Similar comparisons were made in Figure 4-30 Panels C and D with the literature-derived human data. The human ER_{α}, however, achieved a highly significant correlation ($r = 0.996$; $p < 0.0003$) with the murine M/P ratios once nitrofurantoin, topotecan, and cimetidine were removed (riboflavin ER_{α} Ratio was not available for analysis) (Panel C). As seen with the murine in vitro data, the human ER_{α} Ratio could not fully account for the much higher Abcg2 effect observed in the in vivo M/P ratio (nitrofurantoin in particular). The ER_{α} Ratio correlation coefficient for the analysis containing all the compounds was poor at 0.33, whereas the one for containing only the drugs analyzed in Panel C remained significant ($r = 0.996$; $p < 0.0003$). It is important to note that human correlations suffered from a sparse representation of data points in the middle of the curves. The collection of low M/P ratio and efflux ratio drugs

and the single high M/P and high efflux drug, PhIP, likely contributed to the significant correlations and apparently superior ER_{α} human correlation.

Figure 4-30: Correlations between the in vivo ratio of murine milk to plasma ratios in the wild-type and Abcg2 knock-out (M/P wild-type/Bcrp-/-) to the in vitro human and murine asymmetry efflux ratio (ER_α) and ratio of ABCG2 to empty vector-transfected asymmetry efflux ratios (ER_α Ratio).

Panel A. Murine ER_α. The directional flux of riboflavin, nitrofurantoin, cimetidine, and topotecan in the empty vector-transfected cells suggests endogenous transport processes were present for these drugs so they were removed from correlation (open circles). Panel B. Murine ER_α Ratio. Correlations were performed with (dashed line) and without (solid line) the drugs excluded in Panel A. Panels C. Human ER_α. Nitrofurantoin, topotecan, and cimetidine were again removed from correlation for reasons described above. Panel D. Human ER_α Ratio. The best-fit orthogonal regression lines with (dashed line) and without (solid line) the drugs excluded in Panel C are displayed. The Pearson correlation coefficient (r) determined in each scenario is also reported.

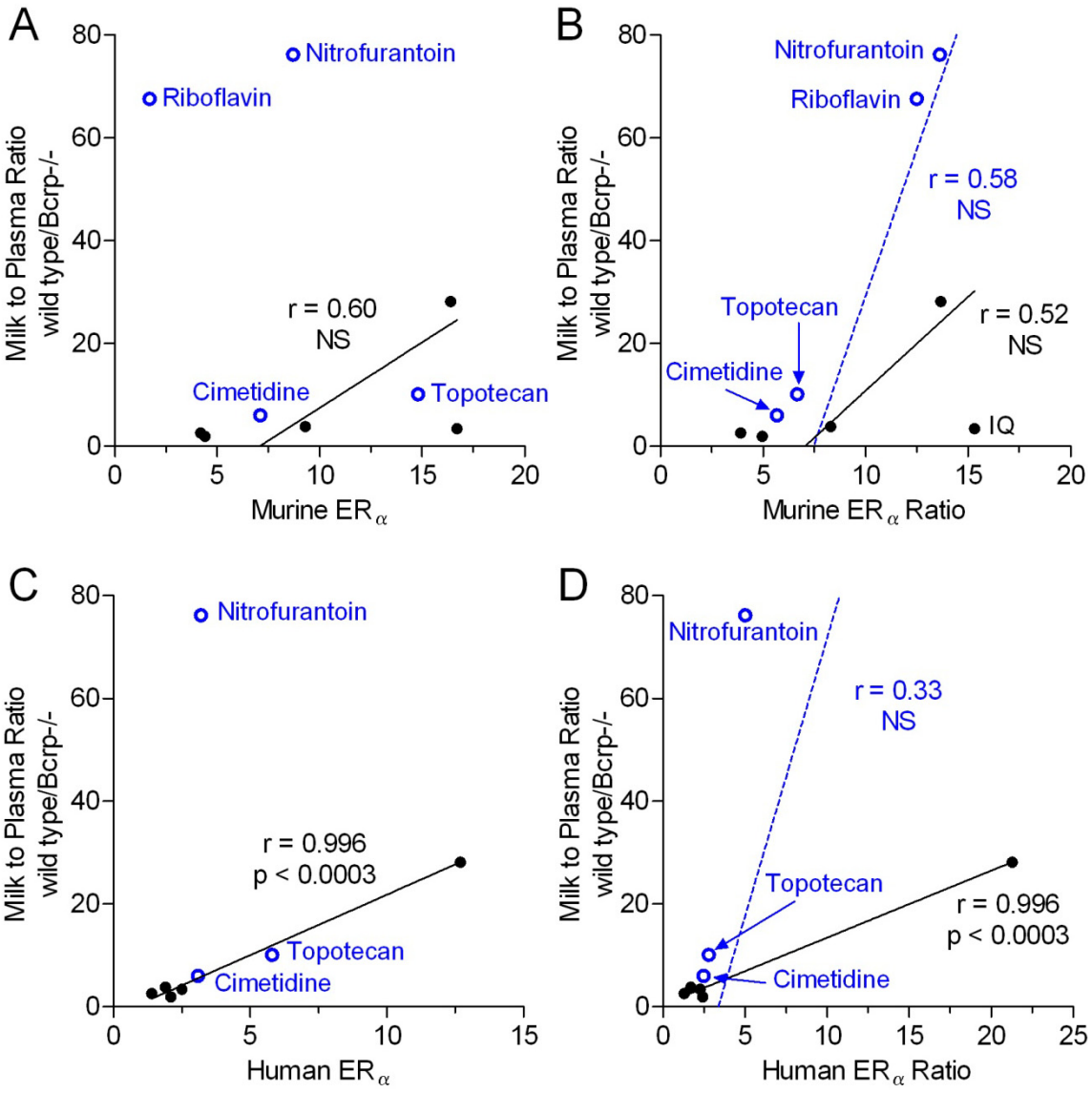

Flux experiments performed in Aim 5 allowed for a more detailed analysis of the model than was possible with the literature-derived data. Accurate measurements of the flux of the paracellular marker used in each assay provided the ability to determine if the correlations could be improved when the efflux ratios were corrected by subtraction of permeability attributed to the paracellular marker (as presented in Eq. 4-12 and Eq. 4-13). Figure 4-31 Panels A and B presents the human efflux ratios from Table 4-2 versus the ratio of the M/P ratios in wild-type and Abcg2 knock-out mice from Table 1-1. An evaluation of the ER_{α} using human data could not be performed as three of the four drugs (ciprofloxacin, cimetidine, nitrofurantoin) showed a directional flux in the empty vector-transfected cells, thereby violating the contraint of this efflux ratio. The ER_{α} Ratio performed fairly well as the rank-order of Abcg2-attributed effect in vivo was observed in vitro for three of the four drugs (ciprofloxacin, cimetidine, PhIP). The nitrofurantoin efflux ratio, however, seemed somewhat blunted compared to that observed in vivo. It should also be noted that some variability was observed with PhIP in the two experiments that were performed. Figure 4-31 Panels C and D present the corrected ER_{α} and ER_{α} Ratio following subtraction of the paracellular marker permeability from that of the substrate measured concurrently (data presented in Table 4-3). Ciprofloxacin was affected the greatest by this correction as the permeability of the paracellular maker was very similar to the A→B flux of ciprofloxacin (2.54 ± 0.5 for ciprofloxacin vs. 2.34 ± 0.7 for mannitol). When all possible combinations of the unmatched permeabilities were evaluated, the variability of the ciprofloxacin efflux ratios following subtraction were much larger than observed without it. The standard deviations surrounding these both the ER_{α} and the ER_{α} Ratio was greater than 100% of the mean and was much larger than observed with the other substrates. The ER_{α} Ratio with the substraction performed better than ER_{α} Ratio without it as the correlation of the in vivo Abcg2-attributed effect and in vitro ER_{α} Ratio for nitrofurantoin and its overall rank order was improved. The Pearson correlation coefficient was 0.94 and trended towards significance with a p-value of 0.06 with ciprofloxacin excluded from the analysis.

Figure 4-31: Correlations between the in vivo ratio of murine milk to plasma ratios in the wild-type and Abcg2 knock-out (M/P wild-type/Bcrp-/-) to the in vitro human asymmetry efflux ratio (ER_α) and ratio of new ABCG2 to empty vector-transfected asymmetry efflux ratios (ER_α Ratio).

Panel A. Human ER_α. Nitrofurantoin, cimetidine, and ciprofloxacin are identified by open circles as all demonstrated directional flux in the empty vector-transfected cells, suggesting endogenous transport processes were present for these drugs. Panel B. Human ER_α Ratio. Panels C/D. The same efflux ratios were calculated for each drug by first subtracting PS_{PC}. Ciprofloxacin is not included due to the very large ER_α and ER_α Ratio variability observed following subtraction of PS_{PC} (see Table 4-3). Panels C. ER_α. Panel D. ER_α Ratio. The best-fit orthogonal regression lines for all drugs are displayed in the ER_α Ratio graphs (Panels B and D). The Pearson correlation coefficient (r) is also reported.

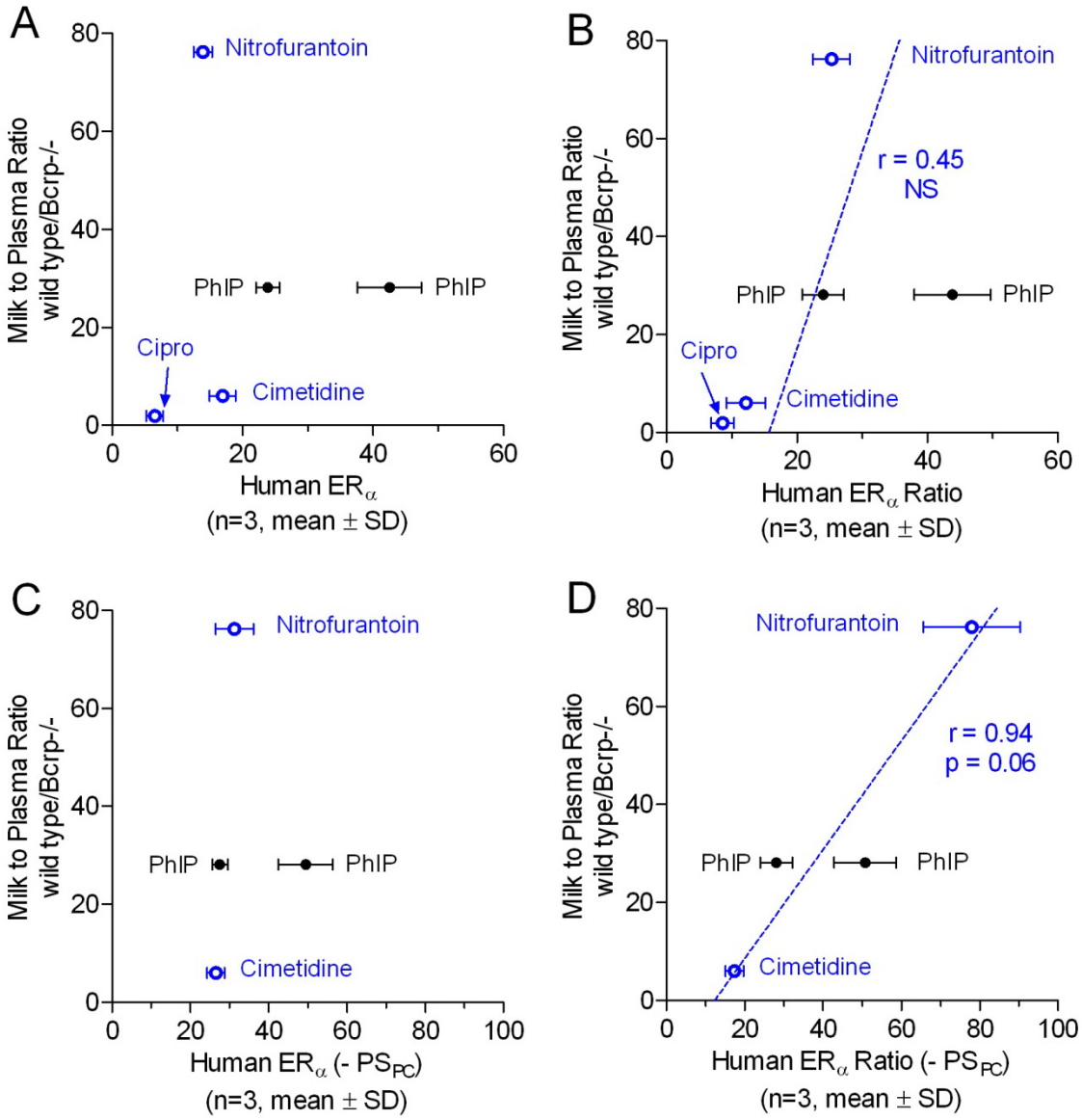

D. Microarray expression profiling of transporter gene expression in murine developmental datasets

1. Specific Aim 8: To identify xenobiotic transporters highly expressed in mice during lactation (in vivo).

Microarray expression profiling was used to identify murine xenobiotic transporters that are differentially expressed during lactation. Nonlactating and lactating mammary gland array data from three independent experiments [174-176] was obtained from the published literature and pooled to increase sample size. Figure 4-32 demonstrates that no substantial experimental bias was seen from the pooling of these datasets as the signal intensities from chips within same group across experiments (nonlactating or lactating) were more highly correlated than those in different groups but within the same experiment.

In order to determine transporters of potential importance for xenobiotic transport during lactation, the signal intensities of the 32 probesets identified in Table 3-2 (subset of transporters genes of interest that are detectable by the Mu74v2A GeneChip®) were compared in lactating vs. nonlactating groups. Of the 32 probesets, 24 were eliminated from the analysis as they were Absent in all 15 lactating samples according to the probeset detection calls. Comparisons of the remaining 8 transporter probesets are presented in Table 4-4 grouped by the genes that are significantly upregulated, downregulated, or with no difference in expression level when comparing lactating vs. nonlactating mammary gland samples. The RNA expression level of Abcg2, Slc22a1, Slc15a2, Slc29a1, Slc16a1, and Abcc5 was higher during lactation, resulting in fold changes of 20, 10, 4, 2, 2, and 2, respectively over virgin mammary glands. To further emphasize the developmental regulation of Abcg2, Slc22a1, and Slc15a2, specifically the higher levels observed during lactation, the array data from all timepoints of one experiment (Stein et al) for these genes as well as the β-casein (positive control) is presented in Figure 4-33. Detection call and signal intensity data from each chip is provided in Appendix 4.

Figure 4-32: Correlations of virgin and lactating murine mammary gland tissue microarray chip signal intensities within and between groups in the Stein et al, Clarkson et al, and Medrano et al. datasets.

Signal concordance was evaluated using Pearson's correlations of the signal values generated by the MAS5 algorithm. The heat map contains all pairwise comparisons where the r^2 values have been converted into a pseudocolor scale.

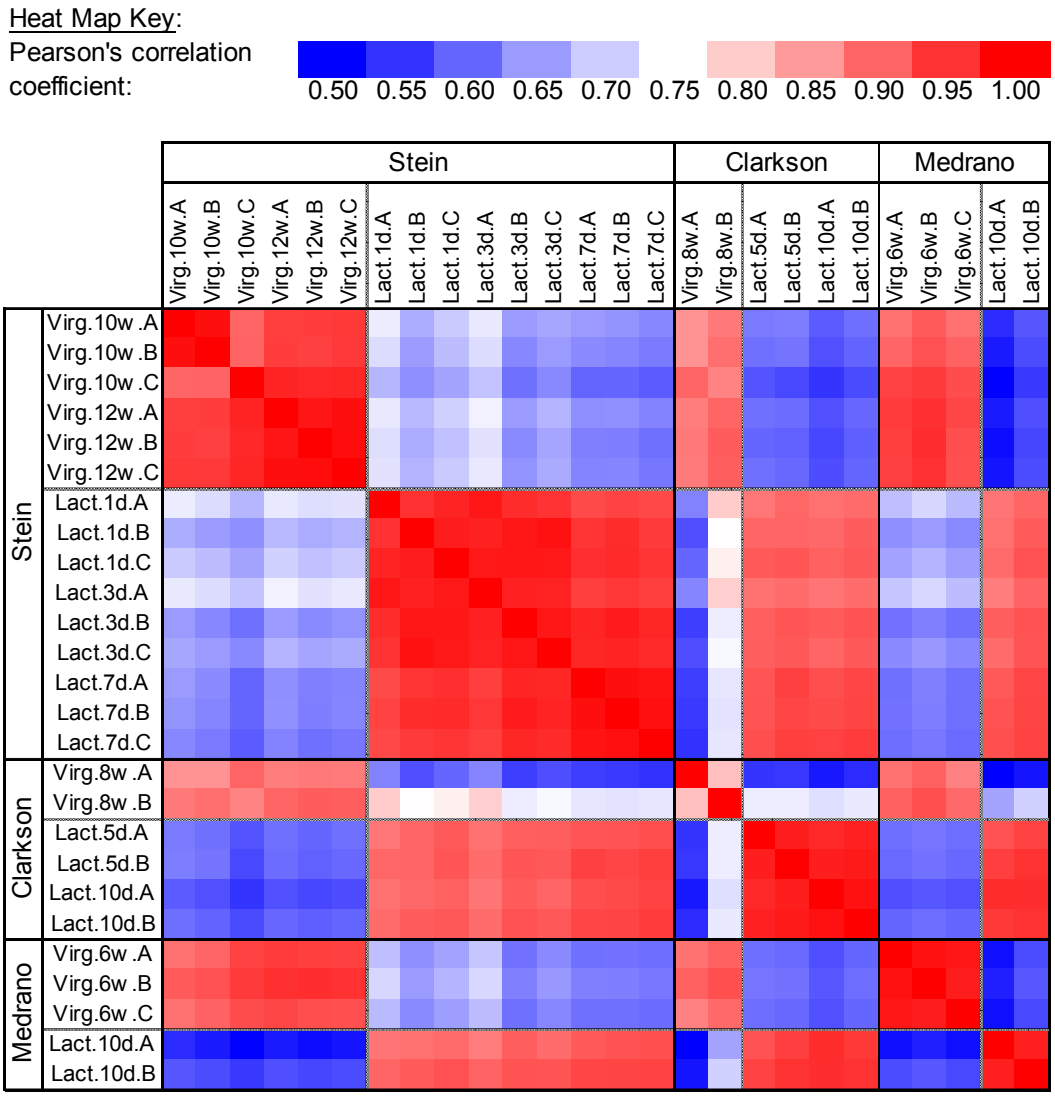

Table 4-4: Comparison of Affymetrix Mu74v2A array transporter probeset expression levels in murine lactating vs. nonlactating mammary gland.

Genes are grouped based on whether they are increased, decreased or not different during lactation. Probesets for the same gene were then grouped into sections of the table sorted by fold change in expression.

Gene Symbol	Probeset ID	p Value	Lactating		NonLactating		Fold Change
			Mean	SD	Mean	SD	
Higher during lactation (p < 0.05, fold change >1)							
Abcg2	93626_at	2.02E-07	1735	682	85	27	**20.49**
Slc22a1	100916_at	6.58E-03	35	38	3	4	**10.07**
Slc15a2	103918_at	5.10E-05	66	34	16	8	**4.06**
Slc29a1	95733_at	6.70E-04	445	193	227	58	**1.96**
Slc16a1	101588_at	1.78E-02	25	13	14	7	**1.73**
Abcc5	103800_at	1.93E-04	155	38	99	23	**1.57**
Lower during lactation (p < 0.05, fold change <1)							
Slc23a2	104267_at	2.72E-04	66	15	101	26	**0.66**
Detectable, but no difference in expression (p > 0.05)							
Slc22a5	98322_at	1.77E-01	55	13	47	17	

Figure 4-33: Affymetrix Mu74v2A array expression levels of β-casein, Abcg2, Slc22a1, and Slc15a2 over the course of murine development.

Data is from 17 developmental time points in the Stein et al. dataset. One mouse mammary gland was used per chip with 3 chips (biological replicates) analyzed per time point. The positive control, B-casein (Panel A) and Abcg2 (Panel B), Slc22a1 (Panel C), and Slc15a2 (Panel D) were significantly all upregulated during lactation.

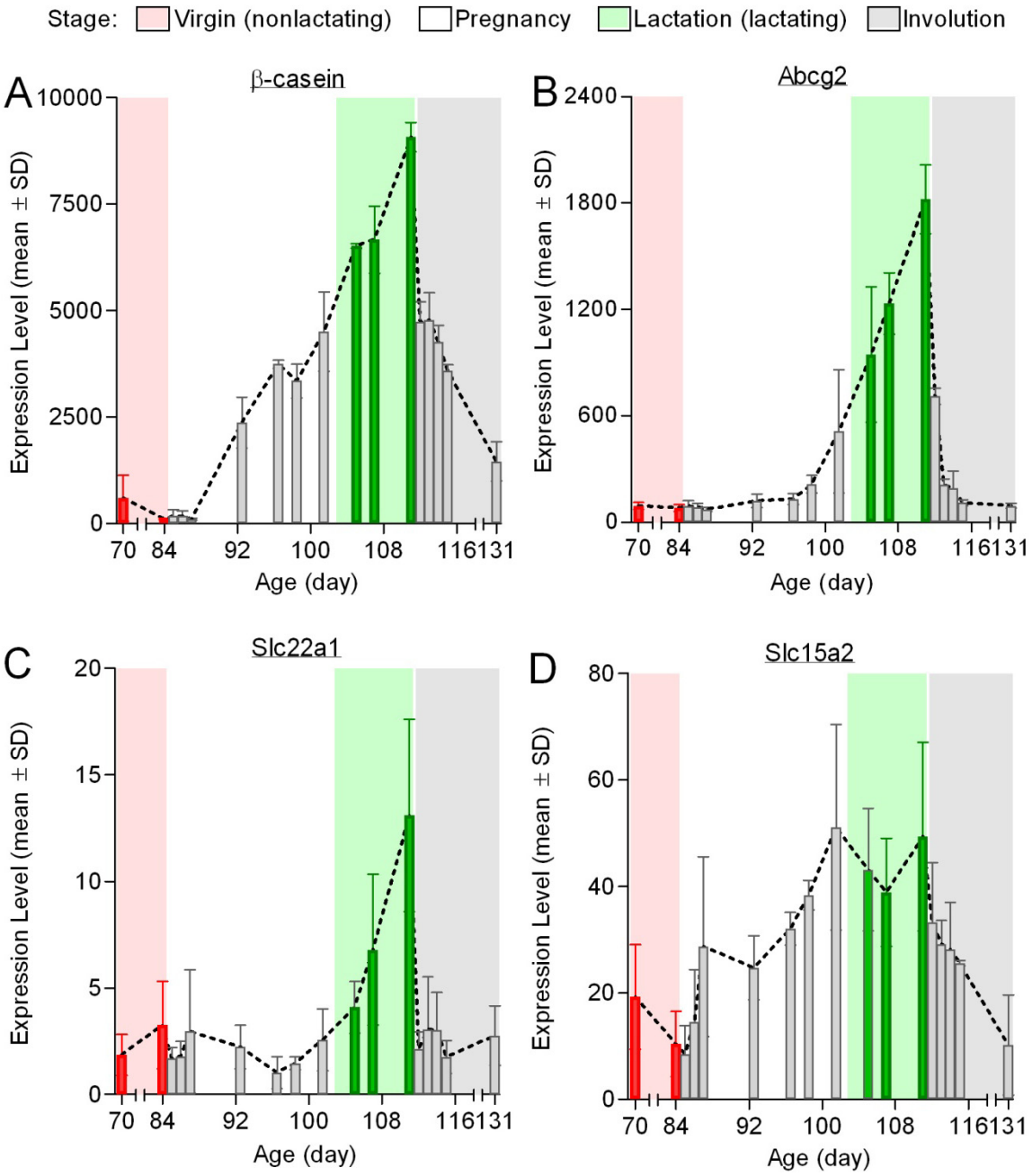

E. Identification of xenobiotic transporters highly expressed in human LMEC clinical samples

1. Specific Aim 9: To develop a robust methodology to isolate a pure population of epithelial cells from human breast milk and reduction mammoplasty clinical samples.

Previous methods using Dynabeads® resulted in >95% purity of MECs from breast milk and breast reduction specimens, but were not robust enough to obtain the numbers of cells needed for microarray analysis. Two new approaches, one using immunomagnetic nanoparticles and the other using FACS, were evaluated with breast milk as it had been difficult to isolate LMECs from this matrix in sufficient numbers previously. The EasySep® immunomagnetic separation system was thoroughly tested with different buffers, blocking agents, incubation times, and nanoparticle conjugation approaches. However, the murine anti-MUC1 (clone 214D4) antibody required by the system did not appear to have the correct specificity for MECs. Figure 4-34 is the best results of the optimized approach and depicts a higher than expected percentage of MUC1 positive (MUC1+) cells prior to selection. This population was enriched to nearly 95% by the procedure, but was not associated with a corresponding increase in cells stained positive by immunocytostaining for simple epithelial cells (Figure 4-35).

The FACS-based method utilizing the rat anti-MUC1 (clone MFGM/5/11[ICR.2]) antibody generated superior results. Figure 4-36 shows the percentage of cells that were MUC1+ in breast milk prior to isolation. A clear bimodal distribution that was not observed with the murine anti-MUC1 (clone 214D4) antibody was apparent with approximately 43% of the initial population MUC1+. LMECs were enriched in the selected population to greater than 99% purity as measure by immunocytostaining (Figure 4-37). The approach was also sufficiently robust with at least 1×10^5 (upwards to 3.5×10^6) cells obtained from a single sample.

Figure 4-34: Flow cytometric analysis of the purity of LMEC cells separated by immunomagnetic separation using the murine anti-MUC1 (clone 214D4) antibody and EasySep® nanoparticles.

Cell-nanoparticle complexes derived breast milk samples were labeled with the FITC-conjugated anti-dextran antibody (green shaded) or FITC-conjugated isotype control (black line). The percentage of cells in MUC1+ gate (set relative to the isotype control) were compared in the before and after isolation.

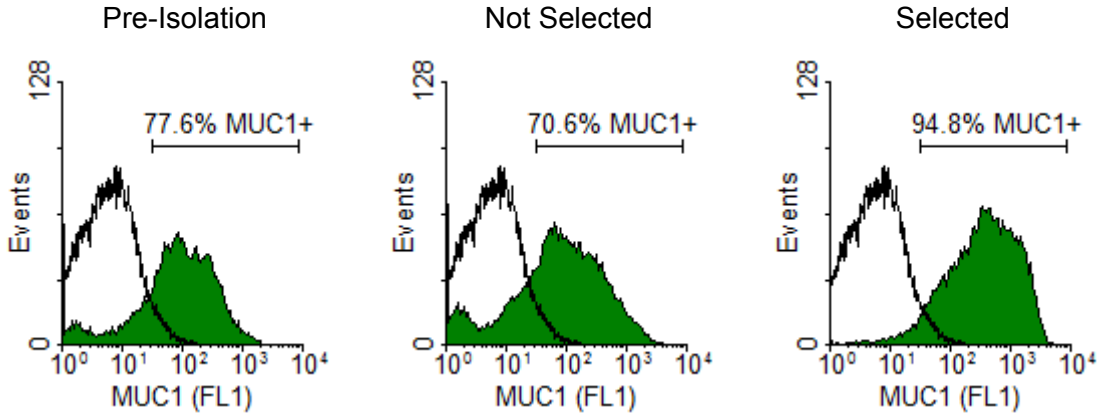

Figure 4-35: Immunocytostaining of luminal epithelial cell specific cytokeratins in the pre-isolated and populations selected by a murine EasySep® nanoparticles to verify purity.

The CK22 simple epithelial cell antibody and Vectastain ABC kit were used to label simple epithelial cells (brown) (20x magnification).

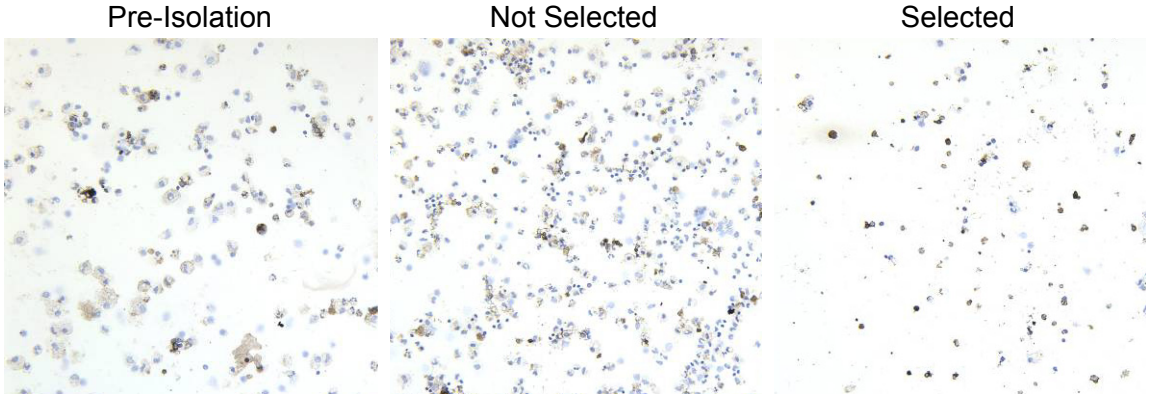

Figure 4-36: FACS isolation of LMEC from breast milk using the rat anti-MUC1 (clone MFGM/5/11[ICR.2] antibody.

Cells were incubated with an anti-MUC1 (clone MFGM/5/11[ICR.2]) (green shaded) or isotype control (black line) antibody and labeled with a FITC-conjugated secondary antibody. The percentage of cells in MUC1+ gate (set at the division of 2 populations in the pre-isolation histogram) were compared in the before and after isolation.

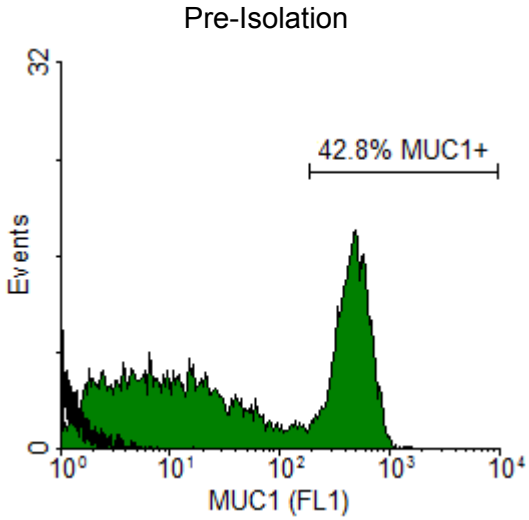

Figure 4-37: Immunocytostaining of luminal epithelial cell specific cytokeratins in the pre-isolated and populations selected by FACS to verify purity.

The CK22 simple epithelial cell antibody and Vectastain ABC kit were used to label simple epithelial cells (brown). Purity was assessed by counting (20x magnification).

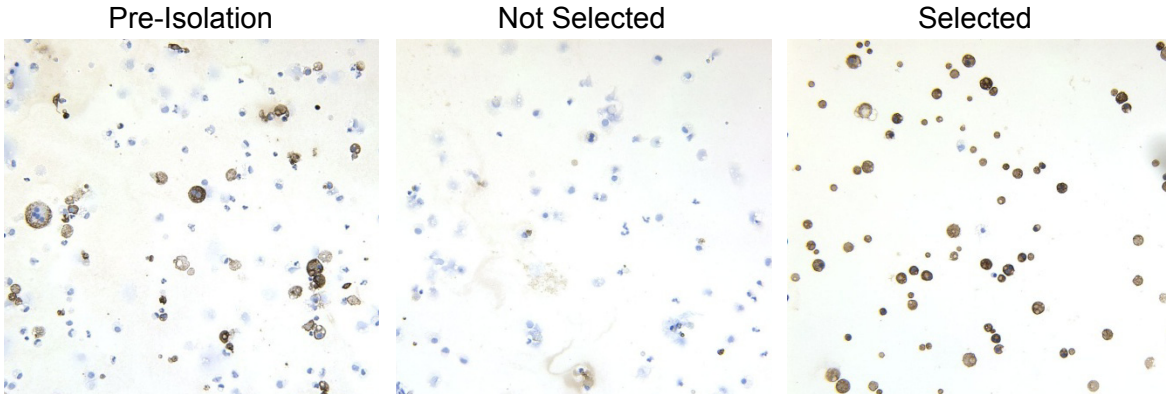

2. Specific Aim 10: To identify xenobiotic transporters highly expressed in human lactating mammary epithelial cells relative to nonlactating mammary epithelial cells and other secretory tissues

Seventeen reduction mammoplasty samples were received from UK surgical pathology from 2002 – 2006. Three were consumed during early method optimization, three samples were small or too fatty to provide enough organoids, four were ruled out due to a pathology reports that were incomplete or indicating significant fibrosis or proliferative changes, and three provided too few cells in the final sorted populations. The remaining four samples were histologically normal and yielded enough cells to generate greater than 2 µg of RNA. From these, the three yielding the greatest amount of high quality RNA were selected for microarray analysis. Subject demographic information that was attainable from the anonymized samples is provided in Table 4-5.

Seven breastfeeding volunteers participated in the study from 2005 – 2006, providing 45 breast milk samples. One subject was used for early method development and three subjects were excluded as they either did not have enough cells in the breast milk or elected to stop participating due to low milk production (weaning). Demographic information from the three subjects who completed the study is provided in Table 4-5. Each provided breast milk over a 6-10 week period and ranged from 9-47 weeks post-partum.

Table 4-5: Sample demographics and FACS isolation results

Number of samples refers to the number of breast milk samples collected from each patient over the post-partum time frame indicated. Number in parenthesis indicates how many samples were successfully processed through FACS to generate enough cells for subsequent RNA isolation. For MEC samples, this refers to the number of frozen organoid vials (split from the original reduction mammoplasty sample) that were processed individually to generate enough cells for subsequent RNA isolation. Number of MEC/LMEC cells isolated is the mean number of MUC1+ cells from each sample collected and is expressed as a percentage of the total number of cells put through the cytofluorimeter during FACS.

					MEC/LMEC isolation results		
Sample	Age	Ethnicity	Weeks post-partum	Number of samples	Number of cells isolated (mean ± SD)	Percentage of total cells (mean ± SD)	Total pooled RNA (µg)
MEC #1	25	Caucasian	-	2	1.7×10^6	33.7	5.6 µg
MEC #2	33	Caucasian	-	8	$7.2 \pm 4.6 \times 10^5$	7.8 ± 2.9	2.2 µg
MEC #3	33	Caucasian	-	4	$8.5 \pm 5.2 \times 10^5$	15 ± 2.9	5.0 µg
LMEC #1	24	Caucasian	39 - 47	7 (6)	1.0 ± 0.7 x 106	29.7 ± 19.2	10.1 µg
LMEC #2	32	Caucasian	27 - 34	10 (9)	0.5 ± 1.1 x 106	25.0 ± 16.5	4.1 µg
LMEC #3	21	Caucasian	9-19	12 (11)	3.9 ± 2.2 x 105	9.5 ± 8.6	3.7 µg

The method performed well, yielding >99% pure populations from both breast milk and reduction samples (Figure 4-38 and Figure 4-39). Approximately 10 – 30% of cells in breast milk were LMECs and 8 – 34% derived from reduction mammoplasty specimens were MECs (Table 4-5). FACs allowed for collection of > 2 µg of RNA in as many as eleven or as few as six collections of eight ounces breast milk or from a single mammary reduction specimen. Due to cell clumping with large samples, the number of cells isolated per specimen was increased when organoids were split into multiple aliquots at the time of freezing and processed via FACS separately. The RNA isolated from each sample was of high quality with little degradation as determined by RNA Integrity Numbers (RIN) of > 9.2 per Bioanalyzer 2100 (Figure 4-40). Sufficient quantities were collected for both microarray analysis and PCR validation from all samples.

Figure 4-38: FACS isolation of mammary luminal epithelial cells from reduction mammoplasty specimens and breast milk.

Cells were incubated with an anti-MUC1 (clone MFGM/5/11[ICR.2]) (shaded) or isotype control (black line) antibody and labeled with a FITC-conjugated secondary antibody. The MUC1+ gate is set at the division of 2 populations in the pre-isolation histogram and served as the population sorted as LMECs/MECs.

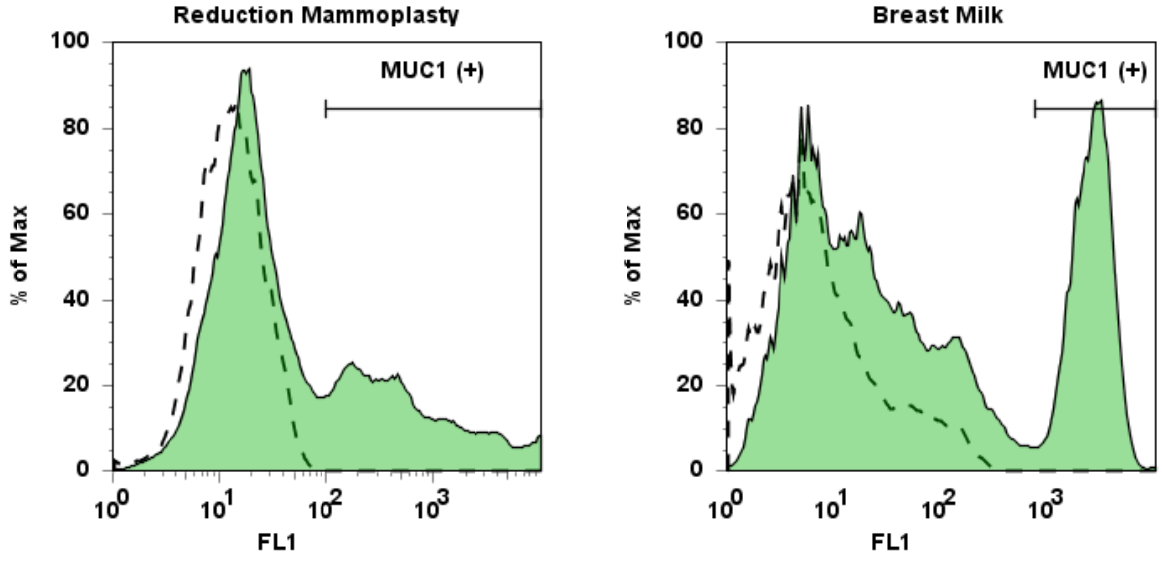

Figure 4-39: Immunocytostaining of luminal epithelial cell specific cytokeratins in the presorted and sorted populations to verify purity.

The CK22 simple epithelial cell antibody and Vectastain ABC kit was used to label simple epithelial cells (brown). Purity was assessed by counting (20x magnification).

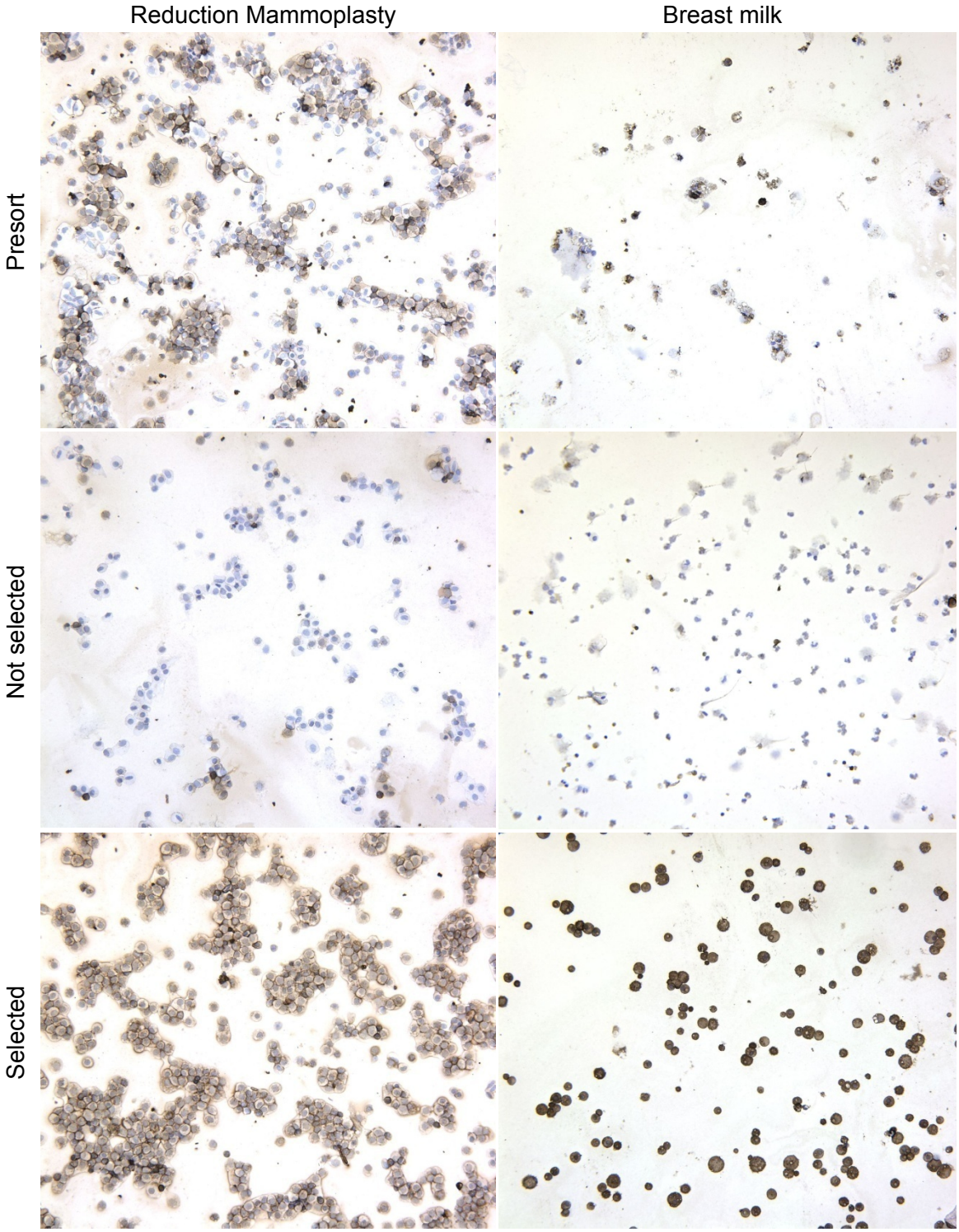

Figure 4-40: Bioanalyer 2100 analysis of LMEC and MEC RNA integrity.

Quality of RNA isolated from LMEC and MEC samples was assessed using the Bioanalyzer 2100 at the UK Microarray Core Facility. Nanogram amounts of RNA were fluorescent labeled and separated by microchannel electrophoresis. RNA integrity was evaluated by integrating the peaks associated with the 28s and 18s bands relative to degradation products. Samples are given a RNA Integrity Number (RIN) on a 10 point scale.

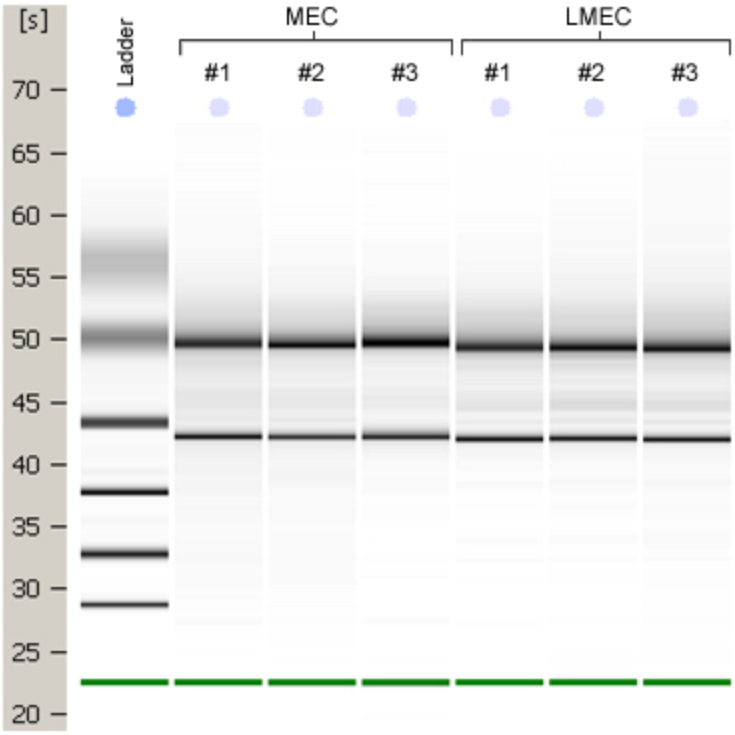

Representative Electropherogram:

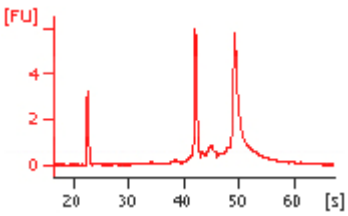

RIN values:

MEC #1 = 9.2
MEC #2 = 9.3
MEC #3 = 10
LMEC #1 = 9.8
LMEC #2 = 9.5
LMEC #3 = 9.7

The external liver and kidney microarray data that were used to determine the relative LMEC expression level when differences between LMEC and MEC samples were not significant was obtained from a study by Khaitovich et al. [183]. The sources of the human liver tissue samples were four males ages 21, 29, and "adult" and 2 females ages 27 and 29. Human kidney tissue samples were from males ages 24, 24, 26, 46, 62, and 64.

Figure 4-41 shows that signal intensities from chips within same group (MEC, LMEC, kidney or liver) were more highly correlated than those in different groups. Also, as one would expect from cells from the same tissue, the MEC and LMEC array signal intensities were also more correlated with each other than with either the kidney or liver.

Figure 4-41: Correlation of LMEC, MEC, liver, and kidney microarray chip signal intensities within and between groups.

Signal concordance was evaluated using Pearson's correlations of the signal values generated by the MAS5 algorithm. The heat map contains all pairwise comparisons where the r^2 values have been converted into a pseudocolor scale.

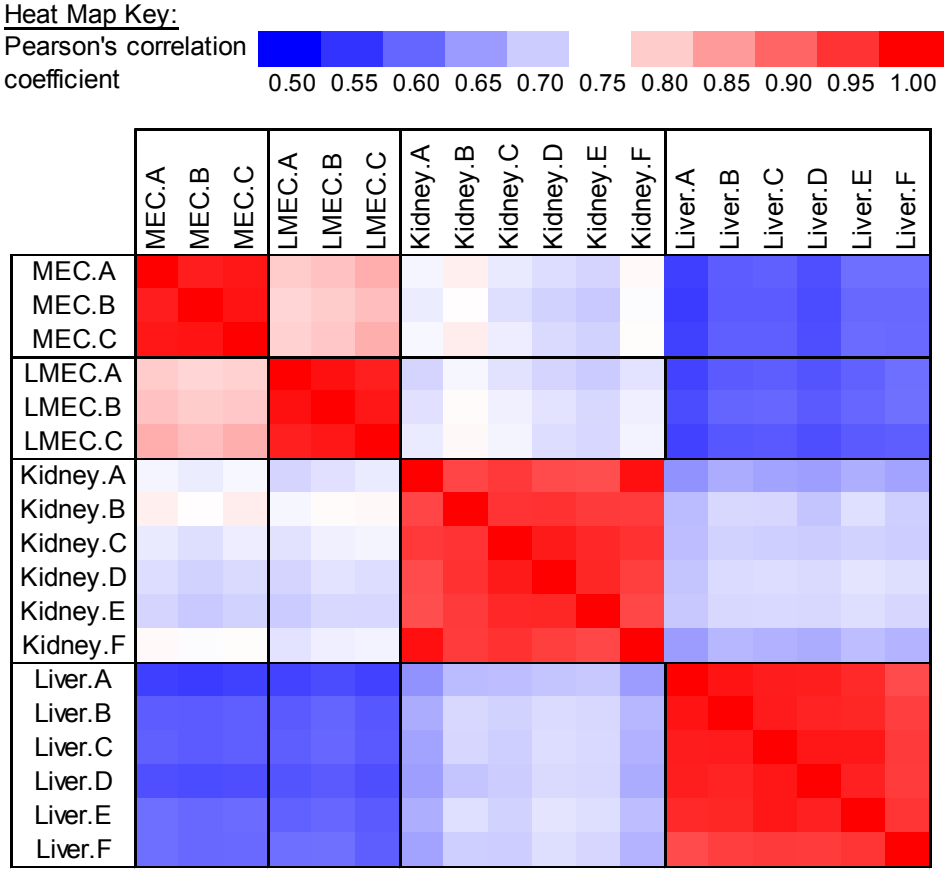

In order to determine transporters of potential importance for xenobiotic transport in LMECs, the signal intensities of the 122 probesets identified in Table 3-2 were first compared in LMEC vs. MEC arrays. Those transporter genes whose expression was significantly upregulated during lactation were of interest whereas those significantly downregulated were not. The transporter probeset comparisons that did not achieve significance were not discarded as similar gene expression in LMEC and MEC cells could still be of importance if that expression level were high. Of the 122 probesets, 85 were eliminated from the analysis as they were Absent in all three LMEC samples according to the probeset detection calls. Comparisons of the remaining 37 transporter probesets are presented in Table 4-6 grouped by the genes that are significantly upregulated, downregulated, or with no difference in expression level when comparing LMEC vs. MEC. The RNA expression level of ABCG2, SLCO4C1, SLC15A2, SLC22A12, and SLC6A14 was higher in LMECs, resulting in fold changes of 164, 70, 41, 8 and 2, respectively over MECs. At least one probeset for ABCB1, ABCB10, ABCC4, SLC10A1, SLC16A1, SLC16A7, SLC17A1, SLC22A3, SLC22A4, SLC22A5, SLC22A9, SLC23A2, SLC28A1, SLC28A3, SLC29A1, SLC29A2, SLCO2B1, and SLC4A1 was detectable, but not different between the groups.

The expression level relative to liver and kidney for the 37 probesets that were not absent on all three LMEC arrays are presented in Table 4-7 and Table 4-8. Versus the liver, SLC6A14, SLC15A, ABCG2, SLCO4C1, SLCO4A1, AND SLC22A4 were upregulated 79, 46, 7, 7, 5, and 2 fold respectively. At least one probeset for ABCB10, SLC16A1, SLC22A12, SLC22A5, SLC28A3, SLC29A, SLC29A2, and SLCO4A1 was detectable, but not different between the groups. The similar comparison versus kidney demonstrated an increase in the level of expression of SLC6A14, ABCG2, SLC15A2, SLC16A1, and SLCO4C1 by 50, 40, 5, 3 and 2 fold. At least one probeset for ABCC10, SLC10A1, SLC16A, SLC22A4, SLC22A9, SLC28A3, SLC29A1, and SCL4A1 was detectable, but not different between the groups. Detection call and signal intensity data from each chip is provided in Appendix 5.

Table 4-6: Comparison of Affymetrix U133 plus 2.0 array transporter probeset expression levels in human LMEC vs. MEC.

Genes are grouped based on whether they are increased, decreased or not different during lactation. Probesets for the same gene were grouped into sections of the table sorted by fold change in expression.

Gene Symbol	Probeset ID	p-Value	LMEC		MEC		Fold Change
			Mean	SD	Mean	SD	
Higher during lactation (p < 0.05, fold change >1)							
ABCG2	209735_at	3.69E-02	17536	5964	107	75	**164.04**
SLCO4C1	222071_s_at	2.39E-03	3362	294	48	31	**69.70**
SLC15A2	205316_at	3.62E-03	3936	421	96	47	**40.80**
	205317_s_at	2.16E-03	868	182	89	62	**9.72**
	240159_at	8.99E-04	243	31	76	10	**3.18**
SLC22A12	237799_at	2.79E-02	184	80	24	19	**7.84**
SLC6A14	219795_at	4.13E-02	3988	1193	1773	500	**2.25**
Lower during lactation (p < 0.05, fold change <1)							
ABCC1	202804_at	8.59E-03	112	21	1400	214	**0.08**
SLCO3A1	219229_at	8.95E-04	51	63	419	34	**0.12**
	227367_at	1.88E-03	160	67	544	62	**0.29**
SLC16A7	207057_at	4.24E-02	125	44	442	181	**0.28**
	210807_s_at	7.83E-03	85	14	191	34	**0.45**
Detectable, but no difference in expression (p > 0.05)							
ABCB1	243951_at	5.29E-01	65	25	52	19	
ABCC10	213485_s_at	1.82E-01	601	169	387	155	
	215873_x_at	3.45E-01	301	43	227	112	
ABCC4	1555039_a_at	7.15E-01	42	53	30	12	
SLC10A1	207185_at	6.26E-01	110	122	70	6	
SLC16A1	1557918_s_at	1.53E-01	954	353	526	230	
	202236_s_at	1.69E-01	3090	473	1908	1127	
	202234_s_at	6.55E-01	736	120	626	375	
	202235_at	6.79E-01	267	47	315	181	
	209900_s_at	9.11E-01	1005	49	1052	639	
SLC17A1	237049_at	4.23E-01	35	32	16	18	
SLC22A3	242578_x_at	1.78E-01	184	54	784	511	
	1570482_at	2.55E-01	29	15	74	56	
SLC22A4	205896_at	2.62E-01	429	82	349	69	
SLC22A5	205074_at	6.34E-01	535	146	477	125	
SLC22A9	241770_x_at	7.26E-01	38	27	47	30	
SLC23A2	211572_s_at	2.95E-01	93	20	109	2	

Table 4-6 cont.

Gene Symbol	Probeset ID	p-Value	LMEC		MEC		Fold Change
			Mean	SD	Mean	SD	
Detectable, but no difference in expression (p > 0.05)							
SLC28A1	207560_at	2.91E-01	200	18	135	91	
SLC28A3	220475_at	6.94E-02	191	219	1422	837	
SLC29A1	201802_at	8.38E-02	591	277	220	45	
	201801_s_at	1.21E-01	1000	468	306	668	
SLC29A2	204717_s_at	5.07E-02	196	38	123	25	
SLCO2B1	203473_at	3.89E-01	152	86	103	23	
SLCO4A1	1554332_a_at	1.40E-01	1345	598	522	24	
	219911_s_at	6.09E-01	907	238	1113	599	

Table 4-7: Comparison of Affymetrix U133 plus 2.0 array transporter probeset expression levels in human LMEC vs. liver.

Genes are grouped based on whether they are increased, decreased or not different during lactation. Probesets for the same gene were then grouped into sections of the table sorted by fold change in expression.

Gene Symbol	Probeset ID	p Value	LMEC		Liver		Fold Change
			Mean	SD	Mean	SD	
Higher relative to liver (p < 0.05, fold change >1)							
SLC6A14	219795_at	2.92E-02	3988	1193	50	36	79.34
SLC15A2	205316_at	3.72E-03	3936	421	85	54	46.06
	205317_s_at	1.89E-02	868	182	184	55	4.72
	240159_at	1.67E-02	243	31	144	49	1.69
ABCG2	209735_at	4.51E-02	17536	5964	2582	1542	6.79
SLCO4C1	222071_s_at	3.46E-06	3362	294	505	313	6.65
SLCO4A1	219911_s_at	1.85E-03	907	238	184	198	4.92
SLC22A4	205896_at	6.61E-04	429	82	186	47	2.30
Lower relative to liver (p < 0.05, fold change >1)							
SLC10A1	207185_at	3.73E-06	110	122	16334	1870	0.01
SLCO2B1	203473_at	2.14E-05	152	86	10989	1752	0.01
SLC23A2	211572_s_at	2.02E-02	93	20	2576	1813	0.04
SLC22A9	241770_x_at	1.17E-04	38	27	802	186	0.05
SLC17A1	237049_at	6.34E-04	35	32	359	91	0.10
ABCB1	243951_at	6.03E-04	65	25	482	117	0.13
SLCO3A1	219229_at	1.42E-02	51	63	328	137	0.15
	227367_at	5.93E-03	160	67	296	40	0.54
SLC22A3	1570482_at	2.26E-02	29	15	185	118	0.16
	242578_x_at	3.65E-03	184	54	837	253	0.22
SLC28A1	207560_at	2.18E-04	200	18	1123	242	0.18
ABCC4	1555039_a_at	9.01E-03	42	53	157	42	0.27
SLC16A7	210807_s_at	2.10E-03	85	14	316	100	0.27
	207057_at	3.23E-02	125	44	378	156	0.33
ABCC1	202804_at	4.10E-03	112	21	371	103	0.30
SLC29A1	201802_at	4.23E-02	591	277	1388	509	0.43

Table 4-7 cont.

Gene Symbol	Probeset ID	p Value	LMEC		Liver		Fold Change
			Mean	SD	Mean	SD	
Detectable, but no difference in expression (p > 0.05)							
ABCC10	215873_x_at	1.75E-01	301	43	395	101	
	213485_s_at	6.41E-01	601	169	552	129	
SLC16A1	202235_at	1.57E-01	267	47	497	336	
	202236_s_at	3.15E-01	3090	473	2314	1161	
	202234_s_at	6.68E-01	736	120	867	486	
	209900_s_at	8.05E-01	1005	49	947	544	
	1557918_s_at	9.65E-01	954	353	943	365	
SLC22A12	237799_at	7.63E-02	184	80	27	10	
SLC22A5	205074_at	9.07E-01	535	146	549	180	
SLC28A3	220475_at	6.50E-01	191	219	240	105	
SLC29A1	201801_s_at	3.13E-01	1000	468	1528	756	
SLC29A2	204717_s_at	6.46E-01	196	38	204	15	
SLCO4A1	1554332_a_at	1.07E-01	1345	598	397	140	

Table 4-8: Comparison Affymetrix U133 plus 2.0 array transporter probeset expression levels in human LMECs vs. kidney.

Genes are grouped based on whether they are increased, decreased or not different during lactation. Probesets for the same gene were then grouped into sections of the table sorted by fold change in expression.

Gene Symbol	Probeset ID	p Value	LMEC		Kidney		Fold Change
			Mean	SD	Mean	SD	
Higher relative to kidney (p < 0.05, fold change >1)							
SLC6A14	219795_at	2.96E-02	3988	1193	79	42	50.19
ABCG2	209735_at	3.82E-02	17536	5964	437	52	40.12
SLC15A2	205316_at	2.24E-06	3936	421	808	263	4.87
	205317_s_at	7.61E-03	868	182	453	148	1.92
SLC16A1	202236_s_at	5.04E-04	3090	473	974	500	3.17
	209900_s_at	9.21E-03	1005	49	400	283	2.51
	202234_s_at	2.01E-02	736	120	383	182	1.92
	202235_at	3.82E-02	267	47	143	76	1.87
SLCO4C1	222071_s_at	5.67E-04	3362	294	1736	417	1.94
Lower relative to Kidney (p < 0.05, fold change >1)							
SLC17A1	237049_at	3.00E-03	35	32	912	404	0.04
SLCO3A1	219229_at	2.79E-04	51	63	637	141	0.08
	227367_at	1.83E-03	160	67	584	140	0.27
SLC22A12	237799_at	1.66E-02	184	80	2227	1416	0.08
ABCB1	243951_at	1.94E-04	65	25	671	164	0.10
SLCO2B1	203473_at	5.92E-03	152	86	1380	669	0.11
ABCC4	1555039_a_at	2.93E-03	42	53	336	105	0.13
SLC16A7	210807_s_at	2.26E-02	85	14	655	429	0.13
	207057_at	3.46E-02	125	44	1400	1085	0.09
ABCC1	202804_at	7.62E-05	112	21	814	156	0.14
SLC22A5	205074_at	3.55E-03	535	146	3014	1200	0.18
SLC22A3	1570482_at	1.36E-04	29	15	143	23	0.21
	242578_x_at	5.33E-03	184	54	894	378	0.21
SLC28A1	207560_at	1.21E-02	200	18	916	457	0.22
SLC29A2	204717_s_at	2.08E-03	196	38	496	103	0.39
SLC23A2	211572_s_at	0.041286	93	20	231	92	0.40
SLC15A2	240159_at	2.52E-02	243	31	556	184	0.44
ABCC10	215873_x_at	1.44E-03	301	43	604	96	0.50

Table 4-8 cont.

Gene Symbol	Probeset ID	p Value	LMEC		Kidney		Fold Change
			Mean	SD	Mean	SD	
Detectable, but no difference in expression (p > 0.05)							
ABCC10	213485_s_at	1.41E-01	601	169	746	99	
SLC10A1	207185_at	7.24E-02	110	122	308	136	
SLC16A1	1557918_s_at	6.35E-02	954	353	194	48	
SLC22A4	205896_at	8.69E-02	429	82	689	212	
SLC22A9	241770_x_at	7.38E-01	38	27	45	24	
SLC28A3	220475_at	9.58E-01	191	219	199	54	
SLC29A1	201801_s_at	3.96E-01	1000	468	710	157	
	201802_at	7.59E-01	591	277	550	123	
SLCO4A1	1554332_a_at	7.40E-02	1345	598	158	74	
	219911_s_at	8.67E-01	907	238	873	284	

Using the two step screening paradigm described previously (Figure 3-5), data from the three comparisons were merged to generate a single list of transporters of interest for potential importance for xenobiotic transport in LMEC (Table 4-9). ABCG2, SLC15A2, SLC22A12, SLC6A14, AND SLCO4C1 are of interest as they were significantly upregulated during lactation. The actual fold change, although certainly the most striking with ABCG2, SLOC4C1, and SLC15A2, should be interpreted cautiously as the signal intensities reported from the MEC arrays (the denominator of the ratio) were often very low with marginal or absent detection calls. Other transporters, such as ABCC10, SLC10A1, SLC16A1, SLC22A4, SLC22A5, SLC22A9, SLC28A3, SLC29A1, SLC29A2, and SLCO4A1 may also be of interest as their expression level was similar to levels in other secretory tissues.

Table 4-9: Results of the microarray analysis screen paradigm for identifying transporters potentially responsible for drug accumulation in breast milk.

Transporter genes upregulated during lactation are shaded. The direction of the differences relative to MEC, liver, and kidney are presented by the arrows. A dash indicates no statistically significant difference was detected. An asterisk denotes a gene detected by other probesets on the chip that were excluded from the analysis (absent on all lactating chips).

			LMEC expression vs.:		
			MEC	Liver	Kidney
ABCC10	**MRP7**	215873_x_at	-	-	↓
		213485_s_at	-	-	-
ABCG2	**BCRP**	209735_at	↑	↑	↑
SLC10A1	**NTCP**	207185_at	-	↓	-
SLC15A2	**PEPT2**	240159_at	↑	↑	↓
		205317_s_at	↑	↑	↑
		205316_at	↑	↑	↑
SLC16A1	**MCT1**	202235_at	-	-	↑
		202236_s_at	-	-	↑
		202234_s_at	-	-	↑
		209900_s_at	-	-	↑
		1557918_s_at	-	-	-
SLC22A12	**URAT1**	237799_at	↑	-	↓
SLC22A4*	**OCTN1**	205896_at	-	↑	-
SLC22A5	**OCTN2**	205074_at	-	-	↓
SLC22A9*	**UST3**	241770_x_at	-	↓	-
SLC28A3	**CNT3**	220475_at	-	-	-
SLC29A1	**ENT1**	201801_s_at	-	-	-
		201802_at	-	↓	-
SLC29A2*	**ENT2**	204717_s_at	-	-	↓
SLC6A14	**ATB(0+)**	219795_at	↑	↑	↑
SLCO4A1*	**OATP-E**	219911_s_at	-	↑	-
		1554332_a_at	-	-	-
SLCO4C1	**OATP-H**	222071_s_at	↑	↑	↑

The observation that SLCO4C1 is upregulated in LMECs, the cells forming the barrier between serum and breast milk was novel and warranted qPCR validation. Quality of the primer pairs used for the quantification of each gene was demonstrated by correlation coefficients > 0.99, PCR efficiencies of 95-100%, and single products on the melt curve analysis and agarose gel electrophoresis (Figure 4-42 and Figure 4-43). Figure 4-44 shows the relative RNA expression levels of SLCO4C1 in each sample and in pooled RNA from human liver and kidney external controls. β-casein RNA expression level was measured in parallel as a positive control. The LMEC expression of SLCO4C1 was confirmed to be much greater than that of MECs (>1000 fold by qPCR). Although striking, the actual magnitude of this fold change must be interpreted cautiously as all three LMEC samples were slightly above the standard curve. The assay was not repeated in order to conserve cDNA for future experiments. SLCO4C1 expression in LMECs was also much higher than that of the kidney and liver samples. Although not the same comparators as were analyzed by microarray analysis, the qPCR shows a higher expression of SLCO4C1 in LMEC relative to these tissues by both methods.

Figure 4-42: Human β-casein amplification curve, melt curve analysis, standard curve, and agarose gel electrophoresis generated from standards over a 5-$\log_{10}$ dilution series.

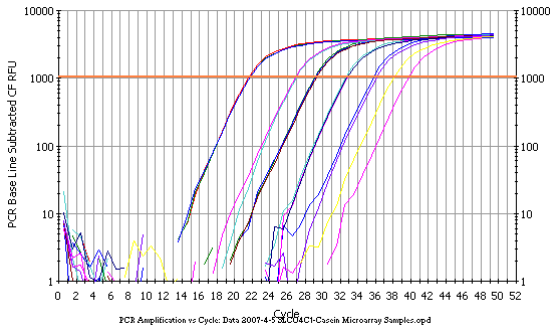

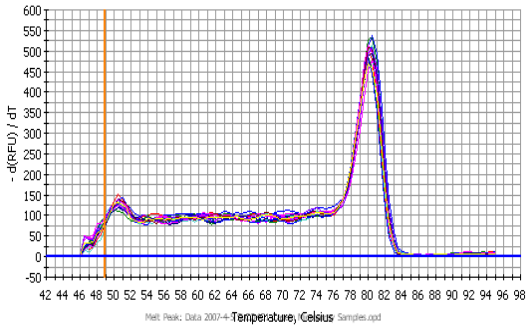

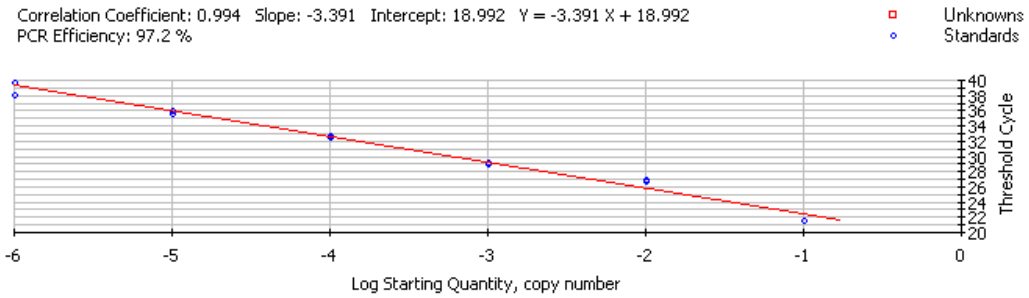

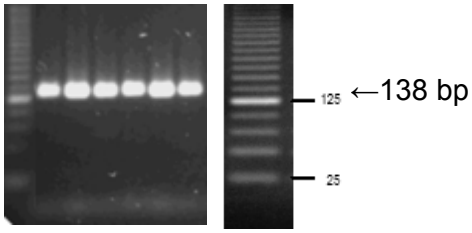

Figure 4-43: Human SLCO4C1 amplification curve, melt curve analysis, standard curve, and agarose gel electrophoresis generated from standards over a 3-$\log_{10}$ dilution series.

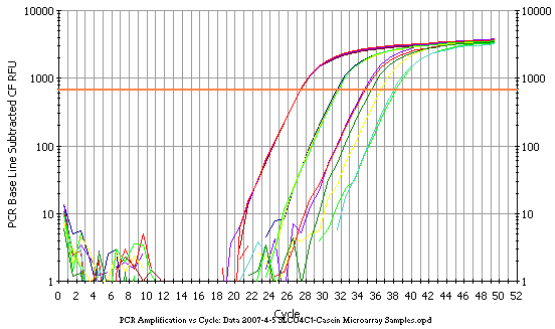

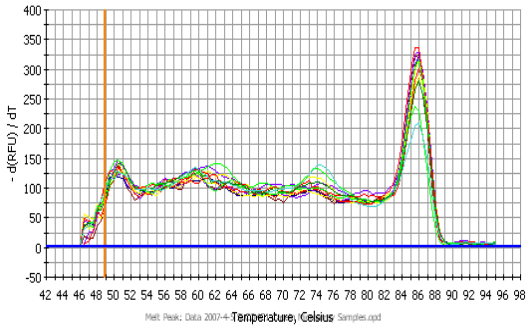

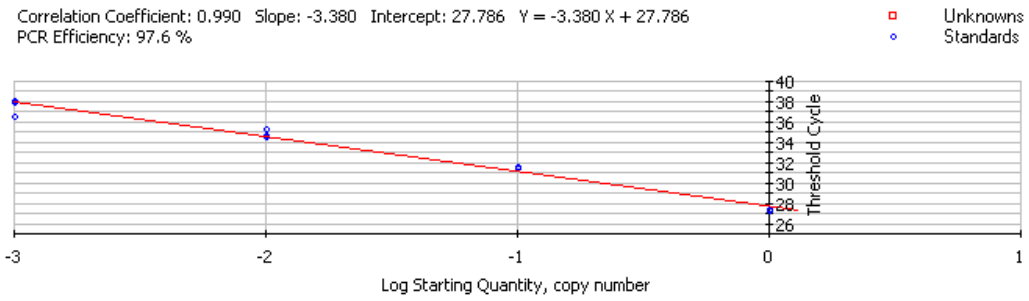

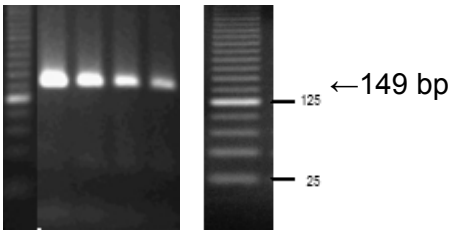

Figure 4-44: Relative RNA expression of β-casein and SLCO4C1 in human LMEC, MEC, and pooled liver and kidney samples as determined by quantitative PCR.

A. Relative β-casein RNA expression. Cells isolated from breast milk were used for generation of a standard curve ($10^{0}\rightarrow10^{-6}$). Samples were prepared in the dilutions indicated. B. Relative SLCO4C1 RNA expression. cDNA from human kidney tissue ($10^{0}\rightarrow10^{-3}$) served as a positive control and samples were prepared in the dilutions indicated. Bars are the mean ± SD of three replicate measurements of the same sample. BLD = below limit of detection.

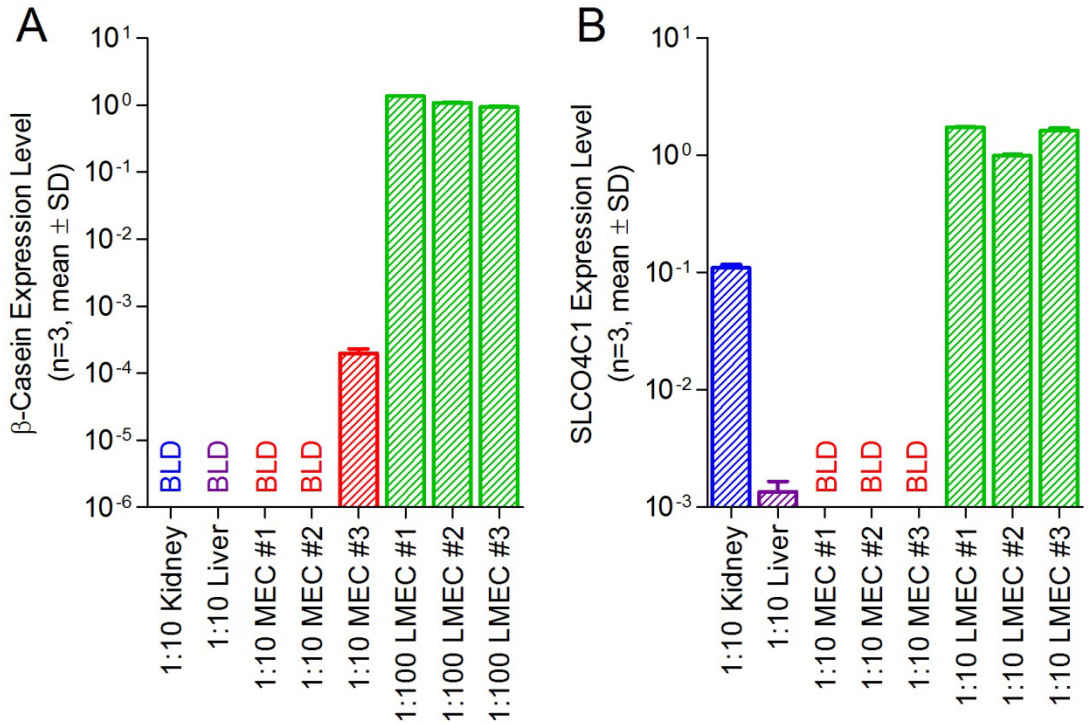

CHAPTER 5: Discussion

A. Expression and functional role of Abcg2 in CIT3 cells

Past efforts have focused on identification of the nitrofurantoin B→A active transport system in the CIT3 cell culture model system. In stimulated CIT3 cells, Gerk et al. have previously shown nitrofurantoin active transport to be sodium dependent and inhibited by dipyridamole, adenosine, and guanosine [87]. Further, inhibition studies measuring radiolabelled nitrofurantoin B→A and A→B flux with and without 250 μM unlabelled nitrofurantoin on the basolateral, apical, and both sides suggested a basolateral localization of the unidentified transport process [88]. Recent data from the lab of Dr. Alfred Schinkel strongly implicate Abcg2 based on several observations: substantial upregulation of Abcg2 protein expression in mammary tissue in several species during lactation as determined by western blotting and immunohistochemistry [124]; nitrofurantoin is an Abcg2 substrate [53]; and perhaps most strikingly, by a study in Abcg2$^{-/-}$ mice that demonstrated a 76-fold decrease in the M/S ratio when the Abcg2 gene was removed [53]. Dipyridamole is known to be an Abcg2 inhibitor [148], but Abcg2 is typically expressed on the apical membrane and ABC transporters are not sodium dependent. Although Abcg2 is known to transport zidovudine [185,186], it is not known if the purines adenosine or guanosine can function as inhibitors. The inconsistencies of these in vitro observations in CIT3 cells with that of the theory that Abcg2 is the unidentified process was the focus of Aims 1-3 of the current work. The hypothesis put forth was that Abcg2 is responsible for the known B→A transport of nitrofurantoin in CIT3 cells.

Abcg2 RNA transcripts and protein were detected in CIT3 cells by qPCR, western blotting, and immunofluorescence. Consistent with the Abcg2 localization in other tissues, the Abcg2 expression in stimulated CIT3 cells was apical when visualized by confocal microscopy. Interestingly, a significant upregulation of mRNA was not observed following the four days of lactogenic hormone stimulation. Protein expression level was noticeable greater by immunofluorescence but was only marginally elevated when quantitated by Western blot. Functionally, both conditions clearly showed a predominant apically-directed nitrofurantoin flux in snapwell assays, but the B→A permeability was slightly greater in stimulated vs. unstimulated cells. This small, but significantly different, nitrofurantoin B→A permeability difference between stimulated and unstimulated cells was not the result of differences in tight junctions, as the graphs of

serial TEER measurements in both conditions were superimposable. The B→A permeabilities achieved (stimulated, 68.0 ± 0.2 μL/h/cm^2; unstimulated, 50.7 ± 5.6 μL/h/cm^2) were similar to that reported by Toddywalla et al. (stimulated, 64.5 ± 4 μL/h/cm^2 [86]) and Gerk et al. (stimulated, 70 ± 10.4 μL/h/cm^2 or 90.5 ± 4.6 μL/h/cm^2 [87]) in the same cell line tested by similar methods. A shorter duration of lactogenic hormone stimulation was used in the current work (4 days vs. 6-7 days in the literature). However, the greatly increased expression of the milk proteins, lactalbumin and β-casein, suggests the duration of hormone exposure was sufficient for a lactogenic response. Unpublished observations from the lab also indicate that the expression level of these two proteins is stable 4-8 days following stimulation of this cell line.

The role that Abcg2 has in nitrofurantoin transport in CIT3 cells is confirmed by the observation that the predominant apically directed flux was ablated by the Abcg2 inhibitor, FTC. The B→A and A→B permeabilities of 10 μM nitrofurantoin collapsed to a common value in both unstimulated and stimulated cells in transwell flux experiments. Similar directionality and inhibition data with 2 μM PhIP further emphasizes the functional importance of Abcg2 in this system whether stimulated with lactogenic hormones or not. Data with the Abcg2 substrate cimetidine, however, was not supportive. Although some trends were demonstrated, statistically significant apically-directed flux and inhibition with FTC was not seen. The relative magnitude of the cimetidine permeability likely contributed to this finding as it is much smaller than that of nitrofurantoin and PhIP, nearing that typically achieved by a paracellular marker. In this situation, it may take additional time to move enough mass for true differences in the permeabilities to be detectable. The growth properties of the CIT3 cells likely compound this problem as these cells tend to form “domes” or “bumps” when grown for the long periods of time typically used in these experiments. The areas where many cell layers exist rather than a simple monolayer function as an additional barrier to transcellular flux.

Overall, the findings presented support the hypothesis put forth. The molecular mechanisms for the sodium dependence and the greater inhibition of B→A nitrofurantoin flux with basolateral placement of 250 μM unlabelled nitrofurantoin previously observed by Gerk et al. [87,88], however, remain unclear. It is possible that there exists a basolateral transport process that by itself does not play a substantial role, but together with Abcg2 forms a vectorial transport process. Such interplay has been suggested to exist in the placental barrier with ABCG2 and SLCO2B1 [162]. SLCO2B1 is expressed in human mammary gland, but it is localized to the myoepithelial cells, not the luminal

mammary epithelial cells [112]. It is not known if any of the organic anion transporting polypeptides are expressed in CIT3 cells. Transcripts for Slc22a1 (Oct1) were detected in both unstimulated and stimulated CIT3 cells and the localization of this transporter is basolateral in other tissues, but this transporter is known to be sodium independent and the concentrative transport of its prototypical substrate tetraethylammonium was not observed in CIT3 cells [105,187]. Gerk et al. also concluded from a series of purine and pyrimidine inhibition experiments that known sodium dependent nucleoside or nucleobase transporters were not involved [87]. Although this dissertation work clearly demonstrates that Abcg2 has role in the transport of nitrofurantoin in CIT3 cells, more work is necessary to elucidate the molecular basis for these observations.

B. Creation of an ABCG2 stably transfected model system

A large number of xenobiotics known to accumulate significantly in breast milk have recently been shown to be ABCG2 substrates [53,93,127]. The objective of this series of experiments was to create and validate an ABCG2-transfected cell system that could potentially be utilized to predict the extent of drug accumulation in vivo.

The MDCKII parent cell line was selected after screening several candidates based on its extensive use in the published literature, ease of transfection and subsequent selection, ability to form a monolayer and tight junctions, and favorable background transporter gene expression. Transcripts for the orthologs of human ABCB1, ABCC1, and ABCC2 in particular have been identified in these cells, but orthologs of human SLCO1A2, SLCO1B1, and most importantly ABCG2 were not detected [160,184]. Despite requiring more than one clonal selection step, ABCG2 was successfully stably transfected. Western blot, flow cytometry, and confocal microscopy data together demonstrated good apical expression of the transporter. Ten clones with various expression levels by Western blot of crude membrane fractions were cataloged and three, clones 40, 46, and 50, were further evaluated in surface expression and functional assays. MDCKII-ABCG2 clone 40 clearly had the greatest surface expression as analyzed by flow cytometry with a $MFI_{ABCG2\text{-}Isotype}$ of 196.8 versus 125.9 and 1.9 for clones 46 and 50 respectively. The Hoechst 33342 efflux assays demonstrated equivalent ABCG2 functionality in clones 40 and 46 whereas clone 50 showed a much lower ability to efflux the dye as was expected based on its surface expression data. MDCKII-ABCG2 clone 40 was selected based on the belief that its high expression level

would be ideal to identify ABCG2-attributed transport phenomena. The new ABCG2 stably overexpressing model system was then validated with directionality and inhibition monolayer flux assays using several established ABCG2 substrates and inhibitors: nitrofurantoin, PhIP, cimetidine, methotrexate, and ciprofloxacin.

The effect of ABCG2 transfection on the flux of 10 μM nitrofurantoin mimicked that observed by Merino et al. in their ABCG2 and Abcg2 transfected MDCKII cell lines [53]. The predominantly A→B directed flux in the empty vector transfected cells was reversed with the addition of ABCG2. Both 1 μM GF120918 and 10 μM FTC blocked this affect, significantly decreasing the B→A flux attributed to ABCG2 by 85.5% and 96.3%, respectively.

Experimental estimates of initial flux rates of the ABCG2 substrate, PhIP, were more difficult to obtain. So much of the mass that was initially placed on the donor side was transferred over the 4 hour experiment that the flux was only linear for the first 2 datapoints. Despite this sparse sampling, a large effect was again observed in the ABCG2-transfected cells as the B→A flux significantly increased and the A→B flux significantly decreased. The ABCG2-attributed flux was completely inhibited with 10 μM FTC, but unlike with nitrofurantoin, 1 μM GF120918 had little effect. A similar, but less obvious difference between the inhibitors was noted in a PhIP study by van Herwaarden et al. [128]. These investigators characterized the flux of a much higher concentration of PhIP (100 μM) in murine Abcg2 transfected LLC-PK1 cells and documented complete inhibition with the potent FTC derivative, Ko143, at 5 μM but only partial inhibition with 5 μM GF120918. Based on Michaelis-Menton enzyme kinetics, if it is assumed that ABCG2 has a single binding site, that both substrates (nitrofurantoin and PhIP) are tested at concentrations below their apparent Michaelis-Menton constant (Km) and that both inhibitors (GF120918 and FTC) are competitive, differences in the inhibitor concentration ([I]) divided by Michaelis-Menton inhibitory constant (Ki), ([I]/Ki), may explain some of these results. Concentrations of GF120918 ranging from 0.1-10 μM [160,188-192] have been used in the literature to inhibit ABCG2 but the relative ABCG2 Ki values of the GF1210918 and FTC have not been directly compared. Allen et al. did study the ability of various inhibitors to increase the accumulation of 20 μM mitoxantrone in drug-resistant mouse MEF3.8/T6400 cells (which have elevated Abcg2), and found that Ko143 was 2- and 10-fold more potent than GF120918 and FTC, respectively [193]. Extrapolating this data and the relative concentrations of FTC and GF120918 used in our experiments suggests that a greater inhibition would be expected with 10 μM FTC

than 1 μM GF120918 if studied with the same substrate, but it is less clear why GF120918 inhibited nitrofurantoin flux, but not PhIP flux when used at the same concentration. An alternative explanation was put forth by Pozza et al. when they observed that 5 μM GF120918 had little effect on the binding of mitoxantrone to purified ABCG2; multiple distinct binding sites may exist for this transporter [194]. These observations are discussed further in the mathematical modeling section.

Similar to nitrofurantoin, experiments involving cimetidine were as expected for an ABCG2 substrate. At 5 μM, cimetidine flux was significantly increased in the B→A direction and decreased in the A→B direction in the ABCG2 transfectants relative to empty vector transfected controls and this directionality was completed ablated by both GF120918 and FTC. These findings are similar to those observed by Pavek et al. with the ABCG2 and Abcg2 transfected MDCKII cells created by the lab of Alfred Schinkel, but are inconsistent with the cimetidine CIT3 data previously discussed [127]. The overall magnitude of the cimetidine flux in the MDCKII-ABCG2 cells was lower than that of nitrofurantoin and PhIP as was also noted in the CIT3 experiments. The very high ABCG2 expression level driven by a constitutively active CMV promoter in this overexpressing system versus the low endogenous Abcg2 expression in CIT3 cells is a likely factor in the conflicting results.

Methotrexate has been used as an ABCG2 substrate in membrane vesicle or cellular accumulation assays performed by many researchers, but monolayer flux data was not available in the literature [153,155,188,190,195]. The present work shows why; the permeability of this very hydrophilic compound across both the empty vector and MDCKII-ABCG2 cells was nearly equal to that of the paracellular marker sucrose. Interesting, clinical M/P data is available from a study conducted in 1972 by Johns et al. [196]. This study measured the M/P ratios at several timepoints following the oral administration of methotrexate to a single patient and found it to achieve a maximum of 0.08. The methotrexate *n*-butanol:water distribution ratios were also measured and found to be 0.02:1 at physiological pH. The conclusion made by the authors that methotrexate is > 98% ionized and in a nondiffusable form and therefore not contraindicated in breastfeeding, is supported by the current observations in the in vitro system. A significant difference in the B→A and A→B ABCG2-attributed permeability was observed, but was small and difficult to interpret as its magnitude in both conditions was less than that in the empty vector comparators.

The final ABCG2 substrate studied was the fluoroquinolone antibiotic, ciprofloxacin at 10 μM. The addition of ABCG2 again generated directionality data that was similar to that of nitrofurantoin, PhIP, and cimetidine and was consistent with published data using the ABCG2 and Abcg2 transfected MDCKII cell lines created by the lab of Alfred Schinkel [93].

Overall, the results with the ABCG2 substrates tested were comparable to that observed with ABCG2/Abcg2 transfected cell lines established by other investigators. Methotrexate, however, performed poorly in this monolayer flux assay. A wide range in the magnitude of the B→A and A→B permeabilities both in the empty vector and ABCG2 transfected cells was noted with the various substrates. Studies using GF120918 and FTC at concentrations comparable to those used for ABCG2 inhibition by other investigators produced the expected results with the exception of the PhIP/GF120918 observation. The mathematical modeling presented in the next section will explore alternative experimental measurements of ABCG2 functional activity in monolayer flux assays in an attempt to explain this observation and to provide guidance for future studies. The successful creation of this ABCG2-transfected cell line will serve as a useful experimental tool for future work.

C. Mathematical modeling and derivation of commonly used measurements of efflux activity.

In a recent publication, Kalvass and Pollack, proposed a simple three-compartment model (apical, cellular, and basolateral) to derive flux equations for the initial rate of flux and steady-state mass transfer in the presence or absence of active efflux [172]. This dissertation work extends this model to include the permeability-surface area products for paracellular flux and the basolateral and apical endogenous transport processes that may be active in transferring substrates in either direction. It then applies the new concepts derived to drug transfer into breast milk and explores the potential utility of the model for estimating the extent of drug accumulation into breast milk and its limitations.

Exploring the model-derived theoretical limitations of the initial B→A and A→B rates when $PS_{B,U}$, $PS_{A,E}$, $PS_{B,E}$, and $PS_{A,U}$ were equal to zero and PS_{PC} was negligible was a useful exercise. Eq. 4-1 (graphically depicted in Figure 4-26) and Eq. 4-2 (graphically depicted in Figure 4-27) show that with increasing $PS_{A,E(ABCG2)}$ the initial

B→A and A→B rates achieve a maximum defined by C_B^0 [PS_D+PS_{PC}] and a minimum defined by C_A^0 [PS_{PC}], respectively. It is intuitive that differences in the permeability-surface area product attributed to paracellular flux (PS_{PC}) and passive diffusion (PS_D) may produce differences in the measured permeabilities of different substrates. PhIP had a greater MDCKII-ABCG2 B→A permeability than nitrofurantoin in the flux assays performed with the new ABCG2-transfected cell line presumably due to a greater PS_D. The empty vector B→A permeabilities of these drugs followed the same pattern. The A→B rates achieved by substrates such as cimetidine, methotrexate, and ciprofloxacin also appeared to achieve a minimum rate that is logically dependent on the leakiness of the cell monolayer (measured by the paracellular marker). However, the observation that increases in $PS_{A,E(ABCG2)}$ do not linearly increase (or decrease) these initial rates is perhaps less obvious. As shown by Eq. 3-8 and Eq. 3-11, neither initial rate is directly proportional $PS_{A,E(ABCG2)}$. This has important implications for how data from experiments such as those performed with the MDCKII-ABCG2 model system (Aim 5) are analyzed and interpretted.

Next, the theoretical limits of the efflux ratios, ER_A and ER_α, in a single apical efflux transporter system was explored when PS_{PC} was assumed to be negligible. As presented by Kalvass and Pollack, when $PS_{A,E(ABCG2)} >> PS_D$, an ER_A upper limit of 2 is reached, but ER_α remains proportional to $PS_{A,E(ABCG2)}$ [172]. The literature-derived flux rates from the cells created by the lab of Alfred Schinkel and permeability data from cell line created in Aim 4 supported these findings after substrates that were clearly affected by endogenous transport processes (ER_α Empty ≠ 1) were removed from the analysis. Despite the likely error associated with manually extracting flux data from the published MDCKII-ABCG2/Abcg2 graphs in the literature, the maximum achieved apical efflux ratio in these cell lines and in the one created in Aim 4 agreed with the model. The asymmetry efflux ratio spanned a much wider range, presumably reflecting the proportionality of ER_α with $PS_{A,E(ABCG2)}$. Many drugs had to be excluded from the analyses, however, based on an ER_α Empty ≠ 1. These observations served to invalidate the model assumption that no other endogenous transporter processes existed. In order to use data from these drugs, the $PS_{B,U}$, $PS_{A,E}$, $PS_{B,E}$, and $PS_{A,U}$ terms were allowed to remain in the equations and a new efflux ratio, the ER_α Ratio, was derived in an attempt to isolate $PS_{A,E(ABCG2)}$ and preserve the proportionality. In the ER_α Ratio, the ER_α of the ABCG2 transfected cells is normalized to the ER_α of the empty vector transfected cells, theoretically removing the confounding effect of $PS_{B,U}$, $PS_{B,E}$,

and $PS_{A,U}$ processes. Contributions of any potential $PS_{A,E}$ process to the ER_{α} Ratio could not be removed. Eq. 4-10 shows that any variability in the cell line $PS_{A,E(ABCG2)}$ and $PS_{A,E}$ (transporter expression levels) or a substrate's ability to cross the membrane by passive diffusion (PS_D) or to interact with either transport process ($PS_{A,E(ABCG2)}$ or $PS_{A,E}$) would be expected to affect this ER_{α} Ratio. The effects of changes in PS_D, $PS_{A,E}$, and $PS_{A,E(ABCG2)}$ on ER_A and the ER_{α} Ratio were illustrated graphically in Figure 4-28. ER_A was included in these graphs despite its lack of direct proportionality with $PS_{A,E(ABCG2)}$ as it is commonly measured in the literature. Increases in $PS_{A,E}$ or a higher relative substrate PS_D lowers the maximal achievable ER_A and blunts the ER_{α} Ratio. The ER_A graph in Panel B of this figure is of particular interest as it may explain the lack of GF120918 inhibition of PhIP flux observation under Aim 5. With the same Michaelis-Menton assumptions made earlier (single binding site, competitive inhibitor, substrate concentration below Km), the addition of GF120918 would serve to effectively decrease $PS_{A,E(ABCG2)}$. In the setting of a high expression level (high baseline $PS_{A,E(ABCG2)}$), as was achieved in the MDCKII-ABCG2 clone 40 cells, this decrease may not result in a substantial change in ER_A due to its nonlinear relationship with $PS_{A,E(ABCG2)}$. It is therefore suggested that any application of Michelis-Menton principles to the transport phenomena be made using an experimental measurement that is directly proportional to $PS_{A,E(ABCG2)}$. It is hypothesized that if ER_{α} was measured in the PhIP flux assay, the expected GF120918 inhibition would have been observed.

The initial assumption that $PS_D >> PS_{PC}$ or that $PS_{PC} \rightarrow 0$ was also shown to be invalid for the experimental data previously presented, as many of the paracellular marker permeabilities approximated that of the substrate studied concurrently. Increases in PS_{PC} blunt both the ER_A and the ER_{α} Ratio, and of specific concern, cause the relationship between $PS_{A,E(ABCG2)}$ and ER_{α} Ratio to become nonlinear as PS_{PC} increases relative to PS_D (as graphically depicted in Figure 4-29). Eq. 4-12 and Eq. 4-13 provide the theoretical basis for a solution, simply subtracting the apparent permeability of the paracellular marker from that of the substrate studied prior to calculation of the efflux ratio. Although easy to implement experimentally, it relies on a currently untested assumption: that the PS_{PC} of the paracellular marker being measured is equal to the PS_{PC} of the drug being studied. This subtraction increased nitrofurantoin's ER_{α} and ER_{α} Ratio, markedly increased these efflux ratios for ciprofloxacin, and had little effect on cimetidine and PhIP. The analysis of methotrexate could not be performed due to its very low permeability. Large increases in ciprofloxacin efflux ratios were attributed to the

very small difference between the ABCG2 A→B and that of mannitol (in the denominator) and the relatively larger difference in ABCG2 B→A permeability (in the numerator). The extreme variability in both the ciprofloxacin ER_{α} and the ER_{α} Ratio, estimated by calculating all possible combinations of the unmatched permeabilities that make up each ratio, decreases confidence in the accuracy of this measurement.

To determine the potential relevance of this model and the utility of the new MDCKII-ABCG2 system for estimations of in vivo accumulation, several correlations were attempted. The in vitro ER_{α} and ER_{α} Ratios were correlated with the ratio of the M/P ratios for the same drugs in wild-type versus Abcg2 knock out mice. As an assumption of the ER_{α} is that no endogenous transport processes exist, drugs for which ER_{α} Empty ≠ 1 were included on the graphs, but excluded from the correlations. At the outset, these correlations were not expected to perform well for several reasons. The in vivo ratio of wild-type to Abcg2-/- M/P ratios obtained were not ideal, as each was calculated by the M/P point ratio method and were only available as the mean observations without any descriptor of variability. The in vitro Schinkel cell line data that was extracted from the literature suffered similar problems due to the way it was obtained (extracted from graphs) and the lack of replicates. The in vitro data generated in the current work was better in that it involved replicates, but only provided data for a handful of drugs. None of the final correlations were overly impressive, but the ER_{α} Ratio did seem to perform well for the drugs where the in vivo ABCG2-attributed effect was large (nitrofurantoin and riboflavin). Ignoring the ciprofloxacin data due to its varibability, the final graph of the ER_{α} Ratio incorporating the PS_{PC} subtraction seems promising, as the rank order of ABCG2-attributed effect was the same in vivo and in vitro. Much more data is needed to compare more appropriately the utility of the various efflux ratios to predict the ABCG2-attributed effect and extent of accumulation in vivo. Even if numerical correlations eventually fail to accurately predict the extent of drug accumulation in breast milk, these data show that in vitro assessment of a potential interaction with ABCG2 holds promise for categorical risk assessment.

To make general recommendations for future work, several principles should be emphasized. Monolayer flux assays with stably transfected ABCG2 overexpressing cell lines are attractive tools as they provide information involving both permeability and transporter interaction. The Kalvass and Pollack publication emphasized the need to understand what is truly measured when flux rates, apparent permeabilities, or any one of the efflux ratios are reported. As shown by the model, when performing in vitro and in

vivo M/S correlations with flux based assays, one needs to consider several variables in the vitro system: potential endogenous transporters ($PS_{B,U}$, $PS_{A,E}$, $PS_{B,E}$, and $PS_{A,U}$), PS_{PC}, PS_D, and $PS_{A,E(ABCG2)}$. Different cell lines or the same cell line under varying growth conditions would be expected to have different values for each of these variables making comparisions challenging. If drugs to be compared are studied in the same cell line under the same experimental conditions (expression level and experimental conditions assumed to be the similar), any variability in ER_α or ER_α Ratio would be expected to be due to differing substrate affinity for ABCG2 or PS_D. Even further, if the substrate affinity of two drugs is equivalent, they would still be expected to have different efflux ratios if they have different PS_D. PS_D is not routinely measured and was not measured in the current work. In a recent review paper, Xia et al. suggests that it should be measured from flux measurements conducted at 4°C (a temperature when transporters would not function) or in the presence of transporter inhibitors [197]. Reversing the relationship shown on the right side of Figure 4-28 Panel B for the situation of constant $PS_{A,E(ABCG2)}$, Figure 5-1 shows the effect of differing PS_D values at several different $PS_{A,E(ABCG2)}$ levels. If PS_{PC} is not neglible or not experimentally subtracted, one can see that at both high and low PS_D values; it is difficult to see ABCG2-attributed effects. Once PS_{PC} is assumed to be zero or is experimentally subtracted, only very high PS_D values obscure ABCG2-attributed effects. This relationship suggests that if experiments with low permeability substrates were conducted long enough for sufficient mass transfer, a potentially large ABCG2-attributed effects could be measured. Work presented with methotrexate and ciprofloxacin underscore the difficulty in accurately measuring flux at minimum permeabilities. It simply may not be possible or practical to conduct experiments for the requisite time needed for accurate measurements. As this relationship shows, it is also difficult to distinguish the contribution of $PS_{A,E(ABCG2)}$ for drugs with high flux rates; selecting clones with lower expression levels may actually improve the ability to measure the ABCG2-attributed effect as the $PS_{A,E(ABCG2)}/PS_D$ ratio would decrease and improve the dynamic range of the possible efflux ratios. Lower expressing MDCKII-ABCG2 clones were identified during development of the model system and are available for future work to explore these relationships.

Figure 5-1: Effect of variable $PS_{A,E(ABCG2)}$ values on the relationship between PS_D and the ER_α Ratio with and without PS_{PC}.

Effect of different $PS_{A,E(ABCG2)}$ values ranging from 0 to 20 on the relationship between PS_D and the ER_α Ratio. Left. PS_{PC} was set to 0.1. Right. PS_{PC} was set to 0. Arrows depict the changes in ER_α Ratio with increasing PS_D. $PS_{A,E}$ was set at 0 in both cases.

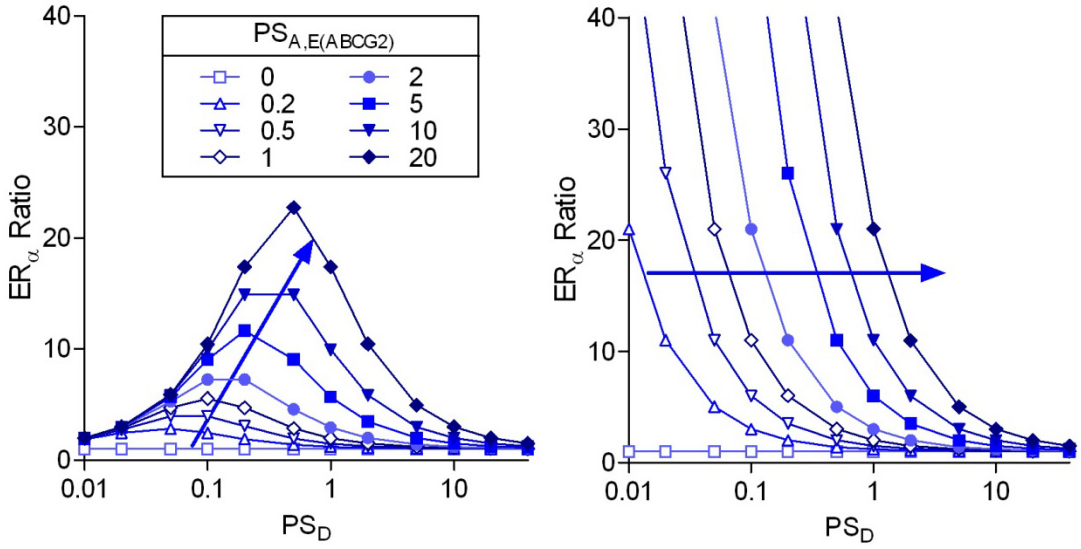

For in vitro data to truly be able to estimate the extent of in vivo accumulation, the ratio of the permeability-surface area product terms (eg. $PS_{A,E(ABCG2)}$ to PS_D) and clearance terms (eg. $Cl_{A,E(ABCG2)}$ to Cl_D) should be roughly equivalent. It is typically assumed that the in vitro and in vivo transporter substrate affinities are similar, but the other factor making up $PS_{A,E(ABCG2)}$ is transporter expression level. In the course of validating in vitro methods for prediction, transporter expression levels should be quantified and any potential day to day variability in expression level be controlled or corrected. Finally, when applying this kinetic model to experimental observations, investigators must be particularly mindful of several of its assumptions; that no unstirred water layers exist, that no intercellular metabolism or binding occur, and that all permeability-surface area products remain constant. Violations of any of these assumptions could yield unexpected results.

D. Microarray expression profiling of transporter gene expression in murine developmental datasets

Knowledge of which xenobiotic transporters are of importance during lactation is incomplete. The literature includes studies focused on individual transporters or organism-wide screens of gene expression in multiple tissues that happens to include

the mammary gland. As discussed previously, these data are either too limited in scope to provide a complete picture or are of questionable usefulness as the data often comes from nonlactating tissue that may not be representative of the lactating condition. The identification of xenobiotic transporters that are highly expressed during lactation specifically may identify those of functional relevance for xenobiotic exposure. Fortunately, three existing datasets (Stein et al., Clarkson et al., and Medrano et al.) were available in public repositories [174-176]. The objective of this first experiment was to mine these data to identify murine xenobiotic transporters that were differentially expressed (upregulated) during lactation using microarray analysis. The pooling of the Affymetrix Mu74v2A GeneChip® Array data from the 3 independent experiments into a lactating and nonlactating group increased power without introducing significant bias between the datasets as shown by the signal intensity correlations. Unfortunately, only a small fraction of the genes of interest were actually detectable by this older chip (Table 3-2). A conservative method of analysis was chosen, only eliminating probesets from the analysis if the detections calls of all 15 samples in the lactating group were labeled "Absent". Despite this approach, only 8 xenobiotic transporter genes were detected in the mouse mammary gland homogenates during lactation. Abcg2, Slc22a1, Slc15a2, Slc29a1, Slc16a1, and Abcc5 were upregulated, Slc23a2 was present but not differentially regulated, and Slc22a5 was downregulated during lactation. Abcg2, Scl22a1, and Slc15a2 were the most substantially upregulated with 20-, 10-, and 4-fold higher expression during lactation in the pooled data, respectively. These overall results were remarkably consistent with existing literature [49,110,116]. The Stein et al. [176] dataset showed the most visually striking patterns of apparent lactation-specific developmental regulation of these transporters as shown in Figure 4-33. Although certainly useful information, the small number of genes detectable by this chip and the fact that the tissue samples were from whole gland homogenates rather than LMECs are limitations of these data.

E. Identification of xenobiotic transporters highly expressed in human LMEC clinical samples

The identification of all xenobiotic transporters in LMECs is necessary to improve M/S predictive models and to determine the drugs for which an active transport mechanism governs transfer into breast milk. The comparison of the RNA transcript

levels of 30 transporter genes in human LMECs and MECs produced in our lab by Alcorn et al. in 2002 remains the most robust investigation of mammary gland xenobiotic transporter gene expression [49]. The immunomagnetic separation procedure used produced highly purified populations of luminal mammary epithelial cells using Dynabeads®, but unfortunately required the pooling of the several breast milk or reduction mammoplasty specimens to assure adequate RNA for the single (n=1 in each group) qPCR comparison. Although the methodology did not allow for biological replicates, each sample was normalized to the β-actin expression in the pool to control for potential processing variability. The small amount of RNA collected also limited the number of genes that could be analyzed and together with the time-consuming nature of qPCR, precluded a complete investigation of the expression level of all known xenobiotic transporters. The omission of ABCG2 provides a good example of potential consequences having to limit the numbers of transporters studied with this methodology.

The current work aimed to expand this work through the development of a more robust method to isolate pure populations of luminal mammary epithelial cells from breast milk or reduction mammoplasty tissue. The goal was to isolate a large enough pure population of cells to provide sufficient RNA for the microarray analysis of biological replicates, as the new arrays allowed for quantification of all known human xenobiotic transporters on a single chip. Initially, the EasySep® immunomagnetic nanoparticle system was tried with a novel murine anti-MUC1 (clone 214D4) antibody as the system was incompatible with the rat antibody used previously. The nanoparticles provided a theoretical benefit, as poor affinity to luminal cells and steric hindrance have been suggested in the literature as the cause of low yields with the Dynabead® method [182]. The end result of rigorously testing this new immunomagnetic nanoparticle system was that the new antibody did not have the correct specificity for luminal mammary epithelial cells. Purification of LMECs through macrophage depletion by glass adherence has been reported in the literature, but this technique only moderately enriched LMEC populations (average 65% pure) so this method was not attempted [198]. Flow cytometry had produced highly purified populations as early as 1991, but low yields (less than 1×10^5 per sample) were commonly reported in these early studies [181,199]. A more recent study by Clayton et al. had greater success, so this method was tested [180]. The optimized FACS-based method eventually developed (using solely the original EMA/MUC1-selective (MFGM/5/11[ICR.2]) antibody to positively sort cells) enriched LMECs and MECs to greater than 99% purity as measured by

immunocytostaining. The approach was also sufficiently robust as at least 1 x 10^5 (upwards to 3.5 x 10^6) cells were typically obtained from a single sample.

Successful development of this method allowed for the clinical study to commence. The number of subjects and number of samples required from each subject to obtain the requisite RNA for microarray was greater than expected, but the methodology was successful as greater than 2 µg of high quality RNA was obtained from each patient. The percentage of total cells in each sample that were sorted as luminal mammary epithelial cells ranged from 7.8 – 29.7%. These percentages are slightly lower than the 20 – 40% reported in the literature; likely due to the high stringency of the sort parameters used in this study [180-182].

Microarray signal intensity correlations showed that signal concordance of chips within the same group was greater than those in different groups and that the MEC and LMEC chips were more highly correlated with one another than with chips from a different tissue. Probesets for all 52 genes of transporter genes of interest were present on the Affymetrix U133 plus 2.0 GeneChip® Array, but only 25 genes were detectable in at least one of the LMEC samples. The final results of screening paradigm (Figure 3-5) are presented in Table 4-9. ABCG2, SLC15A2, SLC22A12, SLC6A14, AND SLCO4C1 are of particular interest as they were significantly upregulated during lactation. Other transporters, such as ABCC10, SLC10A1, SLC16A1, SLC22A4, SLC22A5, SLC22A9, SLC28A3, SLC29A1, SLC29A2, and SLCO4A1 were also identified by the screening paradigm as their expression level was similar to levels in other secretory tissues. The individual findings are put in the context of current knowledge below.

The substantially higher (164-fold) ABCG2 expression in LMECs during lactation mirrors that observed in the murine developmental dataset (20-fold) and underscores the major role ABCG2 plays in drug transfer into breast milk. An appreciation of potential substrate interactions with this transporter is of vital importance for estimating the extent of drug accumulation in breast milk. In CIT3 cells, the current work showed that lactogenic hormones only slightly increased Abcg2 protein expression (Aim 1), but a basal transport function was still observed (Aim 2). Jonker et al. reported, however, that in vivo, ABCG2 expression substantially increased in murine whole tissue homogenates during lactation [124]. It was therefore unclear as to whether ABCG2 is upregulated within individual LMECs during lactation or if expression is constant and mammogenesis causes the expansion of this cell type relative to others within the mammary gland resulting in a higher level in the whole tissue homogenate. This microarray expression

data proves Hypothesis 3b, that it is the expression level within individual LMECs that significantly increases during lactation.

The discovery that SLCO4C1 is expressed in human LMECs and that it is upregulated substantially during lactation (70-fold by microarray) are novel findings of this work. Very little is currently known about this transporter. Mikkaichi et al. originally identified it in 2004 using a human kidney cDNA library and also found it expressed in the rat kidney [200]. OATP4C1 is the first member of the organic anion transporting polypeptide family found expressed in human kidney and has been localized to the basolateral membrane of the proximal tubule. Substrates include the cardiac glycosides (digoxin and ouabain), thyroid hormones (T_3 and T_4), cAMP, methotrexate, and sitagliptin [200,201]. The physiological role of SLCO4C1 is unknown, but it has been suggested that it may work in a concerted effort with P-glycoprotein to eliminate xenobiotics like digoxin in the nephron. The ABCG2 apical and potential SLCO4C1 basolateral localization and significant upregulation of both transporters in the same cells during lactation leads to the interesting possibility that they also may function in concert to create a vectorial transport system in the mammary gland. More work is necessary to confirm SLCO4C1 localization in the mammary gland and to determine if drugs that are known to significantly accumulate in breast milk, such as nitrofurantoin, are substrates.

The higher SLC15A2 expression in LMECs is consistent with data from the murine developmental data and the literature. Alcorn et al. detected this transporter in their pooled human LMEC sample but not in the MEC comparator [49]. Groneberg et al. also detected it in human LMECs and localized SLC15A2 to the ductal epithelium of rat mammary tissue [116]. These investigators proposed a role of SLC15A2 in the high-affinity low-capacity apical uptake of peptides from breast milk. The localization and directionality of this transport system suggests it is involved in scavenging peptides from milk and that it may function to limit infant exposure to substrates such as aminopenicillins and angiotensin converting enzyme inhibitors.

The neutral and cationic amino acid transporter SLC6A14 was also expressed in LMECs at a higher level than in MECs. Similar to ABCG2 and SLCO4C1, its expression in LMECs was also higher than that in liver and kidney compactors. Kwok et al. detected SLC6A14 at the RNA level in human mammary tissue and through uptake studies with MCF-12A cells, proposed that it may have a role in carnitine transport [81]. The localization of SLC6A14 is unknown in the mammary gland; however, Hatanka et al. have determined it is expressed apically in the mouse colon, lung, and eye [202].

Transport appears to bidirectional and is dependent on sodium and chloride gradients [113].

SLC22A12 is the final transporter that had a significantly higher expression level in LMECs vs. MECs in the microarray analysis. No mammary gland expression data currently exists in the literature. Its known physiological function involves the renal reabsorption of urate at the proximal tubule cell apical membrane in exchange for the secretion of anions [105].

In reviewing the transporters identified by the screening paradigm for having an expression level equivalent to or greater than liver or kidney and comparing the results to Alcorn et al. and the murine developmental dataset (Aim 8), some other findings are worth noting. Although SLC22A1 was upregulated over 7-fold in the Alcorn et al. study and over 10-fold in the developmental dataset, its detection call was labeled “Absent” in all three LMEC samples in the current study. SLC22A4, SLC22A5, SLC29A1, and SLCO4A1 were present in LMECs in both human investigations. Despite a much higher expression of SLC28A3 in the previous work from our lab, no differences were detected between LMEC and MEC sample means in the current work. SLC16A1 expression increased during lactation in the mouse, but no changes were evident in this new human data. The datasets were in agreement regarding P-glycoprotein (ABCB1) and the organic anion transporters (SLC22A6-8) as they were either not present or expressed at a very low level during lactation.

Overall, the results were in good agreement with the literature and the screening paradigm did identify transporters currently known to be responsible for drug accumulation in breast milk, thereby supporting Hypothesis 3a. To summarize this large amount of microarray data, a diagram of xenobiotic transporter gene expression in LMECs that incorporates localization and directionality data where available and emphasizes those transporters upregulated during lactation was created (Figure 5-2). As depicted, many combinations of basolateral and apical transporters may work in concert to move xenobiotics across the LMEC barrier towards either breast milk or the maternal circulation to drive exposure risk. The SLCO4C1 observation is the most interesting finding, as it hints at an existence of an undiscovered vectorial pathway with ABCG2 for substrate movement into milk. Other such pathways have been proposed to exist in other tissues such as the placental trophoblast, intestine, kidney, liver, and blood-brain barrier and are the current focus of intensive research and a recent review by Ito et al. [203].

Limitations to this clinical study include the small sample size and variability in lactation stage (postpartum week) of the breastfeeding subjects. Intrapatient (eg. transporter expression level changing with lactation stage) or interpatient differences (eg. due to previous breastfeeding, ethnicity, or age) may exist and affect xenobiotic exposure risk but were not well captured or compared in this small study. Perhaps even more importantly, it is not currently known if these observations at the RNA level translate into similar expression level differences and functional consequences. Future studies should tackle these issues as well as explore the role and significance of SLCO4C1 in LMEC cells. The FACS-based LMEC isolation technique developed and validated in Aim 9 could measure transporter protein surface expression level with relatively small cell numbers if appropriate antibodies were available. The single ABCG2 transfection system created in Aim 4 could be also particularly useful as it may lay the groundwork for the creation of a SLCO4C1/ABCG2 double transfection system. Such a system would be invaluable to study the postulated vectorial process and its functional consequences for xenobiotic accumulation in breast milk.

Figure 5-2: Proposed model of xenobiotic transport in LMEC based on microarray expression data with localization and directionality derived from the published literature.

Panel A. Xenobiotic transporters that were upregulated during lactation with fold change from the microarray analysis. Panel B. Xenobiotic transporters that were expressed at a level equivalent to, or greater than, that in the liver or kidney. Localization and directionality was speculated based on information from other tissues. If data was inconclusive, the transporter is labeled with an asterisk.

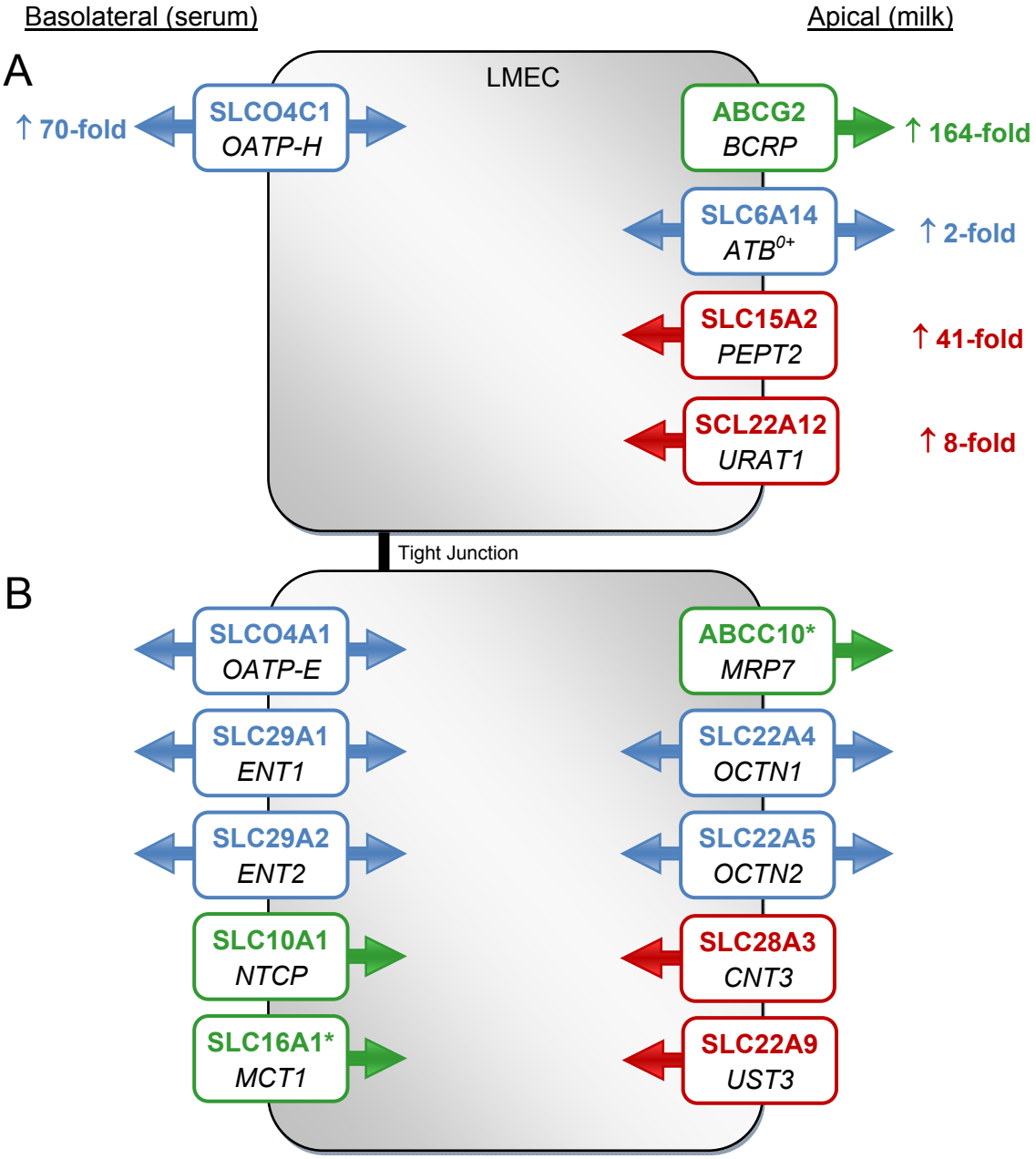

CHAPTER 6: Conclusions

This dissertation work focused on three unresolved issues regarding drug transport into breast milk during lactation: (1) determining if Abcg2, recently identified as having a major role in drug accumulation in breast milk, is the molecular cause of the apically-directed nitrofurantoin flux in CIT3 cells, a commonly used in vitro cell culture model of lactation; (2) developing a mathematical model to aid in understanding of the individual processes that determine xenobiotic flux rates across the mammary barrier, steady-state concentrations, and calculated M/S ratios in order to improve the utility of experimental flux assays; and (3) identifying the subset of all known xenobiotic transporters that are highly expressed, and therefore potentially clinically relevant, during lactation in mice and humans.

Breastfeeding is widely advocated as the best nutritional choice for infants, their mothers, and society [1-3]. Medication use, however, is highly prevalent in the post-partum period and puts patients and health care professions in the difficult position of weighing maternal benefit and potential exposure risks to the suckling infant [41]. The majority of xenobiotics enter breast milk by passive diffusion and mathematical models based on this concept perform well for most drugs, but fail to predict the M/S ratio of xenobiotics that accumulate via active transport [49-53]. Apically-directed nitrofurantoin transport was observed in the CIT3 cell culture model of lactation and clinically this drug was found to concentrate in breast milk. In CIT3 cells, the transport process was sodium-dependent, inhibited by dipyridamole, and believed to be localized to the basolateral membrane, but remained unidentified [88]. Recent literature clearly demonstrates that ABCG2, is responsible for the accumulation of nitrofurantoin and many other drugs in murine breast milk [53,91-93]. The current work was designed to determine if Abcg2 is responsible for CIT3 cell observations. Abcg2 RNA transcripts were detected and the protein was found apically expressed in CIT3 cells. Abcg2 was further demonstrated to be responsible for the directional flux of nitrofurantoin and other Abcg2 substrates such as PhIP, cimetidine, and ciprofloxacin through inhibition studies with the Abcg2-specific inhibitor FTC. Interestingly, the transport was observed both with and without the lactogenic hormone stimulation that was presumed necessary in the cell culture model of lactation. Some inconsistencies with past observations remain (sodium dependence and enhanced inhibition when inhibitors are placed on the basolateral side) and suggest other transport processes may also be present.

Knowledge of a xenobiotic's potential interaction with ABCG2 may help improve in vitro M/S predictions. With this goal in mind, the stable transfection of ABCG2 into a cell line that would be suitable for monolayer flux assays was performed. A MDCKII-ABCG2 clone with high expression was chosen and validated with a series of ABCG2 substrates and the inhibitors GF120918 and FTC. Data was as expected with nitrofurantoin, cimetidine, and ciprofloxacin with the ABCG2-attributed effect significantly altering both the B→A and A→B permeabilities, but results with PhIP and methotrexate were more difficult to explain. PhIP flux was predominantly apically directed and was ablated with 10 μM FTC, but was not affected by the addition of 1 μM GF120918. Methotrexate monolayer flux assays failed due to passive permeability issues. To help explain these results and to provide a greater understanding of the rate processes, a new mathematical model was put forth. A simple three compartment model incorporating several permeability surface area products: $PS_{B,U}$, $PS_{A,E}$, $PS_{B,E}$, and $PS_{A,U}$, PS_{PC}, PS_{D}, and $PS_{A,E(ABCG2)}$ was developed as an extension of the work of Kalvass and Pollack [172]. Derivations demonstrated that ER_A was not proportional to $PS_{A,E(ABCG2)}$ and had a maximal value of 2. ER_α remained proportional to $PS_{A,E(ABCG2)}$ if PS_{PC} was assumed to be negligible. If endogenous transport process existed in the model, it was theoretically shown that the ER_α Ratio is useful as it better preserves the proportionality to $PS_{A,E(ABCG2)}$. Overall increases in $PS_{A,E}$ or a higher relative substrate PS_D lowers the maximal achievable ER_A and blunted the ER_α Ratio. A nonzero PS_{PC} was also shown to blunt these ratios and cause nonlinearity in the relationships. Data extracted from the literature and from the validation of the MDCKII-ABCG2 cell line supported the mathematically derived principles. Correlations with the in vitro efflux ratios from these datasets and the ratio of the milk to plasma ratios in the wild-type and Bcrp1-/- mice were performed. Although most were not significant due to the quality and amount of the data available, ER_α Ratio showed some promise as the in vitro and in vivo rank order of the tested substrates was similar. Much more work is required to demonstrate the utility and understand the limitations of this new model and the model-derived efflux ratios.

In addition to ABCG2, the expression of other members of the SLC and ABC transporter superfamilies has been documented in mammary tissue from a variety of species but interpretation is complicated as expression data is often from nonlactating tissues and/or whole tissue homogenates rather than LMECs. The qPCR analysis of the expression of 30 transporters generated by Alcorn et al. in our lab remains the most

robust investigation of mammary xenobiotic transporter gene expression [49]. The utility of this study is limited however by its lack of biological replicates and the incomplete list of transporters chosen for analysis (ABCG2 was not investigated). To address evaluate the hypotheses that microarray analysis could identify transporters known to accumulate in milk, xenobiotic transporters that were upregulated during lactation were first identified in three murine mammary gland developmental datasets obtained from the literature. The transporters identified as upregulated during lactation was remarkably consistent with the literature and included Abcg2, Slc22a1, Slc15a2, Slc29a1, Slc16a1, and Abcc5. Next, this experimental paradigm was translated to humans and the work of Alcorn et al. was extended through the development of a new robust method to pure populations of luminal mammary epithelial cells from breast milk or breast reduction mammoplasty samples. Microarray expression profiling on the biological replicates (n=3 LMEC and n=3 MEC samples) was then performed to measure the expression level of all known human xenobiotic transporters. The first step of the two step screening paradigm identified ABCG2, SLC15A2, SLC22A12, SLC6A14, AND SLCO4C1 as xenobiotic transporters of potential importance as they were significantly upregulated during lactation. This ABCG2 data addresses an unanswered question in literature by documenting that it is the expression level within individual LMECs that significantly increases during lactation not that the ABCG2 expression is constant in LMECs and that mammogenesis causes the expansion of this cell type relative to others within the mammary gland. The second step identified ABCC10, SLC10A1, SLC16A1, SLC22A4, SLC22A5, SLC22A9, SLC28A3, SLC29A1, SLC29A2, and SLCO4A1 as also of potential interest as their expression level was similar to, or greater than, levels in the kidney or liver. Overall, the significant upregulation of SLCO4C1 (increased 70-fold) is the most interesting finding in this study, as this novel observation suggests that a vectorial pathway with ABCG2 (increased 164-fold) for substrate movement into milk may exist. Future studies will explore the role and significance of SLCO4C1 in LMEC cells.

APPENDICES

Appendix 1: List of Abbreviations

A	membrane surface area
ABC	ATP-binding cassette transporter superfamily
AUC	area under the concentration-time curve
C_0	initial concentration
C_A	concentration in the apical (milk) compartment
C_B	concentration in the basolateral (serum) compartment)
C_C	concentration in the cellular (LMEC) compartment
$C_{infant,serum}$	infant serum concentration
Cl_{infant}	infant systemic clearance
$C_{maternal}$	maternal serum concentration
$C_{milk,\ unbound}$	unbound concentration in the milk
$C_{serum,\ unbound}$	unbound concentration in the serum
DAPI	4',6-diamidino-2-phenylindole
DMSO	dimethyl sulfoxide
ER_A	apical efflux ratio; the ratio of the initial rate of B→A flux when all active transport processes are not inhibited divided by the initial rate of B→A flux when all active transport processes are inhibited completely
ER_α	asymmetry efflux ratio; ratio of the initial rate of B→A flux divided by the initial rate of A→B flux
ER_α Ratio	ratio of asymmetry efflux ratio; ratio of the ER_α in ABCG2-tranfected cells to the ER_α of the empty vector transfectants
FACS	fluorescence-activated cell sorting
F_{infant}	infant bioavailability
FITC	fluorescein isothiocyanate
f_m	fraction protein bound in the milk
f_s	fraction protein bound in the serum
FTC	fumitremorgin C
f_m^{un}	fraction of the drug unionized in the milk
f_s^{un}	fraction of the drug unionized in the serum
HBSS	Hanks balanced salt solution
IRB	institutional review board
J	flux
LMEC	lactating luminal mammary epithelial cell
Km	Michaelis-Menton constant
Ki	Michaelis-Menton inhibitory constant
M/P	milk to plasma ratio
M/S	milk to serum ratio
M/S_{point}	milk to serum point ratio

MEC	nonlactating luminal mammary epithelial cell
MFI	mean fluorescence intensity
MUC1	epithelial basement membrane antigen
P_{app}	apparent permeability
PBS	phosphate-buffered saline
PDR	Physicians Desk Reference
PE	phycoerythrin
PI	propidium iodide
$PS_{A,E}$	permeability-surface area product attributed to passive apical efflux
$PS_{A,E(ABCG2)}$	permeability-surface area product attributed to passive the transfected transporter ABCG2
$PS_{A,U}$	permeability-surface area product attributed to passive apical uptake
$PS_{B,E}$	permeability-surface area product attributed to passive basolateral efflux
$PS_{B,U}$	permeability-surface area product attributed to passive basolateral uptake
PS_{D}	permeability-surface area product attributed to passive diffusion across the LMEC basolateral and apical membranes
PS_{PC}	permeability-surface area product attributed to passive paracellular flux between the cells
qPCR	quantitative PCR
RIN	RNA integrity number
Sk	fat partitioning into skim milk
SLC	solute carrier transporter superfamily
TEER	transepithelial electrical resistance
V_{milk}/τ	milk consumption rate
W	fat partitioning into whole milk

Appendix 2: Chemical Structures

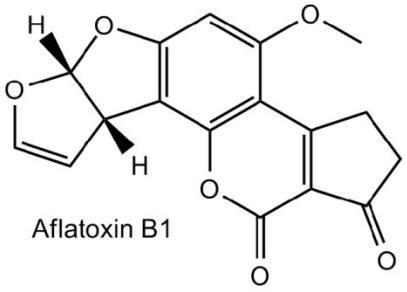

Aflatoxin B1

Albendazole

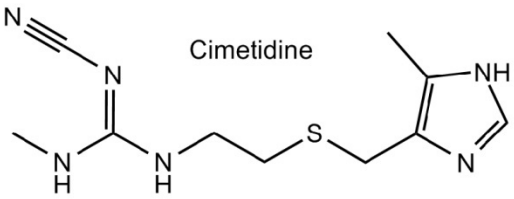

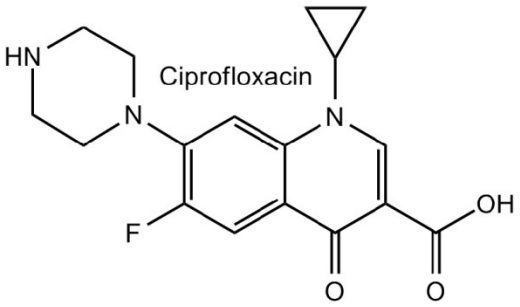

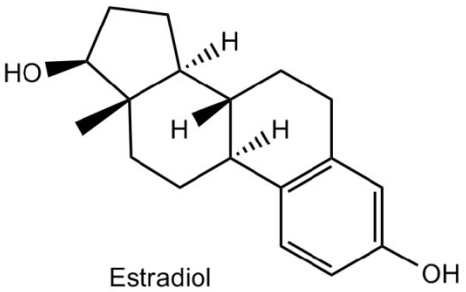

Estradiol

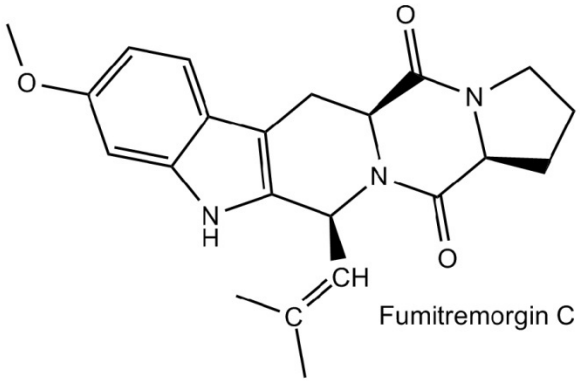

Fumitremorgin C

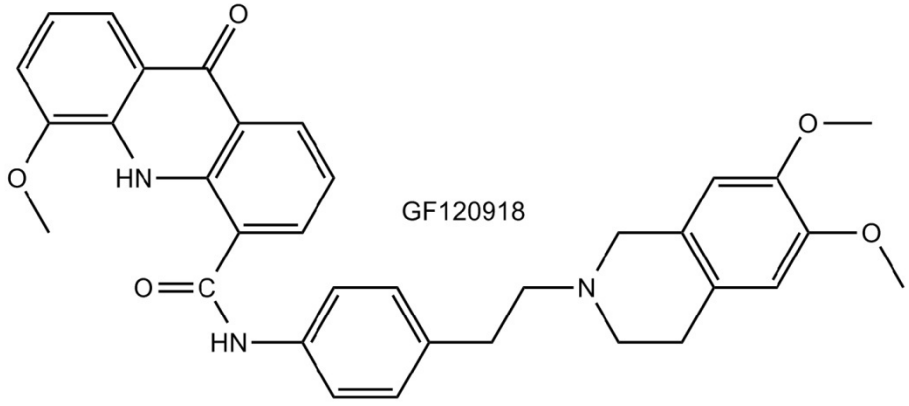

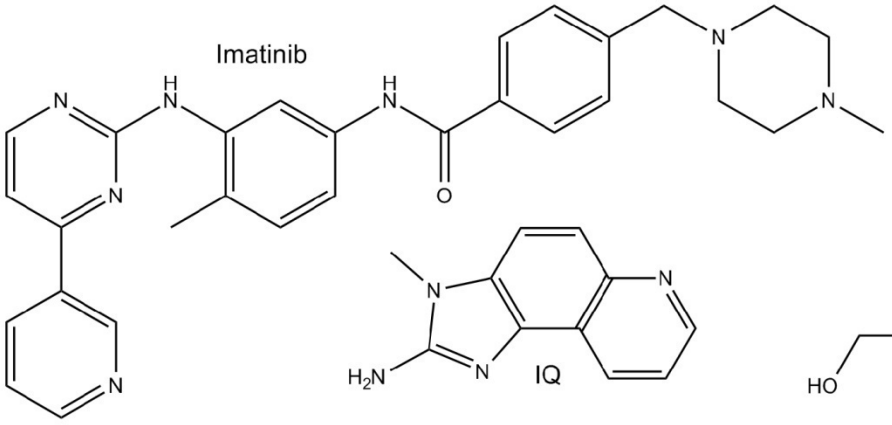
Imatinib

IQ

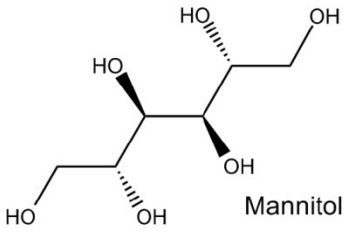
Mannitol

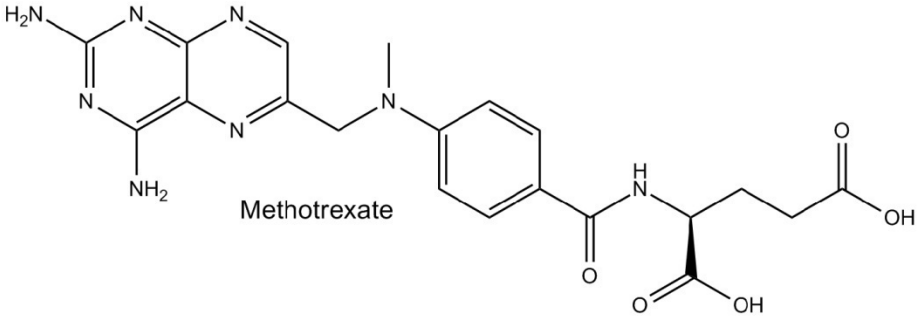
Methotrexate

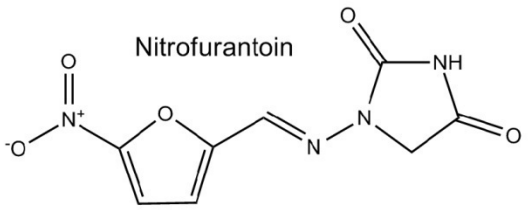
Nitrofurantoin

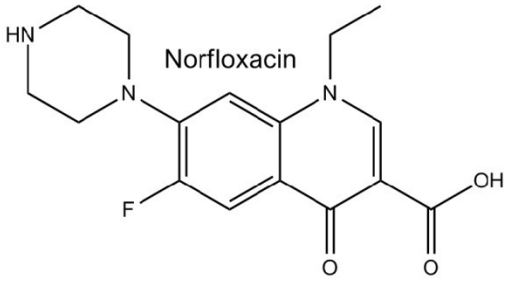
Norfloxacin

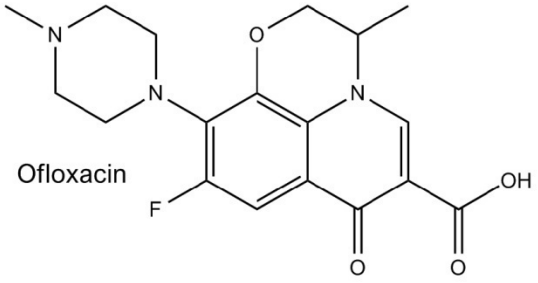
Ofloxacin

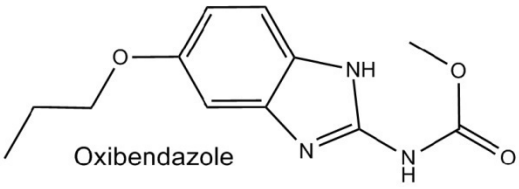
Oxibendazole

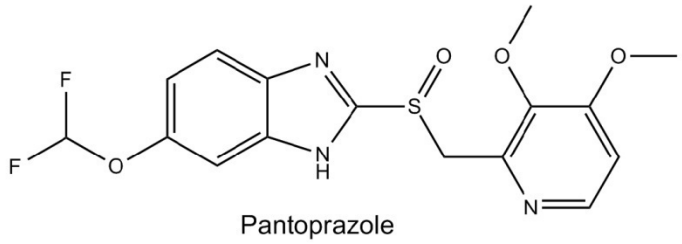
Pantoprazole

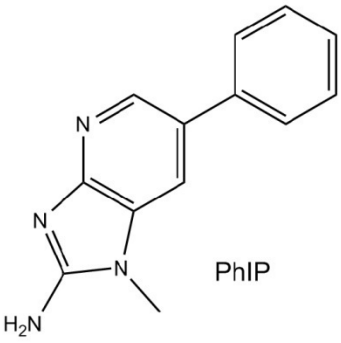
PhIP

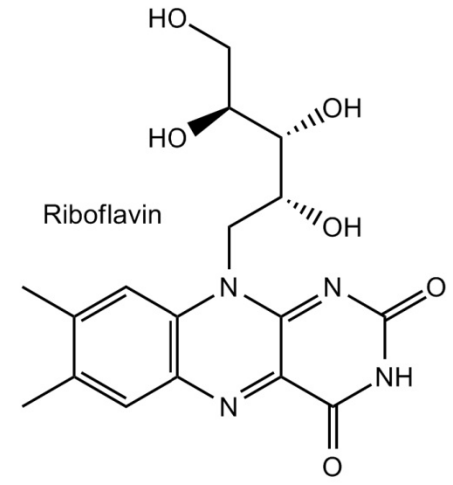

Riboflavin

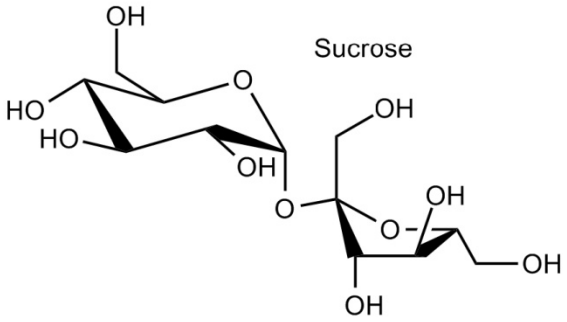

Sucrose

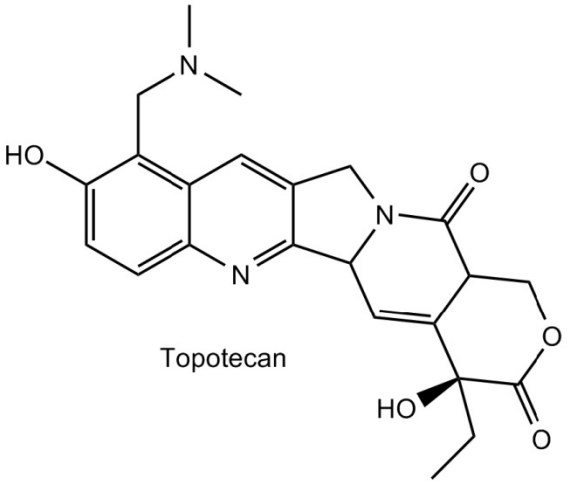

Topotecan

Appendix 3: Mathematical model derivation – Drug transfer from serum into milk with active uptake and efflux in the basolateral and apical membranes.

The following is the expanded derivation of the mathematical model for active flux from serum into milk with active uptake and efflux in the basolateral and apical membranes of LMECs presented in the Methods and Results. Equations are numbered sequentially with any cross-reference to the aforementioned sections noted in parenthesis.

Simple kinetic model for flux across a LMEC monolayer (Figure 3-2).

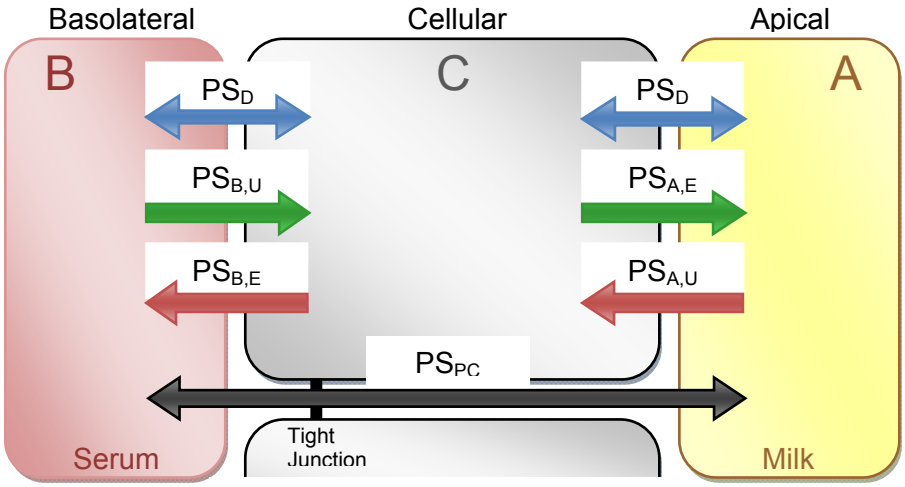

The model incorporates the permeability-surface area products attributed to:

- PS_{PC}: passive paracellular flux between cells
- PS_D: passive diffusion across the LMEC basolateral and apical membranes
- $PS_{B,U}$: basolateral uptake
- $PS_{B,E}$: basolateral efflux
- $PS_{A,U}$: apical uptake
- $PS_{A,E}$: apical efflux

Assumptions:

- 3 compartments, all well-stirred.
- passive diffusion across the basolateral and apical membranes is equal.
- no protein binding, ionization, or fat partioning phenomena exist.
- unstirred water layers are negligible.
- permeabilities are constant.

Substrate flux into and out of the basolateral (serum) compartment:

$$\frac{dX_B}{dt} = C_C(PS_D+PS_{B,E}) - C_B(PS_D+PS_{B,U}) + (C_A-C_B)PS_{PC} \quad \text{Eq. A-1 (Eq. 3-3)}$$

Substrate flux into and out of the cellular (LMEC) compartment:

$$\frac{dX_C}{dt} = C_A(PS_D+PS_{A,U}) + C_B(PS_D+PS_{B,U}) - C_C(2PS_D+PS_{A,E}+PS_{B,E}) \quad \text{Eq. A-2 (Eq. 3-4)}$$

Substrate flux into and out of the apical (milk) compartment:

$$\frac{dX_A}{dt} = C_C(PS_D+PS_{A,E}) - C_A(PS_D+PS_{A,U}) + (C_B-C_A)PS_{PC} \quad \text{Eq. A-3 (Eq. 3-5)}$$

Initial rate: B→A

With initial unidirectional flux into the apical compartment ($C_A = 0$), Eq. A-3 becomes:

$$\frac{dX_{A,B\rightarrow A}}{dt} = C_C(PS_D+PS_{A,E}) + C_B PS_{PC} \quad \text{Eq. A-4}$$

and assuming rapid equilibration between the B and C compartments ($dX_C/dt = 0$) Eq. A-2 can be rearranged to yield:

$$C_C = \frac{C_B(PS_D+PS_{B,U})}{(2PS_D+PS_{A,E}+PS_{B,E})} \quad \text{Eq. A-5}$$

Substitution of Eq. A-5 into Eq. A-4 yields:

$$\frac{dX_{A,B\rightarrow A}}{dt} = C_B^0\left[\frac{(PS_D+PS_{B,U})(PS_D+PS_{A,E})}{(2PS_D+PS_{A,E}+PS_{B,E})}+PS_{PC}\right] \quad \text{Eq. A-6 (Eq. 3-6)}$$

In the absence of both active uptake into and efflux out of the cell ($PS_{B,U}$, $PS_{A,E}$, $PS_{B,E}$, and $PS_{A,U} = 0$), (eg. parent cell line with no endogenous transporter expression):

$$\left(\frac{dX_{A,B\rightarrow A}}{dt}\right)_{parent} = C_B^0\left[\frac{PS_D}{2}+PS_{PC}\right] \quad \text{Eq. A-7 (Eq. 3-7)}$$

In a single apical efflux transporter transfected cell line (like the MDCKII-ABCG2 cells created in Section C), the addition of $PS_{A,E(ABCG2)}$ into a parent cell line with no endogenous transporter expression yields:

$$\left(\frac{dX_{A,B\rightarrow A}}{dt}\right)_{ABCG2} = C_B^0\left[\frac{(PS_D)(PS_D+PS_{A,E(ABCG2)})}{(2PS_D+PS_{A,E(ABCG2)})}+PS_{PC}\right] \quad \text{Eq. A-8 (Eq. 3-8)}$$

Initial rate: A→B

With initial unidirectional flux into the apical compartment ($C_B = 0$), Eq. A-1 becomes:

$$\frac{dX_{B,\,A\rightarrow B}}{dt} = C_C\left(PS_D + PS_{B,E}\right) + C_A PS_{PC} \qquad \text{Eq. A-9}$$

and assuming rapid equilibration between the A and C compartments ($dX_C/dt = 0$), Eq. A-2 can be rearranged to yield:

$$C_C = \frac{C_A\left(PS_D + PS_{A,U}\right)}{\left(2PS_D + PS_{A,E} + PS_{B,E}\right)} \qquad \text{Eq. A-10}$$

Substitution of Eq. A-10 into Eq. A-9 yields:

$$\frac{dX_{B,\,A\rightarrow B}}{dt} = C_A^0\left[\frac{\left(PS_D + PS_{A,U}\right)\left(PS_D + PS_{B,E}\right)}{\left(2PS_D + PS_{A,E} + PS_{B,E}\right)} + PS_{PC}\right] \qquad \text{Eq. A-11 (Eq. 3-9)}$$

In the absence of both active uptake into and efflux out of the cell ($PS_{B,U}$, $PS_{A,E}$, $PS_{B,E}$, and $PS_{A,U} = 0$), (eg. parent cell line with no endogenous transporter expression):

$$\left.\frac{dX_{B,\,A\rightarrow B}}{dt}\right|_{parent} = C_A^0\left[\frac{PS_D}{2} + PS_{PC}\right] \qquad \text{Eq. A-12 (Eq. 3-10)}$$

In a single apical efflux transporter transfected cell line (like the MDCKII-ABCG2 cells created in Section C), the addition of $PS_{A,E(ABCG2)}$ into a parent cell line with no endogenous transporter expression yields:

$$\left.\frac{dX_{B,\,A\rightarrow B}}{dt}\right|_{ABCG2} = C_A^0\left[\frac{(PS_D)^2}{\left(2PS_D + PS_{A,E(ABCG2)}\right)} + PS_{PC}\right] \qquad \text{Eq. A-13 (Eq. 3-11)}$$

Apical efflux ratio: ER_A

The apical efflux ratio, ER_A, is defined as the ratio of the initial rate of B→A flux when all active transport processes are not inhibited (Eq. A-6) divided by the initial rate of B→A flux when all active transport processes are inhibited completely (Eq. A-7):

$$ER_A = \frac{\dfrac{dX_{A,B\rightarrow A}}{dt}}{\left.\dfrac{dX_{A,B\rightarrow A}}{dt}\right|_{inhibited}} = \frac{C_B^0\left[\dfrac{\left(PS_D + PS_{B,U}\right)\left(PS_D + PS_{A,E}\right)}{\left(2PS_D + PS_{A,E} + PS_{B,E}\right)} + PS_{PC}\right]}{C_B^0\left[\dfrac{PS_D}{2} + PS_{PC}\right]} \qquad \text{Eq. A-14 (Eq. 3-12)}$$

If we assume $PS_D >> PS_{PC}$ or that $PS_{PC} \rightarrow 0$, ER_A reduces to:

$$ER_A = \frac{\frac{dX_{A,B\rightarrow A}}{dt}}{\frac{dX_{A,B\rightarrow A}}{dt}_{inhibited}} = \frac{2(PS_D+PS_{B,U})(PS_D+PS_{A,E})}{PS_D(2PS_D+PS_{A,E}+PS_{B,E})} \quad \text{Eq. A-15 (Eq. 3-13)}$$

The ER_A for the transfection of the single apical efflux transporter ABCG2 into the parent cell line with no background endogenous transporter expression (Eq. A-8 divided by Eq. A-7), is:

$$ER_A = \frac{\frac{dX_{A,B\rightarrow A}}{dt}_{ABCG2}}{\frac{dX_{A,B\rightarrow A}}{dt}_{parent}} = \frac{C_B^0\left[\frac{(PS_D)(PS_D+PS_{A,E(ABCG2)})}{(2PS_D+PS_{A,E(ABCG2)})}+PS_{PC}\right]}{C_B^0\left[\frac{PS_D}{2}+PS_{PC}\right]} \quad \text{Eq. A-16}$$

If the same assumption regarding PS_{PC} is made, relationship reduces to:

$$ER_A = \frac{2[PS_D+PS_{A,E(ABCG2)}]}{2PS_D+PS_{A,E(ABCG2)}} \quad \text{Eq. A-17 (Eq. 3-14)}$$

If $PS_{A,E(ABCG2)} >> PS_D$) an ER_A upper limit of 2 is reached as shown by Kalvass et al. [172].

$$\lim_{PS_{A,E}\rightarrow\infty}\left(ER_{A,\frac{ABCG2}{parent}}\right) = 2 \quad \text{Eq. A-18 Eq. 4-3}$$

Asymmetry efflux ratio: ER_α

The asymmetry efflux ratio, ER_α, is defined as the ratio of the initial rate of B→A flux (Eq. A-6) divided by the initial rate of A→B (Eq. A-11):

$$ER_\alpha = \frac{\frac{dX_{A,B\rightarrow A}}{dt}}{\frac{dX_{B,A\rightarrow B}}{dt}} = \frac{C_B^0\left[\frac{(PS_D+PS_{B,U})(PS_D+PS_{A,E})}{(2PS_D+PS_{A,E}+PS_{B,E})}+PS_{PC}\right]}{C_A^0\left[\frac{(PS_D+PS_{A,U})(PS_D+PS_{B,E})}{(2PS_D+PS_{A,E}+PS_{B,E})}+PS_{PC}\right]} \quad \text{Eq. A-19 (Eq. 3-15)}$$

If we assume the initial donor concentrations in the basolateral and apical compartments are equal experimentally ($C_B^0 = C_A^0$), and that PS_{PC} is negligible ($PS_{PC} \rightarrow 0$), the equation can be simplified to:

$$ER_\alpha = \frac{(PS_D+PS_{A,E})(PS_D+PS_{B,U})}{(PS_D+PS_{A,U})(PS_D+PS_{B,E})} \quad \text{Eq. A-20 (Eq. 3-16)}$$

The ER_α for the transfection of the single apical efflux transporter ABCG2 into the parent cell line with no background endogenous transporter expression (Eq. A-8 divided by Eq. A-13), is:

$$ER_\alpha = \frac{\left(\frac{dX_{A,B\rightarrow A}}{dt}\right)_{ABCG2}}{\left(\frac{dX_{B,A\rightarrow B}}{dt}\right)_{ABCG2}} = \frac{C_B^0\left[\frac{(PS_D)(PS_D+PS_{A,E(ABCG2)})}{(2PS_D+PS_{A,E(ABCG2)})}+PS_{PC}\right]}{C_A^0\left[\frac{(PS_D)^2}{(2PS_D+PS_{A,E(ABCG2)})}+PS_{PC}\right]} \qquad \text{Eq. A-21}$$

If the same assumption regarding PS_{PC} and the initial concentrations ($C_B^0 = C_A^0$) is made, relationship reduces to:

$$ER_\alpha = \frac{PS_D+PS_{A,E(ABCG2)}}{PS_D} \qquad \text{Eq. A-22 (Eq. 3-17)}$$

Steady-state concentrations in compartments A, B, and C

The steady-state substrate concentrations in compartments A, B, and C (dX_A/dt, dX_B/dt, and $dX_C/dt = 0$) can be determined by rearranging the differential equations:

Substrate flux into and out of the basolateral (serum) compartment:

$$C_{B,SS} = \frac{C_{A,SS}PS_{PC}+C_{C,SS}(PS_D+PS_{B,E})}{(PS_D+PS_{B,U}+PS_{PC})} \qquad \text{Eq. A-23 (Eq. 3-18)}$$

Substrate flux into and out of the cellular (LMEC) compartment:

$$C_{C,SS} = \frac{C_{A,SS}(PS_D+PS_{A,U})+C_{B,SS}(PS_D+PS_{B,U})}{(2PS_D+PS_{A,E}+PS_{B,E})} \qquad \text{Eq. A-24 (Eq. 3-19)}$$

Substrate flux into and out of the apical (milk) compartment:

$$C_{A,SS} = \frac{C_{B,SS}PS_{PC}+C_{C,SS}(PS_D+PS_{A,E})}{(PS_D+PS_{A,U}+PS_{PC})} \qquad \text{Eq. A-25 (Eq. 3-20)}$$

If we assume $PS_{PC}\rightarrow 0$, Eq. A-23 and Eq. A-25 can be reduced to::

$$C_{B,SS} = \frac{C_{C,SS}(PS_D+PS_{B,E})}{(PS_D+PS_{B,U})} \qquad \text{Eq. A-26 (Eq. 3-21)}$$

$$C_{A,SS} = \frac{C_{C,SS}(PS_D+PS_{A,E})}{(PS_D+PS_{A,U})} \qquad \text{Eq. A-27 (Eq. 3-22)}$$

Recalling that concentrations in this model are unbound drug, the steady-state ratio of a drug in the apical vs. the basolateral compartment can be determined by dividing $C_{A,SS}$ by $C_{B,SS}$ (Eq. A-27 by Eq. A-26). This results in the same asymmetry efflux ratio (ER_α) presented earlier:

$$\frac{C_{A,SS,unbound}}{C_{B,SS,unbound}} = \frac{(PS_D+PS_{A,E})(PS_D+PS_{B,U})}{(PS_D+PS_{A,U})(PS_D+PS_{B,E})} = ER_\alpha \qquad \text{Eq. A-28 (Eq. 3-23)}$$

Relationships to M/S ratio

The in vivo clearance terms that define the unbound ratio of the drug at steady state in the milk and serum are comparable to the in vitro permeability-surface area product terms that define the similar ratio in the model (Eq. A-28), such that:

$$\frac{C_{milk,unbound}}{C_{serum,unbound}} = \frac{(Cl_D+Cl_{A,E})(Cl_D+Cl_{B,U})}{(Cl_D+Cl_{A,U})(Cl_D+Cl_{B,E})} \qquad \text{Eq. A-29 (Eq. 3-24)}$$

The Passive Diffusion model for drug transfer into breast milk is based on total drug concentrations and provides the following prediction for the M/S ratio [68]:

$$\frac{M}{S}_{in\ vivo} \approx \frac{M}{S}_{diffusion} = \frac{(f_s^{un})(f_s)(W)}{(f_m^{un})(f_m)(Sk)} \qquad \text{Eq. A-30 (Eq. 3-25)}$$

It assumes $C_{milk,unbound} = C_{serum,unbound}$ and suggests that the M/S ratio observed in vivo is governed by protein binding and ionization in the milk, and serum and partitioning into milk fat. But, if active processes exist this assumption is not valid ($C_{milk,unbound} \neq C_{serum,unbound}$), so these concentrations need to be added to the prediction:

$$\frac{M}{S}_{in\ vivo} = \left[\frac{C_{milk,unbound}}{C_{serum,unbound}}\right]\left[\frac{(f_s^{un})(f_s)(W)}{(f_m^{un})(f_m)(Sk)}\right] \qquad \text{Eq. A-31 (Eq. 3-26)}$$

Replacing $C_{milk,unbound}/C_{serum,unbound}$ with the clearance in Eq. A-29 allows for the incorporation of active processes to put forth a new in vivo conceptual model and suggests that it may be possible to approximate the in vivo M/S using in vitro ER_α determinations and simple in vitro measurements of protein binding, ionization potential, and skim to whole milk partitioning:

$$\frac{M}{S}_{in\ vivo} = \left[\frac{(Cl_D+Cl_{A,E})(Cl_D+Cl_{B,U})}{(Cl_D+Cl_{A,U})(Cl_D+Cl_{B,E})}\right]\left[\frac{(f_s^{un})(f_s)(W)}{(f_m^{un})(f_m)(Sk)}\right] \qquad \text{Eq. A-32 (Eq. 3-27)}$$

$$\frac{(Cl_D+Cl_{A,E})(Cl_D+Cl_{B,U})}{(Cl_D+Cl_{A,U})(Cl_D+Cl_{B,E})} \approx \frac{(PS_D+PS_{A,E})(PS_D+PS_{B,U})}{(PS_D+PS_{A,U})(PS_D+PS_{B,E})} \quad \text{Eq. A-33 (Eq. 3-28)}$$

$$\frac{M}{S_{in\ vivo}} = \left[\frac{(PS_D+PS_{A,E})(PS_D+PS_{B,U})}{(PS_D+PS_{A,U})(PS_D+PS_{B,E})}\right]\left[\frac{(f_s^{un})(f_s)(W)}{(f_m^{un})(f_m)(Sk)}\right] \quad \text{Eq. A-34 (Eq. 3-29)}$$

$$\frac{M}{S_{in\ vivo}} = ER_\alpha \left[\frac{(f_s^{un})(f_s)(W)}{(f_m^{un})(f_m)(Sk)}\right] \quad \text{Eq. A-35 (Eq. 3-30)}$$

This relationship assumes:

- $PS_D \propto Cl_D$
- No differences in substrate interaction with individual transport processes and that expression level is comparable such that for a series of drugs $PS_{B,U} \propto Cl_{B,U}$, $PS_{B,E} \propto Cl_{B,E}$, $PS_{A,U} \propto Cl_{A,U}$, and $PS_{A,E} \propto Cl_{A,E}$.

Experimental Considerations: Maximum and minimum experimentally achievable initial rates.

The theoretical limits of the initial rates with increasing $PS_{A,E(ABCG2)}$ are explored. Recall the initial B→A rate for a single transfected system with an apical efflux transporter (eg. ABCG2) is described by Eq. A-8:

$$\frac{dX_{A,B\rightarrow A}}{dt}_{ABCG2} = C_B^0 \left[\frac{(PS_D)(PS_D+PS_{A,E(ABCG2)})}{(2PS_D+PS_{A,E(ABCG2)})}+PS_{PC}\right] \quad \text{Eq. A-8 (Eq. 3-8)}$$

If $PS_{A,E(ABCG2)} >> PS_D$, dX_A/dt increases until it achieves a maximal flux for a given initial basolateral concentration:

$$\lim_{PS_{A,E}\rightarrow\infty}\left(\frac{dX_{A,B\rightarrow A}}{dt}_{ABCG2}\right) = C_B^0\,[PS_D+PS_{PC}] \quad \text{Eq. A-36 (Eq. 4-1)}$$

Recall the initial A→B rate for a single transfected system with an apical efflux transporter (eg. ABCG2) is described by Eq. A-13:

$$\frac{dX_{B,\,A\rightarrow B}}{dt}_{ABCG2} = C_A^0 \left[\frac{(PS_D)^2}{(2PS_D+PS_{A,E(ABCG2)})}+PS_{PC}\right] \quad \text{Eq. A-13 (Eq. 3-11)}$$

If $PS_{A,E(ABCG2)} >> PS_D$, dX_B/dt decreases until it achieves a minimum flux for a given initial basolateral concentration:

$$\lim_{PS_{A,E}\to\infty}\left(\frac{dX_{B,\,A\to B}}{dt}_{ABCG2}\right) = C_A^0\,[PS_{PC}] \qquad \text{Eq. A-37 (Eq. 4-2)}$$

Experimental Considerations: Proportionality of $PS_{A,E(ABCG2)}$ to ER_A and ER_α.

Assuming no other transporter processes exist, PS_D can also be measured from $P_{app,B->A}$ or $P_{app,A->B}$ in the empty vector transfected cells such that $PS_D = 2\,PS_{B->A}$. However, an experimental measurement that correlates with the transport phenomena of interest (ie. $PS_{A,E(ABCG2)}$) is less obvious.

Recall, as presented in Eq. A-17, in a single transfected system with an apical efflux transporter (ie. ABCG2) where $PS_D >> PS_{PC}$ or that $PS_{PC}\to 0$, ER_A is:

$$ER_A = \frac{2\left[PS_D+PS_{A,E(ABCG2)}\right]}{2PS_D+PS_{A,E(ABCG2)}} \qquad \text{Eq. A-17 (Eq. 3-14)}$$

Solving for $PS_{A,E(ABCG2)}$ in this equation results in a complex relationship where no direct proportionality to ER_A exists:

$$PS_{A,E(ABCG2)} = \frac{(2PS_D)(ER_{A,\frac{ABCG2}{parent}}-1)}{2-ER_{A,\frac{ABCG2}{parent}}} \qquad \text{Eq. A-38 (Eq. 4-5)}$$

Recall, as presented in Eq. A-22, in a single transfected system with an apical efflux transporter (ie. ABCG2) where $PS_D >> PS_{PC}$ or that $PS_{PC}\to 0$, ER_α is:

$$ER_\alpha = \frac{PS_D+PS_{A,E(ABCG2)}}{PS_D} \qquad \text{Eq. A-22 (Eq. 3-17)}$$

Solving for $PS_{A,E(ABCG2)}$ in this equation, however, shows that this efflux ratio is expected to remain proportional to ER_α as previously shown by Kalvass and Pollack [172].

$$PS_{A,E(ABCG2)} = PS_D(ER_\alpha-1) \qquad \text{Eq. A-39 (Eq. 4-4)}$$

Therefore, the experimental calculation of $ER_{\alpha,ABCG2}$ from $P_{app,B->A}/P_{app,A->B}$ is useful as for a given substrate, it would be expected to be proportional to $PS_{A,E(ABCG2)}$.

Experimental Considerations: Relationship of $PS_{A,E(ABCG2)}$ to ER_A and ER_α when endogenous transporters are present.

Rejecting the assumption that endogenous transporters are absent complicates the relationships between $PS_{A,E(ABCG2)}$ and the efflux ratios. If $PS_{A,E}$ is the endogenous apical efflux transporter and $PS_{A,E(ABCG2)}$ is added to Eq. A-6 and Eq. A-11, the following rate relationships result:

$$\frac{dX_{A,B\rightarrow A}}{dt} = C_B^0\left[\frac{(PS_D+PS_{B,U})(PS_D+PS_{A,E}+PS_{A,E(ABCG2)})}{(2PS_D+PS_{A,E}+PS_{B,E}+PS_{A,E(ABCG2)})}+PS_{PC}\right] \quad \text{Eq. A-40 (Eq. 4-6)}$$

$$\frac{dX_{B,\,A\rightarrow B}}{dt} = C_A^0\left[\frac{(PS_D+PS_{A,U})(PS_D+PS_{B,E})}{(2PS_D+PS_{A,E}+PS_{B,E}+PS_{A,E(ABCG2)})}+PS_{PC}\right] \quad \text{Eq. A-41 (Eq. 4-7)}$$

If ER_A and ER_α are redefined using these new rate equations and we again assume $C_B^0 = C_A^0$ experimentally and $PS_{PC}\rightarrow 0$:

$$ER_A = \left[\frac{PS_D+PS_{A,E}+PS_{A,E(ABCG2)}}{2PS_D+PS_{A,E}+PS_{B,E}+PS_{A,E(ABCG2)}}\right]\left[\frac{(2PS_D+PS_{A,E})}{(PS_D+PS_{A,E})}\right] \quad \text{Eq. A-42 (Eq. 4-8)}$$

$$ER_\alpha = \left[\frac{(PS_D+PS_{A,E}+PS_{A,E(ABCG2)})}{(PS_D+PS_{A,U})}\right]\left[\frac{(PS_D+PS_{B,U})}{(PS_D+PS_{B,E})}\right] \quad \text{Eq. A-43 (Eq. 4-9)}$$

In an attempt to isolate $PS_{A,E(ABCG2)}$, the ER_α was further divided by ER_α of the empty vector-transfected cells ($PS_{B,U}$, $PS_{A,E}$, $PS_{B,E}$, and $PS_{A,U}$ are present, but $PS_{A,E(ABCG2)}$ is not) to produce the ER_α Ratio ($ER_{\alpha(ABCG2)}/ER_{\alpha(Empty)}$):

$$\frac{ER_{\alpha(ABCG2)}}{ER_{\alpha(Empty)}} = \left[\frac{(PS_D+PS_{A,E}+PS_{A,E(ABCG2)})}{(PS_D+PS_{A,E})}\right] \quad \text{Eq. A-44 (Eq. 4-10)}$$

Rearrangement of Eq. A-44 to Eq. A-45 shows $PS_{B,U}$, $PS_{B,E}$, and $PS_{A,U}$ can be removed from the relationship, but it is not possible to isolate $PS_{A,E(ABCG2)}$ from $PS_{A,E}$. However, A proportionality between $PS_{A,E(ABCG2)}$ and this ER_α Ratio still does exist:

$$PS_{A,E(ABCG2)} = (PS_D+PS_{A,E})\left[\left(\frac{ER_{\alpha(ABCG2)}}{ER_{\alpha(Empty)}}\right)-1\right] \quad \text{Eq. A-45 (Eq. 4-11)}$$

Experimentally, any variability in $PS_{A,E(ABCG2)}$ and $PS_{A,E}$ (eg. transporter expression levels), a substrate's ability to cross the membrane by passive diffusion (PS_D), or to interact with either transport process ($PS_{A,E(ABCG2)}$ or $PS_{A,E}$) would be expected to affect the ratio.

Experimental Considerations: Controlling for Variable PS_{PC}

Flux of paracellular markers sucrose and mannitol are somewhat variable between different cell lines (empty vs. transfected) and inter-day. PS_{PC} is therefore not negligible relative to the $PS_{B->A}$ for drugs that either have poor PS_D or relative to $PS_{A->B}$ for drugs that are good substrates for ABCG2. To control for the potential consequences associated with this variable PS_{PC} in the experimental data, the permeability of the paracellular marker can theoretically be subtracted from that of the drug being studied. The rearrangement of Eq. A-40 and Eq. A-41 to Eq. 4-12 and Eq. 4-13, respectively illustrates this solution:

$$\frac{\frac{dX_{A,B\rightarrow A}}{dt}}{C_B^0} - PS_{PC} = \frac{(PS_D+PS_{B,U})(PS_D+PS_{A,E}+PS_{A,E(ABCG2)})}{(2PS_D+PS_{A,E}+PS_{B,E}+PS_{A,E(ABCG2)})} \qquad \text{Eq. A-46 (Eq. 4-12)}$$

$$\frac{\frac{dX_{B,\,A\rightarrow B}}{dt}}{C_A^0} - PS_{PC} = \frac{(PS_D+PS_{A,U})(PS_D+PS_{B,E})}{(2PS_D+PS_{A,E}+PS_{B,E}+PS_{A,E(ABCG2)})} \qquad \text{Eq. A-47 (Eq. 4-13)}$$

It is very important to note that this approach is dependent on one major assumption; that the PS_{PC} of the paracellular marker being measured is equal to the PS_{PC} of the drug being studied.

Appendix 4: Raw data – murine microarray transporter expression levels from each chip.

Mu74v2A Chip detection calls. A=”Absent”; M=”Marginal”; P=”Present”, shading indicates probeset that was “Absent” on all chips in the lactating group.

		Stein															Clarkson						Medrano				
Probe Set ID	Gene Symbol	S_V10 A-detectioncall	S_V10 B-detectioncall	S_V10 C-detectioncall	S_V12 A-detectioncall	S_V12 B-detectioncall	S_V12 C-detectioncall	S_Lac1 A-detectioncall	S_Lac1 B-detectioncall	S_Lac1 C-detectioncall	S_Lac3 A-detectioncall	S_Lac3 B-detectioncall	S_Lac3 C-detectioncall	S_Lac7 A-detectioncall	S_Lac7 B-detectioncall	S_Lac7 C-detectioncall	C_Virgin-1mas5-Detection	C_Virgin-2mas5-Detection	C_Lact-10d-1mas5-Detection	C_Lact-10d-2mas5-Detection	C_Lact-5d-1mas5-Detection	C_Lact-5d-2mas5-Detection	M_Virgin-1mas5-Detection	M_Virgin-2mas5-Detection	M_Virgin-3mas5-Detection	M_Lact-10d-1mas5-Detection	M_Lact-10d-2mas5-Detection
104137_at	Abca2	A	A	P	M	A	A	A	A	A	A	A	A	A	A	A	A	M	A	A	A	A	P	P	A	A	A
102910_at	Abcb1a	P	P	P	A	A	P	A	A	A	A	A	A	A	A	A	A	P	A	A	A	A	A	M	M	A	A
94733_at	Abcb4	A	A	A	A	A	A	A	A	A	A	A	A	A	A	A	A	A	A	A	A	A	A	A	M	A	A
99329_at	Abcc1	A	A	P	A	A	M	A	A	A	A	A	A	A	A	A	A	A	A	A	A	A	P	P	P	A	A
95283_at	Abcc2	A	A	A	A	A	A	A	A	A	A	A	A	A	A	A	A	A	A	A	A	A	A	A	A	A	A
103689_at	Abcc3	M	A	A	A	A	M	A	A	A	A	A	A	A	A	A	A	P	A	A	A	A	A	A	A	A	A
103800_at	Abcc5	A	A	A	A	A	A	A	A	A	A	A	A	A	A	M	A	A	A	P	A	A	A	A	A	M	A
93407_at	Abcc6	A	A	A	A	A	A	A	A	A	A	A	A	A	A	A	A	A	A	A	A	A	A	A	A	A	A
93626_at	Abcg2	P	P	P	P	P	P	P	P	P	P	P	P	P	P	P	P	P	P	P	P	P	P	P	P	P	P
160978_at	Osta	A	A	A	A	A	A	A	A	A	A	A	A	A	A	A	A	A	A	A	A	A	A	A	M	A	A
100339_at	Slc10a1	A	A	A	A	A	A	A	A	A	A	A	A	A	A	A	A	A	A	A	A	A	A	A	A	A	A
100340_at	Slc10a1	A	A	A	A	A	A	A	A	A	A	A	A	A	A	A	A	A	A	A	A	A	A	A	A	A	A
100341_g_at	Slc10a1	A	A	A	A	A	A	A	A	A	A	A	A	A	A	A	A	A	A	A	A	A	A	A	A	A	A
97150_at	Slc10a2	A	A	A	A	A	A	A	A	A	A	A	A	A	A	A	A	A	A	A	A	A	A	A	A	A	A
103918_at	Slc15a2	A	A	A	A	A	A	A	A	M	A	A	A	A	A	A	A	P	P	P	P	P	A	A	A	P	P
101588_at	Slc16a1	A	A	A	A	A	P	A	A	A	A	A	A	A	A	A	A	A	A	A	M	P	P	P	A	A	A
95060_at	Slc16a7	P	P	A	A	A	A	A	A	A	A	A	A	A	A	A	A	A	A	A	A	A	A	A	P	P	A
96077_at	Slc17a1	A	A	A	A	A	A	A	A	A	A	A	A	A	A	A	A	A	A	A	A	A	A	A	A	A	A
96078_g_at	Slc17a1	A	A	A	A	P	A	A	A	A	A	A	A	A	A	A	A	A	A	A	A	A	A	A	A	A	A
100916_at	Slc22a1	A	A	A	A	A	A	A	A	A	A	A	A	A	A	A	A	A	A	A	M	A	A	A	A	A	M
102429_at	Slc22a12	A	A	A	A	A	A	A	A	A	A	A	A	A	A	A	A	A	A	A	A	A	A	A	A	A	A
102947_at	Slc22a2	A	A	A	A	A	A	A	A	A	A	A	A	A	A	A	A	A	A	A	A	A	A	A	A	A	A
92497_at	Slc22a4	A	A	A	A	A	A	A	A	A	A	A	A	A	A	A	A	A	A	A	A	A	A	A	A	A	A
98322_at	Slc22a5	P	M	P	A	P	P	P	P	P	P	P	P	A	P	P	A	M	P	A	M	P	P	P	P	P	P
97431_at	Slc22a6	A	A	A	A	A	A	A	A	A	A	A	A	A	A	A	A	A	A	A	A	A	A	A	A	A	A
104387_at	Slc23a1	A	A	A	A	A	A	A	A	A	A	A	A	A	A	A	A	A	A	A	A	A	A	A	A	A	A
104267_at	Slc23a2	P	P	P	P	P	P	P	A	A	P	M	A	A	A	A	M	P	A	A	A	A	P	P	P	A	M
161687_r_at	Slc29a1	A	A	A	A	A	A	A	A	A	A	A	A	A	A	A	A	A	A	A	A	A	A	A	A	A	A
95733_at	Slc29a1	P	P	P	P	P	P	P	P	P	P	P	P	M	P	P	P	P	P	A	M	P	P	P	A	A	A
92950_at	Slc29a2	A	A	A	A	A	A	A	A	A	A	A	A	A	A	A	A	A	A	A	A	A	A	A	A	A	A
161006_at	Slco3a1	A	A	A	A	A	A	A	A	A	A	A	A	A	A	A	A	P	A	A	A	A	M	A	A	A	A
94663_at	Slco5a1	A	A	A	A	A	A	A	A	A	A	A	A	A	A	A	A	P	A	A	A	A	P	P	P	A	A

Mu74v2A chip signal intensities. “Absent” probesets were excluded.

		Stein															Clarkson					Medrano				
Probe Set ID	Gene Symbol	S_V10 A-signal	S_V10 B-signal	S_V10 C-signal	S_V12 A-signal	S_V12 B-signal	S_V12 C-signal	S_Lac1 A-signal	S_Lac1 B-signal	S_Lac1 C-signal	S_Lac3 A-signal	S_Lac3 B-signal	S_Lac3 C-signal	S_Lac7 A-signal	S_Lac7 B-signal	S_Lac7 C-signal	C_Virgin-1mas5-Signal	C_Virgin-2mas5-Signal	C_Lact-5d-1mas5-Signal	C_Lact-5d-2mas5-Signal	C_Lact-10d-1mas5-Signal	C_Lact-10d-2mas5-Signal	M_Virgin-1mas5-Signal	M_Virgin-2mas5-Signal	M_Virgin-3mas5-Signal	M_Lact-10d-1mas5-Signal	M_Lact-10d-2mas5-Signal
93626_at	Abcg2	104	105	69	101	78	64	542	995	1300	1307	1036	1359	2045	1701	1718	64	149	1909	2084	2291	1897	59	71	67	3179	2666
98322_at	Slc22a5	26	24	73	46	56	61	43	61	57	30	53	73	45	61	76	19	49	58	65	45	41	56	52	51	47	62
95733_at	Slc29a1	193	161	193	251	275	281	535	648	553	605	896	474	300	524	498	327	286	391	312	268	270	199	177	157	202	205
103918_at	Slc15a2	14	13	31	18	7	7	37	36	56	28	49	40	39	70	39	21	31	64	115	90	73	9	12	15	140	108
104267_at	Slc23a2	96	118	94	57	80	100	66	58	57	74	69	82	73	47	33	68	137	67	53	93	65	107	114	141	78	80
103800_at	Abcc5	70	55	116	114	108	112	120	176	175	106	165	183	194	220	195	115	75	117	116	103	183	89	120	114	143	131
101588_at	Slc16a1	14	16	2	19	9	23	20	24	15	21	20	11	21	3	16	19	12	48	47	32	45	22	15	4	28	19
100916_at	Slc22a1	3	1	2	3	6	2	3	4	5	3	7	10	10	11	18	15	3	40	46	89	70	3	1	1	110	94

Appendix 5: Raw data – human microarray transporter expression levels from each chip.

U133 plus 2.0 chip detection calls. A=”Absent”; M=”Marginal”; P=”Present”, shading indicates probeset that was “Absent” on all chips in the lactating group.

Probe Set ID	Gene Symbol	LMEC 1mas5-Detection	LMEC 2mas5-Detection	LMEC 3mas5-Detection	MEC 1mas5-Detection	MEC 2mas5-Detection	MEC 3mas5-Detection	K 1mas5-Detection	K 2mas5-Detection	K 3mas5-Detection	K 4mas5-Detection	K 5mas5-Detection	K 6mas5-Detection	L 1mas5-Detection	L 2mas5-Detection	L 3mas5-Detection	L 4mas5-Detection	L 5mas5-Detection	L 6mas5-Detection
210099_at	ABCA2	A	A	A	A	A	A	A	A	A	A	A	A	A	A	A	A	A	A
210100_s_at	ABCA2	A	A	A	A	A	A	A	A	A	A	A	A	A	A	A	A	A	A
212772_s_at	ABCA2	A	A	A	A	A	P	P	P	P	P	P	P	P	P	P	P	P	P
204343_at	ABCA3	A	A	A	A	A	A	P	P	P	A	A	A	A	A	A	A	A	A
209993_at	ABCB1	A	A	A	A	A	A	P	P	P	P	P	P	P	P	P	P	P	P
243951_at	ABCB1	A	P	P	A	A	A	P	P	P	P	P	P	P	P	P	P	P	P
209994_s_at	ABCB1 /// ABCB4	A	A	A	A	A	A	P	P	P	P	P	P	P	P	P	P	P	P
208288_at	ABCB11	A	A	A	A	A	A	A	A	A	A	A	A	P	P	P	P	P	P
211224_s_at	ABCB11	A	A	A	A	A	A	A	A	A	A	A	A	P	P	A	P	A	P
1570505_at	ABCB4	A	A	A	A	A	A	A	A	A	A	A	A	P	P	M	P	P	A
207819_s_at	ABCB4	A	A	A	A	A	A	A	A	A	A	A	A	P	P	P	P	P	P
237138_at	ABCB4	A	A	A	A	A	A	A	A	A	A	A	A	A	A	A	A	P	A
202805_s_at	ABCC1	A	A	A	P	P	P	A	P	A	A	A	A	A	A	A	A	A	A
202804_at	ABCC1	P	P	P	P	P	P	P	P	P	P	P	P	P	P	P	P	P	P
215873_x_at	ABCC10	A	A	P	A	A	A	P	P	P	A	P	P	A	A	A	A	P	A
213485_s_at	ABCC10	P	P	P	P	P	P	P	P	P	P	P	P	P	P	P	P	P	M
1554911_at	ABCC11	A	A	A	A	A	A	A	A	A	A	A	A	A	A	A	A	A	A
224146_s_at	ABCC11	A	A	A	A	P	P	A	A	A	A	A	A	A	A	A	A	A	A
1552590_a_at	ABCC12	A	A	A	A	A	A	A	A	A	A	A	A	A	A	A	A	A	A
1553410_a_at	ABCC12	A	A	A	A	A	A	A	A	A	A	A	A	A	A	A	A	A	A
206155_at	ABCC2	A	A	A	A	A	A	A	A	P	A	A	A	P	P	P	P	P	P
208161_s_at	ABCC3	A	A	A	P	P	P	A	P	A	A	A	A	P	P	P	P	P	P
209641_s_at	ABCC3	A	A	A	A	A	A	A	A	A	A	A	A	A	A	A	A	A	A
214979_at	ABCC3	A	A	A	A	A	A	A	A	A	A	A	A	P	A	A	A	A	A
230682_x_at	ABCC3	A	A	A	P	A	A	A	A	A	A	A	A	P	A	M	A	P	P
239217_x_at	ABCC3	A	A	A	P	A	P	A	A	A	A	A	A	A	A	A	A	A	P
242553_at	ABCC3	A	A	A	A	A	A	A	A	A	A	A	A	A	A	A	A	A	A
1554918_a_at	ABCC4	A	A	A	A	A	A	P	P	P	P	P	A	A	A	A	A	A	A
203196_at	ABCC4	A	A	A	A	A	A	P	P	P	P	P	P	A	A	A	A	A	A
243928_s_at	ABCC4	A	A	A	A	A	A	A	A	M	A	A	A	A	A	A	A	A	A
244053_at	ABCC4	A	A	A	A	A	A	A	A	A	A	A	A	A	A	A	A	A	A
1555039_a_at	ABCC4	P	A	A	A	A	A	P	P	P	P	P	P	A	A	A	A	A	P
1558460_at	ABCC5	A	A	A	A	A	A	P	P	P	A	A	A	P	M	P	A	P	P
209380_s_at	ABCC5	A	A	A	A	A	A	P	P	P	P	P	P	P	M	P	A	A	P
226363_at	ABCC5	A	A	A	A	A	A	P	P	P	P	P	P	A	A	A	A	A	A
208480_s_at	ABCC6	A	A	A	A	A	A	A	A	A	A	A	A	A	A	A	P	A	P

U133 plus 2.0 chip detection calls. A=”Absent”; M=”Marginal”; P=”Present”, shading indicates probeset that was “Absent” on all chips in the lactating group (cont.).

Probe Set ID	Gene Symbol	LMEC 1mas5-Detection	LMEC 2mas5-Detection	LMEC 3mas5-Detection	MEC 1mas5-Detection	MEC 2mas5-Detection	MEC 3mas5-Detection	K 1mas5-Detection	K 2mas5-Detection	K 3mas5-Detection	K 4mas5-Detection	K 5mas5-Detection	K 6mas5-Detection	L 1mas5-Detection	L 2mas5-Detection	L 3mas5-Detection	L 4mas5-Detection	L 5mas5-Detection	L 6mas5-Detection
215559_at	ABCC6	A	A	A	A	A	A	P	P	P	P	P	P	P	P	P	P	P	P
209735_at	ABCG2	P	P	P	A	P	P	P	A	A	P	A	M	P	P	P	P	P	P
229230_at	OSTalpha	A	A	A	P	A	P	A	A	A	A	A	A	P	P	P	P	P	P
207185_at	SLC10A1	P	A	A	P	A	M	A	A	A	A	A	A	P	P	P	P	P	P
207095_at	SLC10A2	A	A	A	A	A	M	P	P	P	P	P	P	P	A	A	A	A	A
207254_at	SLC15A1	A	A	A	A	A	A	A	A	A	P	P	A	P	P	P	P	P	P
211349_at	SLC15A1	A	A	A	A	A	A	P	A	P	P	P	P	A	P	P	A	A	P
205316_at	SLC15A2	P	P	P	A	A	P	P	P	P	P	P	P	A	A	A	A	A	A
205317_s_at	SLC15A2	P	P	P	A	P	P	P	P	P	P	P	P	A	A	A	A	A	A
240159_at	SLC15A2	P	P	P	P	A	M	P	P	P	P	P	P	M	A	A	A	A	A
202235_at	SLC16A1	P	M	A	P	P	P	A	A	P	A	A	A	P	P	P	P	P	A
1557918_s_at	SLC16A1	P	P	P	A	P	P	A	A	A	A	A	A	P	P	P	P	A	P
202234_s_at	SLC16A1	P	P	P	P	P	P	M	P	P	P	P	A	P	P	P	P	P	P
202236_s_at	SLC16A1	P	P	P	P	P	P	P	P	P	P	P	P	P	P	P	P	P	P
209900_s_at	SLC16A1	P	P	P	P	P	P	A	A	P	A	P	A	P	P	P	P	P	P
241866_at	SLC16A7	A	A	A	P	A	A	P	P	P	P	P	P	P	P	P	P	P	P
210807_s_at	SLC16A7	A	A	P	P	P	P	P	P	P	P	P	P	P	P	P	P	P	P
207057_at	SLC16A7	P	P	P	P	P	P	P	P	P	P	P	P	P	P	P	A	P	P
1560884_at	SLC17A1	A	A	A	A	A	A	P	P	P	P	P	P	A	P	P	A	P	A
1560885_x_at	SLC17A1	A	A	A	A	A	A	P	P	P	A	P	P	A	A	A	A	A	A
206872_at	SLC17A1	A	A	A	A	A	A	P	P	P	P	P	P	P	P	P	M	A	P
242536_at	SLC17A1	A	A	A	A	A	A	P	P	P	P	P	P	P	P	P	A	A	P
237049_at	SLC17A1	A	A	M	A	A	A	P	P	P	P	P	P	P	P	P	P	P	P
207201_s_at	SLC22A1	A	A	A	A	A	A	A	A	A	A	A	A	P	P	P	P	P	P
220100_at	SLC22A11	A	A	A	A	A	A	P	P	P	P	P	P	A	A	A	A	A	A
237799_at	SLC22A12	M	A	A	A	A	A	P	P	P	P	P	P	A	A	A	A	A	A
207429_at	SLC22A2	A	A	A	A	A	A	P	P	P	P	P	P	A	A	A	A	A	A
205421_at	SLC22A3	A	A	A	A	A	A	A	A	A	A	A	A	P	P	P	P	P	P
1570482_at	SLC22A3	A	A	P	A	A	P	A	A	A	A	A	A	A	P	A	A	P	P
242578_x_at	SLC22A3	M	P	M	P	P	P	P	P	P	P	P	P	P	P	P	P	P	P
233900_at	SLC22A4	A	A	A	A	A	A	A	A	A	A	A	A	A	A	A	A	A	A
205896_at	SLC22A4	P	P	P	P	P	P	A	P	P	P	A	A	A	A	A	A	A	A
205074_at	SLC22A5	A	P	P	P	P	P	P	P	P	P	P	P	P	A	M	P	A	P
210343_s_at	SLC22A6	A	A	A	A	A	A	P	P	P	P	P	P	A	A	A	A	A	A
216599_x_at	SLC22A6	A	A	A	A	A	A	P	P	P	P	P	P	A	A	A	A	A	A
244890_at	SLC22A6	A	A	A	A	A	A	P	A	A	M	P	P	A	A	A	A	A	A
1555553_a_at	SLC22A7	A	A	A	A	A	A	A	M	A	P	P	A	P	P	P	P	P	P
220554_at	SLC22A7	A	A	A	A	A	A	P	P	P	P	P	P	P	P	P	P	P	P

U133 plus 2.0 chip detection calls. A=”Absent”; M=”Marginal”; P=”Present”, shading indicates probeset that was “Absent” on all chips in the lactating group (cont.).

Probe Set ID	Gene Symbol	LMEC 1mas5-Detection	LMEC 2mas5-Detection	LMEC 3mas5-Detection	MEC 1mas5-Detection	MEC 2mas5-Detection	MEC 3mas5-Detection	K 1mas5-Detection	K 2mas5-Detection	K 3mas5-Detection	K 4mas5-Detection	K 5mas5-Detection	K 6mas5-Detection	L 1mas5-Detection	L 2mas5-Detection	L 3mas5-Detection	L 4mas5-Detection	L 5mas5-Detection	L 6mas5-Detection
221661_at	SLC22A7	A	A	A	A	A	A	P	P	P	P	P	P	P	P	P	P	P	P
221662_s_at	SLC22A7	A	A	A	A	A	A	A	P	P	P	P	A	P	P	P	P	P	P
231398_at	SLC22A7	A	A	A	A	A	A	P	P	P	P	P	P	P	P	P	P	P	P
221298_s_at	SLC22A8	A	A	A	A	A	A	P	P	P	P	P	P	A	A	A	A	A	A
231352_at	SLC22A8	A	A	A	A	A	A	P	P	P	P	P	P	A	A	A	A	A	A
231625_at	SLC22A9	A	A	A	A	A	A	A	A	A	A	A	A	P	P	P	P	P	P
241770_x_at	SLC22A9	A	A	P	A	A	P	P	A	P	A	P	A	P	P	P	P	P	P
223732_at	SLC23A1	A	A	A	A	A	A	P	P	P	P	P	P	P	P	P	P	P	P
1554692_at	SLC23A2	A	A	A	M	P	P	P	A	A	A	A	A	P	A	M	M	P	A
209236_at	SLC23A2	A	A	A	P	A	A	P	A	M	A	A	A	P	P	P	P	P	P
209237_s_at	SLC23A2	A	A	A	P	A	A	A	A	A	A	A	A	P	A	P	P	A	A
211572_s_at	SLC23A2	P	A	A	P	A	P	A	A	A	A	A	A	P	P	P	P	P	P
216425_at	SLC28A1	A	A	A	A	A	A	A	A	A	A	A	A	A	A	A	A	A	A
216790_at	SLC28A1	A	A	A	A	A	A	A	A	A	A	A	A	A	A	A	A	A	A
231187_at	SLC28A1	A	A	A	A	A	A	P	P	P	P	P	P	P	P	P	P	P	P
207560_at	SLC28A1	M	P	P	A	P	A	P	P	P	P	P	P	P	P	P	P	P	P
207249_s_at	SLC28A2	A	A	A	A	A	A	A	A	A	A	A	A	A	A	A	A	A	A
216432_at	SLC28A2	A	A	A	A	A	A	A	A	A	A	A	A	A	A	A	A	A	A
220475_at	SLC28A3	A	A	P	P	P	P	A	A	A	A	A	A	A	A	A	A	A	A
201802_at	SLC29A1	A	P	P	P	A	P	P	A	A	P	A	M	P	P	P	P	P	P
201801_s_at	SLC29A1	P	P	P	P	P	P	P	P	P	P	P	P	P	P	P	P	P	P
1553540_a_at	SLC29A2	A	A	A	A	A	A	A	A	A	A	A	A	A	A	A	A	A	A
1560062_at	SLC29A2	A	A	A	A	A	A	A	A	A	A	A	A	A	A	A	A	A	A
1560149_at	SLC29A2	A	A	A	A	A	A	A	A	A	A	A	A	A	A	A	A	A	A
1560151_x_at	SLC29A2	A	A	A	A	A	A	A	A	A	A	A	A	A	A	A	A	A	A
204717_s_at	SLC29A2	P	P	P	P	A	P	P	P	P	P	A	P	A	A	A	A	A	A
219344_at	SLC29A3	A	A	A	A	A	A	A	A	A	A	A	P	A	A	M	A	P	P
227281_at	SLC29A4	A	A	A	A	A	A	A	A	A	A	A	A	A	A	A	A	A	A
219795_at	SLC6A14	P	P	P	P	P	P	A	A	A	A	P	P	A	A	A	A	A	P
207308_at	SLCO1A2	A	A	A	A	P	A	P	A	A	A	A	P	P	P	A	A	M	P
211480_s_at	SLCO1A2	A	A	A	A	A	A	A	A	A	A	A	A	A	P	A	A	A	A
211481_at	SLCO1A2	A	A	A	A	A	A	A	A	A	A	A	A	M	P	P	A	P	A
210366_at	SLCO1B1	A	A	A	A	A	A	A	A	A	A	P	P	P	P	P	P	P	P
206354_at	SLCO1B3	A	A	A	A	A	P	A	A	A	A	A	A	P	P	P	P	P	P
220460_at	SLCO1C1	A	A	A	A	A	P	A	A	A	A	A	A	A	A	A	A	A	A
204368_at	SLCO2A1	A	A	A	A	A	A	P	P	P	P	P	P	A	A	A	A	A	A
203472_s_at	SLCO2B1	A	A	A	A	A	A	A	A	A	A	P	A	P	P	P	P	P	P
211557_x_at	SLCO2B1	A	A	A	A	A	A	A	P	A	M	P	A	P	P	P	P	P	P

U133 plus 2.0 chip detection calls. A=”Absent”; M=”Marginal”; P=”Present”, shading indicates probeset that was “Absent” on all chips in the lactating group (cont.).

Probe Set ID	Gene Symbol	LMEC 1mas5-Detection	LMEC 2mas5-Detection	LMEC 3mas5-Detection	MEC 1mas5-Detection	MEC 2mas5-Detection	MEC 3mas5-Detection	K 1mas5-Detection	K 2mas5-Detection	K 3mas5-Detection	K 4mas5-Detection	K 5mas5-Detection	K 6mas5-Detection	L 1mas5-Detection	L 2mas5-Detection	L 3mas5-Detection	L 4mas5-Detection	L 5mas5-Detection	L 6mas5-Detection
203473_at	SLCO2B1	A	P	P	P	A	A	P	P	M	P	P	M	P	P	P	P	P	P
210542_s_at	SLCO3A1	A	A	A	P	P	P	A	A	A	A	A	A	A	A	A	A	A	A
219229_at	SLCO3A1	P	A	A	P	P	P	P	P	P	P	P	P	A	P	P	P	P	P
227367_at	SLCO3A1	P	A	A	P	P	P	P	P	P	P	P	P	P	P	P	P	P	A
229239_x_at	SLCO4A1	A	A	A	A	A	A	A	A	A	A	A	A	A	A	A	A	A	A
1554332_a_at	SLCO4A1	P	P	P	P	P	P	A	A	A	A	A	A	P	A	P	P	P	P
219911_s_at	SLCO4A1	P	P	P	P	P	P	P	P	P	A	P	M	A	A	A	A	A	A
222071_s_at	SLCO4C1	P	P	P	A	P	P	P	P	P	P	P	P	P	P	P	P	P	P
220984_s_at	SLCO5A1	A	A	A	A	A	A	A	A	A	A	A	A	A	A	A	A	A	A
1552745_at	SLCO6A1	A	A	A	A	A	A	A	A	A	A	M	A	A	A	A	A	A	A

U133 plus 2.0 chip signal intensities. Genes “Absent” were excluded.

Probe Set ID	Gene Symbol	LMEC 1mas5-Signal	LMEC 2mas5-Signal	LMEC 3mas5-Signal	MEC 1mas5-Signal	MEC 2mas5-Signal	MEC 3mas5-Signal	K 1mas5-Signal	K 2mas5-Signal	K 3mas5-Signal	K 4mas5-Signal	K 5mas5-Signal	K 6mas5-Signal	L 1mas5-Signal	L 2mas5-Signal	L 3mas5-Signal	L 4mas5-Signal	L 5mas5-Signal	L 6mas5-Signal
202804_at	ABCC1	103	97	135	1185	1403	1613	844	1080	679	784	644	853	410	314	434	507	350	212
213485_s_at	ABCC10	782	447	574	566	298	297	861	799	839	643	643	689	578	477	616	495	759	388
209735_at	ABCG2	23911	16605	12092	28	176	117	383	416	471	483	376	494	4459	4608	1209	1838	2034	1345
205316_at	SLC15A2	4194	4163	3451	50	95	145	998	666	646	832	496	1213	174	69	130	39	49	52
205317_s_at	SLC15A2	1058	850	696	53	161	54	445	464	485	448	204	669	253	109	173	192	139	235
240159_at	SLC15A2	210	271	248	86	66	77	774	297	557	397	588	723	121	124	73	215	175	155
1557918_s_at	SLC16A1	1336	641	885	261	679	637	159	188	233	200	256	124	1005	1317	750	1371	414	799
202234_s_at	SLC16A1	730	858	619	256	1006	616	228	328	411	387	719	228	926	1794	528	856	522	577
202236_s_at	SLC16A1	3535	3141	2593	694	2922	2107	434	850	1475	863	1678	545	2817	4116	1482	2591	753	2124
209900_s_at	SLC16A1	1048	1016	952	348	1594	1214	165	328	535	369	889	116	976	1960	678	1032	479	558
207057_at	SLC16A7	89	175	111	616	254	455	3475	814	750	820	799	1739	673	373	354	252	371	242
242578_x_at	SLC22A3	143	165	245	667	1344	342	1339	435	627	690	1332	938	705	725	627	723	1309	932
205896_at	SLC22A4	510	432	347	413	276	357	334	807	767	800	894	531	228	105	236	173	179	198
207560_at	SLC28A1	180	213	207	85	240	79	323	898	951	1448	1388	486	822	985	1067	1046	1336	1483
201801_s_at	SLC29A1	547	971	1482	279	255	383	822	833	560	666	502	875	1101	1284	1183	1518	1047	3033
204717_s_at	SLC29A2	239	164	184	137	94	138	566	514	512	457	315	610	186	212	197	207	193	229
219795_at	SLC6A14	3193	3411	5360	2287	1289	1742	52	27	97	57	144	99	55	19	14	95	28	90
1554332_a_at	SLCO4A1	875	1142	2017	515	503	549	112	74	141	124	249	249	608	199	362	377	498	340
219911_s_at	SLCO4A1	791	748	1181	1567	434	1339	758	797	1448	712	729	797	195	43	52	559	208	49
222071_s_at	SLCO4C1	3127	3266	3692	21	81	42	1553	2433	1765	1940	1239	1488	339	241	384	562	398	1107
243951_at	ABCB1	53	93	48	51	72	34	759	541	686	949	528	564	389	582	336	538	628	417
202235_at	SLC16A1	314	219	268	202	524	219	21	138	187	169	240	102	524	1146	276	466	277	291
205074_at	SLC22A5	392	528	684	558	541	333	1727	3012	4936	3594	3031	1784	730	480	404	465	396	820

U133 plus 2.0 chip signal intensities. Genes “Absent” were excluded. (cont.)

Probe Set ID	Gene Symbol	LMEC 1mas5-Signal	LMEC 2mas5-Signal	LMEC 3mas5-Signal	MEC 1mas5-Signal	MEC 2mas5-Signal	MEC 3mas5-Signal	K 1mas5-Signal	K 2mas5-Signal	K 3mas5-Signal	K 4mas5-Signal	K 5mas5-Signal	K 6mas5-Signal	L 1mas5-Signal	L 2mas5-Signal	L 3mas5-Signal	L 4mas5-Signal	L 5mas5-Signal	L 6mas5-Signal
201802_at	SLC29A1	294	841	636	197	191	271	720	468	461	647	407	594	1051	1135	1103	1343	1294	2401
203473_at	SLCO2B1	104	252	101	129	89	89	633	1564	801	2346	1892	1044	11339	9207	13054	12753	8841	10741
215873_x_at	ABCC10	346	295	261	264	101	315	622	699	605	497	489	715	513	220	347	443	437	412
1555039_a_at	ABCC4	104	8	15	26	43	20	402	478	185	327	368	256	97	194	155	130	153	212
207185_at	SLC10A1	249	19	64	71	64	75	284	113	207	334	460	449	16004	18281	15816	18623	13561	15722
210807_s_at	SLC16A7	84	100	72	200	153	220	1483	447	402	371	467	758	500	348	283	254	216	296
237049_at	SLC17A1	21	12	71	5	37	5	1211	623	597	616	1583	840	366	409	322	258	508	291
237799_at	SLC22A12	168	272	114	45	10	15	754	2385	2353	4739	2128	1002	31	45	18	25	25	20
1570482_at	SLC22A3	16	26	46	39	44	139	176	105	144	138	140	155	135	79	117	140	400	238
241770_x_at	SLC22A9	10	64	42	14	71	57	20	18	45	41	73	70	747	1136	848	721	777	580
211572_s_at	SLC23A2	110	97	71	110	110	106	346	181	114	174	240	330	6104	1876	2125	2744	1413	1194
220475_at	SLC28A3	31	101	441	2347	1202	717	196	118	237	159	268	215	337	304	200	191	72	339
219229_at	SLCO3A1	124	20	9	454	386	417	837	641	600	461	525	756	198	232	389	384	549	217
227367_at	SLCO3A1	238	121	121	490	611	531	823	554	607	495	410	617	248	340	342	270	308	268

REFERENCES

1. Gartner LM, Morton J, Lawrence RA, Naylor AJ, O'Hare D, Schanler RJ, et al. Breastfeeding and the use of human milk. *Pediatrics* 2005;115(2):496-506.
2. Institute of Medicine. Nutrition during lactation: Report of the subcommittee on nutrution during lactation of the committee on nutritional status during pregancy and lactation. Washington D.D.: National Academy Press; 1991.
3. World Health Organization Fifty-fifth World Health Assembly. Global strategy on infant and young child feeding. Geneva: World Health Organization; 2003.
4. Popkin BM, Adair L, Akin JS, Black R, Briscoe J, Flieger W. Breast-feeding and diarrheal morbidity. *Pediatrics* 1990;86(6):874-82.
5. Bhandari N, Bahl R, Mazumdar S, Martines J, Black RE, Bhan MK. Effect of community-based promotion of exclusive breastfeeding on diarrhoeal illness and growth: a cluster randomised controlled trial. *Lancet* 2003;361(9367):1418-23.
6. Howie PW, Forsyth JS, Ogston SA, Clark A, Florey CD. Protective effect of breast feeding against infection. *Bmj* 1990;300(6716):11-6.
7. Dewey KG, Heinig MJ, Nommsen-Rivers LA. Differences in morbidity between breast-fed and formula-fed infants. *J Pediatr* 1995;126(5 Pt 1):696-702.
8. Oddy WH, Sly PD, de Klerk NH, Landau LI, Kendall GE, Holt PG, et al. Breast feeding and respiratory morbidity in infancy: a birth cohort study. *Arch Dis Child* 2003;88(3):224-8.
9. Lopez-Alarcon M, Villalpando S, Fajardo A. Breast-feeding lowers the frequency and duration of acute respiratory infection and diarrhea in infants under six months of age. *J Nutr* 1997;127(3):436-43.
10. Pisacane A, Graziano L, Zona G, Granata G, Dolezalova H, Cafiero M, et al. Breast feeding and acute lower respiratory infection. *Acta Paediatr* 1994;83(7):714-8.
11. Duncan B, Ey J, Holberg CJ, Wright AL, Martinez FD, Taussig LM. Exclusive breast-feeding for at least 4 months protects against otitis media. *Pediatrics* 1993;91(5):867-72.
12. Cochi SL, Fleming DW, Hightower AW, Limpakarnjanarat K, Facklam RR, Smith JD, et al. Primary invasive Haemophilus influenzae type b disease: a population-based assessment of risk factors. *J Pediatr* 1986;108(6):887-96.
13. Istre GR, Conner JS, Broome CV, Hightower A, Hopkins RS. Risk factors for primary invasive Haemophilus influenzae disease: increased risk from day care attendance and school-aged household members. *J Pediatr* 1985;106(2):190-5.
14. Pisacane A, Graziano L, Mazzarella G, Scarpellino B, Zona G. Breast-feeding and urinary tract infection. *J Pediatr* 1992;120(1):87-9.
15. Marild S, Hansson S, Jodal U, Oden A, Svedberg K. Protective effect of breastfeeding against urinary tract infection. *Acta Paediatr* 2004;93(2):164-8.
16. Ford RP, Taylor BJ, Mitchell EA, Enright SA, Stewart AW, Becroft DM, et al. Breastfeeding and the risk of sudden infant death syndrome. *Int J Epidemiol* 1993;22(5):885-90.

17. Alm B, Wennergren G, Norvenius SG, Skjaerven R, Lagercrantz H, Helweg-Larsen K, et al. Breast feeding and the sudden infant death syndrome in Scandinavia, 1992-95. *Arch Dis Child* 2002;86(6):400-2.

18. McVea KL, Turner PD, Peppler DK. The role of breastfeeding in sudden infant death syndrome. *J Hum Lact* 2000;16(1):13-20.

19. Pettitt DJ, Forman MR, Hanson RL, Knowler WC, Bennett PH. Breastfeeding and incidence of non-insulin-dependent diabetes mellitus in Pima Indians. *Lancet* 1997;350(9072):166-8.

20. Kostraba JN, Cruickshanks KJ, Lawler-Heavner J, Jobim LF, Rewers MJ, Gay EC, et al. Early exposure to cow's milk and solid foods in infancy, genetic predisposition, and risk of IDDM. *Diabetes* 1993;42(2):288-95.

21. Bener A, Denic S, Galadari S. Longer breast-feeding and protection against childhood leukaemia and lymphomas. *Eur J Cancer* 2001;37(2):234-8.

22. Davis MK. Review of the evidence for an association between infant feeding and childhood cancer. *Int J Cancer Suppl* 1998;11:29-33.

23. Chulada PC, Arbes SJ, Jr., Dunson D, Zeldin DC. Breast-feeding and the prevalence of asthma and wheeze in children: analyses from the Third National Health and Nutrition Examination Survey, 1988-1994. *J Allergy Clin Immunol* 2003;111(2):328-36.

24. Gdalevich M, Mimouni D, Mimouni M. Breast-feeding and the risk of bronchial asthma in childhood: a systematic review with meta-analysis of prospective studies. *J Pediatr* 2001;139(2):261-6.

25. Armstrong J, Reilly JJ. Breastfeeding and lowering the risk of childhood obesity. *Lancet* 2002;359(9322):2003-4.

26. Gillman MW, Rifas-Shiman SL, Camargo CA, Jr., Berkey CS, Frazier AL, Rockett HR, et al. Risk of overweight among adolescents who were breastfed as infants. *Jama* 2001;285(19):2461-7.

27. Horwood LJ, Darlow BA, Mogridge N. Breast milk feeding and cognitive ability at 7-8 years. *Arch Dis Child Fetal Neonatal Ed* 2001;84(1):F23-7.

28. Mortensen EL, Michaelsen KF, Sanders SA, Reinisch JM. The association between duration of breastfeeding and adult intelligence. *Jama* 2002;287(18):2365-71.

29. Jacobson SW, Chiodo LM, Jacobson JL. Breastfeeding effects on intelligence quotient in 4- and 11-year-old children. *Pediatrics* 1999;103(5):e71.

30. Reynolds A. Breastfeeding and brain development. *Pediatr Clin North Am* 2001;48(1):159-71.

31. Chua S, Arulkumaran S, Lim I, Selamat N, Ratnam SS. Influence of breastfeeding and nipple stimulation on postpartum uterine activity. *Br J Obstet Gynaecol* 1994;101(9):804-5.

32. Kennedy KI, Labbok MH, Van Look PF. Lactational amenorrhea method for family planning. *Int J Gynaecol Obstet* 1996;54(1):55-7.

33. Cumming RG, Klineberg RJ. Breastfeeding and other reproductive factors and the risk of hip fractures in elderly women. *Int J Epidemiol* 1993;22(4):684-91.

34. Breast cancer and breastfeeding: collaborative reanalysis of individual data from 47 epidemiological studies in 30 countries, including 50302 women with breast cancer and 96973 women without the disease. *Lancet* 2002;360(9328):187-95.

35. Rosenblatt KA, Thomas DB. Lactation and the risk of epithelial ovarian cancer. The WHO Collaborative Study of Neoplasia and Steroid Contraceptives. *Int J Epidemiol* 1993;22(2):192-7.

36. Dewey KG, Heinig MJ, Nommsen LA. Maternal weight-loss patterns during prolonged lactation. *Am J Clin Nutr* 1993;58(2):162-6.

37. Weimer J. The economic benefits of breastfeeding: a review and analysis. Food assistance and nutrition research report. No. 13. In: Food and Rural Economics Division ERS, US Department of Agriculture, editor.; 2001.

38. Ball TM, Wright AL. Health care costs of formula-feeding in the first year of life. *Pediatrics* 1999;103(4 Pt 2):870-6.

39. Ryan AS, Wenjun Z, Acosta A. Breastfeeding continues to increase into the new millennium. *Pediatrics* 2002;110(6):1103-9.

40. Mothers Survey, Ross Products Division, Abbott Laboratories; 2003.

41. Passmore CM, McElnay JC, D'Arcy PF. Drugs taken by mothers in the puerperium: inpatient survey in Northern Ireland. *Br Med J (Clin Res Ed)* 1984;289(6458):1593-6.

42. Schirm E, Schwagermann MP, Tobi H, de Jong-van den Berg LT. Drug use during breastfeeding. A survey from the Netherlands. *Eur J Clin Nutr* 2004;58(2):386-90.

43. Uhl K, Peat R, Toigo T, Kennedy DL, Kweder SL. Review of drug labeling for information regarding lactation. *Clin Pharmacol Ther* 2003;73(2):P39.

44. FDA. Guidance for Industry Clinical Lactation Studies – Study Design, Data Analysis, and Recommendations for Labeling. In; 2005.

45. Lawrence RA, Lawrence RM. Sixth ed. St. Louis, MS: Mosby; 2005.

46. Hennighausen L, Robinson GW. Information networks in the mammary gland. *Nat Rev Mol Cell Biol* 2005;6(9):715-25.

47. Hale TW. Drug therapy and breastfeeding: pharmacokinetics, risk factors, and effects on milk production. *Neoreviews* 2004;5(4):e164-e172.

48. Neville MC, McFadden TB, Forsyth I. Hormonal regulation of mammary differentiation and milk secretion. *J Mammary Gland Biol Neoplasia* 2002;7(1):49-66.

49. Alcorn J, Lu X, Moscow JA, McNamara PJ. Transporter gene expression in lactating and nonlactating human mammary epithelial cells using real-time reverse transcription-polymerase chain reaction. *J Pharmacol Exp Ther* 2002;303(2):487-96.

50. Atkinson HC, Begg EJ. Prediction of drug distribution into human milk from physicochemical characteristics. *Clin Pharmacokinet* 1990;18(2):151-67.

51. Gerk PM, Kuhn RJ, Desai NS, McNamara PJ. Active transport of nitrofurantoin into human milk. *Pharmacotherapy* 2001;21(6):669-75.

52. Ilett KF, Kristensen JH. Drug use and breastfeeding. *Expert Opin Drug Saf* 2005;4(4):745-68.

53. Merino G, Jonker JW, Wagenaar E, van Herwaarden AE, Schinkel AH. The breast cancer resistance protein (BCRP/ABCG2) affects pharmacokinetics, hepatobiliary excretion, and milk secretion of the antibiotic nitrofurantoin. *Mol Pharmacol* 2005;67(5):1758-64.

54. Bitman J, Wood DL, Mehta NR, Hamosh P, Hamosh M. Lipids of human milk. In: Touchstond J, Sherma J, editors. Techniques and applications of thin layer chromatography. New York, NY: John Wiley and Sons; 1985. p. 261-277.

55. Blanc B. Biochemical aspects of human milk--comparison with bovine milk. *World Rev Nutr Diet* 1981;36:1-89.

56. Morriss FH, Jr., Brewer ED, Spedale SB, Riddle L, Temple DM, Caprioli RM, et al. Relationship of human milk pH during course of lactation to concentrations of citrate and fatty acids. *Pediatrics* 1986;78(3):458-64.

57. McNamara PJ, Abbassi M. Neonatal exposure to drugs in breast milk. *Pharm Res* 2004;21(4):555-66.

58. Breitzka RL, Sandritter TL, Hatzopoulos FK. Principles of drug transfer into breast milk and drug disposition in the nursing infant. *J Hum Lact* 1997;13(2):155-8.

59. Wilson JT, Brown RD, Cherek DR, Dailey JW, Hilman B, Jobe PC, et al. Drug excretion in human breast milk: principles, pharmacokinetics and projected consequences. *Clin Pharmacokinet* 1980;5(1):1-66.

60. Begg EJ, Duffull SB, Hackett LP, Ilett KF. Studying drugs in human milk: time to unify the approach. *J Hum Lact* 2002;18(4):323-32.

61. Anderson PO. Drug use during breast-feeding. *Clin Pharm* 1991;10(8):594-624.

62. Fleishaker JC. Models and methods for predicting drug transfer into human milk. *Adv Drug Deliv Rev* 2003;55(5):643-52.

63. Atkinson HC, Begg EJ. The binding of drugs to major human milk whey proteins. *Br J Clin Pharmacol* 1988;26(1):107-9.

64. Howard CR, Lawrence RA. Drugs and breastfeeding. *Clin Perinatol* 1999;26(2):447-78.

65. Wilson JT, Brown RD, Hinson JL, Dailey JW. Pharmacokinetic pitfalls in the estimation of the breast milk/plasma ratio for drugs. *Annu Rev Pharmacol Toxicol* 1985;25:667-89.

66. Findlay JW. The distribution of some commonly used drugs in human breast milk. *Drug Metab Rev* 1983;14(4):653-84.

67. Agatonovic-Kustrin S, Tucker IG, Zecevic M, Zivanovic LJ. Prediction of drug transfer into human milk from theoretically derived descriptors. *Analytica Chimica Acta* 2000;418:181-195.

68. Fleishaker JC, Desai N, McNamara PJ. Factors affecting the milk-to-plasma drug concentration ratio in lactating women: physical interactions with protein and fat. *J Pharm Sci* 1987;76(3):189-93.

69. Fleishaker JC, McNamara PJ. In vivo evaluation in the lactating rabbit of a model for xenobiotic distribution into breast milk. *J Pharmacol Exp Ther* 1988;244(3):919-24.

70. Fleishaker JC, McNamara PJ. Effect of altered serum protein binding on propranolol distribution into milk in the lactating rabbit. *J Pharmacol Exp Ther* 1988;244(3):925-8.

71. McNamara PJ, Burgio D, Yoo SD. Pharmacokinetics of acetaminophen, antipyrine, and salicylic acid in the lactating and nursing rabbit, with model predictions of milk to serum concentration ratios and neonatal dose. *Toxicol Appl Pharmacol* 1991;109(1):149-60.

72. McNamara PJ, Burgio D, Yoo SD. Pharmacokinetics of caffeine and its demethylated metabolites in lactating adult rabbits and neonatal offspring. Predictions of breast milk to serum concentration ratios. *Drug Metab Dispos* 1992;20(2):302-8.

73. McNamara PJ, Burgio D, Yoo SD. Pharmacokinetics of cimetidine during lactation: species differences in cimetidine transport into rat and rabbit milk. *J Pharmacol Exp Ther* 1992;261(3):918-23.

74. McNamara PJ, Meece JA, Paxton E. Active transport of cimetidine and ranitidine into the milk of Sprague Dawley rats. *J Pharmacol Exp Ther* 1996;277(3):1615-21.

75. Oo CY, Kuhn RJ, Desai N, McNamara PJ. Active transport of cimetidine into human milk. *Clin Pharmacol Ther* 1995;58(5):548-55.

76. Oo CY, Kuhn RJ, Desai N, Wright CE, McNamara PJ. Pharmacokinetics in lactating women: prediction of alprazolam transfer into milk. *Br J Clin Pharmacol* 1995;40(3):231-6.

77. Oo CY, Burgio DE, Kuhn RC, Desai N, McNamara PJ. Pharmacokinetics of caffeine and its demethylated metabolites in lactation: predictions of milk to serum concentration ratios. *Pharm Res* 1995;12(2):313-6.

78. Kearns GL, McConnell RF, Jr., Trang JM, Kluza RB. Appearance of ranitidine in breast milk following multiple dosing. *Clin Pharm* 1985;4(3):322-4.

79. Lau RJ, Emery MG, Galinsky RE. Unexpected accumulation of acyclovir in breast milk with estimation of infant exposure. *Obstet Gynecol* 1987;69(3 Pt 2):468-71.

80. Ruprecht RM, Sharpe AH, Jaenisch R, Trites D. Analysis of 3'-azido-3'-deoxythymidine levels in tissues and milk by isocratic high-performance liquid chromatography. *J Chromatogr* 1990;528(2):371-83.

81. Kwok B, Yamauchi A, Rajesan R, Chan L, Dhillon U, Gao W, et al. Carnitine/xenobiotics transporters in the human mammary gland epithelia, MCF12A. *Am J Physiol Regul Integr Comp Physiol* 2006;290(3):R793-802.

82. Dostal LA. Investigation of the mechanisms of the extensive excretion of cimetidine into rat milk. *Biochem Pharmacol* 1990;39(1):207-10.

83. Dostal LA, Weaver RP, Schwetz BA. Excretion of high concentrations of cimetidine and ranitidine into rat milk and their effects on milk composition and mammary gland nucleic acid content. *Toxicol Appl Pharmacol* 1990;102(3):430-42.

84. Kari FW, Weaver R, Neville MC. Active transport of nitrofurantoin across the mammary epithelium in vivo. *J Pharmacol Exp Ther* 1997;280(2):664-8.

85. Oo CY, Paxton EW, McNamara PJ. Active transport of nitrofurantoin into rat milk. *Adv Exp Med Biol* 2001;501:547-52.

86. Toddywalla VS, Kari FW, Neville MC. Active transport of nitrofurantoin across a mouse mammary epithelial monolayer. *J Pharmacol Exp Ther* 1997;280(2):669-76.

87. Gerk PM, Hanson L, Neville MC, McNamara PJ. Sodium dependence of nitrofurantoin active transport across mammary epithelia and effects of dipyridamole, nucleosides, and nucleobases. *Pharm Res* 2002;19(3):299-305.

88. Gerk PM, Moscow JA, McNamara PJ. Basolateral active uptake of nitrofurantoin in the CIT3 cell culture model of lactation. *Drug Metab Dispos* 2003;31(6):691-3.

89. Danielson KG, Oborn CJ, Durban EM, Butel JS, Medina D. Epithelial mouse mammary cell line exhibiting normal morphogenesis in vivo and functional differentiation in vitro. *Proc Natl Acad Sci U S A* 1984;81(12):3756-60.

90. Schmidhauser C, Bissell MJ, Myers CA, Casperson GF. Extracellular matrix and hormones transcriptionally regulate bovine beta-casein 5' sequences in stably transfected mouse mammary cells. *Proc Natl Acad Sci U S A* 1990;87(23):9118-22.

91. van Herwaarden AE, Wagenaar E, Merino G, Jonker JW, Rosing H, Beijnen JH, et al. Multidrug transporter ABCG2/breast cancer resistance protein secretes riboflavin (vitamin B2) into milk. *Mol Cell Biol* 2007;27(4):1247-53.

92. van Herwaarden AE, Schinkel AH. The function of breast cancer resistance protein in epithelial barriers, stem cells and milk secretion of drugs and xenotoxins. *Trends Pharmacol Sci* 2006;27(1):10-6.

93. Merino G, Alvarez AI, Pulido MM, Molina AJ, Schinkel AH, Prieto JG. Breast cancer resistance protein (BCRP/ABCG2) transports fluoroquinolone antibiotics and affects their oral availability, pharmacokinetics, and milk secretion. *Drug Metab Dispos* 2006;34(4):690-5.

94. Rasmussen F. Active mammary excretion of N4-acetylated sulphanilamide. *Acta Vet Scand* 1969;10(4):402-3.

95. Rasmussen F. Active mammary excretion of N4-acetylated p-aminohippuric acid. *Acta Vet Scand* 1969;10(2):193-4.

96. Schadewinkel-Scherkl AM, Rasmussen F, Merck CC, Nielsen P, Frey HH. Active transport of benzylpenicillin across the blood-milk barrier. *Pharmacol Toxicol* 1993;73(1):14-9.

97. Heap RB, Hamon M, Fleet IR. Transport of oestrone sulphate by the mammary gland in the goat. *J Endocrinol* 1984;101(2):221-30.

98. El-Sooud KA. Influence of albendazole on the disposition kinetics and milk antimicrobial equivalent activity of enrofloxacin in lactating goats. *Pharmacol Res* 2003;48(4):389-95.

99. HUGO Gene Nomenclature Committee. http://www.genenames.org. In.

100. Obermeier S, Huselweh B, Tinel H, Kinne RH, Kunz C. Expression of glucose transporters in lactating human mammary gland epithelial cells. *Eur J Nutr* 2000;39(5):194-200.

101. Shillingford JM, Miyoshi K, Flagella M, Shull GE, Hennighausen L. Mouse mammary epithelial cells express the Na-K-Cl cotransporter, NKCC1: characterization, localization, and involvement in ductal development and morphogenesis. *Mol Endocrinol* 2002;16(6):1309-21.

102. Tazebay UH, Wapnir IL, Levy O, Dohan O, Zuckier LS, Zhao QH, et al. The mammary gland iodide transporter is expressed during lactation and in breast cancer. *Nat Med* 2000;6(8):871-8.

103. Ito S, Alcorn J. Xenobiotic transporter expression and function in the human mammary gland. *Adv Drug Deliv Rev* 2003;55(5):653-65.

104. Bleasby K, Castle JC, Roberts CJ, Cheng C, Bailey WJ, Sina JF, et al. Expression profiles of 50 xenobiotic transporter genes in humans and pre-clinical species: a resource for investigations into drug disposition. *Xenobiotica* 2006;36(10-11):963-88.

105. Koepsell H, Endou H. The SLC22 drug transporter family. *Pflugers Arch* 2004;447(5):666-76.

106. Yabuuchi H, Tamai I, Nezu J, Sakamoto K, Oku A, Shimane M, et al. Novel membrane transporter OCTN1 mediates multispecific, bidirectional, and pH-dependent transport of organic cations. *J Pharmacol Exp Ther* 1999;289(2):768-73.

107. Tamai I, Yabuuchi H, Nezu J, Sai Y, Oku A, Shimane M, et al. Cloning and characterization of a novel human pH-dependent organic cation transporter, OCTN1. *FEBS Lett* 1997;419(1):107-11.

108. Tamai I, Ohashi R, Nezu JI, Sai Y, Kobayashi D, Oku A, et al. Molecular and functional characterization of organic cation/carnitine transporter family in mice. *J Biol Chem* 2000;275(51):40064-72.

109. Tamai I, Ohashi R, Nezu J, Yabuuchi H, Oku A, Shimane M, et al. Molecular and functional identification of sodium ion-dependent, high affinity human carnitine transporter OCTN2. *J Biol Chem* 1998;273(32):20378-82.

110. Gerk PM, Oo CY, Paxton EW, Moscow JA, McNamara PJ. Interactions between cimetidine, nitrofurantoin, and probenecid active transport into rat milk. *J Pharmacol Exp Ther* 2001;296(1):175-80.

111. Hagenbuch B, Meier PJ. Organic anion transporting polypeptides of the OATP/ SLC21 family: phylogenetic classification as OATP/ SLCO superfamily, new nomenclature and molecular/functional properties. *Pflugers Arch* 2004;447(5):653-65.

112. Pizzagalli F, Varga Z, Huber RD, Folkers G, Meier PJ, St-Pierre MV. Identification of steroid sulfate transport processes in the human mammary gland. *J Clin Endocrinol Metab* 2003;88(8):3902-12.

113. Chen NH, Reith ME, Quick MW. Synaptic uptake and beyond: the sodium- and chloride-dependent neurotransmitter transporter family SLC6. *Pflugers Arch* 2004;447(5):519-31.

114. Daniel H, Kottra G. The proton oligopeptide cotransporter family SLC15 in physiology and pharmacology. *Pflugers Arch* 2004;447(5):610-8.

115. Sloan JL, Mager S. Cloning and functional expression of a human Na(+) and Cl(-)-dependent neutral and cationic amino acid transporter B(0+). *J Biol Chem* 1999;274(34):23740-5.

116. Groneberg DA, Doring F, Theis S, Nickolaus M, Fischer A, Daniel H. Peptide transport in the mammary gland: expression and distribution of PEPT2 mRNA and protein. *Am J Physiol Endocrinol Metab* 2002;282(5):E1172-9.

117. Gray JH, Owen RP, Giacomini KM. The concentrative nucleoside transporter family, SLC28. *Pflugers Arch* 2004;447(5):728-34.

118. Baldwin SA, Beal PR, Yao SY, King AE, Cass CE, Young JD. The equilibrative nucleoside transporter family, SLC29. *Pflugers Arch* 2004;447(5):735-43.

119. Takanaga H, Mackenzie B, Hediger MA. Sodium-dependent ascorbic acid transporter family SLC23. *Pflugers Arch* 2004;447(5):677-82.

120. Dean M, Hamon Y, Chimini G. The human ATP-binding cassette (ABC) transporter superfamily. *J Lipid Res* 2001;42(7):1007-17.

121. Choudhuri S, Klaassen CD. Structure, function, expression, genomic organization, and single nucleotide polymorphisms of human ABCB1 (MDR1), ABCC (MRP), and ABCG2 (BCRP) efflux transporters. *Int J Toxicol* 2006;25(4):231-59.

122. Cordon-Cardo C, O'Brien JP, Boccia J, Casals D, Bertino JR, Melamed MR. Expression of the multidrug resistance gene product (P-glycoprotein) in human normal and tumor tissues. *J Histochem Cytochem* 1990;38(9):1277-87.

123. van der Valk P, van Kalken CK, Ketelaars H, Broxterman HJ, Scheffer G, Kuiper CM, et al. Distribution of multi-drug resistance-associated P-glycoprotein in normal and neoplastic human tissues. Analysis with 3 monoclonal antibodies recognizing different epitopes of the P-glycoprotein molecule. *Ann Oncol* 1990;1(1):56-64.

124. Jonker JW, Merino G, Musters S, van Herwaarden AE, Bolscher E, Wagenaar E, et al. The breast cancer resistance protein BCRP (ABCG2) concentrates drugs and carcinogenic xenotoxins into milk. *Nat Med* 2005;11(2):127-9.

125. Bera TK, Lee S, Salvatore G, Lee B, Pastan I. MRP8, a new member of ABC transporter superfamily, identified by EST database mining and gene prediction program, is highly expressed in breast cancer. *Mol Med* 2001;7(8):509-16.

126. Bera TK, Iavarone C, Kumar V, Lee S, Lee B, Pastan I. MRP9, an unusual truncated member of the ABC transporter superfamily, is highly expressed in breast cancer. *Proc Natl Acad Sci U S A* 2002;99(10):6997-7002.

127. Pavek P, Merino G, Wagenaar E, Bolscher E, Novotna M, Jonker JW, et al. Human breast cancer resistance protein: interactions with steroid drugs, hormones, the dietary carcinogen 2-amino-1-methyl-6-phenylimidazo(4,5-b)pyridine, and transport of cimetidine. *J Pharmacol Exp Ther* 2005;312(1):144-52.

128. van Herwaarden AE, Jonker JW, Wagenaar E, Brinkhuis RF, Schellens JH, Beijnen JH, et al. The breast cancer resistance protein (Bcrp1/Abcg2) restricts exposure to the dietary carcinogen 2-amino-1-methyl-6-phenylimidazo[4,5-b]pyridine. *Cancer Res* 2003;63(19):6447-52.

129. van Herwaarden AE, Wagenaar E, Karnekamp B, Merino G, Jonker JW, Schinkel AH. Breast cancer resistance protein (Bcrp1/Abcg2) reduces systemic exposure of the dietary carcinogens aflatoxin B1, IQ and Trp-P-1 but also mediates their secretion into breast milk. *Carcinogenesis* 2006;27(1):123-30.

130. Jonker JW, Freeman J, Bolscher E, Musters S, Alvi AJ, Titley I, et al. Contribution of the ABC transporters Bcrp1 and Mdr1a/1b to the side population phenotype in mammary gland and bone marrow of mice. *Stem Cells* 2005;23(8):1059-65.

131. Doyle LA, Ross DD. Multidrug resistance mediated by the breast cancer resistance protein BCRP (ABCG2). *Oncogene* 2003;22(47):7340-58.

132. Krishnamurthy P, Schuetz JD. Role of ABCG2/BCRP in biology and medicine. *Annu Rev Pharmacol Toxicol* 2006;46:381-410.

133. Kusuhara H, Sugiyama Y. ATP-binding cassette, subfamily G (ABCG family). *Pflugers Arch* 2007;453(5):735-44.

134. Robey RW, Polgar O, Deeken J, To KW, Bates SE. ABCG2: determining its relevance in clinical drug resistance. *Cancer Metastasis Rev* 2007;26(1):39-57.

135. Doyle LA, Yang W, Abruzzo LV, Krogmann T, Gao Y, Rishi AK, et al. A multidrug resistance transporter from human MCF-7 breast cancer cells. *Proc Natl Acad Sci U S A* 1998;95(26):15665-70.

136. Xu J, Liu Y, Yang Y, Bates S, Zhang JT. Characterization of oligomeric human half-ABC transporter ATP-binding cassette G2. *J Biol Chem* 2004;279(19):19781-9.

137. Zhang W, Yu BN, He YJ, Fan L, Li Q, Liu ZQ, et al. Role of BCRP 421C>A polymorphism on rosuvastatin pharmacokinetics in healthy Chinese males. *Clin Chim Acta* 2006;373(1-2):99-103.

138. Imai Y, Nakane M, Kage K, Tsukahara S, Ishikawa E, Tsuruo T, et al. C421A polymorphism in the human breast cancer resistance protein gene is associated with low expression of Q141K protein and low-level drug resistance. *Mol Cancer Ther* 2002;1(8):611-6.

139. Ishikawa T, Tamura A, Saito H, Wakabayashi K, Nakagawa H. Pharmacogenomics of the human ABC transporter ABCG2: from functional evaluation to drug molecular design. *Naturwissenschaften* 2005;92(10):451-63.

140. Krishnamurthy P, Ross DD, Nakanishi T, Bailey-Dell K, Zhou S, Mercer KE, et al. The stem cell marker Bcrp/ABCG2 enhances hypoxic cell survival through interactions with heme. *J Biol Chem* 2004;279(23):24218-25.

141. Ebert B, Seidel A, Lampen A. Identification of BCRP as transporter of benzo[a]pyrene conjugates metabolically formed in Caco-2 cells and its induction by Ah-receptor agonists. *Carcinogenesis* 2005;26(10):1754-63.

142. Moffit JS, Aleksunes LM, Maher JM, Scheffer GL, Klaassen CD, Manautou JE. Induction of hepatic transporters multidrug resistance-associated proteins (Mrp) 3 and 4 by clofibrate is regulated by peroxisome proliferator-activated receptor alpha. *J Pharmacol Exp Ther* 2006;317(2):537-45.

143. Wang H, Zhou L, Gupta A, Vethanayagam RR, Zhang Y, Unadkat JD, et al. Regulation of BCRP/ABCG2 expression by progesterone and 17beta-estradiol in

human placental BeWo cells. *Am J Physiol Endocrinol Metab* 2006;290(5):E798-807.

144. Ee PL, Kamalakaran S, Tonetti D, He X, Ross DD, Beck WT. Identification of a novel estrogen response element in the breast cancer resistance protein (ABCG2) gene. *Cancer Res* 2004;64(4):1247-51.

145. Maliepaard M, Scheffer GL, Faneyte IF, van Gastelen MA, Pijnenborg AC, Schinkel AH, et al. Subcellular localization and distribution of the breast cancer resistance protein transporter in normal human tissues. *Cancer Res* 2001;61(8):3458-64.

146. Merino G, van Herwaarden AE, Wagenaar E, Jonker JW, Schinkel AH. Sex-dependent expression and activity of the ATP-binding cassette transporter breast cancer resistance protein (BCRP/ABCG2) in liver. *Mol Pharmacol* 2005;67(5):1765-71.

147. Haimeur A, Conseil G, Deeley RG, Cole SP. The MRP-related and BCRP/ABCG2 multidrug resistance proteins: biology, substrate specificity and regulation. *Curr Drug Metab* 2004;5(1):21-53.

148. Zhang Y, Gupta A, Wang H, Zhou L, Vethanayagam RR, Unadkat JD, et al. BCRP transports dipyridamole and is inhibited by calcium channel blockers. *Pharm Res* 2005;22(12):2023-34.

149. Huang L, Wang Y, Grimm S. ATP-dependent transport of rosuvastatin in membrane vesicles expressing breast cancer resistance protein. *Drug Metab Dispos* 2006;34(5):738-42.

150. Hirano M, Maeda K, Matsushima S, Nozaki Y, Kusuhara H, Sugiyama Y. Involvement of BCRP (ABCG2) in the biliary excretion of pitavastatin. *Mol Pharmacol* 2005;68(3):800-7.

151. Ando T, Kusuhara H, Merino G, Alvarez AI, Schinkel AH, Sugiyama Y. Involvement of Breast Cancer Resistance Protein (ABCG2) in the biliary excretion mechanism of fluoroquinolones. *Drug Metab Dispos* 2007.

152. Merino G, Jonker JW, Wagenaar E, Pulido MM, Molina AJ, Alvarez AI, et al. Transport of anthelmintic benzimidazole drugs by breast cancer resistance protein (BCRP/ABCG2). *Drug Metab Dispos* 2005;33(5):614-8.

153. Breedveld P, Zelcer N, Pluim D, Sonmezer O, Tibben MM, Beijnen JH, et al. Mechanism of the pharmacokinetic interaction between methotrexate and benzimidazoles: potential role for breast cancer resistance protein in clinical drug-drug interactions. *Cancer Res* 2004;64(16):5804-11.

154. Henrich CJ, Bokesch HR, Dean M, Bates SE, Robey RW, Goncharova EI, et al. A high-throughput cell-based assay for inhibitors of ABCG2 activity. *J Biomol Screen* 2006;11(2):176-83.

155. Saito H, Hirano H, Nakagawa H, Fukami T, Oosumi K, Murakami K, et al. A new strategy of high-speed screening and quantitative structure-activity relationship analysis to evaluate human ATP-binding cassette transporter ABCG2-drug interactions. *J Pharmacol Exp Ther* 2006;317(3):1114-24.

156. Goodell MA, Brose K, Paradis G, Conner AS, Mulligan RC. Isolation and functional properties of murine hematopoietic stem cells that are replicating in vivo. *J Exp Med* 1996;183(4):1797-806.

157. Wakabayashi K, Tamura A, Saito H, Onishi Y, Ishikawa T. Human ABC transporter ABCG2 in xenobiotic protection and redox biology. *Drug Metab Rev* 2006;38(3):371-91.

158. Jonker JW, Buitelaar M, Wagenaar E, Van Der Valk MA, Scheffer GL, Scheper RJ, et al. The breast cancer resistance protein protects against a major chlorophyll-derived dietary phototoxin and protoporphyria. *Proc Natl Acad Sci U S A* 2002;99(24):15649-54.

159. Kolwankar D, Glover DD, Ware JA, Tracy TS. Expression and function of ABCB1 and ABCG2 in human placental tissue. *Drug Metab Dispos* 2005;33(4):524-9.

160. Jonker JW, Smit JW, Brinkhuis RF, Maliepaard M, Beijnen JH, Schellens JH, et al. Role of breast cancer resistance protein in the bioavailability and fetal penetration of topotecan. *J Natl Cancer Inst* 2000;92(20):1651-6.

161. Staud F, Vackova Z, Pospechova K, Pavek P, Ceckova M, Libra A, et al. Expression and transport activity of breast cancer resistance protein (Bcrp/Abcg2) in dually perfused rat placenta and HRP-1 cell line. *J Pharmacol Exp Ther* 2006;319(1):53-62.

162. Grube M, Reuther S, Meyer Zu Schwabedissen H, Kock K, Draber K, Ritter CA, et al. Organic anion transporting polypeptide 2B1 and breast cancer resistance protein interact in the transepithelial transport of steroid sulfates in human placenta. *Drug Metab Dispos* 2007;35(1):30-5.

163. Kruijtzer CM, Beijnen JH, Rosing H, ten Bokkel Huinink WW, Schot M, Jewell RC, et al. Increased oral bioavailability of topotecan in combination with the breast cancer resistance protein and P-glycoprotein inhibitor GF120918. *J Clin Oncol* 2002;20(13):2943-50.

164. Rozen S, Skaletsky H. Primer3 on the WWW for general users and for biologist programmers. *Methods Mol Biol* 2000;132:365-86.

165. Ririe KM, Rasmussen RP, Wittwer CT. Product differentiation by analysis of DNA melting curves during the polymerase chain reaction. *Anal Biochem* 1997;245(2):154-60.

166. Bergman AM, Eijk PP, Ruiz van Haperen VW, Smid K, Veerman G, Hubeek I, et al. In vivo induction of resistance to gemcitabine results in increased expression of ribonucleotide reductase subunit M1 as the major determinant. *Cancer Res* 2005;65(20):9510-6.

167. Pearce DJ, Anjos-Afonso F, Ridler CM, Eddaoudi A, Bonnet D. Age-dependent increase in side population distribution within hematopoiesis: implications for our understanding of the mechanism of aging. *Stem Cells* 2007;25(4):828-35.

168. Roche Applied Science. LightCycler: Relative Quantification (Technical Note No. LC 13/2001). 2001.

169. Wierdl M, Wall A, Morton CL, Sampath J, Danks MK, Schuetz JD, et al. Carboxylesterase-mediated sensitization of human tumor cells to CPT-11 cannot override ABCG2-mediated drug resistance. *Mol Pharmacol* 2003;64(2):279-88.

170. Zhou S, Schuetz JD, Bunting KD, Colapietro AM, Sampath J, Morris JJ, et al. The ABC transporter Bcrp1/ABCG2 is expressed in a wide variety of stem cells and is a molecular determinant of the side-population phenotype. *Nat Med* 2001;7(9):1028-34.

171. Horn J, Jordan SL, Song L, Roberts MJ, Anderson BD, Leggas M. Validation of an HPLC method for analysis of DB-67 and its water soluble prodrug in mouse plasma. *J Chromatogr B Analyt Technol Biomed Life Sci* 2006;844(1):15-22.

172. Kalvass JC, Pollack GM. Kinetic considerations for the quantitative assessment of efflux activity and inhibition: implications for understanding and predicting the effects of efflux inhibition. *Pharm Res* 2007;24(2):265-76.

173. Breedveld P, Pluim D, Cipriani G, Wielinga P, van Tellingen O, Schinkel AH, et al. The effect of Bcrp1 (Abcg2) on the in vivo pharmacokinetics and brain penetration of imatinib mesylate (Gleevec): implications for the use of breast cancer resistance protein and P-glycoprotein inhibitors to enable the brain penetration of imatinib in patients. *Cancer Res* 2005;65(7):2577-82.

174. Clarkson RW, Wayland MT, Lee J, Freeman T, Watson CJ. Gene expression profiling of mammary gland development reveals putative roles for death receptors and immune mediators in post-lactational regression. *Breast Cancer Res* 2004;6(2):R92-109.

175. Medrano JF, Ron M, Gregg JP. GSE5831: Analysis of the mammary gland transcriptome in wild type C57BL/6J mice In: NCBI; 2006.

176. Stein T, Morris JS, Davies CR, Weber-Hall SJ, Duffy MA, Heath VJ, et al. Involution of the mouse mammary gland is associated with an immune cascade and an acute-phase response, involving LBP, CD14 and STAT3. *Breast Cancer Res* 2004;6(2):R75-91.

177. Calcagno AM, Ludwig JA, Fostel JM, Gottesman MM, Ambudkar SV. Comparison of drug transporter levels in normal colon, colon cancer, and Caco-2 cells: impact on drug disposition and discovery. *Mol Pharm* 2006;3(1):87-93.

178. Gomm JJ, Browne PJ, Coope RC, Liu QY, Buluwela L, Coombes RC. Isolation of pure populations of epithelial and myoepithelial cells from the normal human mammary gland using immunomagnetic separation with Dynabeads. *Anal Biochem* 1995;226(1):91-9.

179. StemCell Technologies. EasySep® Human MUC1 - Selection Procedure (Version 1.2). In: Catalog #18359; 2004.

180. Clayton H, Titley I, Vivanco M. Growth and differentiation of progenitor/stem cells derived from the human mammary gland. *Exp Cell Res* 2004;297(2):444-60.

181. O'Hare MJ, Ormerod MG, Monaghan P, Lane EB, Gusterson BA. Characterization in vitro of luminal and myoepithelial cells isolated from the human mammary gland by cell sorting. *Differentiation* 1991;46(3):209-21.

182. Clarke C, Titley J, Davies S, O'Hare MJ. An immunomagnetic separation method using superparamagnetic (MACS) beads for large-scale purification of human mammary luminal and myoepithelial cells. *Epithelial Cell Biol* 1994;3(1):38-46.

183. Khaitovich P, Hellmann I, Enard W, Nowick K, Leinweber M, Franz H, et al. Parallel patterns of evolution in the genomes and transcriptomes of humans and chimpanzees. *Science* 2005;309(5742):1850-4.

184. Goh LB, Spears KJ, Yao D, Ayrton A, Morgan P, Roland Wolf C, et al. Endogenous drug transporters in in vitro and in vivo models for the prediction of drug disposition in man. *Biochem Pharmacol* 2002;64(11):1569-78.

185. Wang X, Morris ME. Effects of the flavonoid chrysin on nitrofurantoin pharmacokinetics in rats: potential involvement of ABCG2. *Drug Metab Dispos* 2007;35(2):268-74.

186. Wang X, Nitanda T, Shi M, Okamoto M, Furukawa T, Sugimoto Y, et al. Induction of cellular resistance to nucleoside reverse transcriptase inhibitors by the wild-type breast cancer resistance protein. *Biochem Pharmacol* 2004;68(7):1363-70.

187. Gerk PM. Nitrofurantoin active transport in the mammary epithelium; 2000.

188. Breedveld P, Pluim D, Cipriani G, Dahlhaus F, van Eijndhoven MA, de Wolf CJ, et al. The effect of low pH on breast cancer resistance protein (ABCG2)-mediated transport of methotrexate, 7-hydroxymethotrexate, methotrexate diglutamate, folic acid, mitoxantrone, topotecan, and resveratrol in in vitro drug transport models. *Mol Pharmacol* 2007;71(1):240-9.

189. Maliepaard M, van Gastelen MA, Tohgo A, Hausheer FH, van Waardenburg RC, de Jong LA, et al. Circumvention of breast cancer resistance protein (BCRP)-mediated resistance to camptothecins in vitro using non-substrate drugs or the BCRP inhibitor GF120918. *Clin Cancer Res* 2001;7(4):935-41.

190. Volk EL, Farley KM, Wu Y, Li F, Robey RW, Schneider E. Overexpression of wild-type breast cancer resistance protein mediates methotrexate resistance. *Cancer Res* 2002;62(17):5035-40.

191. Allen JD, Van Dort SC, Buitelaar M, van Tellingen O, Schinkel AH. Mouse breast cancer resistance protein (Bcrp1/Abcg2) mediates etoposide resistance and transport, but etoposide oral availability is limited primarily by P-glycoprotein. *Cancer Res* 2003;63(6):1339-44.

192. Ceckova M, Libra A, Pavek P, Nachtigal P, Brabec M, Fuchs R, et al. Expression and functional activity of breast cancer resistance protein (BCRP, ABCG2) transporter in the human choriocarcinoma cell line BeWo. *Clin Exp Pharmacol Physiol* 2006;33(1-2):58-65.

193. Allen JD, van Loevezijn A, Lakhai JM, van der Valk M, van Tellingen O, Reid G, et al. Potent and specific inhibition of the breast cancer resistance protein multidrug transporter in vitro and in mouse intestine by a novel analogue of fumitremorgin C. *Mol Cancer Ther* 2002;1(6):417-25.

194. Pozza A, Perez-Victoria JM, Sardo A, Ahmed-Belkacem A, Di Pietro A. Purification of breast cancer resistance protein ABCG2 and role of arginine-482. *Cell Mol Life Sci* 2006;63(16):1912-22.

195. Chen ZS, Robey RW, Belinsky MG, Shchaveleva I, Ren XQ, Sugimoto Y, et al. Transport of methotrexate, methotrexate polyglutamates, and 17beta-estradiol 17-(beta-D-glucuronide) by ABCG2: effects of acquired mutations at R482 on methotrexate transport. *Cancer Res* 2003;63(14):4048-54.

196. Johns DG, Rutherford LD, Leighton PC, Vogel CL. Secretion of methotrexate into human milk. *Am J Obstet Gynecol* 1972;112(7):978-80.

197. Xia CQ, Milton MN, Gan LS. Evaluation of drug-transporter interactions using in vitro and in vivo models. *Curr Drug Metab* 2007;8(4):341-63.

198. Thompson PA, Kadlubar FF, Vena SM, Hill HL, McClure GH, McDaniel LP, et al. Exfoliated ductal epithelial cells in human breast milk: a source of target tissue DNA for molecular epidemiologic studies of breast cancer. *Cancer Epidemiol Biomarkers Prev* 1998;7(1):37-42.

199. Smalley MJ, Titley J, O'Hare MJ. Clonal characterization of mouse mammary luminal epithelial and myoepithelial cells separated by fluorescence-activated cell sorting. *In Vitro Cell Dev Biol Anim* 1998;34(9):711-21.

200. Mikkaichi T, Suzuki T, Onogawa T, Tanemoto M, Mizutamari H, Okada M, et al. Isolation and characterization of a digoxin transporter and its rat homologue expressed in the kidney. *Proc Natl Acad Sci U S A* 2004;101(10):3569-74.

201. Chu XY, Bleasby K, Yabut J, Cai X, Chan GH, Hafey MJ, et al. Transport of the dipeptidyl peptidase-4 inhibitor sitagliptin by human organic anion transporter 3, organic anion transporting polypeptide 4C1, and multidrug resistance P-glycoprotein. *J Pharmacol Exp Ther* 2007;321(2):673-83.

202. Hatanaka T, Haramura M, Fei YJ, Miyauchi S, Bridges CC, Ganapathy PS, et al. Transport of amino acid-based prodrugs by the Na+- and Cl(-) -coupled amino acid transporter ATB0,+ and expression of the transporter in tissues amenable for drug delivery. *J Pharmacol Exp Ther* 2004;308(3):1138-47.

203. Ito K, Suzuki H, Horie T, Sugiyama Y. Apical/basolateral surface expression of drug transporters and its role in vectorial drug transport. *Pharm Res* 2005;22(10):1559-77.

VITA

Philip Earle Empey was born on September 13, 1974 in Lowell, Massachusetts. He attended the University of Rhode Island from 1992 to 1998 and received Doctor of Pharmacy (Pharm.D.) degree with highest distinction in May 1998. Philip then completed residencies in both Pharmacy Practice and Critical Care at the University of Kentucky Hospital in 1999 and 2000, respectively. In 2000, he enrolled in the Clinical Pharmaceutical Sciences graduate program at the University of Kentucky College of Pharmacy. He achieved board certification (Board Certified Pharmacotherapy Specialist, BCPS) from the Board of Pharmaceutical Specialties in December 2001.

Dr. Empey has held positions as a Clinical Research Associate in the Neurosurgery Research Program at the University of Kentucky (2001-2003) and as a Pharmacist (1998-2007) at the University of Kentucky Hospital. He has also been the Web Developer for the Department of Pharmacy Services at the University of Kentucky Hospital from 1998 to 2007. Philip received AFPE Predoctoral Fellowships (2004-2006, endowed 2007), Research Challenge Trust Fellowships (2000-2007), was a Predoctoral Trainee in the NIH Training Grant in Reproductive Sciences (T32-HD007436, 2002-2004) and has completed the Clinical Research and Leadership Development Program (K30-HL004163, 2000-2006) at the University of Kentucky. He had the opportunity to present his research at AAPS in 2004 and 2006 and at ISSX in 2006. Dr. Empey has also received the Merck Research Scholar Program Award in 1998; the AAPS Pharmacokinetics, Pharmacodynamics, and Drug Metabolism Section Travel Award in 2004; the Peter J. Glavinos, Ph.D. Graduate Student Endowment Travel Award in 2006, the AFPE Pharmaceutical Sciences Graduate Student Recognition Award in 2007, and was recently elected Chair-Elect of the ACCP Pharmacokinetics and Pharmacodynamics Practice Research Network for 2007-2008.

Publications:

Empey PE, Ren N, McNamara PJ. Microarray analysis of transporter gene expression in lactating mammary epithelial cells. (in preparation)

Empey PE, McNamara PJ. Modeling of drug transport into breast milk and estimation of milk to serum ratio. (in preparation)

Empey PE, Wang L, McNamara PJ. Breast cancer resistance protein (Bcrp1/Abcg2) transports of nitrofurantoin, cimetidine, and PhIP in the CIT3 cell culture model of lactation. (in preparation)

Hatton J, Rosbolt MB, Empey PE, Kryscio R, Young B. Dosing and safety of cyclosporine A in patients with severe brain injury. (accepted, *Journal of Neurosurgery*)

Smith KM, Trapskin PJ, Empey PE, Hecht KA, Armitstead JA. Internally-Developed Online Adverse Drug Reaction and Medication Error Reporting Systems. *Hospital Pharmacy*. 2006 May; 41(5): 428-436.

Empey PE, McNamara PJ, Young B, Rosbolt MB, Hatton J. Cyclosporin A Disposition following Acute Traumatic Brain Injury. *J Neurotrauma.* 2006 Jan; 23(1): 109-16.

Empey PE, Jennings HR, Thornton AC, Rapp RP, Evans ME. Levofloxacin failure in a patient with pneumococcal pneumonia. *Ann Pharmacother.* 2001 Jun;35:687-90. (58 citations)

Jennings HR, Empey PE, Smith KM. Benchmarking ASHP-accredited residencies: A survey of program stipends, benefits, staffing practices, and organization. *American Journal of Health-System Pharmacy* 2000 Nov 15;57(22):2080-6.